PHILOSOPHY DOCTOR THESIS

Centralized transmission techniques for full-duplex reconfigurable WDM optical access networks

Author
Fulvio Grassi Marangione

Supervisors
Dr. José Mora Almerich
Dr. Beatriz Ortega Tamarit

Departamento de Comunicaciones

Universitat Politècnica de València

Valencia, November 2013

Acknowledgements

My foremost appreciation goes to my supervisors, Dr. Beatriz Ortega and Dr. José Mora for having accepted me in the Optical & Quantum Communications Group (OQCG) at Universitat Politècnica de València (UPV) and made this Ph.D. project possible. I am truly grateful for all their guidance, patience and motivation all over my graduate studies. Our regular progress meetings will be remembered for being both entertaining and a source of inspiration. Thank you for keeping your door open and always having time for me.

In addition, I would like to thank the members of my thesis committee for their time and dedication. I have also benefited greatly from the interaction and collaboration with many of the past and present research members of the Optical & Quantum Communications Group (OQCG).

Abstract

This Thesis investigates and develops novel bidirectional and reconfigurable optical access architectures based on WDM technology with the aim of solving the problem of cost and complexity associated to the WDM-PON transceivers. In particular, depending on the capacity requirements of the network, the investigation and development deal with two specific environments of application.

In case of low capacity access platforms, we propose and validate new dispersion tolerant optical transmission systems based on the employment of optical broadband sources operating in the third transmission band and whose adaptability to the transport of RoF signals is realized, for the first time, by means of Mach-Zehnder optical interferometer structures.

The optical bandpass filtering feature of the Mach-Zehnder device is key to overcome the chromatic dispersion-induced limitations arising from the spectral width of the source and, thus, significantly increase the system operative bandwidth to several tens of GHz. The incorporation of a Mach-Zehnder structure has a relatively low degree of implementation complexity and opens the possibility to transmit RoF signals using cost-effective optical broadband sources in optical access platforms being, at the same time, a viable alternative to other dispersion compensation techniques under certain scenarios. Good RoF transmission performance is experimentally achieved over single mode and multi mode fiber links employing optical amplitude and optical phase modulation. The SCM technique is also used for the generation of down- and up-stream signals to improve the link bandwidth utilization and allow converging transport of wired and wireless services. Service flexibility is demonstrated by means of different types of codification concerning the transmitted binary information. In spectrum sliced optical broadband source multichannel applications, the dynamical assignment of capacity is realized by means of a compact routing scheme based on optical switching and validated over different routing scenarios. Moreover, two extra functionalities offered by the Mach-Zehnder device, such as the photonic suppression of harmonic and intermodulation distortion and the all-optical microwaves generation and up-conversion, are demonstrated.

For optical access platforms requiring high capacity transport we propose and validate light sources-centralized optical transmission systems where the PolMUX technique is employed for the first time in the access platform as a novel strategy to minimize the cost and complexity of the terminal units in accordance with the centralization concept.

The PolMUX principle uses light polarization as a degree of freedom to efficiently multiplex two orthogonal optical fields at the same wavelength into the same optical channel. Under this principle, the optical carriers required for the down- and uplink transmission can be provided by a single and centralized coherent source. It means that the terminal unit can be kept source-free and operative wavelength-independent. This concept is firstly validated over a single-channel full-duplex optical transmission system adopting RoF and SCM techniques for the generation and transport of the down- and upstream signals. Apart of fulfilling the requirements of quality

of transmission after the polarization demultiplexing process, we demonstrate that the tracking and control of polarization can be also centralized at the central office for further minimization of the terminal unit complexity. Finally, the effectiveness of the PolMUX technique is exploited in the access network in order to perform full-duplex multichannel communications where reconfiguration of capacity depending on the actual demand and service convergence, required in RoF, are also demonstrated.

Resumen

En esta Tesis doctoral se investigan y desarrollan arquitecturas novedosas de redes de acceso bidireccionales y reconfigurables basadas en tecnología WDM con la finalidad de resolver el problema del coste y la complejidad asociada a los transceptores en las redes ópticas pasivas basadas en WDM. En particular, dependiendo de los requerimientos de capacidad de la red, la investigación y el desarrollo han abarcado dos entornos de aplicación específicos.

En el caso de plataformas de acceso de baja capacidad, se han propuesto y validado nuevos sistemas de transmisión óptica basados en el empleo de fuentes ópticas anchas en tercera ventana de transmisión tolerantes a la dispersión y cuya adaptabilidad al transporte de señales RoF se realiza, por primera vez, por medio de estructuras ópticas interferométricas de Mach-Zehnder.

Las características de transmisión óptica paso banda del dispositivo Mach-Zehnder es clave para superar las limitaciones inducidas por la dispersión cromática debidas a la anchura espectral de la fuente y así incrementar considerablemente el ancho de banda operativo del sistema hasta varias decenas de GHz. La incorporación de la estructura Mach-Zehnder posee un grado de complejidad de implementación relativamente bajo y abre la posibilidad de transmitir señales RoF usando fuentes ópticas anchas de bajo coste en plataformas de acceso óptico. En la transmisión de señales RoF se han logrado buenos resultados experimentales tanto sobre fibra monomodo como en fibra multimodo usando modulación óptica de amplitud y de fase. La técnica de multiplexación por división de subportadora se incorpora para la generación de las señales ascendientes y descendientes con el fin de mejorar la eficiencia espectral del enlace y permitir la transmisión convergente de señales alámbricos y inalámbricos. La flexibilidad de servicio se demuestra usando distintos tipos de codificación de la información binaria transmitida. En aplicaciones multicanal basadas en la subdivisión espectral de la fuente óptica ancha, la reasignación dinámica de capacidad se realiza por medio de compactos esquemas de enrutamiento basados en conmutación óptica y que se validan bajo distintos escenarios de enrutamiento. Además, se demuestra que la estructura Mach-Zehnder permite realizar dos funcionalidades extra tal como la supresión fotónica de la distorsión armónica y de intermodulación, y la generación y conversión óptica de señales de microondas.

Para entornos de acceso óptico de alta capacidad de transporte proponemos y validamos sistemas de transmisión ópticos centralizados donde la técnica de PolMUX se emplea por primera vez en redes de acceso como estrategia novedosa para minimizar el coste y la complejidad de las estaciones terminales de acuerdo con el concepto de centralización de fuentes ópticas.

El principio PolMUX utiliza la polarización de la luz como un grado de libertad para combinar de manera eficiente dos campos ópticos ortogonales y a la misma longitud de onda sobre el mismo canal óptico. Bajo ese

principio, las portadoras ópticas necesarias para la transmisión ascendiente y descendiente pueden ser suministradas por una única fuente óptica coherente centralizada. Por lo tanto la estación terminal quedaría libre de fuentes y transparente a la longitud de onda operativa. Este concepto se valida inicialmente sobre un enlace de transmisión óptica bidireccional de un solo canal adoptando técnicas de RoF y multiplexación por división de subportadora para la generación y el transporte de las señales ascendientes y descendientes. Además de satisfacer los requerimientos de calidad de la transmsión tras el proceso de separación de los campos polarizados, se demuestra que el seguimiento y el control de la polarización pueden también centralizarse en la estación central simplificando aún más la unidad óptica de red. Finalmente, la eficacia de la técnica PolMUX se explota en una red de acceso para realizar comunicaciones multicanal en ambas direcciones donde se demuestran también tanto la asignación dinámica de capacidad dependiendo de la demanda actual como la convergencia de servicios necesaria en aplicaciones RoF.

Resum

En esta Tesi doctoral s'investiguen i desenrotllen arquitectures noves de xarxes d'accés bidireccionals i reconfigurables basades en tecnologia WDM amb la finalitat de resoldre el problema del cost i la complexitat associada als transceptors en les xarxes òptiques passives basades en WDM. En particular, depenent dels requeriments de capacitat de la xarxa, la investigació i el desenrotllament han comprés dos entorns d'aplicació específics.

En el cas de plataformes d'accés de baixa capacitat, s'han proposat i validat nous sistemes de transmissió òptica basats en l'ocupació de fonts òptiques amples en tercera finestra de transmissió tolerants amb la dispersió i amb una adaptabilitat al transport de senyals RoF que es realitza, per primera vegada, per mitjà d'estructures òptiques interferométricas de Mach- Zehnder.

Les característiques de transmissió òptica pasabanda del dispositiu Mach- Zehnder és clau per a superar les limitacions induïdes per la dispersió cromàtica degudes a l'amplària espectral de la font i així incrementar considerablement l'amplada de banda operatiu del sistema fins a diverses desenes de GHz. La incorporació de l'estructura Mach-Zehnder posseïx un grau de complexitat d'implementació relativament baix i obri la possibilitat de transmetre senyals RoF usant fonts òptiques amples de baix cost en plataformes d'accés òptic. En la transmissió de senyals RoF s'han aconseguit bons resultats experimentals tant sobre fibra monomodo com en fibra multimodo usant modulació òptica d'amplitud i de fase. La tècnica de multiplexació per divisió de subportadora s'incorpora per a la generació dels senyals ascendents i descendents a fi de millorar l'eficiència espectral de l'enllaç i permetre la transmissió convergent de senyals alàmbrica i inalàmbrica. La flexibilitat de servici es demostra usant distints tipus de codificació de la informació binària transmesa. En aplicacions multicanal basades en la subdivisió espectral de la font òptica ampla, la reassignació dinàmica de capacitat es realitza per mitjà de esquemes compactes d'enrutament basats en commutació òptica i que es validen davall distints escenaris d'enrutamiento. A més, es demostra que l'estructura Mach-Zehnder permet realitzar dos funcionalitats extra tal com la supressió fotónica de la distorsió harmònica i d'intermodulació, i la generació i conversió òptica de senyals de microones.

Per a entorns d'accés òptic d'alta capacitat de transport proposem i validem sistemes de transmissió òptics centralitzats on la tècnica de PolMUX s'empra per primera vegada en xarxes d'accés com a estratègia nova per a minimitzar el cost i la complexitat de les estacions terminals d'acord amb el concepte de centralització de fonts òptiques.

El principi PolMUX utilitza la polarització de la llum com un grau de llibertat per a combinar de manera eficient dos camps òptics ortogonals i a la mateixa longitud d'ona sobre el mateix canal òptic. Baix eixe principi, les portadores òptiques necessàries per a la transmissió ascendent i descendent poden ser subministrades per una única font òptica coherent centralitzada. Per tant, l'estació terminal quedaria lliure de fonts i transparent a la longitud d'ona operativa. Este concepte es valida

inicialment sobre un enllaç de transmissió òptica bidireccional d'un sol canal adoptant tècniques de RoF i multiplexació per divisió de subportadora per a la generació i el transport dels senyals ascendents i descendents. A més de satisfer els requeriments de qualitat de la transmissió després del procés de separació dels camps polaritzats, es demostra que el seguiment i el control de la polarització poden també centralitzar-se en l'estació central simplificant encara més la unitat òptica de xarxa. Finalment, l'eficàcia de la tècnica PolMUX s'explota en una xarxa d'accés per a realitzar comunicacions multicanal en ambdós direccions on es demostren també tant l'assignació dinàmica de capacitat depenent de la demanda actual com la convergència de servicis necessària en aplicacions RoF.

Contents

band.

Chapter 1

Introduction

1.1   Context.

In today's communication age there is a large, diversified and rapidly growing demand for transporting information from one place to another covering a vast range of distances. Currently, most of the long-haul transport is realized by advanced optical communication systems where the adoption of commercially mature wavelength division multiplexing (WDM) technology is the most powerful way to exploit the spectacular bandwidth of optical fibers and move massive amounts of information at unequalled performance in terms of speed and capacity. Optical communication systems based on WDM technology are now expected to gradually penetrate in the access domain for short-haul communications and the enormous advantages of optical fibers and photonic signal processing promise to relieve the bandwidth limitations of legacy copper-based infrastructures and reduce the bottleneck of actual electronic solutions.

To facilitate a rapid and economically viable migration of optical technology toward the access segment, network architectures and topologies capable of achieve a great sharing of components and resources have been widely pursued from telecommunications service providers and system vendors during the last two decades. In this context, passive optical networks (PONs) has emerged as the more convenient solution to channel the data traffic from core networks to final private home and business subscribers since they use unpowered components instead of active electronics between the central office (CO) headend (attached to the core network) and each optical network unit (ONU) located at user's premises. In present days, the physical layout of a PON is at the base of access technologies and applications, such as for fiber-to-the-x (FTTx), radio over fiber (RoF) and their flexible combination where the transport of both digital baseband and analog GHz signals co-exists on the same fiber trunk line completed by wired and wireless links for the last mile coverage.

Recently, the increase in the number of subscribers and the explosive growth of new diversified broadband services has generated an urgent need for new advanced access architectures capable to fulfill a large set of requirements: high transmission capacity, high per-user bandwidth, great scalability for the accommodation of new subscribers, information security, dynamic assignment of capacity resources based on the actual subscriber's demand, convergence of wired and wireless services and technologies and high flexibility in terms of format and bit rate. To deal with such requirements, the incorporation of WDM technology into the access architecture is a key factor.

By assigning a dedicated pair of wavelengths to each subscriber, WDM systems enable bidirectional communications over a single strand of fiber with capacity multiplication. In other words, the use of multiple

wavelengths creates virtual point-to-point connectivity over a physical point-to-multipoint one. In this way WDM-PONs are uniquely capable to improve network capacity, user's bandwidth, scalability and privacy.

To establish flexible connections, efficient wavelength routing techniques, where the network capacity may be dynamically assigned in response to changing traffic patterns, can be easily implemented by means of selective WDM filters and photonic switches.

WDM-PONs match well with radio links deployed for wireless services delivery. WDM combined with RoF is, in fact, a natural solution to converge the transport of both digital FTTx and analog RoF signals over the (existing) fiber infrastructure of a PON. In such hybrid optical/wireless context, the optical path provides high-capacity backhaul whereas the wireless link assures high mobility of multiple wireless devices. It creates a powerful symbiosis between two different access technologies. In addition, the RoF technique realizes both generation and modulation of high frequency signals with a compact scheme where many signal processing functions are directly performed in the optical domain rather than electrical.

With regard to the generation of the down- and upstream traffic, the electrical subcarrier multiplexing (SCM) technique could be easily employed for some applications in combination with WDM and RoF. In fiber optic communications SCM means translation of a number of parallel radio frequency channels onto an optical carrier which is subsequently modulated. By so doing, the SCM technique is a powerful means to increase the channel spectral efficiency. Capable of mixing different analog and/or digital signals, SCM is also flexible and transparent to the type of service.

Since the worldwide subscribers demand is expected to outgrow the actual network capacity, the exploitation of WDM technology into the access domain is now driving the evolution from current generation time division multiplexing (TDM)-PONs to next generation WDM-PONs. Eventually complemented by RoF techniques for certain applications, WDM-PONs are becoming the most likely broadband access solution for the future.

In this context, the work developed in the present PhD. Thesis has been realized under the framework of the European FP7 ALPHA project (Architectures for fLexible Photonic Home and Access networks), grant agreement no.: 212 352, which main goal was the development of innovative architectural and transmission solutions for access and in-building integrated multi-service Internet/Intranet and 3G/B3G networks with adequate management and control. This project, with a duration of 39 months since January 1st, 2008, was coordinated by ACREO AB (Sweden) and integrated by the following European institutions: the Universitat Politècnica de València, France Telecom R&D, Alcatel-Lucent Bell Labs France, CommScope Italy Srl, University of Bologna, Telefonica I+D, Technical University of Eindhoven, Telsey S.p.A., Bangor University, Politechnico di Torino, Luceat S.p.A., Interdisciplinair Instituut Voor Breedbandtechnologie vzw, Danish University of Technology, Homefibre Digital Network GmbH, 3S Photonics and Telekomunikacja Polska R&D.

1.2 Motivations and objectives.

After conquering the core and metropolitan networks, research and development efforts are focused on extending WDM technology into the access domain. However, here the situation is quite different from that of the backbone network. The access market is, in fact, extremely cost-sensitive and technical solutions that are appropriate for the backbone network, in which costs can be considered to be shared among thousands of subscribers, are frequently too expensive for access. Despite the many potential advantages and benefits of WDM technology, there are some issues that are hampering a large-scale implementation of WDM-based PONs.

In WDM-PONs, to establish bidirectional connectivity between the CO and ONUs, several dedicated transceivers are required in both sides. Each transceiver must be designed and controlled to operate over a specific wavelength channel matching the band pass grid defined by the WDM standard. Therefore optical sources capable of emitting such a narrow and thermally stable grid of wavelengths is very necessary. Generally speaking, the cost and complexity of those transceivers may depend on the particular WDM channel spacing adopted which, in turns, is strictly related to the capacity requirements of the network.

WDM systems are conventionally divided in two different wavelength patterns, coarse WDM (CWDM) and dense WDM (DWDM). Standard CWDM technology, defined in ITU-T G.694.2, uses a maximum number of 18 channels spaced by 20 nm in the 1270 nm-1610 nm band, a large portion of the optical spectrum covering both second (1300 nm) and third (1550 nm) transmission windows. The second and the third transmission windows are characterized by minimum dispersion and minimum attenuation, respectively. Owing to its wide channels spacing, CWDM is considered a low cost technology because it relaxes wavelength stabilization requirements of both optical sources and optical filters/routers deployed at the terminal and intermediate nodes, respectively. This means that inexpensive optical broadband sources (OBS) and optical filters/routers with reduced temperature dependence could be conveniently employed to design less sophisticated and, in principle, cheaper transceivers. Since the economical benefits of CWDM allow the associated costs to approach those of non-WDM optical systems and components, CWDM technology is an interesting upgrading strategy for TDM-PONs in access scenarios with relatively low capacity demand.

The motivation beneath the employment of OBS is justified by their essentiality and cost-effectiveness for the building of spectrum sliced multichannel scenarios where the spectrum of a single OBS is opportunely divided (sliced) by a CWDM filter into a set of narrower channels used as optical carriers to replace several distributed lasers. Although high quality OBSs suitable for spectral slicing applications are commercially available, their tolerance to fiber chromatic dispersion in third transmission window still needs to be improved. The broad spectrum of a sliced channel is, in fact, more vulnerable to dispersion induced power penalties than the narrower spectrum of a coherent laser. Therefore, the operative electrical transmission bandwidth of a link using a sliced channel as optical carrier is drastically reduced allowing the transmission of signals only in a few MHz range. This bandwidth limitation is not significantly unfavorable for the

transmission of baseband FTTx signals but would clearly invalidate the transport of signals in the GHz band as required in RoF applications. It must be remarked that such effect is particularly detrimental when each sliced carrier is amplitude modulated using conventional double sideband (DSB) modulation.

Despite the fact that the effects of dispersion can be successfully surmounted by means of dispersion compensation techniques or adopting single sideband modulation (SSB) format, these solutions either compensate only for one of the two transmission windows or may increase the transceivers cost/complexity. Therefore the convenience of their implementation in access networks requires a careful evaluation. For that reason most of the proposed spectral slicing schemes have been initially applied to OBSs emitting in the second transmission region where the effect of fiber chromatic dispersion could be neglected. However, many CWDM wavelengths falling into the second transmission window are today considered "unusable" due to the increased attenuation in such band and its spectral incompatibility with optical amplifiers such as Erbium doped fiber amplifiers (EDFAs) and Raman amplifiers whose region of maximum amplification gain coincides with the third transmission window. According to such considerations, one first objective of the research presented in this manuscript has been to find a viable solution for the transport of RoF signals by means of spectrum sliced OBS operating in third transmission band and suitable for low-capacity access networks.

With regard to high capacity scenarios, recently we have assisted to a more extensive use of the wavelengths domain offered by conventional WDM technology under the introduction of the ITU-T G.694.1 standard. All conventional WDM systems operate in the third communication band with a channel grid having exactly a 100 GHz (0.8 nm) spacing and a reference frequency fixed at 193.10 THz (1552.52 nm). This grid is placed inside the optical fiber amplifier bandwidth and can be extended to denser channel spacings. In DWDM systems the channels grid varies and a typical system would use 40 channels at 100 GHz (0.8 nm) spacing, 80 channels with a 50 GHz (0.4 nm) spacing or 160 channels with a 25 (GHz) (0.2 nm) spacing. Some variants, sometimes called ultra dense WDM, are capable of 12.5 GHz (0.1 nm) spacing for up to 320 channels operations.

DWDM systems are more expensive and complicated to run than CWDM ones since they have to maintain more stable wavelengths due to the inherent closer spacing. Especially for a dense wavelength packaging, a precise temperature control of laser transmitters is required to prevent "drift" off a very narrow frequency window of the order of a few GHz. DWDM systems provide the highest capacity and are associated with higher modulation rates, thus creating a smaller market for DWDM devices with very high performance levels. For this reason they tend to be used at the highest level of the communications hierarchy, for example, the backbone network.

However, in the long-term, we expect that dense WDM and ultra dense WDM technology may appear in the access network for further enhancement of capacity. On this line, the ongoing research activity aims for finding cost-effective and easy-to-manage solutions using WDM-PON infrastructures based on identical and simple ONUs design. This purpose is justified by the fact that the number of served ONUs increases in high capacity environments. By contrast, the DWDM channels would become

more and more closely spaced imposing strict wavelength specifications which could be only satisfied by means of expensive coherent sources. In a typical access network design, an array of coherent lasers (one for each ONU) would be required at the CO for the downlink transmission whereas a single coherent source would be installed at the ONU for the uplink one. If we add the tight filtering specifications imposed on all wavelength selective devices and routers deployed in the intermediate nodes, the whole access network would be too complex and expensive at the current state of technology. Moreover, these schemes would require wavelength-dependent ("colored") ONUs increasing the inventory, management and maintenance costs of several remote locations. Contrarily to the backbone network, in the access segment the ONU is a key element with a critical impact on the overall capital and operational expenditures. Therefore, in the direction of a cost affordable deployment of WDM- and DWDM-PONs, it is reasonable to find strategies oriented to minimize the cost and architectural complexity of the transceivers. In particular due to the high number of ONUs, most crucial is to avoid the provisioning, management and maintenance of any wavelength specific equipment, as far as possible, at least at the ONU.

With this motivation, many practical and economical considerations have driven the research toward the so-called light sources centralization strategy. The light sources centralization aims to move to the CO the entire optical sources provisioning, required for the uplink transmission (ONU to CO). In this way, the ONU is kept "colorless" and "source-free" gaining a substantial simplification of its architecture and, consequently, the minimization of the overall access network implementation cost and management. Investigating a new alternative light source centralization approach adaptable to high capacity access networks has been another objective of the present work.

Agree with the requirements of the actual state of the art in optical fiber communications concerning the access segment, our work has been carried out with the common aim of investigating and proposing new enabling optical access architectures for an easy deployment and mass-scale implementation of WDM-PONs taking into account whether the environment of application requires low or high network capacity for the transport of broadband services. Therefore, in this thesis we will present the theoretical analysis and the experimental validation of dispersion tolerant optical transmission systems and reconfigurable network architectures based on the employment of centralized OBSs operating in the third transmission band and whose adaptability to the transport of high frequency RoF signals is realized, for the first time, by means of Mach-Zehnder interferometer (MZI) structures. On the other hand, we will propose and experimentally demonstrate high-capacity light sources centralized full-duplex optical transmission systems and reconfigurable network architectures where the polarization multiplexing (PolMUX) technique is employed for the first time into the access platform as a novel strategy to minimize the cost and complexity of the ONU in accordance with the centralization concept.

1.3   Structure.

This dissertation is structured in six chapters organized as follows. Chapter 2 exposes an overview and evaluation of leading broadband access technologies and infrastructures making reference to their historical evolution from legacy copper-based to actual optical fiber-based access solutions. Emphasis is put on those optical architectures adopting a passive infrastructure and their ability to meet the actual and future requirements of the customer with a growing broadband demand. In this context, the principle of operation of the current-generation TDM-PONs and WDM-PONs is described highlighting pros and cons of such access technologies. Due to their outstanding performance, WDM-PONs combined with RoF transport technique is established as the network framework of this research. Possible strategies to enable a large scale implementation of WDM-PONs in the access domain are covered including low-capacity CWDM-PONs based on spectrum sliced OBSs and high-capacity DWDM-PONs based on light source centralization which are identified as the most promising optical access solutions in the direction of cost and complexity minimization. For both approaches, additional challenges such as dynamical optical routing, convergence of FTTx and RoF services and bandwidth utilization are also outlined.

The next chapters 3 and 4 are devoted to the investigation of chromatic dispersion tolerant systems based on OBSs and MZI structures and their implementation in CWDM-PONs. In particular, chapter 3 describes theoretically the fundamental characteristics and limitations of a point-to-point optical transmission system adopting schemes with external modulation of the optical intensity and direct detection. The analysis of the behavior and transmission performance of such reference system takes into account the alternative use of single mode fiber (SMF) and multimode fiber (MMF) links for signal distribution from the CO to a single ONU. In the SMF case, the effect of fiber chromatic dispersion in the third communication band is explored in order to remark the dispersion-induced transmission limitations inherent to the optical modulation format and the spectral width of the optical source. For OBSs the operative bandwidth limitations in presence of a dispersive link are more significant than for coherent sources so as to invalidate the transport of RoF signals. In the MMF links the additional modal dispersion mechanism and the corresponding impact on the electrical transfer function is also investigated. This chapter delineates the topic of the next chapter.

In accordance to the theoretical model and analysis presented in Chapter 3, Chapter 4 proposes and experimentally demonstrates an advanced dispersion tolerant system configuration based on the employment of the MZI structure to overcome the impact of dispersion in presence of an optical carrier generated by a single OBS. The effect of the third order dispersion parameter over the electrical transfer function is also taken into account. The proposed approach is firstly evaluated through the transmission of amplitude modulated (AM) GHz signals. Then, it is extended to a CWDM network environment where the spectral slicing technique is conveniently exploited to create a multiwavelength transmission scenario. Here, the use of optical phase modulation (PM) is also taken as a viable alternative. A short demonstration of some additional features offered by the photonic filtering effect of the MZI is also reported, i.e., the photonic suppression of the non-linear distortion terms generated

by optical modulator and the all-optical frequency up-conversion. Finally, a full-duplex and reconfigurable CWDM access platform adopting a single shared OBS and multiple MZI structures is described and evaluated.

Chapter 5 is entirely focused on the PolMUX technique for centralized access networks. The chapter starts with a short description of the light polarization concept and its typical employment in applications such as optical modulation format and multiplexing technique in long-haul and access networks. The principle of operation of the PolMUX technique as a strategy to achieve light sources centralization is described, characterized and evaluated experimentally in a full-duplex optical transmission system for point-to-point distribution of RoF signals. The effectiveness and potentiality of the PolMUX approach for light-sources centralization and the interesting possibility of realize polarization-insensitive ONUs by means of remote polarization tracking and control is exploited and demonstrated in a novel bidirectional and reconfigurable DWDM optical access network architecture.

Finally, Chapter 6 concludes the thesis where the results achieved throughout the research are summarized and main conclusions are drawn.

Chapter 2

Optical access networks

2.1 Access networks overview.

The access network is that part of a communication network which connects different business and residential subscribers, spread over a local geographical area, to the intermediate service provider CO attached to the core or metropolitan network. The access network is also commonly referred to as the "last mile" network, where the term "mile" refers to the terminal path of the physical infrastructure deployed to reach the end-customer. The networking community has renamed this network segment as the "first mile" to emphasize its priority and importance.

The transmission length of an access network can go as far as 20 km which is the established international standard based on distances from the CO locations to subscribers [Lee 2006, Kaz 2007]. In order to bridge the metropolitan area nodes with local area terminals, the access network enables random bidirectional connections between each subscriber and the CO. For the success of such information transport, both transmission technology and infrastructure play a key role and generally fix the cost effectiveness of the whole architecture. The access network is perhaps one of the oldest assets that telecommunication operators own and is constantly evolving, growing as new customers are connected and new services are offered. This makes it one of the most complex networks in the world to design, maintain and keep track of.

2.1.1 Future services and network requirements.

During the last two decades, the amount and nature of the traffic sent through the access network has been continuously increasing and changing at an unprecedented rate. Such evolution has been fueled by two fundamental reasons. The first one is a worldwide deployment of optical fibers in core and metropolitan networks accompanied by a spectacular advance in photonic technology. The second one is a drastic improvement of digital electronics and desktop computers performance.

It is well-known that, with respect to other copper-based transmission media, optical fibers provide better properties such as lower loss and an essentially unlimited transmission bandwidth over extremely long distances enabling the delivery of any current and foreseeable set of broadband services. However, the utilization of the enormous bandwidth offered by optical fibers is still severely hampered by the bandwidth limitations of electronic devices and systems, which are the primary sources and receivers of the information. This problem, known as the "electronic bottleneck", has pushed both academia and industry world towards the research and development of photonic devices capable to perform optically more and more signal processing tasks that would be more difficult or impossible to do with electronic systems. Today, some of the demanding

functionalities such as generation, filtering, mixing, up- and down-conversion of microwave and mm-wave signals, can be readily implemented in the optical domain [See 2002, Cap 2005, Wil 2008]. For these reasons, optical fibers and photonic technology are very promising to enter the access domain after conquering the core and metropolitan markets [Bor 1997, Shu 2008].

Furthermore, the drastic improvement of digital electronics and desktop computers performance has made possible the expanding of new multimedia services at the customer level. Faster personal computers and larger hard drive storage media are already available at affordable prices. Customer's needs for downloading and uploading information have increased and traffic patterns in access networks have evolved from voice services to data-, image- and video-based services due to the widespread adoption of the Internet [Lee 2006, Kaz 2007]. The emergence of several competing operators due to liberalization is further contributing to the growth of the access network traffic. Consequently, there is an expanding thirst for economical and high-speed connections asking for powerful measures to increase the capacity of the access network infrastructure.

Today the access segment is required to guarantee high capacity transmissions on the order of hundred of Mb/s per customer, symmetric speeds for peer-to-peer file transfer, low delay in real-time and streaming audio/video applications and data security. Actually, the bit rate of services vary from a few Kb/s (some simpler telemetric services) to 24 Gb/s (for immersive ultra high definition TV (HDTV)), the tolerable delay varies from tens of seconds (for e-mail) to a few tens of millisecond (for grid computing), the jitter from seconds (for e-mail) to less than a millisecond (for grid computing), the packet loss from a few percent (on-line gaming) to less than a tenth of percent (thin client). The applications also have varying requirements on the traffic priority and security and may or may not allow mobility of the end-user. The services today include video streaming and medium quality video conferencing, while some others, like remote home monitoring, location based services or ultra high definition video are emerging services of the short or medium term future. Finally, services like web 3D and robotic assistant are more long term services. In addition we see services like TV evolve to HDTV and further into ultra HDTV (see Fig. 2.1). Drawbacks of this development include power consumption in the home and very complex control and management of traffic flows.
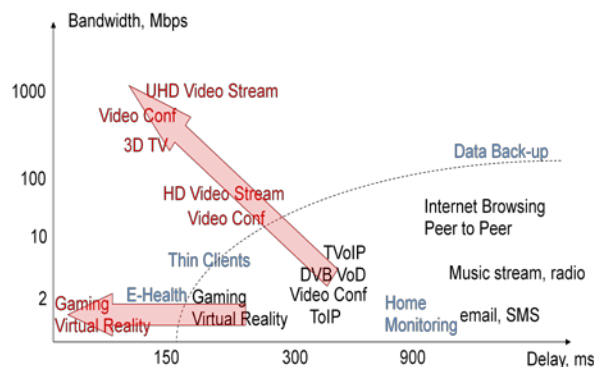

Fig. 2.1 Future services and network specifications

It is clearly observed that the vast number of available and future applications have quite different requirements to the underlying network

architecture, not just in bandwidth requirements, but also in requirements to flow prioritization and delay.

Capacity-on demand and efficient management of the fluctuating traffic patterns is another important requirement. Here, adjustable routing techniques for dynamical assignment of capacity and flexible accommodation of different services are highly pursued. For flexibility, the access network must also be prepared to support the concept of true full-service network where integrated data, audio and video information is delivered by the same transmission infrastructure all the way to the end user. In this context, convergence of both wired and wireless services is also highly desired in order to include the transport of those services supported by emerging wireless technologies into a common infrastructure while satisfying the concept of user's mobility.

One of the most critical decisions for network operators involves the purchase of capital equipment. Among the factors that influence this decision, equipment cost and the resulting potential revenue are two of the most important ones. Network providers face this decision when designing new access networks or upgrading existing ones to expand their functionalities into new areas. They want to minimize the cost of deploying access equipment while maximizing the revenue from the service offerings. The cost of deployment is easier to determine than potential revenue because this last factor involves considerable speculation. As a result, the raw bandwidth capabilities of an access technology are often used as an indicator for potential revenue. Thus, the most important decision a service provider makes when purchasing network equipment is how to strike a balance between minimizing the equipment cost and maximizing the bandwidth.

2.1.2 Legacy infrastructures and technologies.

In the access scenario, there is a strong competition between several technologies and infrastructures [Lee 2006, Kaz 2007, Shu 2008]. Traditional access technologies are the digital subscriber line-over copper (DSL) family and all-coaxial cable television (CATV), which have been devised for the distribution of analog telephony and broadcasting of television signals, respectively. Their native infrastructure is completely based on legacy transmission media, such as, copper twisted pairs and copper coaxial cables. Although they could satisfy the user's demand in their initial stages of deployment, today these two technologies are having difficulties to keep up with the actual traffic and service demands. Indeed, all copper-based transmission media have already reached their bandwidth-distance limitations, becoming the main last-mile bottleneck. Traditional DSL and CATV networks have been proved to be inadequate to satisfy the access network requirements mentioned above.

The most influent telecommunication companies and the academia world agree that the access segment needs new architectural upgrades to alleviate bandwidth bottlenecks and accommodate this new worldwide increasing demand. Now, the penetration of optical fiber-based infrastructures and photonic technology into the access network is taking off and the primary focus of access networks operators is how to facilitate their large scale deployment in terms of higher transmission capability and greater service integration at reasonable costs or alternatively to further

reduce the cost of delivering existing services. At the same time, operators have to consider the hard and necessary migration from working traditional access networks toward hybrid and futuristic all-optical solutions. This includes partial or total substitution of installed electronic hardware and legacy transmission media with optical devices and fibers, respectively. In either case, a smooth migration is expected.

In in-building networks (public, domestic, enterprise areas), though a substantial progress has been made for increasing the bandwidth of copper-based cables (like the Ethernet CAT-5, 6 and 7 cables), this has been done at the expense of complex hardware and processing power.

When moving into the Gb/s area, the use of copper cable is restricted to a very short reach and the cabling and connectors are no longer simple to handle as well as multiple pairs are needed. Furthermore, being normally designed to transport Ethernet traffic only (in a single physical channel), the copper cables in general do not allow for multiplexing of "parallel" information into the medium, as it can be done with an optical fiber using, for example, WDM technology. In the CAT implementation, the copper cables are normally designed to transport single stream of Ethernet traffic only. The inherent difficulty of deploying new cables normally means that a network infrastructure needs to be installed for the long term (tens of years). As a result, this infrastructure must comply with the foreseen evolution of the service requirements over this period. Since such a prediction is a difficult exercise, it is of key importance to ensure that the long term end-user requirements are met with a unified flexible data transport medium that will be able to handle aggregate data rates far larger than what is required today. The optical fiber is the only medium combining a very large bandwidth easily used by WDM technology with a relatively high transparency to signal propagation (both digital and analogue).

As mentioned above, in access networks, the choice for optical fiber to provide connectivity between the large metro or core networks and the end users is accepted throughout the world. In some of the fiber-advanced regions (Asia-Pacific), the deployment of optical access networks is growing while the other technologies (DSL or CATV) are declining as can be seen from Fig. 2.2. As history has already shown, the telecommunication evolution in Europe is correlated to the trends of Asia-Pacific with approximately five years of delay. Whether the optical fiber reaches directly the customer premises (fiber-to-the-home, FTTH) or whether a convenient technology is used to provide the "last mile" connectivity FTTx, the plans and forecasts for optical access network deployments in Europe (and throughout the world) are very ambitious. Today, only 1.5% of the 79 million European broadband users are optically connected but this figure is expected to rise substantially in the coming years similarly to what is currently seen in Asia. Furthermore, the potential to re-use this fiber infrastructure for the deployment of other access methods (fixed wireless access and mobile coverage) will create an ideal environment and business case for the deployment of optical fibers for access networks.
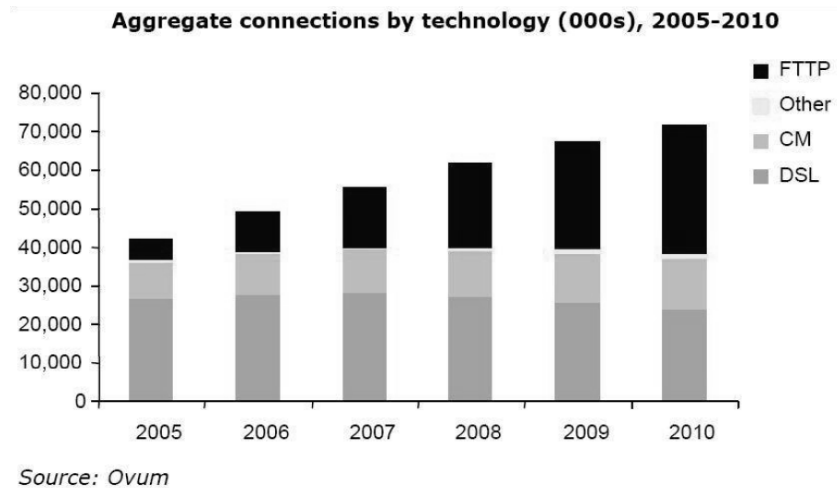
Fig. 2.2 Evolution of the number of broadband lines in Asia-Pacific Region depending on technology.

Concerning specifically the FTTH technology, it is estimated that the number of fiber-connected homes in Europe will roughly double each year for at least a few years perspective and it is expected to reach more than 13 millions of homes by 2011 (see Fig. 2.3).
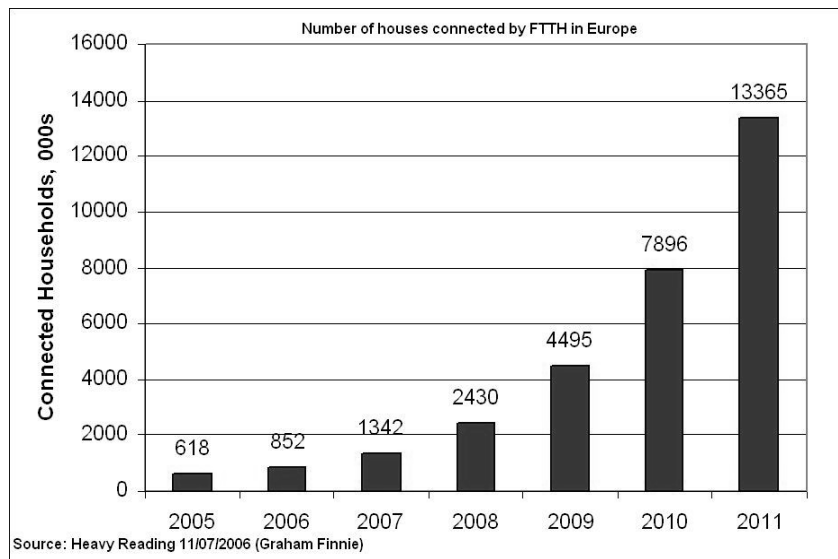
Fig. 2.3 Expected growth of FTTH connection in Europe .

Regarding DSL and hybrid fiber-coaxial (HFC) technology, at the physical level, the basic idea is to introduce the optical fiber into the access network which becomes a natural extension of the optical metropolitan one. However, such penetration is not drastic but gradual. Replacing at least part of these links with SMF shortens the remaining copper segments and allows them to run much faster. In this way, traditional DSL and CATV naturally transform into their hybrid fiber-copper versions. In hybrid DSL networks, fiber is running up to a remote cabinet, from where a DSL copper line goes to the homes. Similarly, in HFC networks, fiber is running up to a remote CATV node and from there coaxial cables run to the homes. In both cases, the existing legacy transmission media is left for the last drop distance to the customer's premises (the aforementioned last-mile paths). A

simplified access infrastructure including hybrid DSL and HFC is schematized in Fig. 2.4.

Fig. 2.4 Hybrid DSL and HFC access network infrastructures.

Hybrid DSL and HFC have gone through several phases of evolution, including standardization and typically deliver up to 25 Mb/s downstream to each customer and lower rates in the return (upstream) direction. Shortening the copper cable creates the possibility to introduce new DSL standards with increased bit rates. Decreasing the 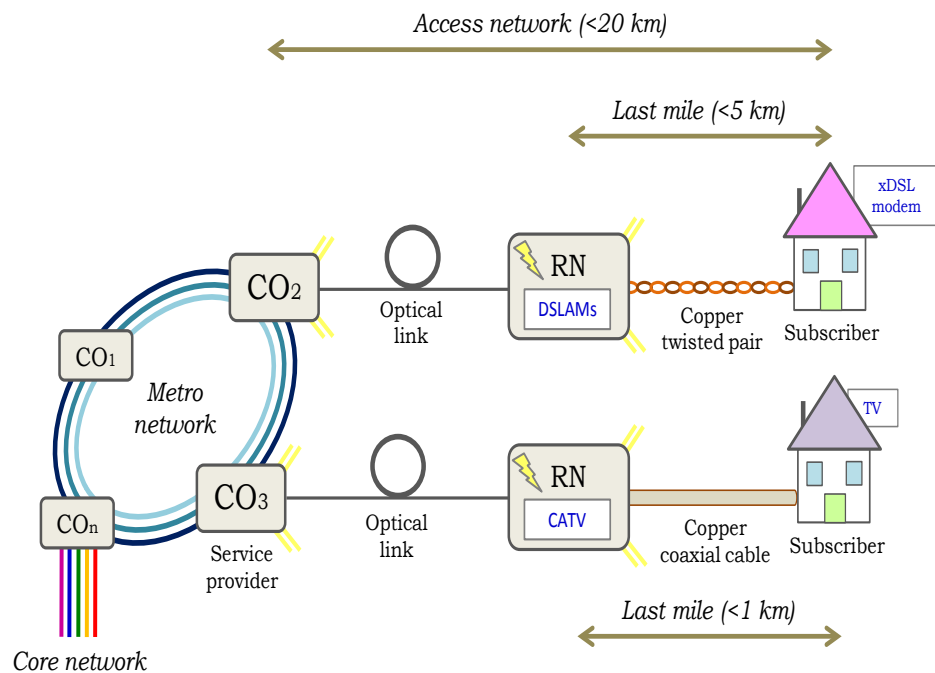copper length means the fiber comes closer to the user, which is the first step in deploying FTTH. With e.g. the very high bit rate DSL (VDSL-2), the maximum copper length measures less than 300 m for providing a 100 Mb/s connection.

HFC networks evolved out of the original TV distribution networks and combine optical fiber with coaxial cable. An optical connection arrives in an optical node that feeds one service area (SA) with a shared coaxial network. The number of homes passed within the same SA is typically from 100 up to 2000. Increasing the capacity requires reducing the SAs, thus increasing the number of optical nodes, and hence increasing the amount of fiber in the access network.

The major advantage of such hybrid access configurations is that they leverage the existing legacy infrastructure already available residences and commercial buildings. However, they are based on a technology that was originally intended for broadcast signal delivery so they do not fit well for the bidirectional communication model of a data network. Moreover, service flexibility and convergence of wired and wireless signals is still far to be satisfied. Another main drawback of these two approaches is that they are noise-limited and require active equipment in the field. This leads to high-operational cost associated with powering, maintaining and managing all remote locations.

Regarding FTTH technology, optical fiber-based access networks can offer bandwidths that are much higher than the DSL, coaxial cable and

other technologies, and can therefore support an enormous variety of services simultaneously. There are two main categories of FTTH networks, either active optical networks (AONs) or PONs. AONs provide a (logical) Point-to-Point (P2P) connection between the CO and each user. Active topologies can be divided in two classes: "home run" fiber architectures which offer a dedicated fiber from the CO to each user and an active star architecture, where a switch or router is installed between the CO and the user, and from this point, a dedicated fiber reaches each user. On the other hand, PONs (mainly deployed as a passive star or tree) are Point-to-Multipoint networks (P2MP), where the access fiber is typically shared by 16 to 128 users. Table 2.1 gives an overview of the current FTTH standards.

Table 2.1 Overview of current FTTH standards.

	Standard	Total bit rate [Mb/s]		Split factor	Bit rate/user (32-split) [Mb/s]	
		Downstream	Upstream		Downstream	Upstream
EFM (P2P)	IEEE 802.3ah	100/1000	100/1000	No split	100/1000	100/1000
Ethernet (P2P)	ITU-T G.985	100	100	No split	100	100
EPON	IEEE 802.3ah	1000	1000	16/32/(64)	31.3	31.3
10GEPON	IEEE 802.3av	10000	1000/10000	16/32/(64)	312.5	31.3/312.5
BPON	ITU-T G.983	156/622/1244	156/622	16/32	38.9	19.4
GPON	ITU-T G.984	1244/2488	156/622/1244	32/64/(128)	77.8	38.9

Today, many FTTH technologies have been deployed, with different standards. Figure 2.5 shows the breakdown of FTTx rollouts around the globe at the end of 2008. In Europe, both PON (primarily B/GPON) and AON are used extensively. In Japan the dominating FTTH technology is the EPON system, with a symmetric physical bit rate of 1.25 Gb/s.
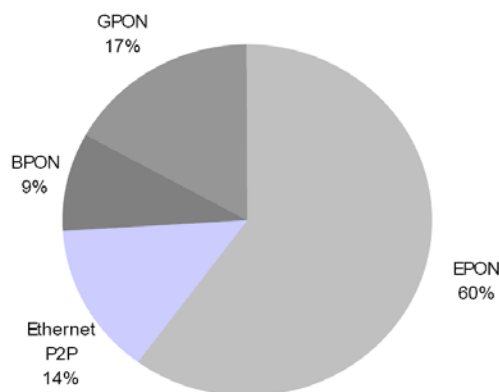

Fig. 2.5 Breakdown of FTTx rollouts around the world at the end of 2008 (source: IDATE).

Furthermore, the benefits brought by the introduction of optical fibers are "future proof" because the speed of the broadband connection is limited

by the terminal equipment rather than the fiber itself. At least in the trunk access segment, from the CO to the remote node (RN), the optical fiber is transparent to the type of service allowing a higher degree of flexibility compared to copper cables. In addition, it represents a nice match to the wireless link through the adoption of emerging RoF technology [Wil 2008]. In RoF systems, radio signals are distributed in the optical domain from a central location (headend) to a set of remote base stations (BSs) or remote antenna units (RAUs) before being radiated through the air. RoF technology takes advantages from the signal transport over SMF. Indeed, it is well known that signals transmitted on optical fiber attenuate much less than through other media, especially when compared to the wireless medium. By using optical fiber, the need of repeaters is further reduced. In addition, RoF technology overcomes spectacularly the physical media constraints of a wireless link in terms of available bandwidth, robustness and security. RoF opens the attractive possibility to merge the transport of both digital and analog signals in the GHz frequency band over the same optical channel. At this point, the concept of service convergence can also be satisfied and customer's mobility can be always assured using a shorter wireless last mile.

2.1.3 Optical access networks.

Unlike hybrid architectures where SMFs are only deployed to shorten the lengths of copper wires, the next step of access operators aims at the deployment of optical fibers to cover the entire distance from the CO to the end customers. A commonly used name to describe this solution is FTTx. FTTx is a generic term for any optical access infrastructure that uses optical fibers to replace all or part of the conventional copper cables used for the last mile paths. The term FTTx comes from a generalization of several configurations of fiber deployment all starting by FTT- but differentiated by the last letter, which is substituted by an x in the generalization. The telecommunications industry differentiates between several configurations. In ascending order of fiber penetration into the last mile, the terms in most widespread use today are: fiber-to-the-node/neighborhood (FTTN), fiber-to-the-curb (FTTC), fiber-to-the-building (FTTB) and FTTH. One more term, fiber-to-the-premises (FTTP), is also used in several contexts, as a blanket term for both FTTB and FTTH or where the fiber reaches both small business and homes. A schematic representation of the FTTx approach is given in Fig. 2.6.

FTTN is an access architecture based on fiber-optic cables running from the CO to a remote active node serving a neighborhood up to some kilometers away from the customer premises. Customers typically connect to this cabinet using traditional coaxial cable or twisted pair wiring. If the cabinet serves an area of less than 300 m in radius, then the architecture is typically an FTTC. FTTN infrastructure allows delivery of all broadband services including the high speed Internet. High speed communications protocols such as broadband cable access or some advanced form of DSL are used between the cabinet and the customers. The data rates vary according to the exact protocol used and according to how close the customer is to the cabinet. Unlike the competing FTTP technology, FTTN often uses the existing coaxial or twisted pair infrastructure to feed the last mile service. For this reason, FTTN may be less costly to deploy. In the long-term, however, its bandwidth potential is relatively limited to implementations which bring the fiber still closer to the subscriber.
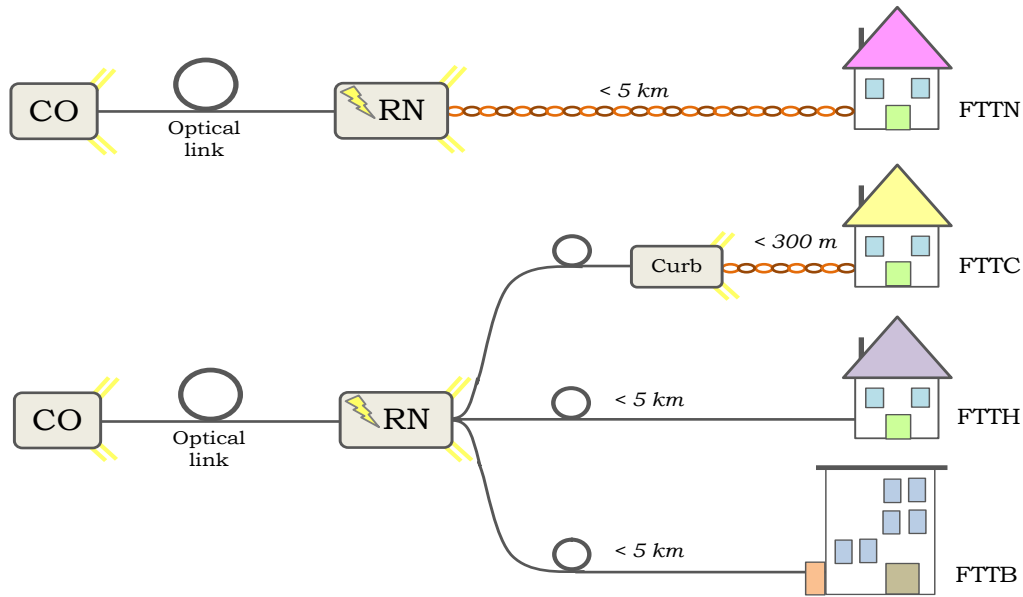
16

Fig. 2.6 Optical access network adopting FTTx infrastructures.

More interesting and challenging solutions are FTTP networks since the optical fiber extends from the CO subscriber's living or working space and is, therefore, the dominant transmission media. The fiber is brought to an active neighborhood node where the signals are broken out onto separate fibers that run to the individual subscribers. Only once at the subscriber's premises, the optical signals may be conveyed throughout the space using any transmission media, including copper twisted pairs, copper coaxial cables, wireless or optical fiber. In the last case, the use of MMF instead of SMF, is especially attractive. Indeed for short reach links, such as inside buildings, MMF may offer the economical advantage of an easier handling than SMF (in particular, in installation activities and splicing) due to its larger core diameter (50 or 62.5 µm versus 10 µm). The bandwidth-distance product is smaller than that of SMF. However, this is not a significant issue for short-reach links. Today, the presence of MMF in already installed local area infrastructures inside home and buildings is dominant [Tyl 2003].

The terms FTTN and FTTP does not restrict the type of fiber architecture used. Basically, three architectures may be deployed for the fiber access network (see Fig. 2.7): the P2P network, the AON and the PON.

Initially, the most logical way to realize a FTTP access infrastructure has been through a P2P topology with dedicated optical fibers running directly from the local exchange CO to each customer located at an average distance of 20 km where an ONU with transceiver functions such as electrical-to-optical conversion and optical-to-electrical conversion is installed (Fig. 2.7(a)). Therefore, in the P2P architecture, two optical transceivers are needed: one at the customer and one in the CO exchange. P2P architectures provided maximum capacity and high flexibility to add new customers and individually upgrade services for customers. Although this would be the ultimate network at the early mid 1980s, it was not yet considered the best solution due to a significant fiber deployment required in the outside plant and whose installation cost increased with the number

of users. By far, the biggest issue in FTTP deployment was cost. Therefore, the market penetration of P2P access networks has been low.
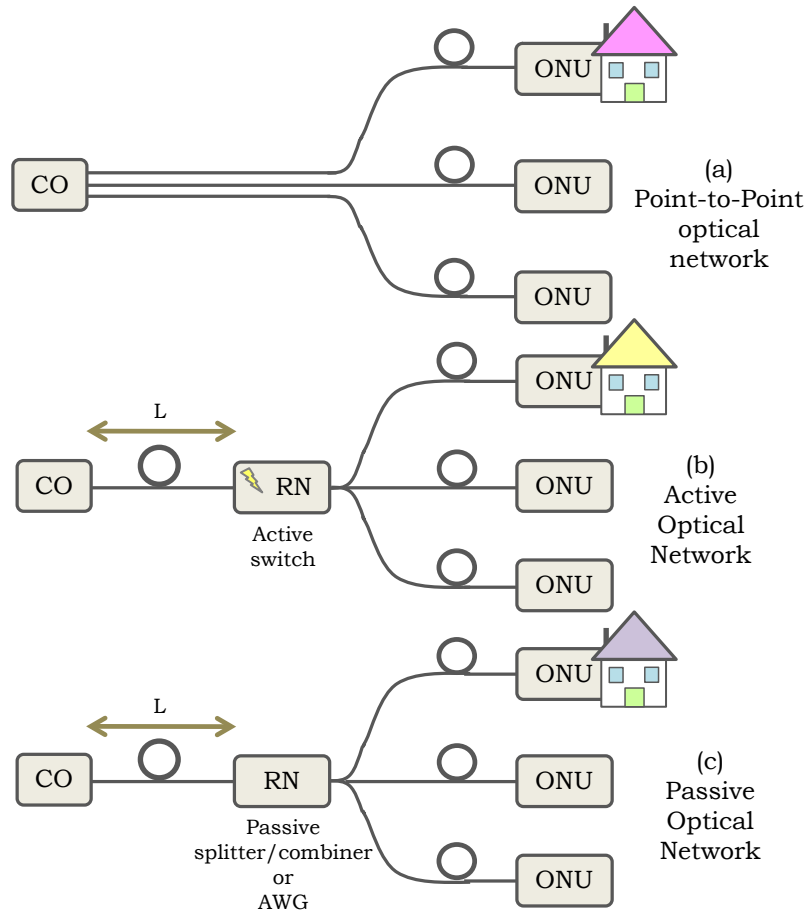

Fig. 2.7 FTTP architectures: (a) P2P, (b) AON and (c) PON.

The major step towards reducing deployment costs has been to redesign the network architecture moving from a dedicated P2P configuration to a P2MP one capable of sharing fibers and key components among the subscribers as much as possible. The first proposed option is the insertion of an active remote switch between the local exchange and the end users. In the so-called active star architecture (active Ethernet), a single trunk fiber carries the traffic from the CO to an active switch from where individual short branching fibers run to each curb/home/building as shown in Fig. 2.7(b). Since only a single feeder fiber is needed, that solution reduces the fiber consumption from the CO to the active switch by the number of customers. Moreover, in the CO only a single transceiver is needed allowing many customers to share its cost. In network upgrading scenarios, from the active node twisted copper pair lines (such as for asymmetric DSL up to some 5 km at speeds up to some 6 Mb/s, or very high speed DSL at speeds up to some 50 Mb/s for lengths of up to 1 km) or coaxial cable lines (such as for HFC) or even wireless links to the customers, may run. Despite the improvement of active architectures in terms of fiber deployment, they require electrical power as well as back-up power at the switching node. In consequence, the downside is the higher cost of installing and maintaining powered equipment cabinets. In addition,

since the sharing of the feeder fiber requires extra measures for avoiding traffic collisions, the CO and ONUs transceivers are more expensive than the ones of P2P architectures.

According to these constraints, it appears that the preferred choice to build an FTTP network is to use passive optical devices at the remote node location in order to achieve the cost sharing of a P2MP topology in a passive way. This approach gives rise to a new architecture called PON.

A PON is a P2MP network where the fundamental difference with respect to the previous solution, is that no active power-consuming elements are deployed. Indeed, in a PON the active node is replaced by a simple inexpensive 1xN passive optical splitter/combiner managing the optical power of the downstream/upstream traffic (Fig. 2.7(c)). In addition to the reduced installation costs of a single fiber feeder link, the completely passive nature of the outside plant avoids costs of powering and maintaining active equipments. A PON maximizes both the infrastructure and hardware sharing among multiple subscribers achieving lower capital and operational expenditures. Furthermore, upgrading to higher bit rates, new data formats and protocols is simpler for a PON than for an active star architecture. Both require upgrading of components in the CO and customer premises, but there is nothing that needs upgrading in the outside plant for a PON, as the passive splitters operate independently of the network speed. For all of the reasons cited above, the PON architecture has been the focus of active research and development for over thirty years [Dav 2006, Lee 2006, Eff 2007, Gro 2008, Shu 2008]. Today, thanks to the fast cost drop of optical components, PON architectures have begun to be deployed and put in service in many countries.

2.1.4 Passive optical networks: architecture description.

In a PON, a CO is connected to multiple ONUs at the customer premises via an optical distribution network made of fibers and passive splitters. In a typical configuration, either a single power splitter or cascaded power splitters are used as branching devices to allow communication between the CO and the many ONUs. Although the use of multiple smaller optical splitters achieve topological flexibility in reaching customers, a single power splitting PON (PS-PON), such as the one depicted in Fig. 2.8, can be taken as reference.

The architecture contains a single transceiver in the CO, one passive optical branching device at the RN and a number N ONUs. The fiber path and the branching device between the CO and ONUs are commonly referred as the outside plant. In the outside plant, there are no active elements.

At the CO transceiver, the downstream traffic (from CO to ONUs) is electrically multiplexed onto a single optical wavelength generated by an optical source. The downlink optical signal is propagated through the fiber path towards the RN. Here, a 1xN power splitter is used as branching device. It divides the downlink light into N optical signals containing the same multiplexed information, one for each ONU. Note that the CO and the outside plant are shared by all subscribers. The total downstream bandwidth is also shared. As a consequence, the number of ONUs may be limited by the splitter attenuation. A PON can serve 16 or more subscribers

(typically N=16, 32, 64, 128), therefore, the average dedicated bandwidth to each subscriber is usually only a few percent of the channel capacity. It can be said that the downlink channel is a broadcast channel or, equivalently, that in downlink direction a PS-PON operates as a broadcast network. All ONUs are composed by a transceiver system. For downlink operations each ONU receives the same optical signal and convert it to electrical through phodetection process. The information contained in the electrical signal is processed to select only that customer's intended traffic (broadcast-and-select) discarding the packets addressed to other ONUs. In uplink direction (from ONUs to CO) the upstream signal generated at the ONU undergoes a symmetrical process as the downstream one. In this case, the power splitter couples only 1/N of the power from each ONU into the feeder fiber for transmission back to the CO. The ONU equipment is installed either at the customer premises for FTTP or eventually in a curb resulting in FTTC architecture.
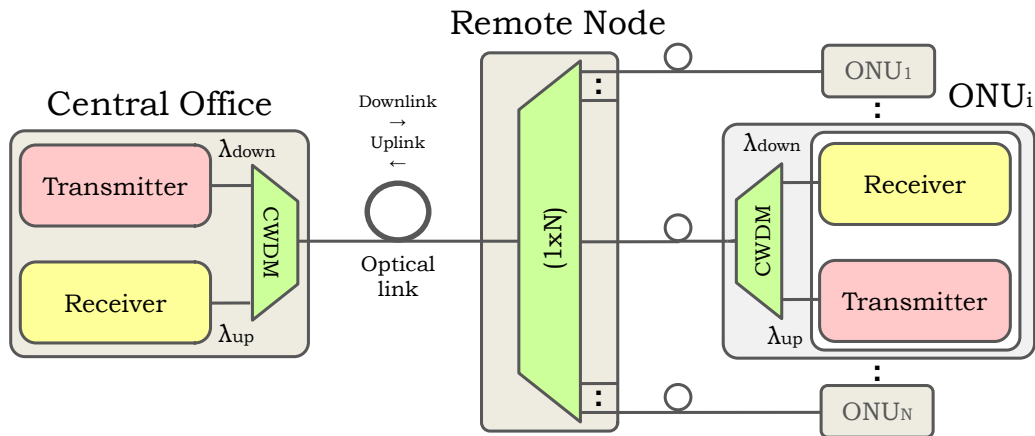

Fig. 2.8 Typical implementation of a PS-PON. The downstream transmission is at 1550 nm, the upstream transmission is at 1300 nm, and they are separated at the CO and each ONU by a coarse WDM.

For the separation of the downstream and upstream traffic, the reuse of the downlink fiber (single-fiber or 1-F) or the installation of an extra fiber (two-fibers or 2-F) are two architectural solutions which have been discussed for several years. Although technically simpler, the 2-F solution has been soon discarded due to added costs and management of the extra path between the CO and RN and to each customer. In contrast, the bidirectional sharing of a single fiber is often preferred since it reduces fiber's installation and handling costs. The 1-F approach can be accomplished in many ways. Some methods use nominally the same wavelength in both directions including directional devices such as couplers and circulators at the CO and each ONU transceivers. A second method is simply to use different wavelengths for downlink and uplink transmission plus an inexpensive CWDM device in each transceiver (see Fig. 2.8). In this case, an optical source emitting in the third communication band is generally preferred for the downlink transmission, whereas the second communication band is exploited for the uplink one. Since the 1300 nm band is centred on the chromatic dispersion minimum, such election benefits from the economical advantage of installing low cost OBSs or multimode Fabry-Perot laser diodes (FPLDs) at the ONU transceivers instead of expensive coherent sources, such as distributed feedback lasers (DFBs).

2.1.5 Multiple access techniques in PONs: TDM-PONs and WDM-PONs.

In the downlink direction, a PS-PON is a P2MP network with star topology. The downstream traffic generated at the CO is optically demultiplexed at the passive optical power combiner before broadcasting to every ONU. Although conceptually similar to the downlink transmission, the uplink transmission deserves much more attention. Indeed, in uplink direction, a PS-PON architecture is no longer a P2MP network but a multipoint-to-point one. It means that multiple ONUs transmit all towards the CO in a multi-access nature. The directional properties of the passive splitter/combiner are such that ONUs transmissions do not interfere to each others. However, since passively combining optical signals provides no capabilities for buffering and retiming, data streams from different ONUs transmitted simultaneously still may experience collisions. In order to multiplex the individual data streams onto the common feeder in a collision-free way, the uplink transmission requires accurate and well-designed multiple access techniques. Two major categories of multiple access mechanism for fiber access networks have been developed: TDM and WDM access. Figure 2.9(a) and (b) schematically shows the TDM and the WDM access principle, respectively.
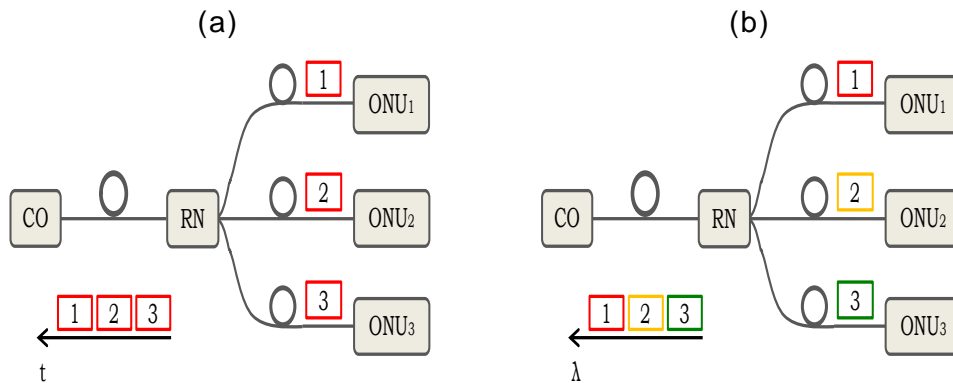

Fig. 2.9 TDM (a) and WDM (b) multiple access principles.

Current generation TDM-PONs.

Currently, TDM is the most popular and widely employed multi-access method. A single fiber full-duplex PS-PON adopting TDM access is also known as a TDM-PON. For the uplink transmission in a TDM-PON, each ONU transmits a burst of data separated by a configurable guard-time. In other words, the TDM access technique relies on assigning dedicated time slots to each ONU which can use the full uplink bandwidth for the duration of its assigned time slot. The upstream packets are, therefore, time-interleaved at the power splitting point and the assignment of time slots is performed by the CO using standard protocols for media access control (MAC) realizing an efficient use of the channel. The CO is provided with a burst mode receiver. The downlink transmission is continuous, so burst receivers are not used in the ONUs. The ONU selects its own part of the downstream signal.

Emerged from two important activities; the Full Service Access Network (FSAN) initiative and the Ethernet in the First Mile (EFM) initiative of the Institute of Electrical and Electronics Engineers (IEEE) group, a number of TDM-PONs have been standardized internationally since early 1990s. In temporal order of development, they include the asynchronous-transfer-mode PON (ATM-PON or APON, ITU-T G983), the broadband PON (BPON, ITU-T G983), the Ethernet PON (EPON, IEEE 802.3ah) and the gigabit PON (GPON, ITU-T G984). A description of the TDM-PONs development history and technology can be found in [Dav 2006, Lee 2006, Eff 2007] for further details.

Apart from the benefit of sharing the CO transceiver and a large part of the fiber infrastructure, TDM-PONs enjoy low complexity of the CO and ONUs equipment as they use the same pair of optical wavelengths for the downlink and uplink transmission. However, they present some limitations in terms of capacity, upgradability, protocol, and security which are inherent to the access method.

Concerning capacity limitations, it must be remarked that, the bandwidth available in a single wavelength is shared amongst all end users. It means that, although a TDM-PON provides higher bandwidth than traditional copper-based access networks, the huge bandwidth of optical fibers is not completely exploited. In the downlink direction, the broadcast nature of TDM access implies that the electronic components in the ONU have to operate at the overall aggregate downstream bandwidth.

Since the downlink carrier is shared by means of a passive splitter, the optical power reaching the ONU reduces in proportion to 1/N as the number of customers increase. The number of ONUs and the upgradability to new users are limited by the splitter attenuation (for example, a 1x32 splitter imposes an insertion/splitting loss typically higher than 17 dB). This solution is suitable as long as the bandwidth demand and the number of users do not become too great.

The protocol time-dependence of TDM-PONs does not satisfy the bandwidth requirements of new real-time applications and the emerging explosive growth of Internet traffic. The management of the upstream transmission is also difficult because, in practice, the MAC algorithms of a TDM-PON network are very complex and require considerable processing power. Moreover, any change in line rate and frame format for upgrading a TDM-PON requires a change of the MAC protocol and all the equipment in the network.

In a TDM-PON all the downstream information is broadcasted to all ONUs over a single wavelength. Therefore, transmission security and privacy are not guaranteed since each customer receives all the information sent to other ONUs subscribed to the network. Security and privacy can be ensured only if encryption is used.

It is agreed that, while current generation TDM-PONs seem to be a satisfactory solution for actual bandwidth demands, future data-rate projections indicates that, as more broadband application appear, they could not cope with future bandwidth requirements (despite trends to increase the total bit rate to 10 Gb/s for the so-called 10GEPON) and the allowable power budget. Therefore, upgrading TDM-PONs is becoming a major challenge. The need for further improvements of TMD-PONs architectures has paved the way to the adoption of effective access method

for sharing a PON infrastructure, the WDM access. Such alternative approach operates in the wavelength domain. WDM is a technology that puts data from different optical sources together, on a single optical fiber, with each signal carried on its own separate light wavelength or optical channel. Today both academia and industry consider WDM-PONs the ideal solution to mitigate the limitations of TDM-PONs and extend the capacity of optical access networks without drastically changing the existing fiber infrastructure.

Next generation WDM-PONs.

A basic WDM-PON configuration, such as the one shown in Fig. 2.10, is composed by a CO, the principal optical fiber link, a RN and a number N of ONUs.

The CO contains a set of optical transceivers. For downlink transmission, the CO generates N optical wavelengths to transport the downstream signals. Each wavelength is univocally and permanently assigned to the corresponding ONU. Before leaving the CO, all downlink wavelengths are combined employing a WDM device and routed towards the RN over a single optical fiber link which is again shared between the N customers as in the basic PS-PON. One architectural difference between a PS-PON and a WDM-PON relies in the RN architecture. Indeed, unlike PS-PON, in a WDM-PON the optical passive splitter is replaced by a passive wavelength router whose function is to separate/combine the downlink/uplink wavelengths received at the input port. In the example of Fig. 2.10, the passive wavelength router is realized by a single $[1]_{In}$ x $[N]_{Out}$ arrayed wavelength grating (AWG) where N is the number of downlink and uplink wavelengths. The AWG is a passive optical device with the special property of periodic routing behavior, which is the cyclic nature by which multiple spectral orders are routed to the same output port from an input port. It allows spatial reuse of the wavelength channels and therefore permits the bidirectional use of the same device. AWGs have an optical loss of around 5 dB (about 12 dB less then that of a typical 1x32 passive splitter), independently on the number of wavelengths and, thus, the number of users.

Once separated, the N downlink wavelengths are routed to the corresponding ONUs through dedicated fiber connections. Each ONU contains a transceiver where the downlink wavelength is photodetected in order to recover the downstream information. In the uplink direction, the transmission from the ONUs to the CO is conventionally run using N different wavelengths. The ONU transceiver, therefore, contains an optical source which provides for a wavelength-specific uplink carrier. The uplink wavelengths are transmitted toward the RN over the same drop fiber. At the RN they are combined before propagation. The uplink multiplexed signal is routed back to the CO over the trunk optical link and demultiplexed into the N individual upstream signals. Each of them is sent to the corresponding receiver.

Compared to a TDM-PON, a WDM-PON is a more powerful multiple access solution for several reasons. By assigning a different pair of dedicated wavelengths to each subscriber, a WDM-PON creates virtual P2P communication channels on a physical P2MP topology. Since multiple channels are introduced over a common fiber infrastructure, the principal advantage of a WDM-PON is a spectacular multiplication of network

capacity with dedicated per user bandwidth whereas, by contrast, in a TDM-PON the same pair of wavelengths is shared among all subscribers.
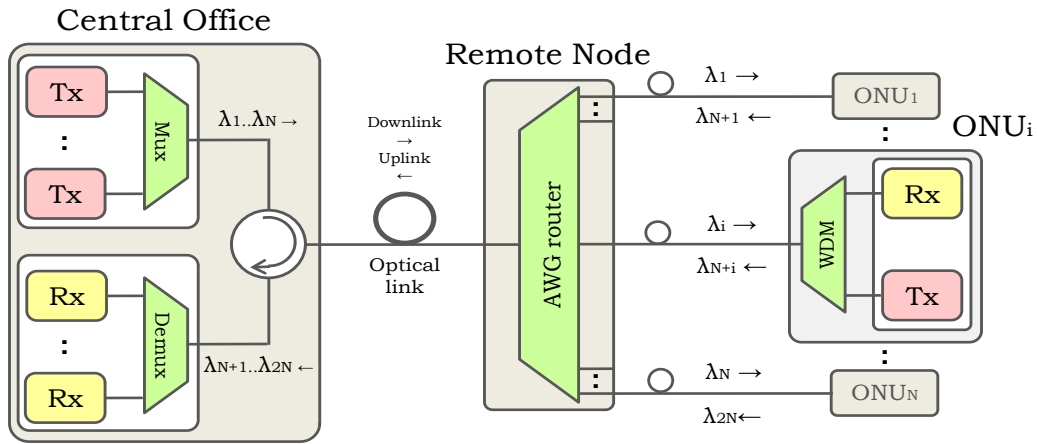

Fig. 2.10 Typical implementation of a WDM-PON using an AWG router at the RN.

In analogy with P2P architectures, a WDM-PON improves network scalability toward a larger number of users by simply adding new wavelengths but without using dedicated fiber connections or modifying the installed infrastructure. It saves the infrastructure investments enabling the evolution of the optical transport towards a unified back-haul and access infrastructure. It must be pointed out that, adding new channels in a WDM-PON can be done either just to provide higher network capacity (here, all channels carry the same type of traffic) or to improve network flexibility (if channels carry different services assigned on an individual basis to each user). Network flexibility is particularly required when the same WDM-PON infrastructure is shared by a diverse set of users such as business customers and home residents, as instance. Network flexibility is useful also for convergence of wired and wireless applications. In this context, hybrid optical/wireless access networks employing WDM-PONs in combination with RoF technology for delivery of wide-fidelity (Wi-Fi), worldwide interoperability for microwave access (WiMax) and cellular services have emerged as a viable access solution and have been successfully demonstrated in several works [Cha 2006, Fer 2006].

Moreover, dedicated downlink and uplink wavelengths allow each user to send/receive data to/from the CO at any time, independently of what the other users are doing. In other words, there is not interaction or coupling between users of a WDM-PON. In this way, there is no need of managing the timing of the ONUs access and, in consequence, the use of sophisticated MAC algorithms for time synchronization and collision avoidance is eliminated.

An additional feature of a WDM-PON is its security and privacy. By employing a passive wavelength router instead of a passive splitter, the downlink signal is no longer broadcasted to every ONU and no optical signals are received by an ONU except the one transported by the corresponding wavelength.

As it will be discussed in the next section, the choice between CWDM or DWDM technology depends on the capacity requirements of the network and also the number of served ONUs. In most cases, the desired network

capacity may be a crucial parameter for providers as it determines the overall cost and architectural complexity of the network.

2.2 Enabling technologies and challenges for a large scale deployment of WDM-PONs.

Besides the several technical advantages brought by WDM technology, there are several issues that are hampering a large-scale implementation of WDM-PONs. Although WDM-PON is ideally a perfect solution, its benefits come with high implementation costs and management complexity due to the need of dedicated transceivers.

In fact, in order to realize a dedicated optical connection to N subscribers, a basic WDM-PON configuration requires N transceivers installed at the CO plus a transceiver at each ONU. This leads to 2N transceivers compared to (N+1) transceivers needed in a TDM-PON. In addition, since in the WDM approach no wavelength is shared between customers, both downlink and uplink communication require 2N different wavelengths matching exactly the transmission window defined by the wavelength router installed at the intermediate node. Although technology advances have allowed the recent commercialization of athermal AWGs whose band-pass channels can remain locked to any standard WDM grid, having a separate wavelength per each ONU imposes serious inventory and maintenance problems for network operators. In fact, instead of having just one type of ONU, a conventional WDM-PON requires colored ONUs based on their specific operating wavelength. Currently, these are fundamental bottlenecks which are slowing down the commercialization of WDM-PONs on a large scale.

A correct choice of the optical sources for the generation of the downlink and uplink wavelengths is the basis of the network design. The network operator's first step is to decide previously the appropriate wavelength assignment and spacing. Therefore, as explained above, the selection of such optical sources involved in the transmission process may differ significantly in terms of cost, complexity and management.

Due to the wide channel spacing between wavelengths, CWDM technology avoids the need to specify tightly and stabilize the central wavelength of the source. Since a strict tuning of wavelengths is not needed, all CWDM wavelengths are easy to manage without worrying about temperature or aging effects in both the CO and ONUs equipment. Although it has been argued that the total system cost of a CWDM-PON may be a 40% cheaper than a DWDM-PON [Ban 2005, Eff 2007, Gro 2008], primary architectural disadvantages of CWDM technology are that the number of channels and network scalability are inherently limited. Therefore, CWDM technology results, in principle, an interesting solution for WDM-PONs whose capacity requirements are not so high. For low-capacity transmissions CWDM-PONs are suitable to be implemented using spectrum sliced OBS in combination with inexpensive wavelength routers with low channel crosstalk at the remote location for further cost minimization. In downlink transmission, the spectral slicing technique allows the shared use of a single OBS installed at the CO, between all ONUs and is an affordable means of simplifying inventory and wavelength stabilization problems at the CO. In the uplink transmission, the installation of a spectrum sliced OBS in

each ONU transceiver, provides cost-effective source provisioning and management.

In contrast to CWDM technology, DWDM technology is characterized by a wavelength spacing that is typically less than 1.6 nm. Due to its inherently narrow wavelength spacing, DWDM technology has been originally employed in very high capacity long-haul communications. Here, in order to take advantages from optical amplifiers, the third communication band has been conveniently exploited. Although DWDM is currently regarded as the most suitable solution for core networks, it has not yet penetrated the access market. Indeed, DWDM technology is envisioned to use multiple closely spaced channels and, in consequence, for each DWDM channel the corresponding optical source must be highly selective. Moreover, each channel must be controlled firstly to operate at the same specific wavelength till the end of the network's lifetime and secondly to avoid crosstalk between adjacent channels. To fulfill such requirements the use of coherent light sources, such as DFB laser or tunable lasers, in both the CO and ONU transceivers is mandatory. For this reason, a conventional implementation of DWDM technology is expensive as it leads to high inventory costs and management complexity, more than those required by a CWDM-PON. In addition, as the number of end-users increases, the installation of several wavelength-specified light sources may be impractical particularly at the ONUs. In order to allow a large scale deployment of DWDM-PONs, much effort has been focused on developing alternative strategies to minimize the ONU complexity. In this context, concepts such as "colorless" ONU or "source-free" ONU have arisen to indicate any strategy to avoid the employment of a wavelength-specific source or to eliminate completely the optical source at the ONU, respectively. A general way to define this last approach is light sources centralization.

Although, CWDM-PONs based on the spectral slicing technique and DWDM-PONs based on light source centralization present significant differences in term of transceivers architecture, they use the same PON topology. In the two following subsections we will take a closer look at those basic approaches.

2.2.1 CWDM-PONs based on the spectral slicing of optical broadband sources.

Since early 90's, the employment of OBSs have been of huge technical interest owing to their great potential for enabling multichannel applications in WDM-PONs minimizing implementation costs and management associated to the generation of the WDM channels. The fundamental motivation for using incoherent sources is their essentiality and cost-effectiveness for the building of multichannel scenarios where the generation of optical channels is made by means of the spectral slicing technique [Ree 1988, Wag 1988, Wag 1990, Lee 1993, Pen 1996, Fel 1997, Lio 1997, Jun 1998, Han 2004, Cho 2007]. The principle of operation of the spectral slicing technique is schematically illustrated in Fig. 2.11.
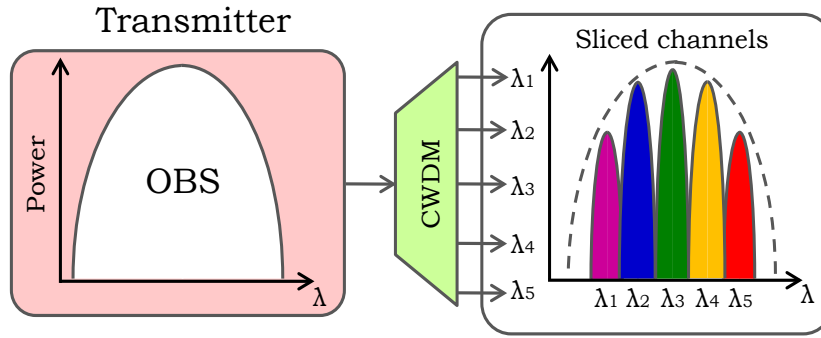
Fig. 2.11 Principle of spectral slicing technique.

As shown in Fig. 2.11, the spectral slicing is a powerful WDM approach whose aim is to exploit a single light source for transmission of several WDM channels and bypass the need of multiple wavelength-selected sources. In the spectral slicing technique, the optical spectrum of a single broadband source is, in fact, conveniently subdivided ("sliced") into a set of narrower bands by means of a conventional WDM filter. All cut slices match the wavelength grid defined by the WDM filter and can be used as optical carriers. For this purpose the full width at half maximum (FWHM) spectral width of the OBS must be at least equal to the wavelength band of the band- pass filter. The most typical examples of optical broadband sources are white sources such as (super-luminescent) light-emitting diodes ((s)LED) and amplified spontaneous emission (ASE) noise spectrum emitted either by an EDFA or a SOA.

The spectral slicing technique can be employed to perform both the generation of downlink and uplink carriers. Downlink operations are accomplished by using the OBS at the CO. In this case, the spectral slicing allows the local generation of the downlink carriers assigned to different subscribers sharing the same optical source. In this way, since the OBS simultaneously provides light for all channels, there is no need to equip the CO with multiple and high-cost lasers. Apart from reducing inventory costs, this strategy relaxes all maintenance operations associated to the temperature-stabilization of wavelengths. In fact, the bandwidth characteristics of an OBS implies that, provided high input powers and low slicing losses are achieved, the generation of all optical carriers can be made with relaxed wavelength spacing conditions avoiding the expensive use of temperature sensitive sources and routing devices. The tolerance to temperature-induced wavelength misalignments increases with the slice bandwidth. However such benefit is achieved at the expense of decrement of the number of available channels. For this reason, the spectral slicing technique is inherently suitable to create CWDM scenarios where the minimization of the transmitter cost and complexity, rather than high-capacity, are the principal targets. Furthermore, with the same principle of operation, a spectrum sliced OBS can be also employed at the CO as an added source to generate "seed" wavelengths for remote modulation of the upstream data at the ONU [Kim 2000]. In this case, the spectral slicing can be regarded also as a particular way to provide source free ONUs and, thus, a centralized network architecture where the uplink carriers are remotely generated.

When the OBS is installed at the each ONU together with a slicing device, the spectral slicing technique just provides locally the

corresponding uplink carrier. In such configuration, the ONUs are identical and colorless [Aki 2003].

Independently on whether the spectral slicing is performed at the CO or ONU, the OBS must fulfill the following requirements: broad bandwidth for the accommodation of various channels and high power spectral density for the relaxation of the spectrum sliced signal power budget. White sources such as LEDs have a spectral width in the range of 50 nm to 100 nm and can be fabricated at reasonably price. Initially, it was often difficult to provide an adequate amount of system margin due to the low output power of LEDs relatively limited to a maximum -10 dBm. With LEDs, the output power and the slicing insertion loss through routers imposed several limitations on the maximum number of sliced channels and, therefore, the number of served ONUs which affected directly the network scalability [Fel 1997, Fel 1998, Lee 2003, Aki 2003]. However, OBSs providing higher output power while maintaining the broad spectrum are now commercially available. In this context, OBSs based on sLEDs and ASE noise are very attractive because a broad emission spectrum with a high power spectral density can be easily generated [Esp 2000]. As instance, the EDFA-based ASE source provides more powerful ASE light (in excess of 20 dBm) into SMF than semiconductor devices [Lee 1993] and is currently considered the most suitable light source for spectral slicing applications.

Although high quality of broadband spectrum suitable for slicing applications can be easily obtained by using conventional ASE sources, the problem related to the dispersion tolerance still needs to be solved. When the spectral slicing technique is applied, a larger slice width increases the power of the corresponding channel but also increases the limitations induced by fiber dispersion on the bandwidth-distance product achievable by that channel [Pen 1996]. For this reason, most of the proposed schemes based on spectral slicing have been originally implemented using OBSs emitting in the second transmission band where the influence of fiber dispersion is lower. By contrast, the influence of fiber dispersion in third communication band is not negligible. As a consequence, any attempt of employing spectrum sliced sources emitting around 1500 nm, has been experimentally demonstrated to offer poor transmission performance. Due to fiber dispersion, the operative electrical bandwidth of a sliced channel only permits the propagation of signals in a few MHz range invalidating the transport at higher frequencies which would be of primary importance in RoF applications. Moreover, the adoption of the spectral slicing approach in third communication band would be favorable in order to achieve a maximum compatibility with standard WDM technology and devices, such as, wavelengths routers and filters already developed and commercially available in such band. In this context, the first aim of this thesis is to demonstrate a new alternative strategy which permits a dispersion tolerant transport of GHz signals by means of spectrum sliced OBSs in the third communication band offering a low implementation complexity and a perfect compatibility with RoF and WDM technology at the same time.

2.2.2 DWDM-PONs based on the centralization of coherent light sources.

Nowadays one of the principal targets pursued by the telecommunication industrial and research community is to offer broadband access connections to a worldwide increasing number of customers. Up to

now, DWDM-based optical access networks are considered the most promising solution where all benefits of optical fiber technology are fully exploited and capacity-per-user can be very high, as indicated in [Ban 2005, Lee 2006, Kaz 2007, Par 2007]. Nevertheless, issues like large bandwidth, easy upgradability and service flexibility usually led to networks with higher complexity and implementation costs especially when the number of ONU deployed throughout the network is high. Therefore, a large scale deployment of DWDM-PONs requires new architectural configurations capable to establish such broadband connections at a reduced cost per customer.

In a DWDM-PON configuration, a large number of remotely located ONUs send/receive different carrier wavelengths to/from a CO. Since all wavelengths are distributed over a dense wavelength grid, expensive coherent light sources such as DFB lasers or tunable lasers are typically used for their generation. Therefore, the operational cost associated with the uplink wavelength provisioning, management and maintenance of each ONU, has a direct and critical impact on the total cost of the access network. The minimization of cost and architecture complexity of the ONU is a key challenge necessary to benefit from a mass-scale production and make DWDM-PONs cost-competitive. Both academic research and networks providers agreed that, making all ONUs identical and source-free, the inventory, installation and maintenance requirements could be drastically reduced [Kaz 2007]. Since early 90's until present days these economical considerations have pushed the research activity toward the so-called light sources centralization approach.
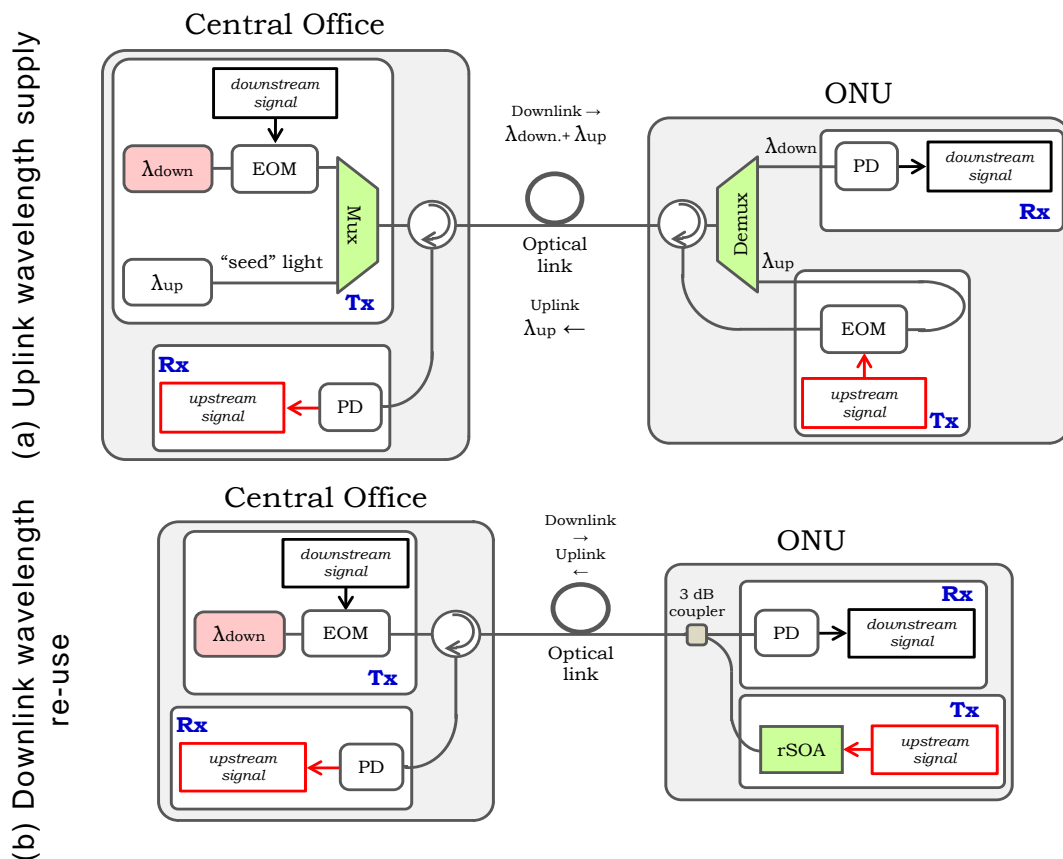

Fig. 2.12 Typical implementations of the light source centralization concept. (a) Uplink wavelength supply and (b) downlink wavelength "re-use" approaches.

From a practical point of view, centralizing the light sources means that the entire optical sources provisioning, required for the uplink transmission (ONU to CO), is made at the CO rather than the ONU. In this way, the ONU is kept completely "source-free" with no wavelength-specific equipments gaining a substantial simplification of its architecture and, consequently, the minimization of the overall access network implementation cost and management. Depending on the degree of network cost/complexity assumed by the operators, the practical realization of centralized architectures follows two alternative ways. The uplink optical carriers can be either provided by additional light sources placed at the CO or optically generated at the ONU employing a portion of the power of the received optical downlink wavelength. These two alternatives are commonly referred to as uplink wavelength supply (or remote modulation) approach and downlink wavelength "re-use" (or re-modulation) approach, respectively. Two typical examples are shown in Fig. 2.12(a) and (b), respectively.

In the first approach, additionally to the light sources employed as optical downlink carriers, extra light sources are installed at the CO. Such extra light sources represent the "seed" lights for the uplink transmission. For each ONU, the CO sends an optical downlink carrier modulated by the downstream data, and an optical uplink carrier which is left as a continuous wave (CW) and so kept unmodulated. All the locally generated downlink and uplink carriers are multiplexed together and launched into the optical link. At the ONU, while the downlink carrier is photo-detected and demodulated for data recovery, the unmodulated emission is used for the uplink transmission. It is modulated with the upstream data and "looped back" from the ONU to the CO. For the upstream modulation, SOAs plus external intensity modulators, reflective SOAs (rSOAs), reflective electro-absorption modulators (rEAMs) or injection locked FPLDs can be also used in alternative to single intensity modulators. With the wavelength supply approach, proposed in [Fel 1998, Ort 2007], the downlink and uplink transmission can be performed using different wavelengths.

Although source-less ONUs with a simple architecture can be easily realized, the insertion of extra light sources at the CO can increase considerably the inventory cost and management especially if distributed or tunable lasers are used. As mentioned in the previous subsection, an interesting alternative is the spectral slicing of an additional high output power OBS installed at the CO where each sliced channel represent the "seed" uplink light for the corresponding ONU [Kim 2000, Hea 2001, Xu 2007, Mun 2008].

To remove the necessity of supply the CO with optical sources dedicated to generate the uplink wavelengths, a second approach is directly re-using the downlink light received at the ONU to perform the uplink transmission at the same optical wavelength. In the so-called downlink wavelength "re-use" approach, the uplink transmission is performed at the ONU by modulating the intensity of a portion of the downlink optical power and then sending this modulated light back to the CO over the same fiber or using a separate fiber. A number of different schemes have been proposed to perform such a wavelength re-use at the ONU employing conventional lasers sources at the CO.

In [Fri 1994], TDM access of a single cost-shared tunable laser is performed in order to let the uplink signal modulated onto the downlink light

without interference. Here, a portion of the temporal period of the downlink signal is left unmodulated and reserved for upstream transmission. While the ONU architecture is only composed by a photo detection circuit and an external intensity modulator, the under utilization of the optical bandwidth and the need of an exact time control protocol inherent to the TDM approach constitutes a limitation. In [Att 2005], a single multi-channel fiber Bragg grating (FBG) is inserted at the ONU to extract, from the downlink light, a pure optical carrier. The reflected optical carrier is then intensity modulated with the uplink data and sent back to the CO. Wavelength stability of the incoming light source is required to match with the reflective bandwidth of the FBG. In [Den 2003, Tia 2008, Yu 2008, Liu 2010, Wan 2010], constant intensity optical frequency shift keying (OFSK), differential phase shift keying (DPSK), optical frequency division multiplexing (OFDM) and polarization shift keying (PolSK) modulation formats are employed at the CO for the downlink transmission to facilitate the uplink data re-modulation at the ONU by superimposing on-off keying (OOK) intensity modulated data. The ONU is again functionally simple at the expense of a complex transmitter at the CO and high-speed electronic processing required at the ONU.

Other approaches of downlink light reuse at the ONU employ power-saturation and intensity modulation properties of a SOA to erase the downlink data from the optical downlink carrier and modulate this one with the uplink signal [Ian 2000, Tak 2000, Tak 2003, Tal 2006, Tak 2006, Yam 2006]. A SOA requires high input power and the use of an extra optical amplifier raises considerably the cost per ONU. Therefore, reflective SOAs are preferred due to their higher power budget. For the uplink transmission the rSOA modulates the optical signal with a higher extinction ratio to "hide" the downlink data instead of erasing it, amplifies the signal and reflects it into the fiber. Source-less ONUs based on rSOAs are demonstrated in [Hea 2001, Pra 2005, Par 2006, Ji 2008, Yeh 2008, Lin 2008] for uplink bit rates up to 10 Gb/s whereas better bandwidth performances can be obtained by combining the rSOA with an EAM at the ONU [Tow 2008] at the expense of a much higher cost and insertion losses.

Several data remodulation schemes, using injection-locked multimode FPLDs, have been proposed to realize a low-cost upstream transmitter. In such approaches, an FPLD located at the ONU is injection locked by a portion of the received optical power of the downlink wavelength and simultaneously directly modulated to produce the upstream signal. The downstream light is generated at the CO either by a laser [Che 2001, Hun 2003, Cha 2002] or by an unmodulated ASE-based OBS source [Kim 2000]. However, these schemes require high injection powers.

While downlink wavelength re-use avoids the difficulty of having a dedicated optical source at the ONU, it introduces its own set of limitations apart of operational bandwidth restrictions, laser stabilization and transceiver complexity. In wavelength re-using, the output power of the CO source is required to be large enough to handle the round-trip uplink transmission as well as the downlink one. This requirement translates into a larger output power for the source. The insertion of an optical amplifier in each ONU would be an expensive solution. Secondly, most of these schemes perform the wavelength reuse at the ONU employing the same wavelength of the downlink transmission for the uplink one. If the transmission runs over the same fiber, which is economically desirable in

optical access network, unwanted back-reflections (from connector and splices in the fiber link) of the downlink light from the CO and the uplink light from the ONU must be prevented to avoid significant power degradations at the receiving ends. Separating optical fibers for downlink and uplink transmission can be helpful against back-reflections although, it implies doubling the fiber infrastructure size.

As described, these centralization strategies are compatible with WDM technology and PON topology although present different technical issues. In general, the approaches based on downlink wavelength "re-use" pose certain technical restrictions and increase the architecture complexity. On the other hand, the schemes based on the uplink wavelength supply facilitate the scalability but increase the overall cost of the network due to the high number of light-sources employed. In this research area, the second contribution of the thesis is represented by a novel light sources centralized DWDM-PON architecture. Our strategy is based on the polarization multiplexing (PolMUX) technique as a cost-effective means to implement the wavelength supply approach. In fact, for each DWDM channel, the PolMUX technique allows the generation of both the optical downlink and uplink carrier using a single coherent light source placed at the CO instead of two separate sources. In this way, one of the principal advantages brought by the PolMUX strategy is to save the installation costs associated to the additional source.

2.2.3 Network reconfigurability.

One of the main challenges of a WDM-PON is to share efficiently the available transmission capacity between all ONUs maintaining full-duplex connectivity. The issue of developing appropriate architectures oriented to achieve a fair sharing of capacity resources has been an important topic of research and two main strategies have been proposed: the fixed channel allocation (FCA), and the dynamic channel allocation (DCA) also referred to as network reconfigurability [Lee 2006, Shu 2008].

FCA-based networks allocate channels to every ONU in a fixed way in every service cycle. The first generations of access networks focused on static connections or FCA, in which a fixed channel was assigned to every subscriber at a certain wavelength. This static model underutilized the network resources wasting capacity in idle connections. Therefore, while it was a simple approach, FCA did not perform optimally in terms of capacity management. By contrast, DCA-based networks have the ability to reconfigure the channels distribution, providing each ONU a variable transmission capacity, depending on its actual request. Consequently, a dynamic scheme provides a more realistic, efficient and flexible capacity assignment by virtually increasing the capacity of the corresponding set of channels. Today, the growing interest in using DCA strategies in the access segment is further justified by the following consideration.

In the emerging market of broadband access networks, there is a wide range of bandwidth usage among different customers, by time of the day and by type of services. As instance, the traffic patterns may change from the before-noon business-centric file transfer and video conference, to afternoon entertainment-centric video-on-demand and voice-over-IP communications. In this case, the location of the traffic congestion changes

on a specific time-scale-basis. Significant fluctuations in the traffic load are also observed in access networks distributing wireless services through the integration of RoF technology. Here, the mobility of the users in the radio cells requires dynamic capacity assignment solutions to avoid any waste of capacity and keep reduced costs. In any case, the ability to dynamically reassign the transmission capacity in a shared network topology like a PON is an important added value. In a more general scenario. one customer can be temporarily granted greater bandwidth than average if other customers on the network are using less than average. Furthermore, since traffic, especially web-browsing traffic, is often bursty, some of the multiplexed channels can operate with higher apparent bandwidth than the shared bandwidth imposed by the multiplexing device. Here a shared channel is virtually divided into a set of variable bit-rate channels which adapt to the instantaneous needs of the customers. In this context, the DCA approach achieves the highest efficiency in terms of available per-channel bandwidth and can be considered a statistical multiplexing gain.

Although DCA can increase the PON efficiency when user demand is not uniform, it adds some architectural complexity at the RN location. In a reconfigurable network, the optical physical layer must have a wavelength routing capability to provide DCA to all wired and/or wireless services operating at the top of the network stack. Current reconfigurable optical networks are being developed by using all-photonic technology in order to avoid optical-to-electronic-to-optical conversions in transponders.

Optical devices such optical cross-connects (OXCs), reconfigurable optical add-drop multiplexers (ROADMs), fast wavelength selective switches, AWGs and their combination are typically used to setup the optical circuits that define the virtual topology of the agile network. With such optical devices, the light-paths are automatically reconfigured in the remote location avoiding the manual assignment of wavelength by network administrators. By so doing, the operative costs are greatly reduced. Moreover, the actual topology can be modified at any time to form different topologies or when new ONUs are added to or removed from the network. The principle of operation of these optical routing technologies is described in [Bor 1997]. The use of flexible wavelengths routers to dynamically assign a different number of WDM channels has been previously proposed in [Düs 2002, Boc 2005, Hsu 2005, Ort 2007, Urb 2008, Urb 2009] amongst others. In most cases, either a large and costly number of components or limitations to the ONUs upgrading may render feasibility and scalability a rather complicated and costly task. In this thesis DCA capabilities are implemented using a compact RN architecture using conventional WDM devices and realizing the channels selection by means of single or multiple optical switches.

2.2.4 Radio over fiber technology for wired and wireless service convergence in WDM-PONs.

The integration of RoF technology into existing WDM-PON infrastructures is a natural solution to allow the convergent transport of both wired digital and wireless analog signals over the same PON infrastructure (see Fig. 2.13). The use of optical fiber links in radio networks for the transport and distribution of radio signals is now a reality. The mobile and fixed wireless systems where RoF technology is now finding applications include indoor distributed antenna systems offering

mobile radio services, first, second and third generation microcellular mobile networks, indoor wireless local area networks (LANs), fixed broadband radio access and satellite communications which can provide very high bandwidth services to users [Gli 1998, Oga 1992, Lim 2000, Hui 2002, Lim 2003, Cha 2006, Jia 2007].
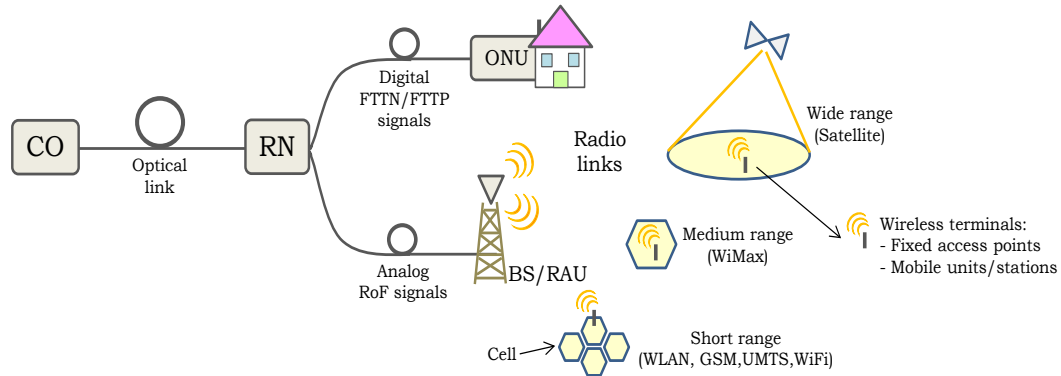

Fig. 2.13 WDM-PON infrastructure incorporating RoF technique for radio signal distribution to/from different wireless networks.

RoF technology entails the use of optical fiber links to distribute RF signals from the CO to a group of remote of BSs. Each antenna BS is adapted to communicate over a radio link with at least one user's wireless terminal located within a given radio range (cell radius), which may vary depending on the application. RoF systems achieve a maximum simplification of the BSs/RAUs architecture through consolidation of many signal processing functions (such as, frequency up-conversion, mixing and multiplexing) at the centralized headend whose equipment is shared by multiple stations. Therefore, the BSs are simplified significantly, as they only perform optoelectronic conversion and amplification functions, when required. In addition to the sharing of the CO equipment, the centralization of RF signal processing functions enables dynamic allocation of resources, and remote control and maintenance of the radio signal distribution via the fiber link. These benefits can translate into major system installation and operational savings especially in wide-coverage broadband wireless communication systems where a high density of BSs is necessary.

In a simplified RoF link, such as the one depicted in Fig 2.14, a radio signal, containing data pre-modulated electrically, is generated at the CO. The radio signal modulates the optical carrier provided by an optical source. There are two ways of modulating the light source. One way is to let the RF signal directly modulate the laser diode's current (direct modulation). The second option is to operate the laser in CW mode and then use an external electro optical modulator (EOM) to modulate the intensity of the light (external modulation). In any case, the resulting optical modulated signal is transmitted through the optical fiber to the remote BS. At the BS it is back converted to the radio frequency band via photodetection. The photocurrent, which is a replica of the modulating RF signal, undergoes transimpedance amplification to yield a voltage that is in turn used to excite the antenna. If the RF signal used to modulate the transmitter is itself modulated with data, then the detected RF signal at the receiver will be carrying the same data. The modulation format of the data is preserved. Finally, the antenna radiates the RF signal toward wireless mobile and fixed stations through the radio link. The uplink signal, coming

from the wireless terminal, is sent from the antenna to the CO in the same way.
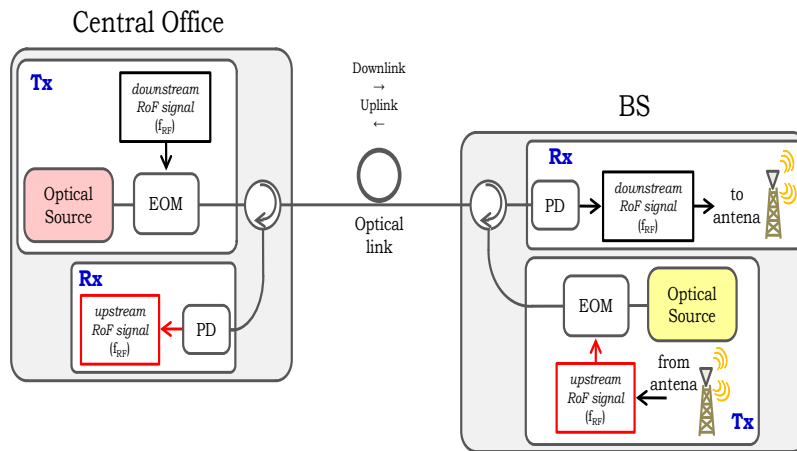

Fig. 2.14 RoF transmission system employing the IM-DD scheme with external modulation of the optical carrier.

Despite its architectural simplicity the RoF signal transport of wireless services operating at GHz frequencies presents some challenges due to the need of suitable high-speed optical modulation techniques that have the ability to generate µ-wave and mm-wave modulated optical signals as well as high-speed photodetection devices for carrier recovery.

As shown in Fig. 2.14, both the CO and the BS should perform an optical modulation function which is strictly required to operate in a wide electrical range to support modulation of baseband-to-GHz signals in both downlink and uplink transmission. Concerning the technological aspect of optical modulation of radio signals, it must be remarked that, although less complex than external modulation, direct modulation of lasers is not so appropriate for RoF links especially at mm-wave frequencies. Indeed, the main drawback of directly modulated lasers for high bit rate transmission beyond very short-reach access applications is their inherent frequency chirp, i.e., a residual phase modulation accompanying the desired amplitude modulation. Laser chirp broadens the optical spectrum impeding WDM channel packing and increasing the signal distortion caused by the interaction with fiber chromatic dispersion and fiber nonlinearity. At frequencies of 10 GHz or higher, the frequency chirp becomes large enough that direct modulation of semiconductor lasers is rarely used [Kot 1997, Ack 2002].

Unlike directly modulated lasers, external modulators can operate with mm-wave signals approaching 100 GHz. This is the fundamental reason for which in RoF technology external modulation is preferred to direct modulation. In the architecture of high-speed transmitters employing external modulation, the optical source is biased at a constant current to provide the CW output, and an optical modulator placed next to the laser converts the CW light into a data-coded pulse train with the right modulation format. Commonly used external EOMs are the Mach-Zehnder-type interferometric modulator (MZM) or the EAM. Another advantage that external modulation brings to the link designer is the versatility to support both amplitude and phase modulation formats in both their analog and

digital versions. Photodetectors should also be present with similar performance in this frequency band.

At this point, it is of great importance to consider another technological issue related to the schemes adopted for the modulation and recovery of carriers in the CO and BS transceivers. To accomplish modulation and recovery functions two basic approaches are possible. These are the intensity modulation with direct detection (IM-DD) scheme and coherent detection (CD) scheme. In the simplest IM-DD scheme, the optical source intensity is passed through an EOM to which the input electrical signal is applied. The resulting intensity modulated signal is propagated over the fiber link, and injected directly in the optical receiver where the modulation is returned to the electrical domain via photodetection. In the CD scheme, the optical source can be modulated in intensity, phase or frequency by the input electrical signal through the external EOM. After fiber propagation the modulated signal reaches the optical receiver where, prior to photodetection, it is coherently mixed with a CW optical field generated locally using a narrow width laser called local oscillator (LO). A sufficiently phase-stable LO acts as a phase reference for the received signal. The combined signal illuminates the photodetector to produce an electrical signal centred on the difference frequency between unmodulated optical source and the LO laser. Post-detected, this signal is further electrically processed to recover the original signal.

A potential advantage of using the CD scheme is that both amplitude and phase of the received optical signal can be detected and measured. This feature opens up the possibility of sending the information by modulating the amplitude, phase or frequency of the optical carrier. However, apart from requiring additional mixing components and optical sources, two main disadvantages of CD systems relative to those using direct detection are their phase sensitivity and polarization-dependence. With regard to the first disadvantage, since the photodetector response depends on the relative phase between the two mixed signal, the phase of both optical carrier and LO should ideally stay constant except for the intentional phase modulation of the optical carrier. In practice both phases fluctuate randomly with time and, thus, must be controlled either through an optical phase-looked loop (homodyne detection) or using narrow width semiconductor lasers for both optical sources (heterodyne detection). It makes the design of coherent receivers quite complicate and puts stringent requirements on the two optical sources for the matching of the transmitter and LO frequencies at the receiver.

By contrast, for IM-DD system, any unintentional phase changes are not seen by the detector (as the detector responds only to the optical power) and are not of major concern. Moreover, in IM-DD systems it is only necessary that the source frequency be suitable for the photodiode used. With regard to the second disadvantage, in coherent systems the polarization state of the signal and LO must be matched at the photodiode. In consequence, coherent systems need always to track the signal polarization by the LO polarization using either a polarization controller at the receiver or two parallel coherent receivers, one for each of the two orthogonal polarizations. In both cases, to make a coherent receiver polarization-independent more hardware components are required. Therefore, the use of CD schemes infringes the premise of low-complex ONU architecture. Owing to its lower complexity, the IM-DD scheme is

generally the most preferred option for practical implementation of optical transmitter/receiver blocks especially in access networks. For this reason, the IM-DD scheme has been employed in all architectures proposed in this dissertation.

2.2.5 Subcarrier multiplexing technique to increase the bandwidth utilization in WDM-PONs.

The wide operative bandwidth provided by a RoF link can be conveniently exploited by implementing the SCM technique in the electrical domain. The principal advantage of SCM is an increase of the bandwidth utilization of the link [Smi 1998, Hui 2002, Lim 2003, Mar 2003, Loa 2003, Che 2004, Woo 2004].

A traditional application of SCM technique in fiber optic systems is analog CATV distribution [Dar 1990]. With the explosion in the demand in access networks, CATV systems are being upgraded to handle full-duplex communication of voice, video and data through the addition of digitally modulated subcarriers and integration of WDM technology. Owing to its simple implementation, SCM has also been proposed to carry control information in a circuit switched network or label information in packet-based architectures [Cap 2005].

The SCM approach is based on subdividing the radio frequency spectrum transmitted by an optical carrier in several narrower independent channels. In a SCM scheme as the one of Fig. 2.15, multiple independent baseband digital signals are mixed by a set of equally spaced microwave subcarriers at the electrical level. The modulated subcarriers are then combined electrically creating a single composite SCM signal. Subsequently, the composite SCM signal is used to drive the external modulator to modulate one single optical carrier. This process is performed at the CO location. After fiber propagation, the received optical signal is converted back to the electrical domain at the ONU side. The resulting SCM signal is then separated into constituent electrical subcarriers each one filtered and demodulated to recover the original baseband data. Uplink SCM can be realized in a similar way.
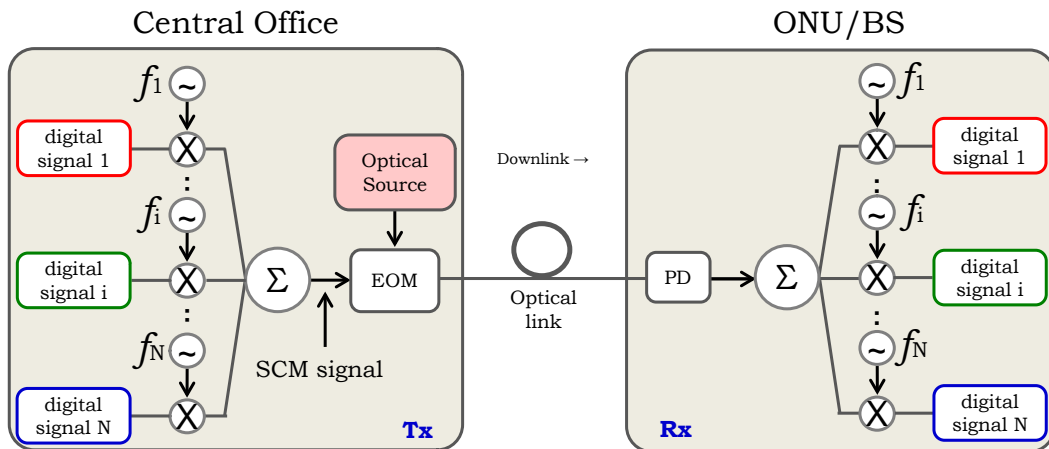

Fig. 2.15 Schematic description of the SCM technique.

Since each subcarrier frequency band constitutes an independent communication channel, it may carry the same signal or a signal in a format

different from that carried by another channel. As instance one subcarrier may carry a high-speed digital stream, while another subcarrier may be modulated with an analog signal such as video or telephone traffic). The SCM technique is, thus, completely transparent to the type of service. The capability to support the multiplexing of various types broadband data represents an efficient and flexible way to satisfy the concept of service convergence. Apart from improving the spectral efficiency of the optical channel, this is another advantage of SCM.

In hybrid WDM-SCM configurations, each WDM optical carrier would undergo the same process before/after optical multiplexing/demultiplexing. SCM is therefore compatible with both CWDM and DWDM technology. In this dissertation, such compatibility is exploited in order to convey the RF subcarriers on the fiber plant of a PON infrastructure so that independent baseband data streams and RoF signals can be simultaneously delivered to wired and wireless users, respectively [Kam 2001, Mar 2001].

One major disadvantage of SCM is that being an analogue communication technique, it is more sensitive to signal distortions. This characteristic places stringent linearity requirements especially on optical components such as the EOM and the PD which are inherently non-linear. In this context, the modulation index that could be obtained at the transmitter plays an important role. Indeed, when the optical modulator is driven by high amplitude SCM signals, the system electrical response may be degraded by the presence of harmonic (HD) and intermodulation distortion (IMD) terms arising from the non-linear characteristic of the optical modulator and photodetectors. Such undesired terms, may affect the recovery of the original signals at the receiver.

2.3   Summary.

In this chapter, we have reviewed the historical evolution of the access networks and their enabling technologies making a special emphasis on those infrastructures based on the optical fiber as transmission media. In this context, the PON architecture has been considered as the basic and most promising solution to satisfy the increasing capacity demand in the access segment owing to its maximum degree of infrastructure sharing. To provide multiple access capabilities, PONs infrastructures can be adapted to host multiplexing technique such as TDM and WDM. TDM-PONs are the current-generation PON where the bandwidth provided by a single feeder optical channel and the hardware in the CO are shared among several ONUs. However in TDM-PONs the transmission capacity is inherently limited by the shared use of one single optical wavelength for downlink and uplink communications. In order to increase significantly the capacity of the access segment, WDM-PONs has been addressed as the best solution for the next generation PONs.

WDM-PONs offer high capacity, service flexibility, easy upgradability and security. Moreover the high compatibility of WDM technology with RoF technology allows the convergent transport of both wired and wireless signals over the same infrastructure. However, due to the increased number of transceivers required to realize WDM access, the overall network complexity and its subsequent implementation cost are the most critical issues preventing WDM-PONs from a large scale deployment.

The implementation complexity and cost of a WDM-PON is associated to the transmitter architecture and in particular to the optical sources dedicated to carry out the bidirectional transport of signals. A correct choice of the transmitter technology is, therefore, the basis of the network design and depends on the capacity requirements of the network. In this context, two viable alternatives have been selected and described: CWDM and DWDM technology. CWDM technology requires a reduced number of optical sources for its practical implementation. Therefore, the spectral slicing of typical broadband sources, such as LEDs and ASE, can be conveniently used as an effective means to avoid the installation of multiple wavelength-selective lasers simplifying the transmitter architecture and its management at the same time. Although spectral slicing is an interesting solution for CWDM-PONs, the maximum per-channel bandwidth of a sliced channel can be severally limited by fiber chromatic dispersion. In consequence, the principal drawback of spectrum sliced broadband sources is their inability to transport GHz signals as required in RoF applications.

For high capacity networks, DWDM technology is necessary. In a DWDM-PON configuration, the optical carrier wavelengths are distributed over a dense grid. Therefore expensive coherent light sources such as distributed feedback lasers (DFB) lasers or tunable lasers must be used for their generation. Being a high-capacity solution, DWDM-PONs provides multi channel communications between the CO and a number of ONUs which can be significantly higher than in CWDM-PONs. Here, the operational cost associated with the uplink wavelength provisioning, management and maintenance of each ONU, has a strong impact on the overall cost of the access network. In DWDM-PONs the architecture complexity of the ONU must be minimized to allow cost-competitive implementations. To fulfill this requirement, the centralization of all wavelengths provisioning, monitoring and stabilization at the CO has been proposed. In the so-called centralized light source approach no light sources are incorporated in the ONU reducing the overall implementation cost and management of the network.

In both CWDM- and DWDM-PONs the dynamical channel assignment is an advanced strategy to increase the actual capacity of the network. Network reconfigurability provides an efficient sharing of the available bandwidth resources avoiding any waste of capacity in case of fluctuations of the traffic load. The use of flexible wavelengths routers at the RN location is the most typical solution to dynamically assign a different number of WDM channels depending on the actual ONUs demand.

A detailed description of a reference RoF link has been also presented remarking the importance use of external optical modulators for the generation of high frequency optical signals and the advantages brought by the IM-DD scheme in order to reduce the complexity of the ONU architecture. Finally, the incorporation of the SCM technique to increase the spectral efficiency of a WDM channel has been described remarking the great flexibility of such technique to provide convergent transport of different services over the same link.

2.4   References.

[Ack 2002]   D. A. Ackermann, J. E. Johnsonn, L. J. P. Ketelsen et al., "Telecommunication lasers", In Optical Fiber Telecommunications IV, (I. Kaminow and T. Li, eds), Academic Press, pp. 587-665, 2002.

[Aki 2003]   K. Akimoto, J.-I Kani, M. Teshima, K. Iwatsuki, "Super-Dense WDM Transmission of Spectrum-Sliced Incoherent Light for Wide-Area Access Network", J. Lightwave Technol., Vol. 21, pp. 2715-2722, 2003.

[Att 2005]   M. Attygalle, N. Nadarajah, A. Nirmalathas, "Wavelength reused upstream transmission scheme for WDM passive optical networks", Electron. Lett., Vol. 41, pp. 1025-1027, 2005.

[Ban 2005]   A. Banerjee, Y. Park, F. Clarke, H. Song, S. Tang, G. Kramer, K. Kim, B. Mukherjee, "Wavelength-division-multiplexed passive optical network (WDM-PON) technologies for broadband access: a review [Invited]", J. Opt. Netw., Vol 4, pp. 737-758, 2005.

[Bor 97]   M. S. Borella, J. P. Jue, D. Banerjee, B. Ramamurthy, B. Mukherjee, "Optical Components for WDM Lightwave Networks", Proceedings of the IEEE, Vol. 85, pp. 1274-1307, 1997.

[Boc 2005]   C. Bock, J. Prat, S. Walker, "Hybrid WDM/TDM PON using the AWG and featuring centralized light generation and dynamic bandwidth allocation", J. Lightwave Technol., Vol. 23, pp. 3981-3988, 2005.

[Cap 2005]   J. Capmany, B. Ortega, D. Pastor, S. Sales, "Discrete-time optical processing of microwave signals", J. Lightwave Technol., Vol. 23, pp. 702-723, 2005.

[Cha 2002]   L.Y. Chan, C.K. Chan, D.T.K Tong, E Tong, L.K. Chen, "Upstream traffic transmitter using injection-locked Fabry-Perot laser diode as modulator for WDM access networks", Electron. Lett., Vol. 38, pp. 43-45, 2002.

[Cha 2006]   G. K. Chang, J. Yu, Z. Jia, J. Yu, "Novel optical-wireless access network architecture for simultaneously providing wireless and wired services", presented at the Optical Fiber Communications Conf. (OFC), Anaheim, CA, March 2006.

[Che 2001]   S. Y. Cheung, L. Y. Chan, C. K. Chan, D. T. K. Tong, F. Tong, L. K. Chen, "Demonstration of an ONU for WDM Access Network with Downstream BPSK and Upstream Remodulated OOK Data Using Injection-Locked FP Laser", Proc. 27th Eur. Conf. on Opt. Comm. (ECOC),Amsterdam, 2001.

[Che 2004]   W. H. Chen, W. I. Way, "Multichannel Single-Sideband SCM/DWDM Transmission Systems", J. Lightwave Technol., Vol. 22, pp. 1679-1693, 2004.

[Cho 2007]   J. Cho, J. Kim, D. Gutierrez, L.G. Kazovsky, "Broadcast Transmission in WDM-PON using a Broadband Light Source", in Proceedings of Optical Fiber Communication Conf (OFC),

Anaheim, CA, March 2007.

[Dar 1990]   T. E. Darcie, "Subcarrier multiplexing for lightwave networks and video distribution system", IEEE J. Sel. Areas Commun., Vol. 8, pp. 1240-1248, 1990.

[Dav 2006]   R. Davey, J. Kani, F. Bougart, K. McCammon, "Options for Future Optical Access Networks", IEEE Communications Magazine, pp. 50-56, 2006.

[Den 2003]   N. Deng, C.K. Chan, L.K. Chen, F. Tong, "Data remodulation on downstream OFSK signal for upstream transmission in WDM passive optical network", Electron. Lett., Vol. 39, pp. 1741-1743, 2003.

[Düs 2002]   M. Düser, P. Bayvel, "Analysis of a Dynamically Wavelength-Routed Optical Burst Switched Network Architecture", IEEE J. Lightwave Technol., Vol. 20, pp. 574-585, 2002.

[Eff 2007]   F. Effenberger, D. Cleary, O. Haran, G. Kramer, R. D. Li, M. Oron, T. Pfeiffer, "An Introduction to PON Technologies", IEEE Communications Magazine, pp. 17-25, 2007.

[Esp 2000]   R.P. Espindola, G. Ales, J. Park, T.A. Strasser, "80 nm spectrally flattened, high power erbium amplified spontaneous emission fibre source", Electron. Lett., Vol. 36, pp. 1263-1265, 2000.

[Fel 1997]   R. D. Feldman, "Crosstalk and Loss in Wavelength Division Multiplexed Systems Employing Spectral Slicing", J. Lightwave Technol., Vol. 15, pp. 1823-1831, 1997.

[Fel 1998]   R. D. Feldman, E. E. Harstead, S. Jiang, Thomas H. Wood, Martin Zirngibl, "An Evaluation of Architectures Incorporating Wavelength Division Multiplexing for Broad-Band Fiber Access", J. Lightwave Technol., Vol. 16, pp. 1546-1559, 1998.

[Fer 2006]   X. Fernando, "Radio over Fiber in Multimedia Access Networks", invited paper, International Conference on Access Networks, Athens, Greece, September, 4-6, 2006.

[Fri 1994]   N. J Frigo, P. P. Iannone, P. D. Magill, T. E. Darcie, M. M. Downs, B. N. Desai, U. Koren, T. L. Koch, C. Dragone, H. M. Presby, G. E. Bodeep, "A Wavelength Division Multiplexed Passive Optical Network with Cost-Shared Components", IEEE Photon. Technol. Lett., Vol. 6, pp. 1365-1367, 1994.

[Gli 1998]   U. Gliese, "Multi-functional fiber-optic microwave links", Opt. Quantum Electron., Vol. 30, pp. 1005-1019, 1998.

[Gro 2008]   K. Grobe, J.-P. Elbers, "PON in Adolescence: From TDMA to WDM-PON", IEEE Communications Magazine, pp. 26-34, 2008.

[Han 2004]   K. H. Han, E. S. Son, H. Y. Choi, K. W. Lim, Y. C. Chung, "Bidirectional WDM PON Using Light-Emitting Diodes Spectrum-Sliced With Cyclic Arrayed-Waveguide Grating", IEEE Photon. Technol. Lett., Vol. 16, pp. 2380-2382, 1993.

[Hea 2001]   P. Healey, P. Townsend, C. Ford, L. Johnston, P. Townley, I. Lealman, L. Rivers, S. Perrin, R. Moore, "Spectral slicing WDM-

PON using wavelength-seeded reflective SOAs", Electron. Lett., Vol. 37, pp. 1181-1182, 2001.

[Hui 2002]   R. Hui, B. Zhu, R. Huang, C. T. Allen, K. R. Demarest, D. Richards, "Subcarrier Multiplexing for High-Speed Optical Transmission", J. Lightwave Technol., Vol. 20, pp. 417-427, 2002.

[Hun 2003]   W. Hung, C.-K. Chan, L.-K. Chen, F. Tong, "An Optical Network Unit for WDM Access Networks With Downstream DPSK and Upstream Remodulated OOK Data Using Injection-Locked FP Laser", IEEE Photon. Technol. Lett., Vol. 15, pp. 1476-1478, 2003.

[Hsu 2005]   Y-L. Hsueh, M. S. Rogge, S. Yamamoto, L. G. Kazovsky, "A Highly Flexible and Efficient Passive Optical Network Employing Dynamic Wavelength Allocation", IEEE J. Lightwave Technol., Vol. 23, pp. 277-286, 2005.

[Ian 2000]   P. P. Iannone, K. C. Reichmann, A. Smiljanic, N. J. Frigo, A. H. Gnauck, L. H. Spiekman, R. M. Derosier, "A Transparent WDM Network Featuring Shared Virtual Rings", J. Lightwave Technol., Vol. 18, pp. 1955-1963, 2000.

[Ji 2008]   H.-C. Ji, I. Yamashita, K.-I. Kitayama, "Cost-effective colorless WDM-PON delivering up/down-stream data and broadcast services on a single wavelength using mutually injected Fabry-Perot laser diodes", Opt. Express, Vol. 16, pp. 4520-4528, 2008.

[Jia 2007]   Z. Jia, J. Yu, A. Chowdhury, G. Ellinas, G.-K. Chang, "Simultaneous Generation of Independent Wired and Wireless Services Using a Single Modulator in Millimeter-Wave-Band Radio-Over-Fiber Systems", IEEE Photon. Technol. Lett., Vol. 19, pp. 1691-1693, 2007.

[Jun 1998]   D. K. Jung, S. K. Shin, C.-H. Lee, Y. C. Chung, "Wavelength-Division-Multiplexed Passive Optical Network Based on Spectrum-Slicing Techniques", IEEE Photon. Technol. Lett., Vol. 10, pp. 1334-1336, 1998.

[Kam 2001]   T. Kamisaka, T.Kuri, K. Kitayama, "Simultaneous modulation and fiber-optic transmission of 10 Gb/s baseband and 60 GHz band radio signals on a single wavelength", IEEE Trans. Microwave. Theory Tech., Vol. 49, pp. 2013-2017, 2001.

[Kaz 2007]   L. G. Kazovsky, S.W.T. Shaw, D. Gutierrez, N. Cheng, S.W. Wong, "Next-Generation Optical Access Networks", J. Lightwave Technol., Vol. 24, pp. 3428-3442, 2007.

[Kot 1997]   T. L. Koch, "Laser sources for amplified and WDM lightwave systems", In Optical Fiber Telecommunications III, (I. P. Kaminow and T. L. Koch, eds), Academy Press, pp.115-162, 1997.

[Kim 2000]   H. D. Kim, S.-G. Kang, C.-Hee Lee, "A Low-Cost WDM Source with an ASE Injected Fabry–Perot Semiconductor Laser", IEEE Photon. Technol. Lett., Vol. 12, pp. 1067-1069, 2000.

[Lee 1993]   J. S. Lee, Y. C. Chung, D. J. Di Giovanni, "Spectrum-Sliced Fiber Amplifier Light Source for Multichannel WDM Applications", IEEE

Photon. Technol. Lett., Vol. 5, pp. 1458-1461, 1993.

[Lee 2006]   C.-H. Lee, W. V. Sorin, B. Y. Kim, "Fiber to the Home Using a PON Infrastructure", J. Lightwave Technol., Vol. 24, pp. 4568-4583, 2006.

[Lim 2000]   C. Lim, A. Nirmalathas, D. Novak, R. Waterhouse, G. Yoffe, "Millimeter-wave broad-band fiber-wireless system incorporating baseband data transmission over fiber and remote LO delivery", J. Lightwave Technol., Vol. 18, pp. 1355-1363, 2000.

[Lim 2003]   C. Lim, A. Nirmalathas, M. Attygalle, D. Novak, R. Waterhouse, "On the Merging of Millimeter-Wave Fiber-Radio Backbone With 25-GHz WDM Ring Networks", J. Lightwave Technol., Vol. 21, pp. 2203-2210, 2003.

[Lin 2008]   S.-C. Lin, S.-L. Lee, C.-K. Liu, "Simple approach for bidirectional performance enhancement on WDM-PONs with direct-modulation lasers and RSOAs", Opt. Express, Vol. 16, pp. 3636-3643, 2008.

[Lio 1997]   K.-Y. Liou, U. Koren, E. C. Burrows, J. L. Zyskind, K. Dreyer, "A WDM Access System Architecture Based on Spectral Slicing of an Amplified LED and Delay-Line Multiplexing and Encoding of Eight Wavelength Channels for 64 Subscribers", IEEE Photon. Technol. Lett., Vol. 9, pp. 517-519, 1997.

[Liu 2010]   B. Liu, X. Xin, L. Zhang, J. Yu, Q. Zhang, Chongxiu Yu, "A WDM-OFDM-PON architecture with centralized lightwave and PolSK-modulated multicast overlay", Opt. Express, Vol. 18, pp. 2137-2143, 2010.

[Loa 2003]   A. Loayssa, C. Lim, A. Nirmalathas, D. Benito, "Optical Single-Sideband Modulator for Broad-Band Subcarrier Multiplexing Systems", IEEE Photon. Technol. Lett., Vol. 15, pp. 311-313, 2003.

[Mar 2001]   A. Martinez, V. Polo, J. Marti, "Simultaneous baseband and RF optical modulation scheme for feeding wireless and wireline heterogeneous access network", IEEE Trans. Microwave Theory Technol., Vol. 49, pp. 2018-2024, 2001.

[Mar 2003]   C. Marra, A. Nirmalathas, C. Lim, M. Attygalle, D. Novak, B. Ashton, L. Poladian, W. Rowe, T. Wang, J. A. Beasley, and L. Reekie, "A WDM fiber-radio system with improved optical spectral efficiency incorporating remote LO delivery and novel FBG optical filtering", in Proc. OFC2003, Atlanta, GA, Mar. 2003, pp. 730–731.

[Mun 2008]   S.-G. Mun, J.-H. Moon, H.-K. Lee, J.-Y. Kim, C.-H. Lee, "A WDM-PON with a 40 Gb/s (32×1.25 Gb/s) capacity based on wavelength-locked Fabry-Perot laser diodes", Opt. Express, Vol. 16, pp. 11361-11368, 2008.

[Oga 1992]   H. Ogawa, D. Polifko, and S. Banba, "Millimeter-wave fiber optics systems for personal radio communications", IEEE Trans. Microwave Theory Tech., Vol. 40, pp. 2285-2292, 1992.

[Ort 2007]   B. Ortega, J. Mora, G. Puerto, J. Capmany, "Symmetric reconfigurable capacity assignment in a bidirectional DWDM

access network", Opt. Express, Vol. 15, pp. 16781-16786, 2007.

[Par 2006]   S.-B. Park, D.K. Jung, D.J. Shin, H.S. Shin, I.K. Yun, J.S. Lee, Y.K. Oh and Y.J. Oh, "Demonstration of WDM-PON with 50 GHz channel spacing employing spectrum-sliced reflective semiconductor optical amplifiers", Electron. Lett., Vol. 42, 2006.

[Par 2007]   S.-J. Park, Y.-B. Choi, J.-M. Oh, S.-G. Koo, D. Lee, "An Evolution Scenario of a Broadband Access Network Using R-SOA-Based WDM-PON Technologies", J. Lightwave Technol., Vol. 25, pp. 3479-3487, 2007.

[Pen 1996]   G. J. Pendock, D. D. Sampson, "Transmission Performance of High Bit Rate Spectrum-Sliced WDM Systems", J. Lightwave Technol., Vol. 14, pp. 2141-2148, 1996.

[Pra 2005]   J. Prat, C. Arellano, V. Polo, C. Bock, "Optical Network Unit Based on a Bidirectional Reflective Semiconductor Optical Amplifier for Fiber-to-the-Home Networks", IEEE Photon. Technol. Lett., Vol. 17, pp. 250-252, 2005.

[Ree 1988]   M. H. Reeve, A. R. Hunwicks, W. Zhao, S. G. Methley, L. Bickers, S. Hornung, "Led Spectral Slicing for Single-Mode Local Loop Applications", Electron. Lett., Vol. 24, pp. 389-390, 1988.

[See 2002]   A. Seeds, "Microwave photonics", IEEE Trans. Microw. Theory Tech., Vol. 50, pp. 877-887, 2002.

[Shu 2008]   P. W. Shumate, "Fiber-to-the-Home: 1977–2007", J. Lightwave Technol., Vol. 26, pp. 1093-1103, 2008.

[Smi 1998]   G. H. Smith, D. Novak, C. Lim, "A Millimeter-Wave Full-Duplex Fiber-Radio Star-Tree Architecture Incorporating WDM and SCM", IEEE Photon. Technol. Lett., Vol. 10, pp. 1650-1652, 1998.

[Tak 2000]   H. Takesue, F. Yamamoto, T. Sugie, "Novel Node Configuration for DWDM Photonic Access Ring Using CMLS", IEEE Photon. Technol. Lett., Vol. 12, pp. 1698-1700, 2000.

[Tak 2003]   H. Takesue, T. Sugie, "Wavelength Channel Data Rewrite Using Saturated SOA Modulator for WDM Networks With Centralized Light Sources", J. Lightwave Technol., Vol. 21, pp. 2546-2556, 2003.

[Tak 2006]   H. Takesue, N. Yoshimoto, Y. Shibata, T. Ito, Y. Tohmori, T. Sugie, "Wavelength Channel Data Rewriter Using Semiconductor Optical Saturator/Modulator", IEEE J. Lightwave Technol., Vol. 24, pp. 2347-2354, 2006.

[Tal 2006]   G. Talli, P.D. Townsend, "Hybrid DWDM-TDM long-reach PON for next-generation optical access", IEEE J. Lightwave Technol., Vol. 21, pp. 2827-2834, 2006.

[Tia 2008]   Y. Tian, Q. Chang, Y. Su, "A WDM passive optical network enabling multicasting with color-free ONUs", Opt. Express, Vol. 16, pp. 10434-10439, 2008.

[Tow 2008]   P. D. Townsend, G. Talli, E. K. MacHale, C. Antony, "Long Reach

PONs", Proceedings of COIN2008, 2008.

[Tyl 2003]   E. J. Tyler, P. Kourtessis, M. Webster, E. Rochart, T. Quinlan, S. E. M. Dudley, S. D. Walker, R. V. Penty, I. H. White, "Toward Terabit-per-second capacities over multimode fiber links using SCM/WDM techniques", J. Lightwave Technol., Vol. 21, pp. 3237-3243, 2003.

[Urb 2008]   P.J. Urban, M. M. de Laat, E. J. Klein, A. M. J. Koonen, G. D. Khoe, H. de Waardt, "25 Gbit/s Bidirectional Link in an Access Network Employing a Reconfigurable Optical Add/Drop Multiplexer and a Reflective Semiconductor Optical Amplifier", in Proc. 10th Int. Conf. on Transparent Optical Networks (ICTON), pp. 166-169, paper We.B4.5., 2008.

[Urb 2009]   P.J. Urban, B. Huiszoon, R. Roy, M. M. de Laat, F. M. Huijskens, E. J. Klein, G. D. Khoe, A. M. J. Koonen, H. de Waardt, "High-Bit-Rate Dynamically Reconfigurable WDM-TDM Access Network", J. of Opt. Commun. Netw., Vol. 1, pp. A143-A159, 2009.

[Wag 1988]   S. S. Wagner, H. Kobrinsky, T. J. Robe, H. L. Lemberg, L. S. Smoot "Experimental Demonstration of a Passive Optical Subscriber Loop Architecture", Electron. Lett., Vol. 24, pp. 344-346, 1988.

[Wag 1990]   S. S. Wagner, T. E. Chapuran "Broadband High-Density WDM Transmission using Superluminescent Diodes", Electron. Lett., Vol. 26, pp. 696-697, 1990.

[Wan 2010]   R. Wang, S. Fu, P.P. Shum and C. Lin "10 Gbit/s WDM-PON using downstream PolSK coded by polarization modulator and upstream intensity re-modulation", Electron. Lett., Vol. 46, 2010.

[Wil 2008]   R.C. Williamson, R. D. Esman "RF Photonics", J. Lightwave Technol., Vol. 26, pp. 1145-1153, 2008.

[Woo 2004]   S. L. Woodward, Mary R. Phillips, "Optimizing Subcarrier-Multiplexed WDM Transmission Links", J. Lightwave Technol., Vol. 22, pp. 773-778, 2004.

[Xu 2007]   Z. Xu, Y. J. Wen, W.-D. Zhong, C.-J. Chae, X.-F. Cheng, Y. Wang, C. Lu, J. Shankar "High-speed WDM-PON using CW injectionlocked Fabry-Pérot laser diodes", Opt. Express, Vol. 15, pp. 2953-2962, 2007.

[Yam 2006]   S. S.-H. Yam, J. Kim, D. Gutierrez, F. Achten "Optical access network using centralized light source, single-mode fiber+broad wavelength window multimode fiber", J. Optical. Network., Vol 5, pp. 604-610, 2006.

[Yeh 2008]   C. H. Yeh, C. W. Chow, C. H. Wang, F. Y. Shih, H. C. Chien, S. Chi "A self-protected colorless WDM-PON with 2.5 Gb/s upstream signal based on RSOA", Opt. Express, Vol. 16, pp. 12296-12301, 2008.

[Yu 2008]   J. Yu, M.-F. Huang, D. Qian, L. Chen, G.-K. Chang "Centralized Lightwave WDM-PON Employing 16-QAM Intensity Modulated OFDM Downstream and OOK Modulated Upstream Signals", IEEE

Photon. Technol. Lett., Vol. 20, pp. 1545-1547, 2008.

Chapter 3

Fundamental transmission features and limitations in fiber-based optical communication links

3.1   Introduction

As anticipated in Chapter 2, an optical communication system based on the IM-DD of the optical carrier owns a simpler conceptual structure of the transmitter and receiver blocks than a system based on coherent detection. As a result, the commercial implementation of coherent systems has lagged behind that of IM-DD systems. The IM-DD approach is the most preferred option for modulation and recovery of optical signals especially in optical access networks where a reduction of the hardware complexity of the terminal nodes may facilitate a large-scale implementation. Concerning the technological aspect, the external modulation of the optical carrier is, compared to direct modulation, the most versatile and transparent choice since it offers the possibility of sending information by independently modulating all physical parameters of the optical carrier and, at the same time, offers high-bandwidth performance enabling the transport of both digital baseband and analog microwave signals.

The optical device most routinely used as external modulator in IM-DD lightwave systems for digital and analog signal distribution is a refractive modulator based on the electro-optic effect and typically manufactured in Lithium Niobate ($LiNbO_3$). The electro-optic effect causes the change of the optical refractive index in non linear optical crystals, such as $LiNbO_3$, due to the application of an external voltage. The index change leads to changes in the phase of the light traveling along the device. The optical phase is, thus, the physical parameter manipulated by the electrical voltage applied externally. In this way, the simplest type of EOM consists of a crystal of $LiNbO_3$ which is intrinsically an optical phase modulator (PM). All phase modulated signals have a constant envelope which cannot be directly detected by the photodiode as required in IM-DD schemes. To recover the electrical signal, the phase modulated optical carrier should be converted to an intensity modulated signal prior to direct photodetection. As will be discussed later, such required phase-to-intensity (PM-IM) conversion can be conveniently realized thanks to the dispersive nature of the optical link inserted between the transmitter and the receiver.

A phase modulating EOM can also be used as an intensity modulator by means of interferometric structures. The above described EOM becomes an intensity modulator once two $LiNbO_3$ waveguides are used to form a Mach-Zehnder interferometer configuration. In such a particular EOM, known as MZM, the incoming light is split into two optical paths at an input coupler. One (or both) paths are equipped with $LiNbO_3$-based conventional phase modulators. The phase modulators let the optical fields acquire some phase difference relative to each other by controlling the applied phase modulation voltages. The two fields are then recombined at an output

coupler. Changing the electrical field on the phase modulating paths determines whether the two beams interfere constructively or destructively at the output, thereby controlling the amplitude of the light launched into the modulator. In this way, the resulting intensity-modulated optical signal can be directly detected at the receiver.

From a practical point of view, the design and fabrication of a $LiNbO_3$-based EOM as optical phase modulator is much simpler than that of an EOM made in the same technology but conceived for amplitude modulation since a Mach-Zehnder interferometer is no longer needed and a single waveguide can be used. Therefore, a phase modulator may offer a lower degree of implementation complexity than a MZM. However, owing to the capacity of generating both amplitude and phase modulation of the optical carrier, the MZM is, in principle, the most versatile optical modulator device. Moreover its analytical model is perfectly compatible with DSB, SSB and PM formats and, thus, it is chosen as a basis for the analytical description presented in the next section.

3.2 Theoretical description of the transmission architecture over SMF links.

The block diagram depicted in Fig. 3.1 illustrates the general architecture of a traditional optical transmission system employing external modulation of the optical carrier.
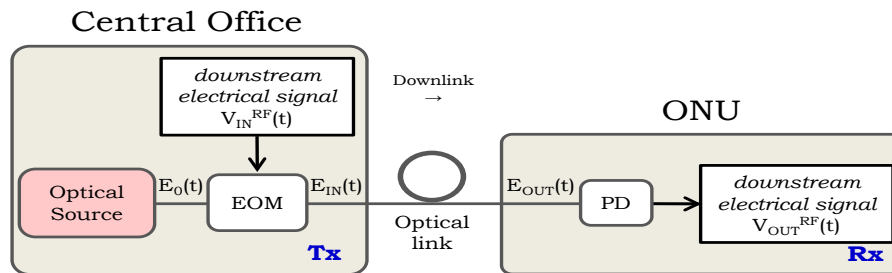
Fig. 3.1 Traditional optical transmission system using external modulation of the optical carrier.

The system is composed of a CO and one single ONU connected by a communication channel which use an optical fiber-based transmission media. According with the objective of this chapter, and without loss of generality, the architecture design is centred on the downlink path. Therefore, as shown in Fig. 3.1 the only two blocks considered in the CO and ONU are, respectively, the CO transmitter (Tx) and the ONU receiver (Rx). They are described as follows:

In the CO, a generic optical source supplies the downlink optical carrier wavelength. The optical carrier is modulated by the downstream electrical signal by means of a versatile dual-drive (DD) MZM. Note that, if the SCM technique is implemented, the downstream electrical signal would be the result of a previous modulation step performed entirely in the electrical domain where digital baseband data modulate a set of analog tones at higher frequencies called electrical subcarriers.

Moving back to the scheme, the resulting optically modulated signal is propagated through the optical link. Then, it reaches the receiver structure

of the ONU where is directly photodetected by means of a photodetector (PD) for the recovery of the downstream electrical signal.

In the field of optical communications, such a combination of photonic devices has the fundamental function of transporting the information, in form of electrical (digital or analog) signal, from one place (in this case, the CO) to another (the ONU). In order to deliver the electrical signal with the highest quality, these operations are performed entirely in the optical domain. The optical technology, in fact, guarantees better performance than the electrical one in terms of signal attenuation and distortion, bandwidth, capacity, electromagnetic immunity (EMI) and security amongst others.

From a more general perspective, the above optical devices perform a set of operations which can be regarded as a sequence of photonic signal processing tasks over the input electrical signal, whose optical transport from sender to destination is just one between several applications in the broad field of photonic processing of electrical signals [Cap 2005]. The block diagram of Fig. 3.1 is representative of a particular photonic circuit with two electrical input/output ports to/from which the signal processed is applied/extracted. Therefore, the behavior of the optical transmission system, shown in Fig. 3.1, as well as its features and limitations can be analytically described by means of its electrical impulse response, $h(t)$ or equivalently its electrical response $H(\Omega) = V_{OUT}^{RF}(\Omega)/V_{IN}^{RF}(\Omega)$. Such function is necessary to characterize an optical link in terms of maximum bandwidth-distance performance. In particular, the operative electrical 3dB bandwidth associated to the electrical response, serves as a measure of the maximum rate at which the input power may be modulated without significant increase of attenuation. The impulse response and the electrical response are related by the Fourier transform (FT).

The possibility to define an electrical transfer function is feasible only if the effects taken into account in the optical modulation stage, the optical link and the photodetection stage are linear and, thus, independent on the input power of the optical signal. Therefore, since we are interested in obtaining a general analytical expression of the output electrical signal, our description will be based on this working hypothesis. In order to find such general expression, let's $V_{IN}^{RF}(t)$ and $V_{OUT}^{RF}(t)$ be the input and output electrical signals respectively. Moreover let's define and model each one of the above photonic devices separately.

With regard to the optical source block dedicated to provide the optical carrier wavelength, its time domain representation is generically given by the optical field:

$$E_0(t) = \frac{1}{\sqrt{2\pi}} \int_{-\infty}^{+\infty} E_0(\omega)e^{j\omega t}d\omega \quad (3.1)$$

where $E_0(\omega)$ is the complex amplitude of the optical field for each optical angular frequency $\omega = 2\pi f$. In the theoretical analysis we assume that the optical field generated by this block obeys the following general condition:

$$\langle E_0(\omega)E_0^*(\omega_0)\rangle = S_0(\omega)\delta(\omega - \omega_0) \quad (3.2)$$

where $S_0(\omega)$ is the power spectral density (PSD) of the optical field.

The EOM is modeled by its discrete electrical transfer function or, equivalently, its electrical impulse response, s(t) which can be generically expressed as follows [Cor 2001]:

$$s(t) = \sum_{n=-\infty}^{\infty} s_n e^{jn\Omega t} \quad (3.3)$$

where $\Omega = 2\pi f$ is the electrical angular frequency and the nth-order coefficients, s_n, are defined in Table 3.1 for three types of modulation format, DSB-AM, SSB-AM and PM:

Table 3.1 Expression of the s_n coefficients for three different modulation format.

DSB-AM	SSB-AM	PM
$s_n = \cos\left(\varphi_{DC} \pm n\dfrac{\pi}{2}\right) J_n(m) e^{jn\theta_{RF}}$	$s_n = \cos\left(\varphi_{DC} \pm n\dfrac{\pi}{4}\right) J_n(m) e^{j\frac{n\theta_{RF}}{2}}$	$s_n = j^n J_n(m)$

In the expressions of Table 3.1, $J_n(\bullet)$ is the Bessel function of the first kind and harmonic order n which depends on the normalized amplitude of the driving signal, m. The parameter m is also known as the modulation index and V_π as the half-wave switching voltage of the modulator. For amplitude modulated signals, the parameter φ_{DC} is the normalized bias phase related to the bias voltage applied to the EOM, and θ_{RF} is a constant phase shift. In equation (3.3), the insertion losses of the modulator have been voluntarily omitted for the sake of simplicity.

The impulse response of the EOM is helpful to define the analytical form of the modulated optical signal at its output port which, in turn, represents also the optical signal launched into the dispersive link. Let's call such signal $E_{IN}(t)$. It is the product between $E_0(t)$ and s(t):

$$E_{IN}(t) = \left(\frac{1}{\sqrt{2\pi}}\right) \sum_{n=-\infty}^{\infty} s_n \left(\int_{-\infty}^{+\infty} E_0(\omega) e^{j(\omega+n\Omega)t} d\omega \right) \quad (3.4)$$

From the above equation, we find that the complex amplitude of the modulated optical field consists of the original carrier (n=0) plus infinite optical modulated sidebands with frequency deviation of $\pm n\Omega$, whose amplitudes are determined by the s_n coefficients.

The generic optical link is modeled as a linear time invariant (LTI) system by its optical impulse response:

$$h^{OPT}(t) = \frac{1}{\sqrt{2\pi}} \int_{-\infty}^{+\infty} H^{OPT}(\omega) e^{j\omega t} d\omega \quad (3.5)$$

where the optical transfer function, $H^{OPT}(\omega)$, is the FT of $h^{OPT}(t)$. In this way the optical field, $E_{OUT}(t)$, at the output of the optical link, can be expressed as a function of the optical input field, $E_{IN}(t)$, and the optical impulse response, $h_{OPT}(t)$, can be obtained as follows:

$$E_{OUT}(t) = \frac{1}{2\pi} \sum_{n=-\infty}^{\infty} s_n \left(\int_{-\infty}^{+\infty} E_0(\omega) H^{OPT}(\omega+n\Omega) e^{j(\omega+n\Omega)t} d\omega \right) \quad (3.6)$$

As happens to the signal at the input of the optical link, the signal at the output of the optical link contains infinite number of optical components, each one now multiplied by the contribution of the optical link.

Following the scheme of Fig. 3.1, the optical field $E_{OUT}(t)$ represents the optical input to the PD. The PD is a sensor of light, thus, it is sensitive to the received optical power associated to $E_{OUT}(t)$. Therefore, it is more convenient to express the received optical power in terms of $E_{OUT}(t)$ by means of the following average relation:

$$P_{OUT}(t) = \left\langle E_{OUT}(t) \cdot E_{OUT}^{*}(t) \right\rangle \quad (3.7)$$

Substituting the expression (3.6) into (3.7) and taking into account the assumption in eq. (3.2) we obtain the final expression of $P_{OUT}(t)$:

$$\begin{cases} P_{OUT}(t) = \dfrac{1}{4\pi^2} \sum_{k=-\infty}^{\infty} p_k e^{jk\Omega t} \\ p_k = \sum_{n=-\infty}^{\infty} s_n s_{n-k}^{*} \left(\int_{-\infty}^{+\infty} S_0(\omega) H^{OPT}(\omega+n\Omega) H^{*OPT}(\omega+(n-k)\Omega) d\omega \right) \end{cases} \quad (3.8)$$

The PD averages the incident optical power and converts it into a photocurrent $i_{OUT}^{RF}(t)$ according to an ideal response:

$$i_{OUT}^{RF}(t) = \Re \cdot P_{OUT}(t) \quad (3.9)$$

where $\Re$ is the PD responsivity. Finally, the electronic stage of the PD through its load impedance Z_L, provides the output electrical signal $V_{OUT}^{RF}(t)$:

$$V_{OUT}^{RF}(t) = Z_L \cdot i_{OUT}^{RF}(t) \quad (3.10)$$

Finally, using eq. (3.8) and eq. (3.9), eq. (3.10) can be expressed as follows:

$$\begin{cases} V_{OUT}^{RF}(t) = \left(\dfrac{\Re Z_L}{4\pi^2} \right) \sum_{k=-\infty}^{\infty} p_k e^{jk\Omega t} \\ p_k = \sum_{n=-\infty}^{\infty} s_n s_{n-k}^{*} \left(\int_{-\infty}^{+\infty} \underbrace{S_0(\omega)}_{\substack{\text{Optical source} \\ \text{contribution}}} \underbrace{H^{OPT}(\omega+n\Omega) H^{*OPT}(\omega+(n-k)\Omega)}_{\text{Optical link contribution}} d\omega \right) \end{cases} \quad (3.11)$$

The above equation is the general expression of the overall electrical signal at the output of the photodetection stage. It is expressed as a discrete sum of infinite power components, p_k, each one associated to the corresponding k^{th}-order electrical frequency. Moreover each kth-contribution depends on

the input optical source employed through the term $S_0(\omega)$, and the optical response of the link, $H^{OPT}(\omega)$.

We remark that until now, since all optical modulated sidebands are included in the beating process at the photodetection stage, this general expression is a strict and accurate solution which applies to all types of optical source, optical modulation format and optical communication link.

At this point we particularize the general expression given in eq. (3.11) for a specific type of optical communication channel consisting in a SMF link where only linear propagation effects such as attenuation and dispersion are taken into account in the theoretical model. Under this assumption, the optical response of the SMF link can be expressed as follows:

$$
\begin{cases}
H_{SMF}(\omega)= e^{-\frac{\alpha L}{2}} e^{-j\beta(\omega)L} \\
\beta(\omega) \approx \beta_0 + \beta_1(\omega - \omega_0) + \frac{\beta_2}{2}(\omega - \omega_0)^2 + \frac{\beta_3}{6}(\omega - \omega_0)^3
\end{cases}
\tag{3.12}
$$

where α is the optical attenuation factor of the fiber and L is the fiber length. The optical propagation constant $\beta(\omega)$ has been expanded in a Taylor series around ω_0 retaining all terms up to third order. Here ω_0 is the frequency at which the light pulse spectrum is centred, also referred to as the optical carrier frequency and each coefficient of the optical propagation constant is the ith derivative of $\beta(\omega)$ with respect to ω and evaluated at ω_0. This type of expansion is made under the condition that (ω-ω_0) is much smaller than ω_0. Apart from the linear phase shift, β_0, the coefficients β_1 and β_2 represent per unit of length, the group delay and the chromatic dispersion parameter, respectively.

In eq. (3.12) together with the higher-order dispersion coefficients, also the cubic coefficient β_3, called third-order dispersion parameter or dispersion slope, could be neglected if the optical source bandwidth is sufficiently small, that is, when the optical source verifies the quasi-monochromatic approximation. Indeed, we expect that the effect of the third-order dispersion would be, in principle, more relevant for optical sources whose width is as high as to invalidate such approximation. The lector is referred to Chapter 4 for studying the analytical condition over the source width, under which the effects of the third order dispersion must be taken into account showing experimentally the influence of such parameter on the system electrical transfer function.

Therefore, in order to obtain the analytical expression of the output electrical signal particularized for the SMF link, let's neglect from eq. (12) the last term depending on β_3. In this case taking $H^{OPT}(\omega)= H_{SMF}(\omega)$ and after some mathematical simplifications, eq. (3.11) can be expressed as:

$$
\begin{cases}
V_{OUT}^{RF}(t)=\left(\frac{\Re Z_L}{4\pi^2}\right)\sum_{k=-\infty}^{\infty} p_k e^{jk\Omega t} \\
p_k = e^{-\alpha L} e^{-j\beta_1 L(k\Omega)} e^{j\frac{1}{2}\beta_2 L(k\Omega)^2}\left(\sum_{n=-\infty}^{\infty} s_n s_{n-k}^* e^{-jn\beta_2 L(k\Omega^2)}\right)\int_{-\infty}^{+\infty} S_0(\omega) e^{-j\beta_2 L(k\Omega)\Delta\omega}d\omega
\end{cases}
\tag{3.13}
$$

The above equation completely characterizes the variation of each kth-order harmonic component photodetected after propagation over the dispersive

fiber. The overall electrical signal at the output of the PD is the sum of all harmonic components.

Now, we use the linearity of the PD. It means that from eq. (3.13), we can take into account only for the harmonics with index k=0 and k=±1. Concerning the optical modulation stage, we use the working hypothesis under which also the EOM is operating in the linear region of its optical transmittance characteristic curve. In practice, such condition is verified amplitude of the electrical signal driving the modulator is much smaller than the switching voltage V_π, or equivalently, when the modulation index is much smaller than unity. In particular, for amplitude modulated signals, we assume the EOM biased in the quadrature point ($V_{DC}=V_\pi/2$), that is, where the characteristic curve exhibits the maximum degree of linearity.

Under small modulation index, the optical modulated field is a close replica of the applied electrical field corresponding to the input electrical signal, $V_{IN}^{RF}(t)$ and the resulting optical spectrum at the output of the EOM contains the optical carrier (for n=0) and only two optical modulated sidebands at ±Ω (for n=±1). Therefore after some mathematical simplification, expression (3.13) reduces to:

$$
\begin{cases}
V_{OUT}^{RF}(t) \approx \left(\dfrac{\Re Z_L}{4\pi^2}\right)\left(p_0 + p_1 e^{j\Omega t} + p_1^* e^{-j\Omega t}\right) \\[2mm]
p_0 = P_0 e^{-\alpha L}\left(\left|s_0^2\right| + \left|s_1^2\right|\right)H_0^{RF}(0) \\[2mm]
p_1 = P_0 s_0 e^{-\alpha L} e^{-j\beta_1 L\Omega}\left(s_{-1}^* e^{j\frac{\beta_2 L}{2}\Omega^2} + s_1 e^{-j\frac{\beta_2 L}{2}\Omega^2}\right)H_0^{RF}(\Omega)
\end{cases}
\qquad (3.14)
$$

where the term $H_0^{RF}(\Omega)$ is defined as:

$$
H_0^{RF}(\Omega) = \frac{\displaystyle\int_{-\infty}^{+\infty} S_0(\omega)e^{-j\beta_2 L\Omega\Delta\omega}d\omega}{\displaystyle\int_{-\infty}^{+\infty} S_0(\omega)d\omega}
\qquad (3.15)
$$

being the denominator of (3.15) the total power of the source, P_0.

Equation (3.14) describes analytically the photodetected signal. Note that, the first order power component, p_1, in (3.14) represents the electrical transfer function, $H_{RF}(\Omega)$, of the SMF-based optical transmission system depicted in Fig 3.1 under small signal approximation. Note that, from eq. (3.14) it can be demonstrated that $p_{-1}=p_1^*$.

The electrical response depends, firstly, on some constants related to the detection and modulation efficiency. Secondly two more factors include the power loss and the delay caused by the signal propagation through the channel. In addition, another term takes into account the effect of fiber chromatic dispersion on the electrical characteristics of the modulation process, such as the modulation format and the bandwidth of the modulating electrical signal. A final term, $H_0^{RF}(\Omega)$, takes into account the effects of fiber chromatic dispersion over the spectral power distribution $S_0(\omega)$ of the input optical source. We anticipate now that such last term gains more relevance especially for optical sources with a significant

spectral width. This aspect will be treated with great depth in the next section.

The electrical transfer function can be easily specified for three different optical modulation formats, DSB-AM, SSB-AM and PM.

(a) DSB-AM format

In case of DSB-AM format, the Bessel coefficients s^*_{-1} and s_1, calculated from eq. (3.3) and taking into account Table 3.1, are equals. Therefore, taking $s^*_{-1}=s_1$, the electrical transfer function can be written as:

$$H^{RF}(\Omega) = \left(\frac{\Re Z_L}{2\pi^2}\right) P_0 s_0 s_1 e^{-\alpha L} e^{-j\beta_1 L\Omega} \cdot CSE(\Omega) \cdot H_0^{RF}(\Omega) \quad \text{(DSB-AM)} \quad (3.16)$$

where the term $CSE(\Omega)$ is defined as:

$$CSE(\Omega) = \cos\left(\frac{1}{2}\beta_2 L\Omega^2\right) \quad (3.17)$$

Under linear modulation assumption, eq. (3.16) is the well known formula that gives the electrical response of a DSB-AM-based optical transmission system for a generic optical source externally modulated and propagated over a dispersive SMF link. As observed, the particular condition verified by the Bessel coefficients in case of DSB-AM and the presence of the dispersive link, analytically generates the term $CSE(\Omega_{RF})$ known as carrier suppression effect (CSE). From eq. (3.17) we observe that the CSE is caused by the dispersive nature of the fiber link and is inherent to the propagation of optical carriers modulated in DSB-AM format.

(b) SSB-AM format

In case of SSB-AM format, the Bessel coefficients are such that $s_1\neq0$ and $s^*_{-1}=0$. Therefore, the electrical transfer function becomes:

$$H^{RF}(\Omega) = \left(\frac{\Re Z_L}{4\pi^2}\right) P_0 s_0 s_1 e^{-\alpha L} e^{-j\beta_1 L\Omega} \cdot e^{j\frac{\beta_2 L}{2}\Omega^2} \cdot H_0^{RF}(\Omega) \quad \text{(SSB-AM)} \quad (3.18)$$

This is the electrical response of a SSB-AM-based optical transmission system with a dispersive SMF link under linear modulation assumption. It is important to remark the absence of the CSE term.

(c) PM format

For the PM format the Bessel coefficients are such that $s^*_{-1}=-s_1$. In this case, the electrical transfer function can be arranged as follows:

$$H^{RF}(\Omega) = \left(\frac{\Re Z_L}{2\pi^2}\right) P_0 s_0 s_1 e^{-j\frac{\pi}{2}} e^{-\alpha L} e^{-j\beta_1 L\Omega} \cdot PM\text{-}IM(\Omega) \cdot H_0^{RF}(\Omega) \quad \text{(PM)} \quad (3.19)$$

where the term $PM\text{-}IM(\Omega)$ is defined as:

$$PM\text{-}IM(\Omega) = \sin\left(\frac{\beta_2 L}{2}\Omega^2\right) \quad (3.20)$$

Equation (3.19) gives the electrical response of an optical transmission system where the optical carrier is phase modulated and propagated under small signal modulation over a dispersive SMF link. In this case a new factor, PM-IM(Ω), appears in the electrical response as a result of a phase modulated optical signal propagated over the fiber. It represents the phase-to-intensity (PM-IM) conversion effect. The PM-IM conversion effect is inherent to the optical phase modulation of an optical source in presence of a dispersive link. Moreover, the existence of such effect is the fundamental reason for which a phase modulated signal can be directly photodetected [Yao 2005, Zen 2005, Chi 2009].

3.3   Impact of fiber chromatic dispersion in third communication band.

From the analytical description of the previous section is evident that the signal propagation over SMF links is characterized by the constant presence of the fiber chromatic dispersion parameter. The role played by fiber chromatic dispersion in the system response is critical and not only depends by the link parameters itself but also on two more fundamental aspects: the characteristics of the optical modulation process, and the spectral characteristics of the source. After a brief qualitative description of the chromatic dispersion mechanism, this section provides a theoretical study of the dispersion-induced transmission limitations where, just for commodity of description, the aspects related to the modulation process and the source characteristics will be treated separately.

3.3.1 Description of the chromatic dispersion mechanism.

A light pulse is a wave-packet composed of a spectrum of components of different wavelengths. In case of SMF propagation, the energy of the injected light pulse is transported by the fundamental mode. Therefore, the group delay parameter, $\beta_1 L$ appearing in the optical transfer function of a SMF link (see eq. (3.12)) represents the transit time required by the single pulse to travel the link distance L at the corresponding group velocity. The group velocity is the velocity at which energy or information is conveyed. The specific group delay β_1 associated with the fundamental mode exhibits frequency dependence. Consequently, different spectral components of the light pulse travel at slightly different group velocities. In other words, the frequency dependence of the group delay leads to pulse broadening simply because such spectral components disperse during propagation and do not arrive simultaneously at the fiber output.

Such wavelength dependence of the group delay is due to the combined effect of two fundamental linear dispersion mechanisms present in optical fibers: the material dispersion arising from the wavelength dependence of the glass refractive index and the waveguide dispersion resulting from the dependence of the field distribution in the fiber on the ratio between the core radius and the operative wavelength. The combined effect of material and wavelength dispersion is referred to as chromatic dispersion to emphasize its wavelength-dependent nature, and is the most

important distortion contribution in all optical communication systems based in SMF. Chromatic dispersion is sometimes called group-velocity dispersion (GVD) to emphasize the role of the group velocity, or intramodal dispersion to distinguish it from the modal dispersion inherent to MMF propagation.

The extent of the pulse temporal broadening represents the overall response time of the fiber. It is proportional to the fiber length and the source spectral width through the specific second-order dispersion parameter, β_2 also known as GVD parameter or simply chromatic dispersion parameter, which involves the combination of material and waveguide. If dispersion is too high, the group of light pulses representing the bit-stream, will spread in time and merge together, up to a point where pulses overlap each others rendering the bit-stream unintelligible at the receiver. For correct reception, the extent of pulses broadening should not exceed the allocated bit slots. This phenomenon is known as intersymbol interference (ISI). Therefore, while fiber attenuation limits the magnitude of the optical power received, fiber dispersion governs the temporal spreading of the optical pulses carrying the data and, thus, limits the fiber length that a certain signal can be sent down without regeneration or, the signal bandwidth that can be transmitted through a given fiber length.

Since also the β_2 parameter is wavelength dependent, the amount of the pulse broadening will depend on the source wavelength region of emission or, equivalently, on the operative communication band designate for transmission. For a standard SMF-based link designed to work in the second communication window β_2 is relatively small ($\beta_2 \sim -0.9$ ps^2/km). For example, in this wavelengths region, the bandwidth-distance (BL) product of SMF can reach few hundred of GHz·Km for optical sources with a spectral width of some nanometers. The chromatic dispersion parameter can vary considerably when the operating wavelength is shifted from 1300 nm. In particular, in the wavelength area of more interest for optical communications that is the third communication band typical values of β_2 are between -19 ps^2/km and -23 ps^2/km. Here, dispersion becomes a more limiting factor. To give an idea, in the best case (lower chromatic dispersion parameter), the BL product would reduce to few tens of GHz·km (one order of magnitude) using optical source with similar spectral widths. However, owing to its lowest fiber attenuation (around 0.2 dB/km), the third communication band is of considerable interest for optical communication systems and networks. In such environments, the advantage of operating in the minimum fiber attenuation range is generally frustrated by the limiting effect of dispersion. Therefore, to ensure adequate quality of service, it is extremely important that carriers compensate for this type of signal distortion. The widespread use of WDM architectures covering the C-L bands (1530-1625 nm) certainly creates the need for wideband accurate strategies oriented to reduce or compensate the impact of dispersion.

3.3.2 Transmission limitations inherent to the optical modulation format.

The principal characteristics of the optical modulation process can be described once the bandwidth of the modulating electrical signal and the modulation format employed are known. The effect of fiber dispersion may change depending on both factors. In fact, the modulation operated by the electrical signal over the optical carrier tends to enhance the optical spectrum transmitted over the fiber link and, thus, the dispersion effect. In

turns, the optical modulated spectrum depends itself on the specific modulation format adopted. In order to investigate such modulation-dependent effects of fiber dispersion, let's evaluate the electrical transfer function of a SMF-based optical transmission system in the ideal case where the optical carrier wavelength is provided by a coherent source.

In accordance to definitions in eq. (3.1) and eq. (3.2) the PSD function of a coherent source can be expressed as:

$$S_0(\omega) = P_0 \cdot \delta(\omega - \omega_0) \quad (3.21)$$

where P_0 is the optical power emitted by the coherent source centred at the carrier frequency ω_0.

Substituting the definition (3.21) in relations (3.16), (3.18) and (3.19) we find the expressions of the electrical transfer functions of a SMF-based system for optical coherent sources modulated in DSB-AM, SSB-AM and PM format respectively:

$$H^{RF}(\Omega) = \left(\frac{\Re Z_L}{2\pi^2}\right) P_0 s_0 s_1 e^{-\alpha L} e^{-j\beta_1 L\Omega} \cdot CSE(\Omega) \quad (DSB-AM) \quad (3.22.a)$$

$$H^{RF}(\Omega) = \left(\frac{\Re Z_L}{4\pi^2}\right) P_0 s_0 s_1 e^{-\alpha L} e^{-j\beta_1 L\Omega} \cdot e^{j\frac{\beta_2 L}{2}\Omega^2} \quad (SSB-AM) \quad (3.22.b)$$

$$H^{RF}(\Omega) = \left(\frac{\Re Z_L}{2\pi^2}\right) P_0 s_0 s_1 e^{-j\frac{\pi}{2}} e^{-\alpha L} e^{-j\beta_1 L\Omega} \cdot PM\text{-}IM(\Omega) \quad (PM) \quad (3.22.c)$$

Note that, since a coherent source is employed, in all the three cases the term $H_0^{RF}(\Omega)$, defined in eq. (3.15), is reduced to a unity factor multiplying P_0.

Figure 3.2 plots the normalized electrical responses obtained using the theoretical model for an optical modulated coherent source emitting a monochromatic radiation at 1550 nm and propagated over 10 km of SMF link with a $\beta_2 = -22.6$ ps^2/km. In particular case (a) refers to amplitude modulation formats DSB-AM and SSB-AM, whereas, case (b) refers to the PM format.

As shown in Fig 3.2(a) (black curve), when a coherent source is modulated by using DSB-AM format, the received electrical power exhibits fading due to fiber dispersion. The mechanism under which such power degradation occurs can be understood as follows. When DSB-AM is adopted, the optical spectrum at the output of the modulator is characterized by both electrical lower and upper sidebands transmitted around the optical carrier. If the optical fiber was not dispersive, at the optical receiver each sideband would beat with the optical carrier generating two beat signals which would constructively interfere to produce a single electrical component at radio frequency. Actually, the wavelength dependent nature of fiber dispersion causes each spectral component of the optical modulated signal to experience different phase shifts during propagation. The amount of such phase shifts depends on the fiber link distance, and chromatic dispersion parameter β_2. Therefore, at the optical

receiver, such phase shifts cause relative phase differences between the carrier and each sideband and produces a phase difference in the two beat signals at electrical frequency. It results in a power degradation of the photodetected electrical signal. When the phase difference is π (counter phase sidebands condition) a complete cancellation (suppression) of the electrical signal occurs or, equivalently, a notch in the electrical response appears.

(a) Amplitude modulation formats (b) Phase Modulation format
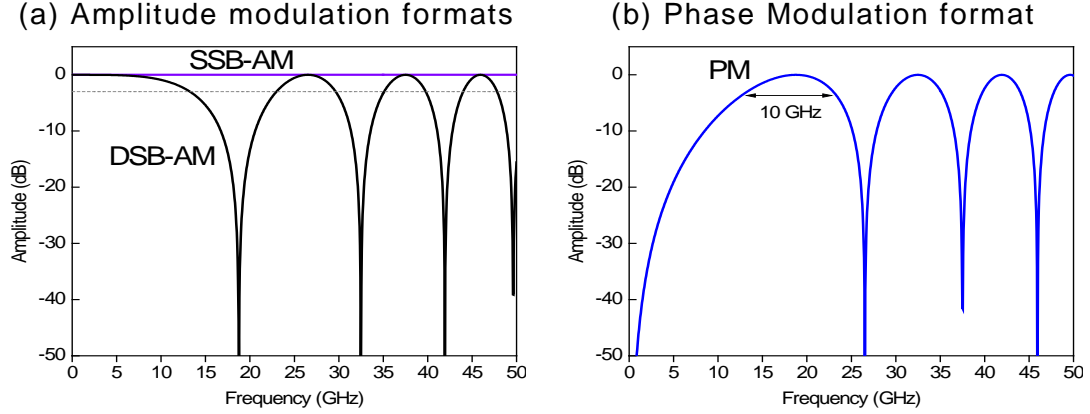
Fig. 3.2 Theoretical normalized electrical responses of a 10 Km SMF-based transmission system when a coherent source emitting at 1550 nm is modulated using (a) DSB-AM (—) and SSB-AM (—) format and (b) PM (—) format.

Quantitatively, such power degradation follows cosine-like fluctuations given by the CSE function defined in eq. (3.17). Therefore the power of the photodetected signal periodically disappears at the fading nodes. From eq. (3.17) we find easily that the kth frequency nulls for which the electrical power experiences its maximum fading can be calculated as:

$$CSE(\Omega)=\cos\left(\frac{1}{2}\beta_2 L\Omega^2\right) \Rightarrow \Omega_k=\sqrt{\frac{(2k+1)\pi}{\beta_2 L}} \quad , k \in Z \quad (3.23)$$

Using the link parameters L=10 km and β_2=-22.6 ps^2/km in eq. (3.23), the first four notches of the electrical response are placed at frequencies: 18.7 GHz, 32.5 GHz, 41.9 GHz and 49.6 GHz in accordance with the electrical response of Fig. 3.2(a). From the above equation, it can be observed that, for a given chromatic dispersion parameter, the notches moves toward lower frequencies as the link distance increases and that, for a given link distance, the effect of dispersion is even higher at higher frequencies. In any case, the operative electrical bandwidth of the system defined at the 3dB point of the response is determined by the first CSE notch. Note that, certain services could also be transmitted at frequencies higher than the one established by the 3dB point if they are conveniently far from the notches.

In Fig. 3.2(a), the operative electrical 3dB bandwidth is around 13 GHz. It means that any electrical signal transmitted in a frequencies range larger than 0-13 GHz could be drastically attenuated at the receiver after 10 km. The operative system bandwidth would reduce down to 9 GHz and 7 GHz for 20 km and 30 km distance, respectively, as example.

Therefore, it can be affirmed that in SMF-based transmission systems employing coherent sources modulated in DSB-AM format, fiber dispersion manifest itself through the CSE which directly imposes a fundamental limitation over the bandwidth-distance product of the transmission link. The performance fading problem becomes extremely important especially when the electrical operative frequency approaches the CSE notch. In this region any RoF application based on the transport of microwave and millimeter-wave signals would not be feasible.

When the SSB-AM format is adopted, the situation completely changes. In fact, from the response of fig. 3.2 (blue plot), we immediately see that, although the propagation runs over a dispersive link, the CSE-induced electrical power fading is not present just as we found in eq. (3.22b). Note that it doesn't mean that fiber dispersion has been compensated. In fact, the elimination of one sideband, inherent to the SSB-AM format, avoids only the carrier power fluctuations caused by the presence of both sidebands in the DSB-AM format. It can be said that the SSB is just immune to the CSE rather than dispersion itself. It is however a positive result since the operative electrical bandwidth provided by a SSB-AM system is limited, in principle, only by the operative electrical bandwidth of the optical modulator and photodetector employed.

When PM is applied to the optical carrier, the electrical response of Fig. 3.2(b) again exhibits electrical power degradation similarly to the DSB-AM case. However, this time, the power fluctuations are governed by the sin-like function defined in eq. (3.20) called PM-IM conversion effect. Mathematically, the notch frequencies of the electrical response, Ω_k, can be easily extracted from eq. (3.20) as follows:

$$PM\text{-}IM(\Omega)=\text{sen}\left(\frac{1}{2}\beta_2 L\Omega^2\right)\Rightarrow \Omega_k=\sqrt{\frac{2\pi k}{\beta_2 L}}\quad , k\in Z \quad (3.24)$$

In accordance to the above equation, the first four notches of the response fall at dc and frequencies 26.5 GHz, 37.5 GHz and 45.9 GHz using the same link parameters. It can be seen that, due to the first notch at the dc frequency, the PM-IM function shows a band-pass characteristic. Between the first and the second notches the electrical response exhibits a frequency region whose 3dB bandwidth calculated in correspondence of the maximum peak amplitude defines the operative range of the system. In the example of Fig. 3.2(b) this range is around 10 GHz. It means that the system allows the transport of RoF signals always when they falls in the available range offered by the PM-IM conversion curve. The lector may also observe that the transmission of baseband signals is prevented since they would be drastically attenuated due to the notch at dc. As the factor $\beta_2 L$ increase, the peak amplitude shifts to lower frequencies and the pass-band region becomes more selective reducing the available transmission bandwidth.

As mentioned previously, the PM-IM conversion effect occurs only when a phase modulated carrier is propagated through a dispersive media. As known, a phase modulated signal has a constant envelope. It means that if it is directly detected using a photodiode, only a dc component would be obtained as the photodetector is only sensitive to intensity variations of the input optical signal. However, if the phase modulated signal passes through a dispersive device, for example a length of SMF, the phase

relationship between all spectral components will be changed to fully or partially in phase thanks to chromatic dispersion. When the dispersed optical signal is fed to a PD frequency components either than dc may be obtained which indicates that the phase modulating signal has been converted to an amplitude modulated one.

Therefore, the PM-IM conversion allows the employment of the IM-DD scheme also for optical PM signals where the use of a phase EOM offers several implementation facilities with respect to MZMs. In addition, the PM-IM conversion process generates a pass-band transmission region in the electrical transfer function where the RoF transport is permitted in a wide operative range similarly to the case of employing coherent sources modulated in DSB-AM format.

3.3.3 Typical strategies to reduce the impact of fiber chromatic dispersion.

This subsection provides a descriptive review of the most commonly adopted strategies to compensate the chromatic dispersion effects in SMF-based links employing externally modulated coherent sources. This is not intended as a complete review on this topic, rather as a quick walk-through with references to further information.

For SMF-based links operating in third communication band adopting external modulation of coherent sources, several commonly adopted strategies to enhance the operative electrical bandwidth of the link have been proposed during the last two decades. In general these strategies are oriented to either mitigate or cancel completely the CSE-induced power fading due to fiber dispersion still maintaining the use of DSB-AM format.

Concerning the mitigation of the CSE, the basic idea is to displace conveniently the CSE notches in function of the transmitted electrical signal frequency. It can be done by means of introducing a phase chirp in the output signal from the EOM. In the specific case of an MZM, such chirp can be imposed by varying the relative amplitude and sign of the electrical driving signals applied to each electrode. Since the phase chirp affects the phase of the spectral components of the modulated signal, it will also affect the fiber distance at which the electrical beat signals cancel after photodetection and, thus the position of the CSE notches. It has been demonstrated in [Gna 1991, Smi 1997-01, Pol 1999] that the distance can be increased for a large and negative chirp. In this case, the notches are shifted to the right, enhancing the 3 dB bandwidth of the system. Otherwise, if the chirp is positive the bandwidth is reduced. The optimum electrical range can be obtained by biasing the MZM at the quadrature point and using the appropriate modulation index.

Analogous techniques to achieve similar results are based on imposing the chirp variations by means of a SOA operating in saturation mode [Mar 2001] or using fiber-induced self phase modulation (SPM) [Ram 1998]. Although those solutions successfully mitigate the CSE, they do not eliminate it completely. Moreover, in most cases they are either bandwidth-limited, too complex or introduce non-linear distortion in the received signal.

Amongst the techniques oriented to achieve a fading-free transport of DSB-AM signals we remark the optical dispersion compensation (ODC) [Nie

2000, Knu 2002] and the electronic pre-distortion [Buc 2000, Woo 2003, Cur 2004]. ODC is used in transmission lines to reduce the accumulation of dispersion, and thus, minimize signal distortions at the receiver. An option to realize ODC consists in adding a second fiber span characterized by another chromatic dispersion parameter in such a way to compensate the dispersion accumulated over the principal path. Optical fibers used for ODC are called dispersion compensating fibers (DCFs) with typical β_2 parameters in the 100-130 ps^2/km range at 1550 nm. To obtain these high values of β_2, DCFs are fabricated with sophisticated refractive index profiles and tend to be expensive. In addition DCFs present high loss ($\approx$0.5 dB/km at 1550 nm) that must be compensated with optical amplification increasing hardware costs. DCFs are, therefore, economically justified in the context of high-capacity transport over very large distances. An alternative ODC option is the insertion of FBGs to equalize the group delay between the upper and lower sidebands [Will 1994, Mar 1997, Mor 2004]. Probably the most important advantage of ODC, as an all-optical technique, is its ability to be applied directly in the optical path. It is, however, always difficult to achieve zero dispersion conditions with coherent sources since a very precise control of their emission wavelength is needed. Also in the hypothesis that it was possible, these methods would fit only for one single wavelength. Therefore their use would be prevented in multi-channel environments such as WDM-based networks where the users lie at different locations and the optical paths could dynamically change in terms of distance.

In this context, the electronic predistortion (pre-chirping) operated at the transmitter may be employed. Electronic predistortion is a technique to generate at the transmitter arbitrary dispersion tolerant waveforms. In combination with digital signal processing at the receiver, it opens up the possibility to compensate for dispersion accumulation. In general, the amount of increase dispersion tolerance depends on the degree of complexity affordable at the transmitter for the generation of a specific waveform and at the receiver for the corresponding electronic equalization and processing. However, especially in the receiver stage, the electronic technology, although extensively mature and sophisticated, may impose some limitations on the maximum bit rate of the electrical signal.

Concerning the SSB-AM format, it seems to be the ideal solution against chromatic dispersion impairments since it overcomes totally the CSE and is even more efficient than the DSB-AM format in terms of bandwidth. However, its implementation is not without difficulties [Smi 1997-02, Sie 1997, Hui 2001, Loa 2003, Che 2004]. The practical generation of an optical SSB-AM modulated signal can be made with either an electrical phase shift of the driving signals at the modulator input or inserting an ultra narrowband optical filter at the transmitter or receiver to suppress one sideband at the modulator output. In practice, the first method needs to divide the input electrical signal into two electrical paths with a $\pi/2$ radians phase shift at the same power. Therefore, a MZM must be used. Since the sideband suppression ratio depends on the accuracy of the phase shift and the power balance, such approach has a great difficulty in realizing high sideband suppression ratio over a wide electrical range of frequencies. In contrast, the second method yields to high sideband suppression ratio with good stability at the high frequencies at the expense of introducing some limitations related to the spectral characteristics of the optical filter employed for the sideband suppression. Moreover, both

methods can increase the transmitter complexity. Therefore, the employment of SSB modulation format may be more complex to implement than the conventional DSB format.

3.3.4 Transmission limitations due to the spectral characteristics of the source.

The pulse broadening caused by fiber chromatic dispersion depends also on the spectral power distribution of the optical source, and in particular the source bandwidth. All optical sources used in communications systems do not emit a monochromatic radiation. In practice, they have a certain spectral bandwidth which tends to increase the chromatic dispersion effect. The present subsection is entirely focused on the influence of the optical spectrum emitted by the source over the electrical transfer function of a SMF-system.

In section 3.2, we found that, independently on the modulation format adopted, a factor taking into account the combined effect of chromatic dispersion and spectral distribution of the input optical power appears in the electrical response of the link. We anticipated that such term takes a special relevance for optical sources with a significant width. This term, previously defined in eq. (3.15), is $H_0^{RF}(\Omega)$:

$$H_0^{RF}(\Omega) = \frac{\int_{-\infty}^{+\infty} S_0(\omega) e^{-j\beta_2 L\Omega\Delta\omega} d\omega}{\int_{-\infty}^{+\infty} S_0(\omega) d\omega}$$

Observing the analytical expression of $H_0^{RF}(\Omega)$, it can be noted a great similarity with the well-known analytical structure of a FT operating over two specific domains: the electrical domain in Ω and the optical domain in ω. Mathematically, the existence of a FT relationship between $H_0^{RF}(\Omega)$ and $S_0(\omega)$ explains the reason under which the term $H_0^{RF}(\Omega)$ is simply reduced to a constant P_0 just in the particular case of coherent source with PSD defined as in eq. (3.21). Nevertheless, for optical sources with a finite spectral bandwidth, such condition is no longer verified and $H_0^{RF}(\Omega)$ owns a more complex expression which has to be calculated for a specific form of the PSD distribution.

Using eq. (3.15) we have analytically expressed $H_0^{RF}(\Omega)$ for three typical PSD distributions: (a) Lorentzian, (b) Gaussian, and (c) rectangular (uniform). The first profile, is appropriate to describe the optical emission spectrum of distribute feedback (DFB) lasers. The second profile describes the typical spectral power distribution of a light emitting diode (LED). The last profile is most representative of the combination of a LED with an optical channel selector and, in a first approximation, the spectrum "sliced" portions of ASE-based light sources.

For each case, Table 3.2 shows the analytical expression of the PSD function and the corresponding $H_0^{RF}(\Omega)$ term, where P_0 and $\delta\omega_{3dB}$ are the total average power and the 3dB optical bandwidth of the source, respectively.

Table 3.2 PSD and $H_0^{RF}(\Omega)$ functions for typical non-coherent optical sources.

	(a) Lorentzian	(b) Gaussian	(c) Rectangular
$S_0(\omega)$	$\dfrac{P_0}{\pi} \cdot \dfrac{\left(\dfrac{\delta\omega_{3dB}}{2}\right)}{\left(\Delta\omega\right)^2 + \left(\dfrac{\delta\omega_{3dB}}{2}\right)^2}$	$\dfrac{P_0}{\sqrt{2\pi}} \cdot \dfrac{1}{\delta\omega} \cdot e^{-\left(\frac{\Delta\omega}{\delta\omega}\right)^2}$ $\delta\omega = \dfrac{\delta\omega_{3dB}}{2\sqrt{\ln 2}}$	$\begin{cases} \dfrac{P_0}{\delta\omega_{3dB}} & \|\Delta\omega\| < \dfrac{\delta\omega_{3dB}}{2} \\[2ex] 0 & \|\Delta\omega\| \geq \dfrac{\delta\omega_{3dB}}{2} \end{cases}$
$H_0^{RF}(\Omega)$	$e^{-\left\|\frac{\beta_2 L\Omega \cdot \delta\omega_{3dB}}{2}\right\|}$	$e^{-\left(\frac{\beta_2 L\Omega \cdot \delta\omega}{2}\right)^2}$	$\mathrm{sinc}\left(\dfrac{\beta_2 L\Omega \cdot \delta\omega_{3dB}}{2}\right)$

According to the analytical expression of the source PSD, the term $H_0^{RF}(\Omega)$ corresponding to the Lorentzian and Gaussian profiles exhibits an exponential dependence whereas for the rectangular profile, $H_0^{RF}(\Omega)$ gives the well-known sinc function. Note that all profiles can be used to describe theoretically an ideal coherent source when $\delta\omega_{3dB}$ tends to limit zero. In this case $H_0^{RF}(\Omega)$ tends to the unity, as expected.

We have performed a theoretical study of the term $H_0^{RF}(\Omega)$ by varying the optical 3dB bandwidth parameter $\delta\omega_{3dB}$ according to the values listed in Table 3.3 and considering each of the above defined source spectral profiles. In the theoretical model, we have considered the transmission of an optical source over 10 km of SMF with β_2 = -22.6 ps^2/km at 1550 nm.

Table 3.3 Optical source $\delta\omega_{3dB}$ values used in the theoretical model.

i	0 (—)	1 (—)	2 (—)	3 (—)	4 (—)
$(\delta\omega_{3dB}/2\pi)_i$ (GHz)	0.125	12.5	50	100	500
$\delta\lambda_i$ (nm)	0.001	0.1	0.4	0.8	4

Figure 3.3 plots the frequency behavior of $H_0^{RF}(\Omega)$ in the following cases: (a) Lorentzian profile, (b) Gaussian profile and, c) rectangular profile and using the $\delta\omega_{3dB}$ values of Table 3.3. Fig 3(d) plots the electrical 3dB bandwidth degradation of $H_0^{RF}(\Omega)$ as a function of the optical 3dB bandwidth of the source for the three reference PSD distributions:
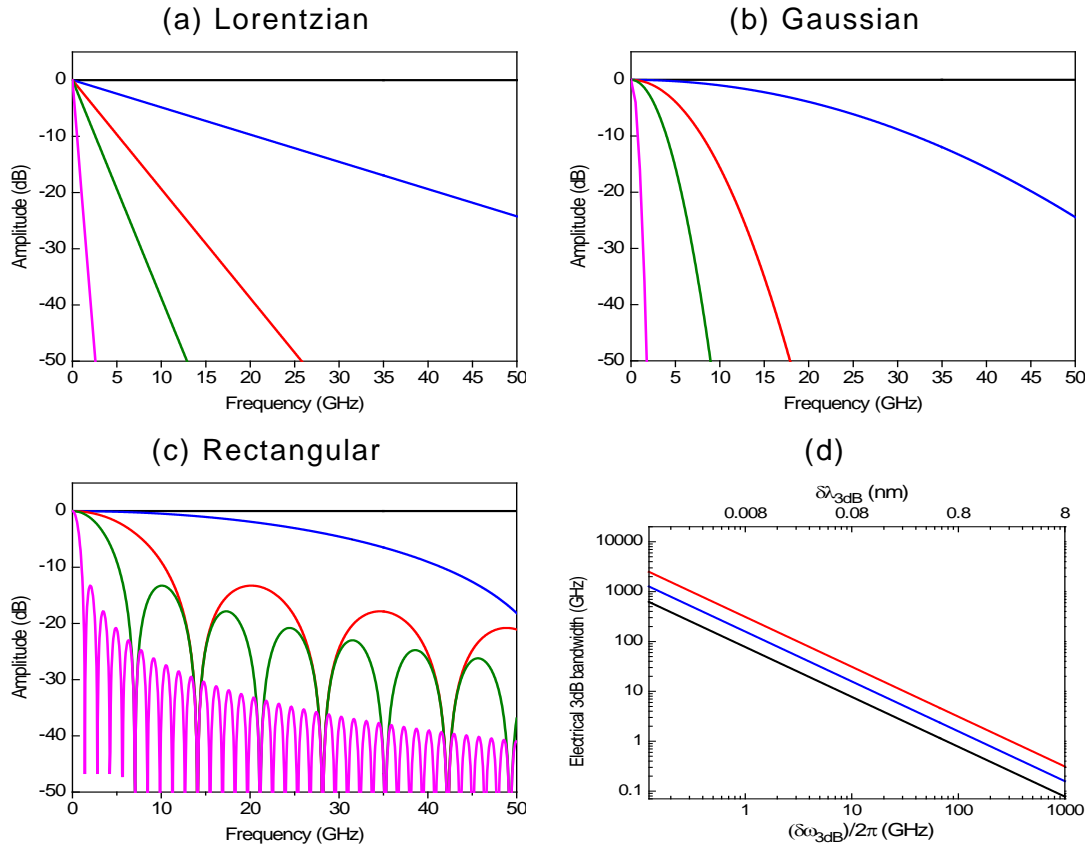
Fig.3.3 Theoretical normalized frequency behavior of $H_0^{RF}(\Omega)$ using an optical source with different values of $(\delta\omega_{3dB})/2\pi$: 0.125 GHz (—), 12.5 GHz (—), 50 GHz (—), and 500 GHz (—) in cases (a) Lorentzian distribution, (b) Gaussian distribution and (c) Rectangular distribution. (d) Electrical 3dB bandwidth degradation vs. source optical 3dB bandwidth for the three reference distributions: Lorentzian (—), Gaussian (—), Rectangular (—).

As shown in Fig. 3.3(a), (b) and (c), the theoretical frequency behavior of $H_0^{RF}(\Omega)$ is strongly influenced by the spectral characteristics of the source and, in particular by the optical source bandwidth. For all profiles, in the best case, that is, when the source optical bandwidth is extremely narrow, the response of $H_0^{RF}(\Omega)$ is frequency-flat and approximates the response that would be obtained employing a monochromatic source. However, as the source bandwidth increases, the electrical behavior of $H_0^{RF}(\Omega)$ becomes frequency selective in the dc region. An increasing/decreasing of the optical source bandwidth induces a narrowing/broadening of the $H_0^{RF}(\Omega)$ function in the dual domain. In the worst case, at the wider source bandwidth, the bandwidth limitation is maximum. The term $H_0^{RF}(\Omega)$ owns, therefore, an electrical low-pass filter characteristic.

Qualitatively, the behavior of $H_0^{RF}(\Omega)$ could have been also predicted thanks to the FT relationship. In fact, by using the scaling property of the FT, if the PSD of the source broadens in the optical domain, the corresponding $H_0^{RF}(\Omega)$ function narrows in the electrical one, and vice versa. The filtering effect is more or less abrupt depending on the source optical bandwidth. Note that, independently on the specific optical source profile and bandwidth, the role of the β_2 parameter is determinant for the

existence of the low-pass effect. In fact, $H_0^{RF}(\Omega)$ would have an all-pass response in absence of chromatic dispersion.

Figure 3.3(d) displays the theoretical 3dB bandwidth degradation of the filter $H_0^{RF}(\Omega)$ as a function of the optical source bandwidth for the three reference profiles. The curves show clearly a common increasing of the selectivity with the source bandwidth. A slight difference is found depending on the profile. For a given $(\delta\omega_{3dB})/2\pi$ parameter, the rectangular profile offers the higher electrical bandwidth.

Once described analytically the $H_0^{RF}(\Omega)$ function, we remind the lector back to the general expression of the electrical transfer function given in eq. (14) which characterize completely the signal propagation over a SMF-based optical transmission system. Here, the term $H_0^{RF}(\Omega)$ appears as a multiplicative factor. Therefore, the low-pass filtering characteristic inherent to $H_0^{RF}(\Omega)$ will reflect directly in the system response independently on the modulation format adopted.

Figure 3.4 shows, for the three modulation formats, the theoretical system responses obtained in case of using an optical broadband source with rectangular profile and a source bandwidth $\delta\lambda_i$ of 4 nm assuming signal propagation over 10 km of SMF and a chromatic dispersion coefficient β_2=-22.6 ps^2/km at 1550 nm. All plots of the first column obey the analytical expressions given in (16), (18) and (19) for (a) DSB-AM, (b) SSB-AM, and (c) PM format, respectively. The theoretical results related to the coherent case given in subsection 3.3.2 have been also plotted in the right column for comparison purposes. From the figure, we observe that the employment of an optical broadband source instead of a coherent source has a strong impact on the electrical transfer function of the system. This modification is carried out by $H_0^{RF}(\Omega)$ which takes into account the effect of the optical source bandwidth.

When DSB-AM format is adopted, the electrical transfer function in Fig. 3.4(a) exhibits a low-pass response whose envelope is governed by $H_0^{RF}(\Omega)$ unless the frequency regions where the CSE notches force a maximum power degradation. The operative range of the system calculated at the 3dB point is given by the electrical bandwidth of the filter $H_0^{RF}(\Omega)$ and, thus, depends on the source width. The theoretical operative range of the link is around 0.6 GHz in perfect agreement with the curve shown in Fig 3.3(d) referred to the source with rectangular profile and width of 4 nm. In Fig. 3.3(d) we can find the theoretical values of the system bandwidth for optical sources up to 8 nm of width. Case (a) of Fig. 4 should be compared with the corresponding right plot referred to a coherent source where the operative bandwidth of the system is determined by the first CSE notch.

For the SSB-AM format, Fig 3.4(b) shows that the only difference with respect to the DSB-AM format is the absence of the power degradation in correspondence of the CSE notches. Since the CSE is no longer present, the electrical response owns the same low-pass profile of the filter $H_0^{RF}(\Omega)$, which is the only dominant factor. Note that, the great advantage of cancelling the CSE effect, brought by the transmission of one electrical sideband (see corresponding right plot), is totally wasted by the employment of a broadband source. In this case, the DSB-AM and SSB-AM formats are practically equivalent from the point of view of the system operative bandwidth.

For phase modulated carriers, the filter $H_0^{RF}(\Omega)$ modifies the amplitude response in the band-pass region provided by the P-I conversion effect around the first two notches (see Fig 3.4(c)). It means that any signal transmitted in such region will be drastically attenuated at the receiver. Therefore, an optical phase modulated broadband source does not allow any signal propagation over the link since the P-I conversion effect also intrinsically precludes the signal transport in the baseband region.
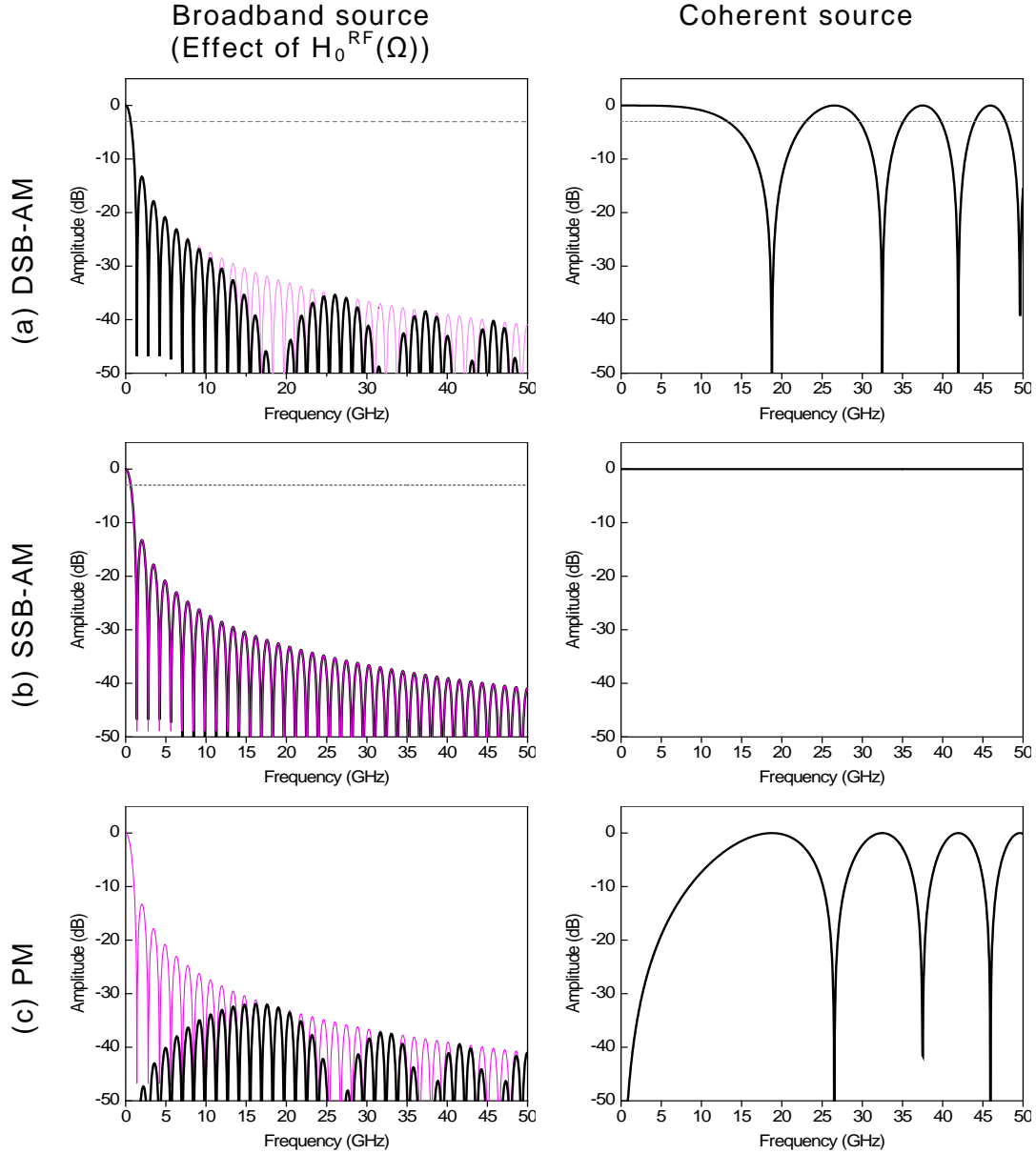
Fig.3.4 Theoretical normalized electrical responses of a 10 Km SMF-based transmission system in case of using an OBS with spectral bandwidth of 4 nm. (a) DSB-AM format, (b) SSB-AM format and (c) PM format. The behavior of the $H_0^{RF}(\Omega)$ term is also included (——). The right plots refer to a coherent source using the corresponding modulation format.

We can conclude that, for all modulation formats considered, an increasing of the optical source width has a detrimental influence on the system response especially for the propagation of high-frequency signals. The amplitude degradation of the system response is imposed by the term

$H_0^{RF}(\Omega)$ whose spectral behavior presents a low-pass characteristic due to the presence of the fiber chromatic dispersion parameter. This is the fundamental fiber chromatic dispersion-induced transmission limitation arising when an optical broadband source is employed. For amplitude modulated carriers with several nanometers of width, the system would only permit the transport of baseband signals with a maximum bandwidth of few hundred of MHz preventing the transmission of GHz signals. For phase modulated carriers the baseband transport is also intrinsically prohibited.

3.4   Transmission over MMF links: impact of modal dispersion.

In section 3.3, the effects of fiber chromatic dispersion have been described emphasizing the influence of the modulation format and the source spectral width over the electrical transfer function of the optical communication system shown in Fig.1 in the specific case of an optical link consisting in a length of SMF operating in third communication band. However, if the SMF channel is substituted by a MMF channel, another source of dispersion, known as modal dispersion, and its corresponding propagation effects over the electrical transfer function of the system must be taken into account. The present section is focused on the description of this aspect with emphasis on the modal dispersion-induced transmission limitations for coherent and broadband sources emitting in the spectral region around 1550 nm.

3.4.1 Description of the modal dispersion mechanism.

When the optical propagation is performed through a MMF, the energy of a single light pulse injected by the source spreads into various light pulses (composite pulse) which are transported by a large number of transversal optical modes. Due to different effective refractive index, each mode propagates at a different group velocity. It means that all modes excited at the fiber input will reach the fiber output with a different group delay. For a fiber length L, if M is the number of modes, the group delays experienced are $\beta_{1q}L$ (q=1..M) where q represents the mode group number and β_{1q} is the specific group delay per unit of length of mode q. Such variety of travel times leads to a time spreading of the original light pulses received at the fiber output. The received composite pulse is a delayed and distorted copy of the transmitted ones. This effect is called modal dispersion and is inherent to MMF propagation. Since the modes are generally not excited equally, the overall shape of the received composite pulse has a smooth profile. The amount of the time interval over which the composite pulse spreads, is governed principally by the β_{1q} parameters of the modes propagating with the smallest and largest velocities. The overall width of the received composite pulse represents the overall response time of the fiber. Modal dispersion is directly proportional to the fractional refractive index change and the fiber length L except for long fibers, where, random irregularities of the fiber surface or homogeneities of the refractive index permit some power exchange between modes adjacent. When a certain critical length is exceeded the pulses broaden at a slower rate proportional to the square root of L [Sal 2001].

In SMF, there is obviously no modal dispersion since only one mode with one group velocity is propagated. The received pulse is, therefore, only a

delayed but not distorted copy of the transmitted one. In contrast, for MMF links, chromatic dispersion is also present affecting the delay times of the pulses associated to individual optical carriers. In multimode step-index fibers, modal dispersion is usually much greater than the chromatic contribution and dominates the response time of the fiber. In multimode graded-index fibers, where the group delay times of the modes are very similar, modal dispersion can be reduced to extremely low values and, thus, the pulse broadening can be comparable to the one induced by chromatic dispersion in SMF. The overall pulse width, in this case, involves both dispersion contributions. However, when such condition is verified, chromatic dispersion may become important, especially in third communication band, depending on the modulation format and spectral width of the source as discussed before in section 3.3.

In any case, the pulse broadening caused by the differential mode delay in MMF propagation may generate ISI limiting the speed at which adjacent pulses can be sent without overlapping at the receiver and, thus, the speed at which the communications system can operate. The response time of a MMF-link is just the width of its impulse response in the time domain. Since the impulse response and the electrical response are related by the FT, the operative bandwidth of the MMF system is inversely proportional to the response time and, thus, is directly affected by both modal and chromatic dispersion sources. Therefore, as for SMF-based links, the system electrical response function continues being a powerful analytical tool to characterize the MMF link in terms of maximum bandwidth-distance performance once provided the modal dispersion effect is taken into account.

There are two theoretical formulations to describe the electrical transfer function of MMF-based links and their related propagation effects. The first one is based on power flow equations [Yab 2000] and the second one employs an electric field propagation model [Gas 2006]. The power flow equations are adequate for the description of digital pulse propagation through MMF but present several limitations either when considering the propagation of analogue signals or when a detailed knowledge of the electrical transfer function is required since, in these situations, the effect of the signal phase may be critical on the behavior of the electrical response due to the omnipresent effect of chromatic dispersion. To overcome these limitations the second method, based on the propagation of electric field signals rather than optical power signals, result more effective and convenient. However, in order to describe the chromatic dispersion characteristic of all the propagating modes, both models consider an average value of the second order dispersion coefficient ($\beta_{2q} \approx \beta_2$, q=1..M) appearing in the Taylor expansion of eq. (3.12). Under this assumption, the combined effect of chromatic dispersion and modal dispersion can be conveniently uncoupled in two separate factors. Relying on the theoretical results presented and validated in [Gas 2006], a general closed-form analytic expression of the electrical transfer function of a MMF link, under the approximation of small signal modulation, is given by:

$$H_{MMF}^{RF}\left(\Omega\right) = H_{Chromatic}^{RF}\left(\Omega\right) \cdot H_{Modal}^{RF}\left(\Omega\right) \quad (3.25)$$

where the chromatic contribution, namely $H_{Chromatic}{}^{RF}(\Omega)$, is defined as:

$$H_{Chromatic}^{RF}\left(\Omega\right)=\left(\frac{\Re Z_L}{2\pi^2}\right)P_0s_0e^{-\alpha L}e^{-j\beta_1 L\Omega}\left(s_{-1}^*e^{\frac{j\beta_2 L}{2}\Omega^2}+s_1e^{-\frac{j\beta_2 L}{2}\Omega^2}\right)H_0^{RF}\left(\Omega\right) \quad (3.26)$$

and the modal contribution, $H_{Modal}{}^{RF}(\Omega)$, is given by:

$$H_{Modal}^{RF}\left(\Omega\right)=\sum_{q=1}^{M}2q\left(C_q+G_q\right)e^{-2\alpha_q L}e^{-j\beta_{1q}L\Omega} \quad (3.27)$$

As observed in eq. 3.26, the chromatic contribution of eq. (3.25) corresponds to the electrical transfer function of the SMF case once we have considered all guided modes having the same second order dispersion coefficient, β_2.

The modal contribution, defined in (3.27), is inherent to MMF propagation. It contemplates the modal dispersion effect arising by the simultaneous propagation of the M modes. The modal term can be considered as a microwave transversal filter where each sample corresponds to a different mode group q carried by the fiber. Each sample is time delayed by a specific amount β_{1q} corresponding to the group delay of its mode group q. This term takes into account also for the modes attenuation. The amplitude of the samples depends on the modal attenuation, α_q, and the sum of coefficients Cq and Gq which take into account the power coupling between propagating modes.

As the lector may observe, under the assumption of considering the same value of the second order dispersion parameter for all mode groups, the electrical transfer function of a MMF links own a very compact structure similar to the SMF case. Indeed, such assumption permits to associate the same chromatic dispersion contribution to all modes (as only one mode was propagating over the fiber) and to describe the overall intermodal dispersion-induced effects by means of a weighted summation of modal group delays. Therefore the same considerations made in section 3.3 regarding the transmission limitations induced by chromatic dispersion over the electrical response apply also if the signal transport is performed over MMF. The substantial difference between the two types of fiber is pointed out by the modal term which gives rise to amplitude fluctuations in the electrical response whose amplitude, in absence of modal noise, is governed by the amplitude of the coupling coefficients through the β_{1q} parameter.

Actually, modal noise is another difficulty inherent to MMF propagation and is directly related to the random interference of the modes [Dai 1979, Kan 1984]. The origin of such mechanism can be understood as follows. As a result of uncontrollable mechanical disturbances, such as vibrations and micro-bends as well as temperature fluctuations, each mode undergoes a random phase shift so that the sum of the complex amplitude of the modes has an intensity which fluctuates randomly with time. This randomness is a form of additive noise known as modal noise which leads to small fluctuations in the optical received power and, thus, in the electrical transfer function of the system. The effect of modal noise is very similar to the multipath transmission fading of radio-signals.

In [Gas 2008-01] the statistical fluctuations due to modal noise in radio over fiber signals propagated through a graded-index MMF have been

deeply investigated. It has been confirmed that the modal noise is strongly related to the coherence properties of the optical source. Modes interference occurs, in fact, only if the coherence time of the emitted light is larger than the intermodal delay time. Therefore, the modal noise can be reduced by increasing the spectral width of the optical source. For broadband sources the optical bandwidth is large enough that the above condition is satisfied. It is another reason for which most MMF-based lightwave systems use LEDs to avoid the modal-noise problem. Modal noise becomes a serious problem when semiconductor lasers are used. It has been also demonstrated that modal noise is independent on the frequency of the modulating signal, while the evaluation of the modal noise in function of the link length showed that it becomes almost negligible for distances above the 3 Km. For shorter distances the random fluctuations of modal noise become comparable with the amplitude fluctuations caused by the modal dispersion. This behavior, however, widely supports the feasibility of implementing high-frequency radio over fiber transmission through MMF links for short and middle reach distances employing coherent sources.

3.4.2 Transmission limitations for coherent sources.

In graded-index MMF-based systems employing coherent sources operating in third communication band, the principal limitation over the operative transmission bandwidth arises from the combined effect of chromatic and modal dispersion. In particular, the chromatic effect depends on the modulation format adopted as for coherent sources the low-pass effect due to the source width is negligible. The presence of modal dispersion implies a certain phase coupling between modes during propagation. The resulting effect over the electrical response is represented by statistic amplitude fluctuations whose amount is directly proportional to the L for short to middle distance links.

The electrical response of the system shown in Fig. 3.1 has been obtained theoretically in case of employing an optical DSB-AM modulated coherent source emitting a monochromatic radiation at 1550 nm and transmitted over a 62.5 µm graded-index MMF with β_2=-18.47 ps/km^2. In the theoretical model we have used center-launching technique in order to guarantee robustness against the offset between the fiber connectors, fiber bending and fiber shaking [Haa 1993, Rad 1998, Yam 2007, Sim 2007]. Figures 3.5 (a) and (b) plot the normalized electrical response obtained for 1 km and 5 km of MMF, respectively.

In Fig. 3.5(a) we can observe the amplitude fluctuation in the electrical response due to modal dispersion. However, it is not higher than 1 dB and does not induce a significant attenuation of the signal. Since the transmission is tested over 1 km of MMF, the CSE power fading inherent to the DSB-AM modulation format is not influent in the dc-20 GHz range, as for 1 km the first CSE notch appears around frequency 65 GHz. In this case, the MMF transport of both baseband and high frequency signals is clearly viable over the entire electrical operative range dc-20 GHz. We remark the 20 GHz limitation is just inherent to the bandwidth characteristics of the modulator and photodetector used in the theoretical model.

The curve obtained in Fig. 3.5(b) for the 5 km case, exhibits a slightly different behavior. Firstly, the amplitude fluctuation is more pronounced

(around 1.7 dB) due to an increasing of the temporal mode spreading with the distance. This value tends to increase at longer distances and may cause an important electrical power penalty independently on the electrical frequency. Secondly, for a length of 5 km, the first CSE notch appears around 30 GHz and causes the power fading observed at higher frequencies in the electrical response. As for SMF, the CSE would further limit the operative range of the system at longer distances as discussed in section 3.3.

(a)   (b)
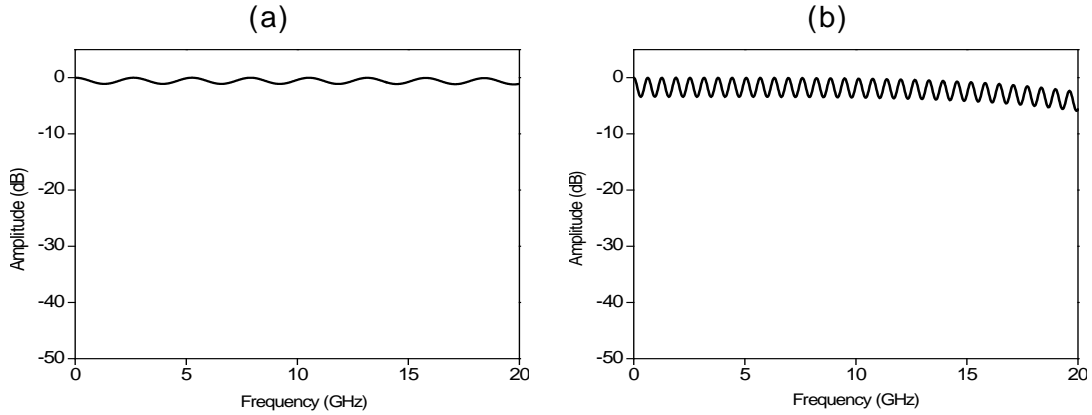
Fig.3.5 Theoretical normalized electrical response of a MMF-based transmission system excited by a DSB-AM modulated coherent source emitting at 1550 nm and propagated over (a) 1 km and (b) 5 km of MMF.

3.4.3 Transmission limitations employing broadband sources.

Commercially available MMFs are still optimized for signal transmission in second communication bandwidth. Here, since chromatic dispersion is minimal, the requirement for a narrow spectral width of the source is not so crucial and allows the combination of MMF transmission with broadband LED sources to achieve a great minimization of transceiver and infrastructure costs. For this reason, MMFs and LEDs have been widely proposed for last mile applications. Here, the transmission performance was only limited by fiber attenuation and modal dispersion. However, in the last years, the widespread use of WDM technology has pushed many research efforts to develop techniques to operate in third communication band which was initially rejected due to chromatic dispersion. Here, the principal bandwidth limitation of a MMF link strongly depends on the combined effect of chromatic dispersion and modal dispersion.

In this context, only the use of high quality lasers would permit 1550 nm operations with an increasing of the operative bandwidth up to few GHz km once the modal noise can be neglected. By contrast, with optical broadband sources, the bandwidth limitations would become strongly susceptible to the source spectral width just as occurred in the SMF case. Here, the low-pass filtering effect of $H_0(\Omega)$ would be the dominating source of transmission limitations.

We have theoretically obtained the electrical transfer function in case of replacing the coherent source with a 38.4 nm-wide LED emitting in the third band and using a 5 km length of 62.5 µm graded-index MMF with β_2=-18.47 ps/km^2. In particular, in order to investigate the dependence of the electrical response on the width of the source, the LED is followed by an optical channel controller (OCC) operating in the same band. The OCC

permits to modify the bandwidth of the source by filtering a maximum number of 48 channels spaced by 0.8 nm from the input LED spectrum, emulating a source with a variable width and an arbitrary power spectral profile. In the model the power spectral profile has been kept rectangular. Figure 3.6 shows the theoretical normalized electrical response for different line widths.
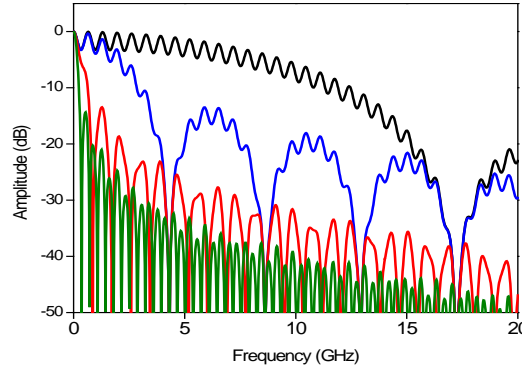
Fig.3.6 Theoretical electrical responses of a 5 km MMF-based link excited by a LED source of width 0.8 nm (—), 3.2 nm (—), 16 nm (—) and 38.4 nm (—).

The responses of Fig. 3.6 demonstrate that also when the propagation is made over MMF, the operative electrical 3dB bandwidth of the amplitude response strongly depends on the optical source width through the presence of $H_0(\Omega)$. The minimum low-pass selectivity is found for the 1-channel equivalent source which has the minimum width of 0.8 nm. As more channel are added, the equivalent source width imposes a more abrupt filtering effect. The transmission bandwidth is reduced to a minimum value around 0.2 GHz in case of simulating the original LED source of 38.4 nm. In all cases, the modal dispersion-induced fluctuations are also present. However, the curves show that the dominant transmission limitation is clearly represented by the source width. Similar results have been achieved simulating the SSB and PM formats. Therefore, we can conclude that independently on the modulation format adopted, the transport of GHz signals over MMF is not permitted when a broadband source is employed instead of coherent lasers at the transmitter. The dependence of the electrical transmission range on the spectral width of the source is similar to the one found in SMF links.

3.5   Summary.

In this chapter we have theoretically described the fundamental issues and transmission limitations of IM-DD optical communication systems adopting external modulation of the optical carrier in conventional amplitude and phase modulation formats. It has been demonstrated that, for SMF transmission in third communication band (1550 nm) the principal cause of signal distortion and amplitude degradation of the electrical response is represented by the chromatic dispersion. Chromatic dispersion manifests itself with two principal effects. The first one is a power fading of the electrical response related with the modulation format of the optical carrier. Modulation formats such as DSB-AM and PM are particularly

influenced by such effect as the transport of RoF signals may be not permitted at frequencies close to the amplitude notches arising in the electrical response. The notch frequency depends on the link parameters, such as, the second-order dispersion coefficient β_2 and the length L. In third transmission band, the notches moves toward lower frequencies as the link distance increases. The position of first notch is particularly important since it defines the electrical bandwidth of the system.

For DSB-AM format such effect is known as CSE and the position of the first notch is particularly important since it defines the operative electrical bandwidth of system. For PM format the CSE transforms into its complementary function known as PM-IM effect. The power fading of the PM-IM effect owns a band-pass characteristic where the transmission of radio signals is allowed. The band-pass region starts at dc (first notch) and extends to the second notch frequency whose value depends on the $\beta_2 L$ parameter through a sin-like function. The presence of a dispersive link allows phase modulated carriers to be directly photodetected without the necessity of employing coherent detection schemes. In this context, we see chromatic dispersion as a positive factor since it enables the employment of phase modulators. The electrical response obtained with the generation and propagation of one single electrical sideband is free from CSE-induced penalties. However, the implementation of the SSB-AM format requires additional devices which may be too complex and not practical for optical access applications.

The second effect of chromatic dispersion is directly associated to the spectral characteristics of the source. Concerning this aspect, the difference between coherent sources and broadband source must be clearly remarked since the width of the source plays an important role in the final determination of the transmission capacities of the system. We have found that chromatic dispersion creates a strongly dependence between the operative bandwidth of the system and the spectral bandwidth of the source. This effect is taken into account by the factor $H_0(\Omega)$ in the electrical transfer function. The analytical form of $H_0(\Omega)$ (see eq. (3.15)) has a frequency selective characteristic typical of a low-pass electrical filter whose response depends on the source bandwidth. In particular, an increasing/decreasing of the optical source bandwidth produces a narrowing/broadening of the $H_0^{RF}(\Omega)$ function in the dual electrical domain. Such low-pass filter characteristic reflects in the electrical response. When coherent sources are employed, the effect of $H_0^{RF}(\Omega)$ can be neglected. However, for broadband sources it becomes the dominant transmission limitation which prevents the transport of high frequency signals. For broadband sources with several nanometers of bandwidth, the capacity of the system is reduced to few hundred of MHz whereas coherent sources allows the transport in a bandwidth of few tens of GHz. The hard limitation caused by the source bandwidth is independent on the modulation format.

In MMF links another source of dispersion is modal dispersion inherent to the propagation delays of several guided mode groups. The mechanism of modal dispersion is governed by the group delay parameter of each mode and analytically is expressed by a multiplicative factor which takes into account for the modal delay, as well as the attenuation and coupling of the modes. The effect of multi mode propagation over the electrical transfer function is represented by amplitude fluctuations whose amount increases with the link distance. For short-to-medium distances typical of in-building

networks and last-mile access such fluctuations does not cause excessive power penalty on the received signal and the high-frequency transport is just limited by the chromatic dispersion effects in third communication band. Modal noise arising by the statistical behavior of the optical intensity received also leads to small fluctuations in the electrical transfer function. Modal noise is pronounced when the coherence time of the emitted light is larger than the intermodal delay time. Therefore, it can be avoided by employing broadband sources. For coherent sources modal noise becomes negligible only for distances above few kilometers.

In order to cover short-to-medium distances, the employment of multimode fiber is attractive because MMF is easy to fabricate, to connect and manipulate in combination with broadband sources for further minimization of hardware costs and the inherent reduction of modal noise contribution. However, due to the source width induced limitations, broadband sources are not devised to transmit modulated signals at frequencies either than baseband. For this reason the employment of MMF for RoF applications in third communication band has been only proposed in combination with coherent sources such as LEDs(???seria lasers???). In this context, different advanced and complex strategies have been proposed to improve the bandwidth distance product including mode group diversity multiplexing (GDM) [Koo 2006, Sch 2006], optical frequency multiplication (OFM) [Lar 2006] and multiple input multiple output (MIMO) transmission [Gre 2008] in addition to two more conventional techniques such as the electrical SCM [Kan 2003, Ami 2007] and its combination with optical WDM [Tyl 2003,Gas 2008-02].

The SCM technique is especially interesting for both SMF- and MMF-based links since it provides the potential convergence of both wired FTTx and wireless RoF signals over the same fiber infrastructure. Another important approach to force less intermodal dispersion consists in reducing the number of modes propagated through the fiber by means of practical mode filtering implementations at the transmitter and/or receiver side, [Haa 1993, Rad 1998, Yam 2007, Sim 2007]. The transmitter side mode-filtering is performed by exciting a limited number of lower order modes in the MMF and thus coupling only a small portion of the total power into the rest of the transmitted modes. Using this approach in combination with WDM techniques and low width lasers has recently pushed the capacity of MMF links toward THz·Km [Gas 2008-02].

However, the employment of OBSs for RoF transmission in SMF and MMF systems and networks still needs a significant improvement in order to offer transmission capabilities comparable to those permitted by coherent sources. Such improvement constitutes the central topic of next chapter and is the first innovative contribution of the thesis.

3.6   References.

[Ami 2007]   M. Amin, E.-A. Diab, J. D. Ingham, R. V. Penty, I. H. White, "10-Gb/s Transmission on Single-Wavelength Multichannel SCM-Based FDDI-Grade MMF Links at Lengths Over 300 m: A Statistical Investigation", J. Lightwave Technol., Vol 25, pp. 2976-2983, 2007.

[Buc 2000]   F. Buchali, H. Bülow, W. Baumert, R. Ballentin, and T. Wehren, "Reduction of the chromatic dispersion penalty at 10 Gbit/s by integrated electronic equalizers", in Technical Digest Optical Fiber Communication Conference, OFC'00, Baltimore, Maryland, U.S.A., pp. 268-270, Paper ThS1, March 2000.

[Cap 2005]   J. Capmany, B. Ortega, D. Pastor, S. Sales, "Discrete-time optical processing of microwave signals", J. Lightwave Technol., Vol. 23, pp. 702-723, 2005.

[Che 2004]   W. H. Chen, W. I. Way, "Multichannel Single-Sideband SCM/DWDM Transmission Systems", J. Lightwave Technol., Vol. 22, pp. 1679-1693, 2004.

[Chi 2009]   H. Chi, X. Zou, J. Yao, "Analytical Models for Phase-Modulation-Based Microwave Photonic Systems With Phase Modulation to Intensity Modulation Conversion Using a Dispersive Device", J. Lightwave Technol., Vol. 27, pp. 511-521, 2009.

[Cor 2001]   J. L. Corral, J. Marti, J. M. Fuster, "General expressions for IM/DD dispersive analog optical links with external modulation or optical up-conversion in a Mach-Zehnder electrooptical modulator", IEEE Trans. Microwave. Theory Tech., Vol. 49, pp. 1968-1976, 2001.

[Cur 2004]   V. Curri, R. Gaudino, A. Napoli, P. Poggiolini, "Electronic equalization for advanced modulation formats in dispersion-limited systems", IEEE Photon. Technol. Lett., Vol. 16, pp. 2556-2558, 2004.

[Dai 1979]   B. Daino, G. de Marchis, S. Piazzolla, "Analysis and measurement of modal noise in an optical fibre", Electron. Lett., Vol. 15, pp. 755-756, 1979.

[Gas 2006]   I. Gasulla, J. Capmany, "Transfer function of multimode fiber links using an electric field propagation model: Application to Radio over Fibre Systems", Opt. Express, Vol. 14, pp. 9051-9070, 2006.

[Gas 2008-01]   I. Gasulla, J. Capmany, "Modal noise impact in Radio over Fiber multimode fiber links", Opt. Express, Vol. 16, pp. 121-126, 2008.

[Gas 2008-02]   I. Gasulla, J. Capmany, "1 Tb/s·km Multimode fiber link combining WDM transmission and low-linewidth lasers", Opt. Express, Vol. 16, pp. 8033-8038, 2008.

[Gna 1991]   A. H. Gnauck, S. K. Korotky, J. J. Veselka, J. Nagel, C. T. Kemmerer, W. J. Minford, D. T. Mower, "Dispersion penalty reduction using an optical modulator with adjustable chirp", presented at the Topical Meeting Integrated Photon. Res., Monterrey, CA, Apr. 1991.

[Gre 2008]   M. Greenberg, M. Nazarathy, M. Orenstein, "Efficient hierarchical list decoder for massive optical MIMO Transmission", Opt. Express, Vol. 16, pp. 718-724, 2008.

[Haa 1993]   Z. Haas and M. A. Santoro, "A mode-filtering scheme for omprovement of the bandwidth-distance product in multimode fiber systems", J. Lightwave Technol., Vol. 11, pp. 1125-1131, 1993.

[Hui 2001]   R. Hui, B. Zhu, R. Huang, C. Allen, K. Demarest, D. Richards, "10-Gb/s SCM Fiber System Using Optical SSB Modulation", IEEE Photon. Technol. Lett., Vol 13, pp. 896-898, 2001.

[Kan 1984]   T. Kanada, "Evaluation of Modal Noise in Multimode Fiber-optic Systems", J. Lightwave Technol., Vol. 5, pp. 11-18, 1984.

[Kan 2003]   S. Kanprachar, I. Jacobs, "Diversity of coding for subcarrier multiplexing on multimode fibers", IEEE Trans. Commun., Vol. 51, pp. 1546-1553, 2003.

[Knu 2002]   S. N. Knudsen, "Design and manufacture of dispersion compensating fibers and their performance in systems", in Technical Digest Optical Fiber Communication Conference, OFC'02, Anaheim, California, U.S.A., pp. 330-332, Paper WU3, March 2002.

[Koo 2002]   A. M. J. Koonen, H. P. A. van den Boom, F. Willems, J. W. M. Bergmans, G. D. Khoe, "Broadband multiservice in-house networks using mode group diversity multiplexing", in *Proceedings of POF conference,* pp. 87-90, 2002.

[Lar 2006]   M. G. Larrode, A. M. J. Koonen, J. J. V. Olmos, A. Ngoma, "Bidirectional radio-over-fiber link employing optical frequency multiplication", IEEE Photon. Technol. Lett., Vol. 18, pp. 241-243, 2006.

[Loa 2003]   A. Loayssa, C. Lim, A. Nirmalathas, D. Benito, "Optical Single-Sideband Modulator for Broad-Band Subcarrier Multiplexing Systems", IEEE Photon. Technol. Lett., Vol. 15, pp. 311-313, 2003.

[Mar 1997]   J. Marti,. J.M. Fuster, R.I. Laming, "Experimental reduction of chromatic dispersion effects in lightwavemicrowave/millimetre-wave transmissions using tapered linearly chirped fibre gratings", Electron. Lett., Vol. 33, pp. 1170-1171, 1997.

[Mar 2001]   J. Martí, F. Ramos, J. Herrera, "Experimental Reduction of Dispersion-Induced Effects in Microwave Optical Links Employing SOA Boosters", IEEE Photon. Technol. Lett., Vol.13, pp. 999-1001, 2001.

[Mor 2004]   M. Morin, M. Poulin, A. Mailloux, F. Trépanier, Y. Painchaud, "Full C-band slope-matched dispersion compensation based on a phase sampled Bragg grating", in Technical Digest Optical Fiber Communication Conference, OFC'04, Los Angeles, California, U.S.A., Paper WK1, February 2004.

[Nie 2000]   L. G. Nielsen, S. N. Knudsen, B. Edvold, T. Veng, D. Magnussen, C. C. Larsen, H. Damsgaard, "Dispersion compensating fibers", Optical Fiber Technology, Vol. 6, pp. 164-180, 2000.

[Pol 1999]   V. Polo, J. Marti, F. Ramos, "Mitigation of chromatic dispersion effects employing electroabsorption modulator-based transmitters", IEEE Photon. Technol. Lett., Vol. 11, pp. 883-885, 1999.

[Rad 1998]   L. Raddatz, I. H. White, D. G. Cunningham, M. C. Nowell, "An Experimental and Theoretical Study of the Offset Launch Technique for the Enhancement of the Bandwidth of Multimode Fiber Links", J. Lightwave Technol., Vol. 16, 324-331, 1998.

[Ram 1998]   F. Ramos, J. Marti, V. Polo, J.M. Fuster, "On the use of fiber-induced self-phase modulation to reduce chromatic dispersion effects in microwave/millimeter-wave optical systems", IEEE Photon Technol. Lett., Vol. 10, pp.1473-1475, 1998.

[Sal 2001]   B. E. A. Saleh, M. C. Teich, "Fundamentals of Photonics", (John Wiley & Sons, Inc), 2001.

[Sch 06]   S. Schoellmann, C. Xia, W. Rosenkranz, "Experimental Investigations of Mode Group Diversity Multiplexing on Multimode Fibre", in Optical Fiber Communication Conference and Exposition and The National Fiber Optic Engineers Conference, Technical Digest (CD) (Optical Society of America, 2006), paper OWR3.

[Sie 1997]   M. Sieben, J. Conradi, D. Dodds, B. Davis, S. Walklin, "Optical signal sideband (OSSB) transmission for dispersion avoidance and electrical dispersion compensation in microwave subcarrier and baseband digital systems", Electron. Lett., Vol. 33, pp. 971-973, 1997.

[Sim 2007]   D. H. Sim, Y. Takushima, Y. C. Chung, "Transmission of 10-Gb/s and 40-Gb/s signals over 3.7 km of multimode fiber using mode-field matched center launching technique", in Proceedings of OFC 2007, (Anaheim, USA, 2007), OTuL3.

[Smi 1997-01]   G. H. Smith, D. Novak, Z. Ahmed, "Overcoming Chromatic-

Dispersion Effects in Fiber-Wireless Systems Incorporating External Modulators", IEEE Trans. Microwave. Theory Tech., Vol. 45, pp. 1410-1415, 1997.

[Smi 1997-02]   G. H. Smith, D. Novak, Z. Ahmed, "Technique for optical SSB generation to overcome fiber dispersion penalties in fibre-radio system", Electron. Lett., Vol. 33, pp. 74-75, 1997.

[Tyl 2003]   E. J. Tyler, P. Kourtessis, M. Webster, E. Rochart, T. Quinlan, S. E. M. Dudley, S. D. Walker, R. V. Penty, I. H. White, "Toward Terabit-per-second capacities over multimode fiber links using SCM/WDM techniques", J. Lightwave Technol., Vol. 21, pp. 3237-3243, 2003.

[Will 1994]   J. A. R. Williams, I. Bennion, K. Sugden, N. J. Doran, "Fibre dispersion compensation using a chirped in-fibre Bragg grating", Electron. Lett., Vol. 30, pp. 985-987, 1994.

[Woo 2003]   S. Woodward, S.-Y. Huang, M. Feuer, and M. Boroditsky, "Demonstration of an electronic dispersion compensator in a 100 km 10 Gb/s ring network", IEEE Photon. Technol. Lett., Vol. 15, pp. 867-869, 2003.

[Yab 2000]   G. Yabre, "Comprehensive Theory of Dispersion in Graded-Index Optical Fibers", J. Lightwave Technol., Vol. 18, pp. 166-177 (2000).

[Yam 2007]   S. S. Yam and F. Achten, "Toward 100 Gbits/s Ethernet with broad wavelength window multimode fiber", J. Opt. Netw., Vol. 6, pp. 527-534, 2007.

[Yao 2005]   J. Yao, G. Maury, Y. Le Guennec, B. Cabon, "All-Optical Subcarrier Frequency Conversion Using an Electrooptic Phase Modulator", IEEE Photon. Technol. Lett., Vol 17, pp. 2427-2429, 2005.

[Zen 2005]   F. Zeng, J. Yao, "All-Optical Microwave Mixing and Bandpass Filtering in a Radio-Over-Fiber Link", IEEE Photon. Technol. Lett., Vol 17, pp. 899-901, 2005.

Chapter 4

Chromatic dispersion-tolerant optical transmission systems based on optical broadband sources and Mach-Zehnder interferometers

4.1 Optical transmission system adapted to RoF signal transport.

In chapter 3, we have theoretically described the electrical response of a traditional optical transmission system where, using the IM-DD scheme, externally modulated optical carriers are propagated over a dispersive link. The analysis has been performed in case of employing coherent sources or broadband sources both operating in third communication band taking into the account amplitude and phase modulation formats.

It has been demonstrated that, when the transmission is performed over a dispersive SMF link, fiber chromatic dispersion is the most important source of impairments. Apart from the power fading effects (CSE and PM-IM) inherent to the signal propagation of DSB-AM and PM carriers, respectively, the electrical operative range of the system is severally influenced and limited by the mutual interaction between chromatic dispersion and the spectral characteristics of the input optical source, in particular the spectral width. Such limitation is caused by the presence of the term $H_0^{RF}(\Omega)$ in the electrical response expressed in the general eq. (3.14) of Chapter 3. The factor $H_0^{RF}(\Omega)$ is defined in eq. (3.15) and acts as a low-pass electrical filter in such a way that the low-pass characteristic, observed in the electrical response, is more abrupt as the spectral width of the optical source increases. The low-pass effect depends on the spectral width of the source and is independent on the optical modulation format adopted as well as the type of optical fiber. Unlike coherent optical sources, for broadband sources the transport of signals is restricted to an electrical operative range of few MHz especially in third transmission band where fiber chromatic dispersion effect is more significant. Such transmission limitation, therefore, completely prevents the transport of radio signals, and thus, radio over fiber applications. In other words, it means that the employment of a broadband source for RoF applications would be unviable, in principle.

In this context, the main objective pursued throughout the chapter is to demonstrate a new dispersion-tolerant optical transmission system oriented to the RoF signal transport using broadband sources emitting in the 1550 nm region. The key of our approach is the insertion of a MZI structure to optically enhance the operative electrical bandwidth achievable in OBS-based optical transmission links in order to reach good performance comparable with that obtained with optical coherent sources.

4.1.1 Theoretical description of the transmission architecture.

Figure 4.1 illustrates the first proposed configuration of an OBS-based optical transmission system tolerant to dispersion adapted to RoF signal transport.
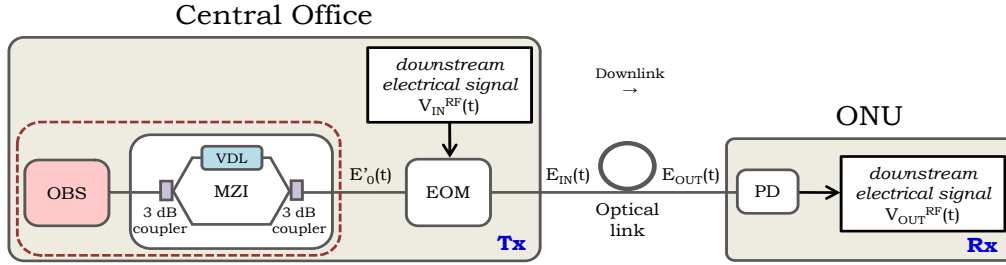
Fig. 4.1 First optical transmission system tolerant to dispersion. The MZI is located before the EOM.

The architecture is composed by a CO connected to an ONU by a dispersive SMF link. The CO and the ONU are both composed of a transmitter (Tx) and a receiver (Rx) part described as follows.

Focusing on the downlink, in the CO, an OBS operating in third transmission band generates the optical carrier wavelength. Before entering the EOM, the optical field runs through a MZI structure. The optical signal resulting from the combined OBS-MZI subsystem is modulated by the downstream electrical signal via EOM. The modulated optical signal is launched into a dispersive optical link. After propagation, it reaches the ONU receiver where is photodetected in order to recover the downstream electrical signal.

The MZI is an optical device with one input and one output port. It is formed by two optical 3dB 1x2 power couplers with an optical variable delay line (VDL) inserted in one of the two fiber arms. The function of the VDL is to set a certain variable propagation time delay between the two branches of the MZI. A schematic representation of the MZI is given in fig. 4.2(a).

(a)   (b)
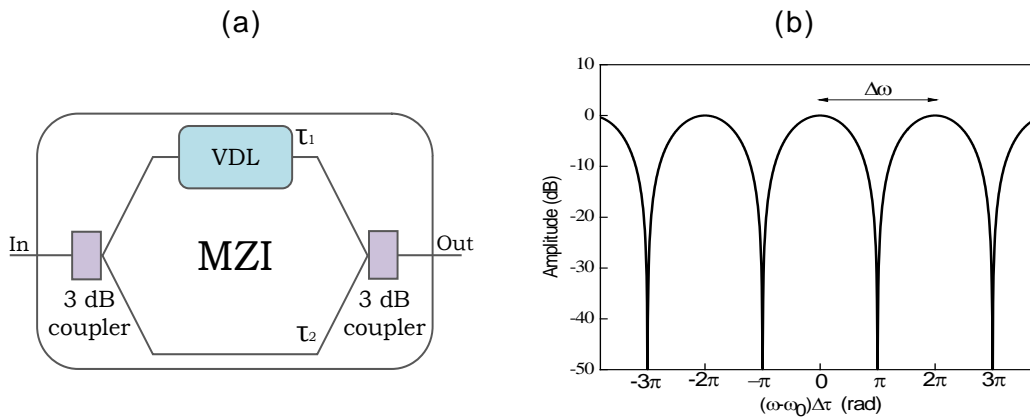
Fig. 4.2 (a) Scheme of a tunable MZI, (b) Normalized theoretical amplitude response of the MZI for a time delay $\Delta\tau = 80$ ps between the two arms.

In order to express the optical response of the MZI structure, we assume an equal power splitting and same states of polarization of the two MZI branches. Under these conditions, the optical response of the MZI can

be expressed as [Agr 2001]:

$$H_{MZI}(\omega) = \frac{1}{\sqrt{2}}\left[e^{-j(\omega-\omega_0)\tau_1} + e^{-j(\omega-\omega_0)\tau_2} \right] \quad (4.1)$$

Where τ_1 and τ_2 are the optical delay for each MZI branch. We define $\Delta\tau = \tau_1 - \tau_2$ as the differential time delay between both MZI branches which is related to the optical frequency periodicity $\Delta\omega = 2\pi/\triangle\tau$ as plotted in Fig. 2(b). The amplitude response exhibits a spectrum periodicity determined by the time delay $\Delta\tau$.

As the lector may observe, the transmission system described in Fig. 4.1 is a particular case of the general architecture of a traditional IM-DD optical transmission system described in Fig. 3.1 where the optical source block of the transmitter is now represented by the subsystem OBS-MZI, being the MZI located just before the optical modulator. The term $E'_0(t)$ is the corresponding generated optical field whose frequency domain representation is simply the product between the optical spectrum of the field emitted by the source, $E_0(\omega)$, and the optical response, $H_{MZI}(\omega)$, of the MZI defined in eq. (4.1). In terms of PSD function, such optical field can be expressed as:

$$S'_0(\omega) = S_0(\omega) \cdot \frac{1}{2}\left[1 + \cos\left((\omega-\omega_0)\Delta\tau\right) \right] \quad (4.2)$$

where $S_0(\omega)$ is the PSD of the optical source and the second term of eq. 4.2 is the power transfer function, $|H_{MZI}(\omega)|^2$, of the MZI.

Following the same steps of the theoretical description of Chapter 3, we find that the presence of this new subsystem modifies the general expression (3.11) of the overall photodetected electrical signal and, in particular, the optical source contribution term. Therefore, eq. (3.11) can be rewritten by substituting $S'_0(\omega)$ for $S_0(\omega)$ and, assuming that the signal propagation is realized over a dispersive length of SMF, the analytical expression of the output voltage is given by:

$$
\begin{cases}
V_{OUT}^{RF}(t) = \left(\dfrac{\Re Z_L}{4\pi^2}\right)\displaystyle\sum_{k=0}^{\infty} p_k e^{jk\Omega t} \\[2em]
p_k = e^{-\alpha L} e^{-j\beta_1 L(k\Omega)} e^{j\frac{1}{2}\beta_2 L(k\Omega)^2} \left(\displaystyle\sum_{n=-\infty}^{\infty} s_n s_{n-k}^* e^{-jn\beta_2 L(k\Omega^2)}\right) \left(\begin{array}{l} \dfrac{1}{2}\displaystyle\int_{-\infty}^{+\infty} S_0(\omega) e^{-j\beta_2 L(k\Omega)\Delta\omega}d\omega + \\[1.5em] +\dfrac{1}{2}\displaystyle\int_{-\infty}^{+\infty} S_0(\omega)\left[\cos\left((\Delta\omega)\Delta\tau\right)\right]e^{-j\beta_2 L(k\Omega)\Delta\omega}d\omega \end{array}\right)
\end{cases} \quad (4.3)
$$

Finally, under the assumption of small signal modulation, the above equation simplifies in:

$$
\left\{
\begin{aligned}
V_{RF}^{OUT}\left(t\right) &\approx \left(\frac{\Re Z_L}{4\pi^2}\right)\left(p_0 + p_1 e^{j\Omega t} + p_1^* e^{-j\Omega t}\right) \\
p_0 &= \frac{P_0}{2} e^{-\alpha L}\left(\left|s_0\right|^2 + \left|s_1\right|^2\right)\left(H_0^{RF}\left(0\right) + \frac{1}{2}H_0^{RF}\left(-\Omega_0\right) + \frac{1}{2}H_0^{RF}\left(+\Omega_0\right)\right) \\
p_1 &= P_0 s_0 e^{-\alpha L} e^{-j\beta_1 L\Omega}\left(s_{-1}^* e^{j\frac{\beta_2 L}{2}\Omega^2} + s_1 e^{-j\frac{\beta_2 L}{2}\Omega^2}\right)\left(H_0^{RF}\left(\Omega\right) + \frac{1}{2}H_0^{RF}\left(\Omega-\Omega_0\right) + \frac{1}{2}H_0^{RF}\left(\Omega+\Omega_0\right)\right)
\end{aligned}
\right. \qquad (4.4)
$$

The first order power component of eq. (4.4), p_1, represents the electrical response $H_{RF}(\Omega)$ of the SMF-based optical transmission system depicted in Fig. 4.1 corresponding to the first transmission configuration tolerant to dispersion. It should be compared with the analogous eq. (3.14) obtained in the absence of the MZI structure. In this new system configuration, the electrical response depends, firstly, on some constants related to the modulator and photodetection efficiency as well as the attenuation and delay caused by signal propagation over the SMF channel. Within eq. (4.4), we identify again the factor taking into account the effect of fiber chromatic dispersion on the electrical characteristics of the modulation process, such as the modulation format and the bandwidth of the transmitted electrical signal. The important variation with respect to the conventional system described in Chapter 3 is represented by the last factor which is composed by a group of terms. The first one is $H_0^{RF}(\Omega)$, the same term defined in eq. (3.15) which is responsible for the low-pass filter characteristic of the electrical response arising from the interaction between the chromatic dispersion and the spectral width of the optical source. Such term was also present when the MZI was not inserted in the scheme. In addition and, inherently to the presence of the MZI, the same factor, but scaled and shifted to another electrical frequency region, appears. The term $H_0^{RF}(\Omega\pm\Omega_0)$ owns the same analytical structure of $H_0^{RF}(\Omega)$ apart from its spectral position. Therefore, it can be referred to as a pass-band filter. The central frequency, Ω_0, of the pass-band region over which the filter $H_0^{RF}(\Omega\pm\Omega_0)$ operates is given by:

$$
\Omega_0 = \frac{\Delta\tau}{\left|\beta_2\right|L} \qquad (4.5)
$$

where $\Delta\tau$ is the differential time delay between the MZI fiber arms, β_2 is the chromatic dispersion parameter at the central wavelength of operation ω_0 and L is the fiber length.

The band-pass factor is generated optically by the interference of the two optical fields at the output port of the MZI. As mentioned before, the term $H_0^{RF}(\Omega\pm\Omega_0)$ is a replica of $H_0^{RF}(\Omega)$ shifted at $\pm\Omega_0$, which modifies the electrical transfer function of the system.

Since the spectral position of $H_0^{RF}(\Omega\pm\Omega_0)$, is governed by Ω_0, it can be said that the band-pass filter is tunable over the entire electrical range offered by the system equipment, in principle. The tuning of the central electrical frequency can be made either by changing the optical time delay $\Delta\tau$ using the VDL or varying the total fiber chromatic dispersion parameter, $\beta_2 L$.

The generation of a band-pass region in the electrical transfer function opens the possibility of propagating high-frequency signals through it, thus, allowing RoF transport in the GHz frequency band. Indeed, every electrical signal at radio frequency, Ω_{RF}, can be propagated always when Ω_{RF} is equal to Ω_0. The insertion of the MZI is a countermeasure strategy to avoid the transmission limitation problems arisen from the employment of optical broadband sources. The apparition of the band-pass filter is a result which indistinctly applies to all modulation formats of the optical carrier. However, there are some differences from case to case. They can be easily highlighted by previously specifying the general expression (4.4) for DSB-AM, SSB-AM and PM formats respectively:

$$H^{RF}(\Omega)=\left(\frac{\Re Z_L}{4\pi^2}\right)P_0 s_0 s_1 e^{-\alpha L}e^{-j\beta_1 L\Omega}\cdot CSE(\Omega)\cdot\left(H_0^{RF}(\Omega)+\frac{1}{2}H_0^{RF}(\Omega-\Omega_0)+\frac{1}{2}H_0^{RF}(\Omega+\Omega_0)\right) \quad \text{(DSB-AM)} \quad (4.6a)$$

$$H^{RF}(\Omega)=\left(\frac{\Re Z_L}{8\pi^2}\right)P_0 s_0 s_1 e^{-\alpha L}e^{-j\beta_1 L\Omega}\cdot e^{j\frac{\beta_2 L}{2}\Omega^2}\cdot\left(H_0^{RF}(\Omega)+\frac{1}{2}H_0^{RF}(\Omega-\Omega_0)+\frac{1}{2}H_0^{RF}(\Omega+\Omega_0)\right) \quad \text{(SSB-AM)} \quad (4.6b)$$

$$H^{RF}(\Omega)=\left(\frac{\Re Z_L}{4\pi^2}\right)P_0 s_0 s_1 e^{-j\frac{\pi}{2}}e^{-\alpha L}e^{-j\beta_1 L\Omega}\cdot PM\text{-}IM(\Omega)\cdot\left(H_0^{RF}(\Omega)+\frac{1}{2}H_0^{RF}(\Omega-\Omega_0)+\frac{1}{2}H_0^{RF}(\Omega+\Omega_0)\right) \quad \text{(PM)} \quad (4.6c)$$

Concerning the DSB-AM case, from eq. 4.6(a) it can be observed that, since the MZI is located before the optical modulator, the band-pass term $H_0^{RF}(\Omega\pm\Omega_0)$ results also multiplied, and thus, affected by the CSE. Therefore, the transmission of any band-pass signals would be possible only at electrical frequencies sufficiently far from the CSE transmission nulls where the power fading would be as high as to invalidate the band-pass filtering effect. Analogous considerations would apply when optical phase modulation is adopted. As shown by eq. 4.6(c), in this case, the amplitude of the pass-band transmission region generated by $H_0^{RF}(\Omega\pm\Omega_0)$, would be gradually attenuated as the frequency Ω_0 approaches the notches of the PM-IM conversion function. Therefore, the tuning of the band-pass filter should be conveniently made in the band-pass response of the PM-IM conversion curve and especially around frequencies where the amplitude of the PM-IM curve presents maximum values. For the remaining SSB-AM format, there are no restrictions over the spectral position of the pass-band region since the electrical response of a SSB-AM system is intrinsically free from the CSE power fading. In this case, the tuning range of the pass-band filter depends only on the electrical modulation and photodetection bandwidths.

Therefore, it can be affirmed that the generation of the pass-band transmission window realized by placing the MZI before the optical modulator, would overcome successfully the bandwidth limitations of the electrical transfer function in all cases. However for both AM-DSB and PM modulation formats, the pass-band filter is still vulnerable to the CSE and PM-IM notches, respectively.

In this context, only for DSB-AM carriers, we have proposed a second system configuration capable to remove the restrictions caused by the CSE notches over the tuning range of the pass-band filter. The difference with respect to the first configuration is the new location of the MZI in the CO

transmitter. The schematic diagram of the second optical transmission system configuration tolerant to dispersion is shown in Fig. 4.3.
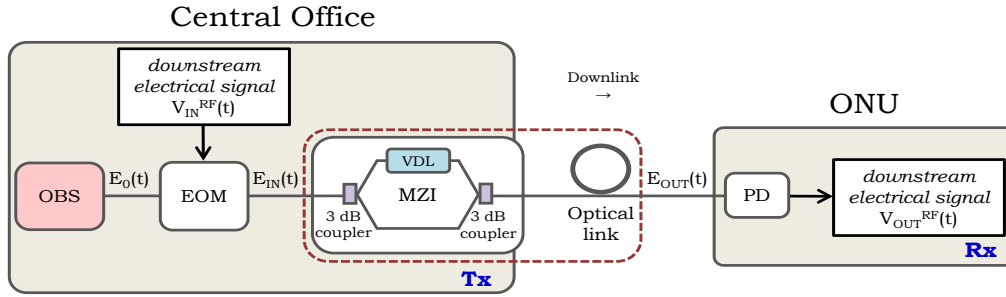
Fig. 4.3 Second optical transmission system tolerant to dispersion. The MZI is located after the optical modulator.

In this second configuration, the MZI is inserted just after the optical modulator. The variation of the MZI position into the scheme results analytically in a significant change of the electrical response of the system. This time, referring to the general expression of eq. 3.11, the insertion of the MZI behind the optical modulator modifies the optical link contribution term. Since now the MZI and the optical link are adjacent, the optical response of the combination between MZI and optical link is the product between the optical response of the MZI, $H_{MZI}(\omega)$ (eq. 4.1) and the optical response of the SMF fiber, $H_{SMF}(\omega)$ (eq. 3.12). In this case, the electrical response is given by:

$$H^{RF}\left(\Omega\right)=\left(\frac{\Re Z_L}{4\pi^2}\right)\frac{P_0}{4}s_0 e^{-\alpha L}e^{-j\beta_1 L\Omega}\cdot\left[\begin{array}{l}2\cos\left(\frac{\Delta\tau}{2}\Omega\right)\cdot\left(s_{-1}^{*}e^{j\frac{\beta_2 L}{2}\Omega^2}+s_1 e^{-j\frac{\beta_2 L}{2}\Omega^2}\right)\cdot H_0^{RF}\left(\Omega\right)+\\[2mm]\left(s_{-1}^{*}e^{j\frac{\beta_2 L}{2}\Omega(\Omega+\Omega_0)}+s_1 e^{-j\frac{\beta_2 L}{2}\Omega(\Omega+\Omega_0)}\right)\cdot H_0^{RF}\left(\Omega+\Omega_0\right)+\\[2mm]\left(s_{-1}^{*}e^{j\frac{\beta_2 L}{2}\Omega(\Omega-\Omega_0)}+s_1 e^{-j\frac{\beta_2 L}{2}\Omega(\Omega-\Omega_0)}\right)\cdot H_0^{RF}\left(\Omega-\Omega_0\right)\end{array}\right] \quad (4.7)$$

Equation (4.7) analytically expresses the electrical response of the second transmission system tolerant to dispersion depicted in Fig. 4.3. As described previously, the second configuration is characterized by the new position of the MZI inserted behind the optical modulator and not before as in the first one. Moreover, such new configuration has been specifically conceived to remove the transmission restrictions caused by the presence of the CSE notches in case of employing DSB-AM carriers. The improvement of the second system configuration with respect to the first proposed, is better remarked by specifying eq. (4.7) for the DSB-AM format case. The electrical response of the second configuration when the optical carrier is DSB-AM modulated is:

$$H^{RF}(\Omega) = \left(\frac{\Re Z_L}{4\pi^2}\right) P_0 s_0 s_1 e^{-\alpha L} e^{-j\beta_1 L\Omega} \cdot \left(\begin{array}{l} \cos\left(\frac{\Delta\tau}{2}\Omega\right) \cdot CSE(\Omega) \cdot H_0^{RF}(\Omega) + \\ +\frac{1}{2}CSE(\Omega-\Omega_0) \cdot H_0^{RF}(\Omega-\Omega_0) + \\ +\frac{1}{2}CSE(\Omega+\Omega_0) \cdot H_0^{RF}(\Omega+\Omega_0) \end{array} \right) \quad \text{(DSB-AM) (4.8)}$$

From eq. (4.8) it can be observed that the band-pass filter results now multiplied by a modified version of the CSE, defined as follows:

$$CSE(\Omega \pm \Omega_0) = \cos\left(\frac{\beta_2 L}{2}\Omega(\Omega \pm \Omega_0)\right) \quad \text{(4.9)}$$

The variation of the MZI position affects directly the behavior of the CSE function and, in consequence, its effect over the band-pass filter. In fact, eq. (4.9) shows clearly that the CSE function is also frequency shifted by an amount which depends on the central frequency of the band-pass filter in such a way that the power fading is completely avoided just in correspondence of that frequency, that is, Ω_0. Indeed, when $\Omega=\Omega_0$, the cosin function would give a constant and unitary value. It means that no power fading would be experienced if the filter approaches the CSE notches as occurred with the first configuration. In other words, the CSE never affects the spectral region where the pass-band filter is tuned. Therefore, once the band-pass window is opened, the second configuration allows the transmission of electrical signals even at frequencies close to the CSE notches where a conventional laser and the first configuration could not do. This represents the most important improvement brought by the second system configuration. Note that, a certain flexibility is permitted regard the position of the MZI in the second configuration. The MZI could be also be inserted after the fiber link and eventually in the ONU prior to photodetection without changing the system performance against fiber chromatic dispersion.

At this point, we remark that for PM carriers, the second configuration would not give an equivalent improvement as the one achieved for DSB-AM carriers. In this case the electrical response is shown in the following expression:

$$H^{RF}(\Omega) = \left(\frac{\Re Z_L}{4\pi^2}\right) P_0 s_0 s_1 e^{-j\frac{\pi}{2}} e^{-\alpha L} e^{-j\beta_1 L\Omega} \cdot \left[\begin{array}{l} \cos\left(\frac{\Delta\tau}{2}\Omega\right) \cdot PM\text{-}IM(\Omega) \cdot H_0^{RF}(\Omega) + \\ +\frac{1}{2}PM\text{-}IM(\Omega) \cdot H_0^{RF}(\Omega+\Omega_0) + \\ +\frac{1}{2}PM\text{-}IM(\Omega) \cdot H_0^{RF}(\Omega-\Omega_0) \end{array} \right] \quad \text{(PM) (4.10)}$$

where the modified version of the PM-IM conversion function multiplying the band-pass filter is defined as below:

$$PM\text{-}IM(\Omega \pm \Omega_0) = \sin\left(\frac{\beta_2 L}{2}\Omega(\Omega \pm \Omega_0)\right) \quad \text{(4.11)}$$

From eq. (4.11) it can be observed that, the sin function calculated in correspondence of the Ω_0 frequency would be nullified and so would the amplitude of the band-pass filter. It means that when the second system configuration is implemented for phase modulated carriers, the band-pass window cannot be generated at any frequency of the available electrical range. Therefore, contrarily to DSB-AM carriers, for PM carriers the generation and operability of the band-pass filter through the second transmission configurations is not viable. Despite such limitation, however, the transport of RoF signals in the GHz band is always possible by implementing the first configuration.

Observe that, in case of employing a MMF link, the term defined in eq. 3.27 should be inserted in the electrical responses of both system configurations to take into account for the effects of modal dispersion.

4.1.2 Experimental characterization for transmission of DSB-AM carriers.

In this subsection, we experimentally characterize the electrical response of the first and the second configurations tolerant to dispersion focusing on the transport radio signals modulating DSB-AM optical carriers. The experimental characterization is also supported by the results obtained with the theoretical model. For this purpose, we have implemented the schemes of Fig. 4.1 and Fig. 4.3.

In the experimental setup, the input optical source is a C-L band EDFA-based ASE light with an optical bandwidth higher than 85 nm (at 10 dB point) extended from 1525 nm to 1610 nm and centred at 1567.5 nm. The ASE source has a total optical power of 13 dBm. The ASE source is followed by an optical channel controller (OCC) operating in the conventional "Erbium window", that is, the C-band (1530 nm to 1565 nm). The optical channel controller allows the enabling of maximum 48 channels with a spacing of 0.8 nm, each one with a settable attenuation range of 20 dB. In this way an equivalent variable-bandwidth OBS with an arbitrary power spectral profile can be built just by selecting the number of channels. The VDL employed in the setup, permits a manual path variation of 18 cm which corresponds to 600 ps maximum delay in time domain with a maximum insertion loss of 1 dB. In the other arm, a manual polarization controller (PC) is inserted in order to guarantee the same state of polarization (SoP) of the two optical fields at the output of the MZI.

Figure 4.4(a) and 4.4(b) plot, respectively, the optical spectrum of the ASE source and the optical spectrum at the output of the optical channel controller when 20 channels are selected, as instance. The resulting spectrum at the output of the optical channel controller is equivalent to an OBS centred at wavelength λ_0=1550.68 nm and with a 3dB optical width around 17 nm. Figure 4.4(c) plots the spectrum of the OBS at the output of the MZI when the optical time delay, $\Delta\tau$, between the two arms is set to 3.5 ps, as instance. Observe the interferometric effect of the MZI on the OBS spectrum represented by the periodical amplitude variations. The wavelength periodicity $\Delta\lambda$ of the fluctuations is inversely proportional to the optical time delay $\Delta\tau$. In this case, for $\Delta\tau$ =3.48 ps, we experimentally find a wavelength periodicity $\Delta\lambda$=2.30 nm at λ_0=1550.68 nm.

(a) (b) (c)
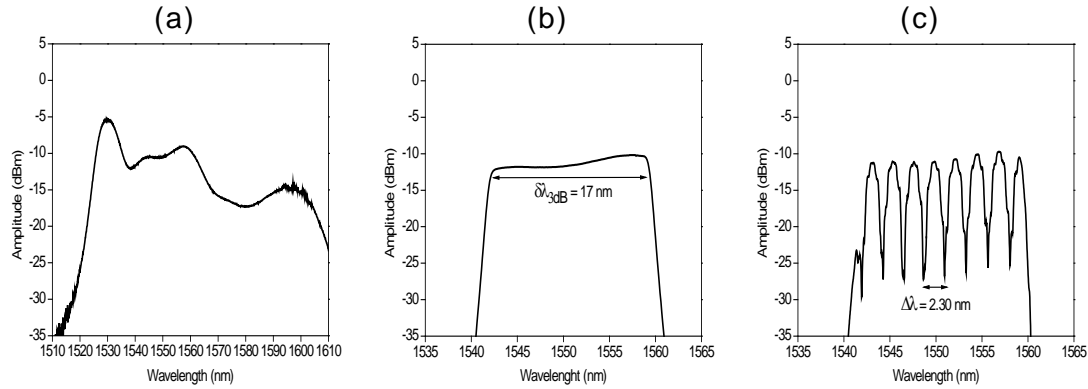
Fig. 4.4 (a) Optical spectrum of the ASE source, (b) optical spectrum at the output of the OCC and (c) optical spectrum at the output of the MZI for an optical time delay $\Delta\tau$ of 3.30 ps.

The optical modulator used in the experimental setup has a 3dB electrical bandwidth of 30 GHz. The optical detector has a 3dB electrical bandwidth of 50 GHz with a responsivity of 0.63 A/W. Finally, the optical link employed in the setup is a SMF link with the following characteristics at λ_0=1550 nm: attenuation coefficient α=0.2 dB/km, chromatic dispersion β_2=-22.62 ps^2/km and zero dispersion slope β_3=-0.125 ps^3/km. In order to reduce the impact of the dispersion slope on the optical source width, for the experimental characterization we build an equivalent OBS by enabling only 7 of the 48 channels, so that the resultant OBS has a 3dB bandwidth of 5.6 nm with a quasi-squared spectral shape centred at 1550 nm. Finally we use 10 km of SMF transmission link. All these characteristics and parameters have been also employed also in the theoretical model.

(a) First configuration tolerant to dispersion.

Figure 4.5 shows the experimental measurements together with the theoretical predictions of the normalized electrical transfer function when the first system configuration tolerant to dispersion is used. Here, the VDL is adjusted manually to set different time delays between the two arms of the MZI. In the experiment the optical time delays are varied sequentially and, for each one of them, the electrical response is measured at the output of the PD. In addition, the experimental and analytical response that would be obtained employing a coherent source emitting at 1550 nm has been also included in the figure using a grey line.

(a) Experimental   (b) Theoretical
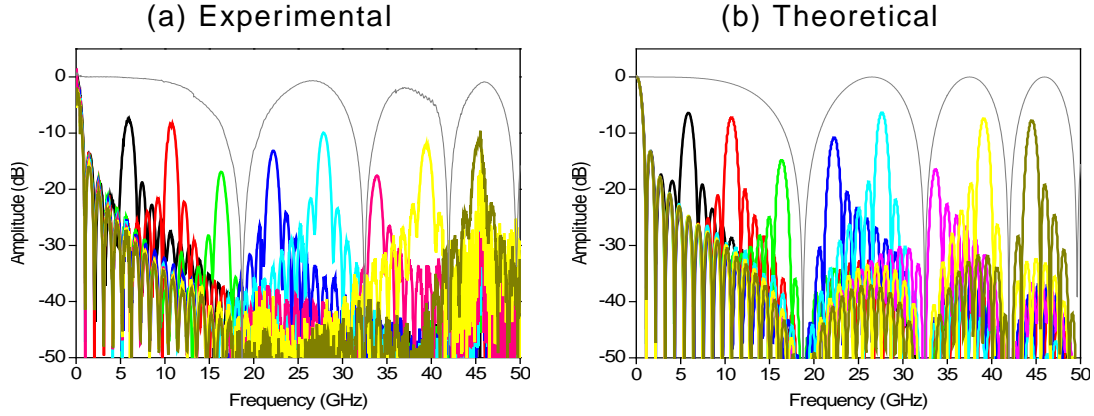
Fig. 4.5 Normalized (a) experimental and (b) theoretical amplitude responses of the first configuration tolerant to dispersion for different optical time delays. Electrical response for a conventional laser at 1550 nm (—).

In Fig. 4.5(a) for a given optical time delay, the corresponding electrical response exhibits a narrow baseband window with an electrical 3dB bandwidth around 0.5 GHz due to the effect of the low-pass term, $H_0(\Omega)$ which is invariantly present when broadband sources are employed. In addition, inherently to the insertion of the MZI, a new single and very selective band-pass window appears, as predicted theoretically by eq. (4.7a). The band-pass window is generated directly in the optical domain due to the interferometric action of the MZI in presence of a dispersive SMF link. The interferometric effect reflected in the electrical response takes the characteristic form of a band-pass filter centred at frequency Ω_0, which is analytically represented by the term $H_0(\Omega \pm \Omega_0)$.

In accordance with eq. (4.5) the central frequency Ω_0 of the band-pass filter can be continuously tuned by varying the path delay imbalance of the MZI, that is $\Delta\tau$, using the optical VDL. Therefore, the tunability features of the MZI structure allow changing the position of the band-pass filter over the entire available electrical bandwidth provided by the system equipment. In this case the band-pass window, has been tuned over a maximum electrical range of 50 GHz. Comparing Fig. 4.5(a) with Fig. 4.5(b) there is a good agreement between the experimental and the theoretical curves.

Nevertheless, it can be observed that, when the band-pass filter is tuned close to the CSE notches (for 10 km SMF the notches appear around 18.7 GHz, 32.5 GHz, 41.9 GHz and 49.6 GHz), the peak amplitude experiments a significant attenuation (see curves (—) and (—), for example). The attenuation of the band-pass window is also shown in the theoretical results of Fig. 4.5(b).These measurements confirm that when the MZI is located before the optical modulator, the CSE degrades the band-pass window in such a way that in the electrical region close to the CSE nulls, the amplitude attenuation of the band-pass window may invalidate the transmission of any electrical signal through it.

Note that, apart from the notch regions, the amplitude of the band-pass window is 6 dB lower than the amplitude of the low-pass window demonstrating the presence of the scaling factors in the analytical expression (4.6a).

At this point, we show a detailed analysis of some principal parameters related to the band-pass window which can be extracted from the results presented in Fig.4.5 These parameters are the central frequency

Ω_0, the electrical 3dB bandwidth of the filter, the peak amplitude and the ratio between the main lobe and the secondary left and right lobes. Figure 4.6(a) and (b) plots the central frequency and the electrical 3 dB bandwidth of the band-pass window as a function of the corresponding optical delay time, respectively.
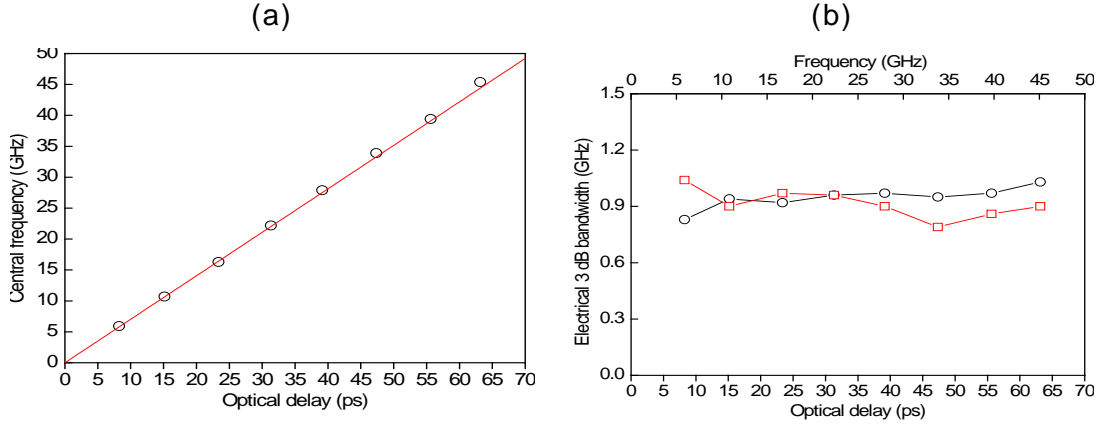
Fig. 4.6 Characterization of the band-pass window with respect to the optical time delay: (a) Experimental central frequency points (○), theoretical slope (—). (b) Electrical 3dB bandwidth: experimental (○) and theoretical (□).

From fig. 4.6(a), we observe a linear dependence between the central frequency, Ω_0, and the optical time delay, $\Delta\tau$, as established by eq. (4.5). For the measured points (○) we find an experimental slope of 0.71 GHz/ps. This value is in a very good agreement with the theoretical slope (—) calculated from the equation which is 0.70 GHz/ps. From a practical point of view, the linear dependence between Ω_0 and $\Delta\tau$ results very convenient. Depending on the application, certain flexibility is offered since the band-pass window position can be tuned by varying the total link dispersion and keeping a fixed optical time delay using tunable dispersion modules based on FBG and AWG technology as in [Hun 1996, Mor 2002, Mor 2003, Cap 2005].

In Fig. 4.6(b) we observe that the electrical 3dB bandwidth of the band-pass window is kept between 0.8 GHz and 1 GHz over the entire operation range for both the experimental (○) and theoretical (□) plots. This value establishes a limitation on the maximum bandwidth of the electrical signal which can be propagated through the link and may change depending on the particular spectral profile of the broadband source. Note also that the electrical 3dB bandwidth of the band-pass filter uses to double the electrical 3dB bandwidth of the low-pass filter. The band-pass filter is, in fact, a replica of the low-pass filter at higher frequencies.

Fig. 4.7(a) and (b) plots the peak amplitude evolution (○) of the band-pass window together with the ratio between the main lobe and the secondary left (▽) and right (△) lobes as a function of the optical time delay for the experimental and theoretical cases, respectively. In Fig. 6 the grey plot indicates the electrical response that would be obtained if a conventional laser would be inserted in the same setup.
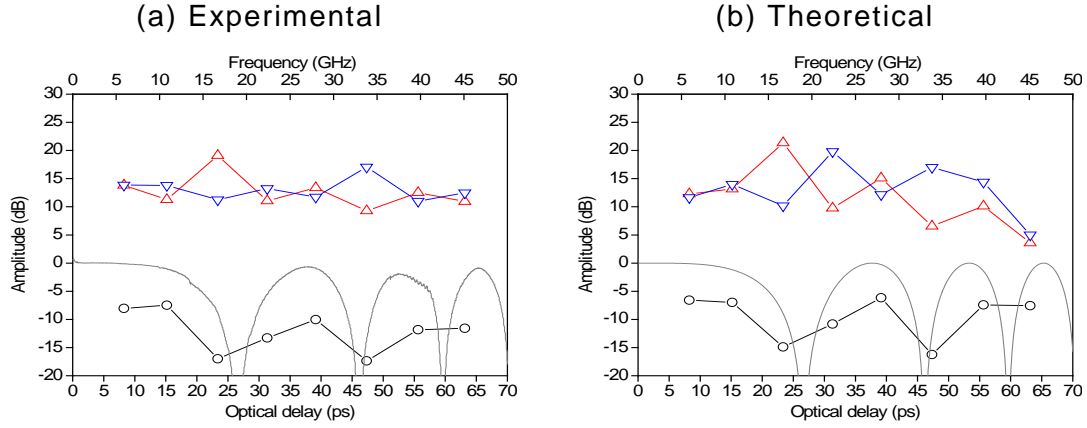
Fig. 4.7 (a) Experimental and (b) theoretical characterization of the band-pass window with respect to the optical time delay: peak amplitude (○), ratio between the main lobe and the left (▽) and right (△) secondary lobe. Electrical transfer function employing a conventional laser emitting at 1550 nm (—).

Figure 4.7(a) shows clearly the attenuation induced by the CSE notches over the electrical peak amplitude of the band-pass window (○). The peak level experiments a maximum attenuation of 10 dB in both the experimental and theoretical plots, confirming the results of Fig. 4.5. This behaviour is reflected also into the ratio between the main and secondary lobes, where an asymmetry between the main to secondary left (▽) and right (△) lobes ratio is found just in correspondence of the CSE nulls, as expected.

(b) Second configuration tolerant to dispersion.

The same characterization has been performed for the second system configuration for a 10 km SMF-based optical link. Fig. 4.8 shows the experimental and theoretical electrical response obtained for different optical time delays selected by tuning the VDL.
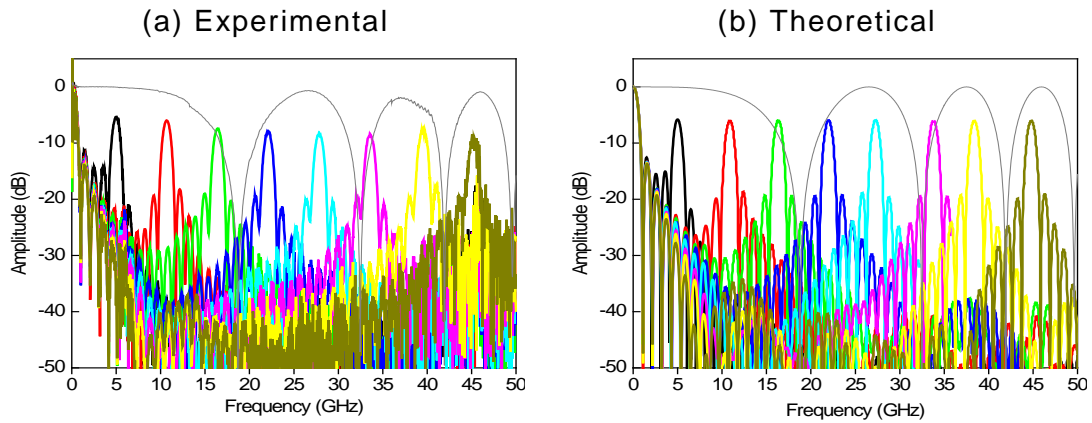
Fig. 4.8 Normalized (a) experimental and (b) theoretical amplitude responses for different optical time delays. Electrical transfer function employing a conventional laser at 1550 nm (—).

Again, the electrical responses of Fig. 4.8(a) contain a common low-pass window and different pass-band windows whose central frequency corresponds, in each case, with the corresponding optical time delay selected. The most important difference caused by the change in the MZI

position is represented by the fact that, now the CSE does not affect the band-pass region of the filter. In fact, all band-pass windows own the same peak amplitude independently of the electrical frequency. The improvement of this second configuration with respect to the first one is more evident especially at frequencies close to the CSE notches where the peak amplitude of the band-pass window remains practically constant whereas in the first configuration it was drastically reduced (see again curves (—) and (—)). This result, already predicted analytically by equation eq. (4.8), is now confirmed both experimentally and theoretically as shown in Fig. 4.8(b). Figure 4.8 should be compared with figure 4.5 referred to the first configuration.

Now, we remark that the second transmission configuration not only overcomes the CSE-induced power fading affecting the first one, but also performs even better than a conventional laser source-based optical transmission system.

A detailed analysis of the principal parameters extracted by the experimental and theoretical results of Fig. 4.8 follows in order to complete the characterization of the second configuration. In Fig. 4.9(a) and Fig 4.9(b) we plot the central frequency and the electrical 3dB bandwidth of the band-pass region over the optical time delay, respectively.
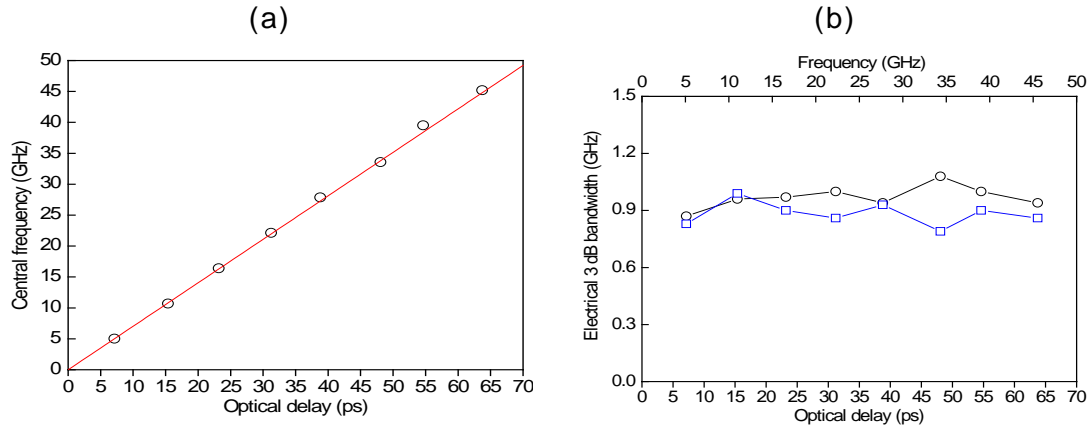
Fig. 4.9 Characterization of the band-pass window with respect to the optical time delay: (a) Experimental central frequency points (○), theoretical slope (—). (b) Electrical 3dB bandwidth: experimental (○) and theoretical (□).

In Fig. 4.9(a), we find a linear dependence between the central frequency of the band-pass window (○) and the optical time delay set by the MZI. The slope of the experimental points is the same obtained with the first configuration and agrees with the theoretical one. The electrical 3dB bandwidth is around 1 GHz in a range of 50 GHz as shown by Fig. 4.9(b). Therefore, with respect to these two parameters; the performance of the first and second configuration is practically equivalent.

Finally, Fig. 4.10 plots the peak amplitude (○) of the band-pass window and the relation between the main lobe and the secondary left (▽) and right (△) lobes as a function of the optical time delay in the experimental (a) and theoretical (b) case.

(a) Experimental   (b) Theoretical
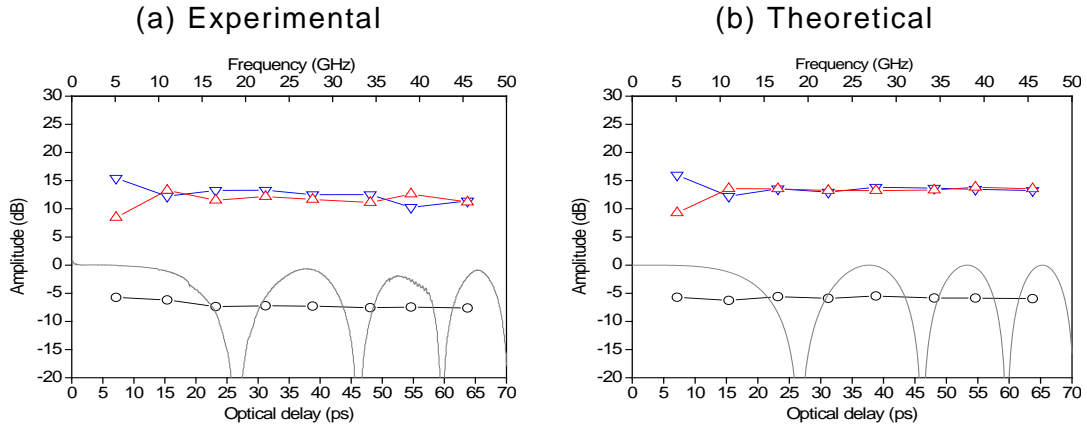
Fig. 4.10 (a) Experimental and (b) theoretical characterization of the band-pass window with respect to the optical time delay: peak amplitude (○), ratio between the main lobe and the left (▽) and right (△) secondary lobe. Electrical transfer function employing a conventional laser at 1550 nm (—).

Figure 4.10(a) and (b) show that the experimental peak amplitude (○) of the band-pass window maintains a level close to -6 dB over the frequency range as it is practically transparent to the CSE. In consequence, the ratio between the main and secondary left (▽) and right (△) lobes remains almost constant.

In summary, the insertion of the MZI overcomes the transmission bandwidth limitations induced by fiber chromatic dispersion when DSB-AM optical broadband sources are employed in third communication band. The pass-band filter generated by the MZI is key to enhance the operative transmission bandwidth. As added value, when the second configuration is implemented, that is, when the MZI is located behind the optical modulator, the signal propagation is not affected by the CSE. Therefore, a total increase of the operative bandwidth is achieved which could not be realized with a conventional DSB-AM laser source. This functionality is optically realized without employing any dispersion compensation technique, or others additional devices.

4.1.3 Comparison between the first and second system configuration.

In this subsection, we compare the performance of the two transmission configurations tolerant to dispersion regarding the CSE. For this purpose, we have measures the electrical responses of the two configurations when the central frequency of the band-pass window is tuned to the first and second CSE notch frequencies which are f_1=18.7 GHz and f_2=32.5 GHz, respectively. In order to center the band-pass filter at the first notch frequency, the optical time delay is set to 26.2 ps for the first configuration and 26.3 ps for the second one. Fig. 4.11 plots the experimental (a) and theoretical (b) responses obtained with the first configuration whereas the experimental and theoretical response of the second configuration are shown in (c) and (d) respectively. Both plots the electrical response of the conventional laser source-based system.

Experimental

(a)

First configuration

Theoretical

(b)

(c)

Second configuration

(d)
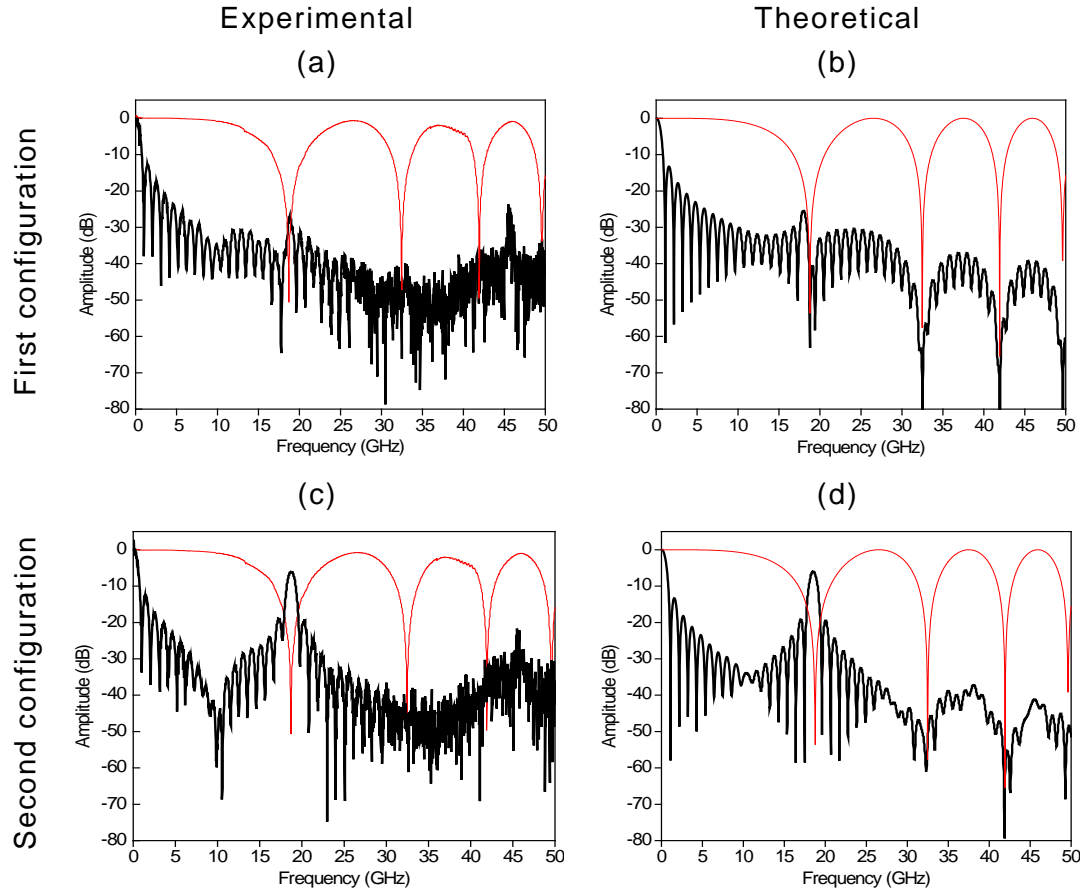
Fig. 4.11 Normalized electrical responses when the band-pass window is centred on the first CSE notch. First configuration: (a) experimental and (b) theoretical. Second configuration: (c) experimental and (d) theoretical.

Comparing Fig. 4.11(a) and (c) it is clearly evident that regarding the first CSE notch, the band-pass window vanishes if the first configuration is implemented, invalidating all transmission possibilities around that frequency. Nevertheless, its amplitude is not degraded with the second configuration. In fact, where the experimental peak amplitude is around -27 dB for the first configuration, the peak amplitude is around -6 dB in the second one. In this last case, the performance of the second configuration is even better than the one obtained employing a conventional laser. The experimental measurements in (a) and (c) completely agree with the theoretical results of (b) and (d).

The behaviour of the band-pass window in the second notch is measured by setting the optical time delay to 45.9 ps for the first configuration and 45.6 ps for the second one. Theoretical results and experimental measurement of the electrical response are shown for both configurations in Fig. 4.12.

The experimental plots of Fig. 4.12(a) and (c) show that the peak amplitude values of the band-pass window are -27 dB and -7 dB for the first and second configuration respectively. We observe again that the CSE notch at 32.5 GHz disappears only if the second configuration is employed, whereas, when the first configuration is employed, the band-pass window is drastically attenuated at the notch frequency.

Experimental

Theoretical

(a)

(b)

(c)

(d)
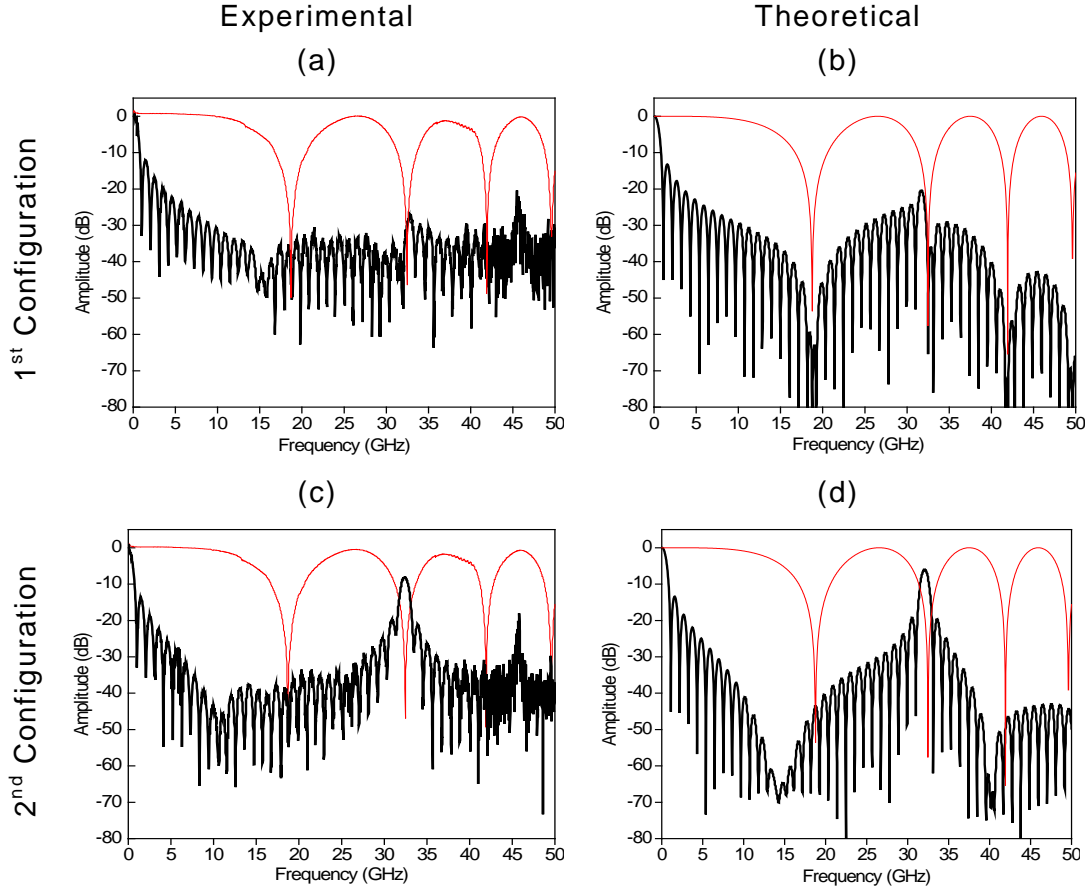
Fig. 4.12 Normalized electrical responses when the band-pass window is centred on the second CSE notch. First configuration: (a) experimental and (b) theoretical. Second configuration: (c) experimental and (d) theoretical.

4.1.4 Effect of the third order dispersion parameter.

In Chapter 3, we have demonstrated that the optical source width has a huge impact on the electrical response and in particular on its electrical 3dB bandwidth. Actually, for a given optical link, the increasing of the source width produces a decreasing of the 3dB bandwidth in the electrical domain allowing only the transmission of few MHz signals. This effect is governed by the chromatic dispersion parameter in combination of the source width and represented by the term $H_0^{RF}(\Omega)$ defined in eq. 3.15.

When the first and second configurations have been described, we have remarked the apparition, of a new band-pass replica of $H_0^{RF}(\Omega)$ centred at Ω_0 inherent to the insertion the MZI. Both low-pass and band-pass filters have the same analytical structure and their experimental behavior is very similar (apart from the spectral position). Therefore, a certain influence of the source width on the bandwidth of the band-pass filter should be also expected.

In order to investigate the dependence of the band-pass filter characteristics on the spectral width of the source, we measure the electrical transfer function of a 10 km SMF link when the system is transmitting a fixed 25 GHz electrical signal and the spectral width of the broadband source is varied by using the optical channel controller. In particular, the optical time delay of the MZI is set to 35.7 ps for a band-

pass window centred at 25 GHz and the source width variation is made by enabling progressively a maximum number of 20 channels. In this way, we generate a series of equivalent OBSs with spectral width going from 0.8 nm (one channel) to 16 nm (20 channels). In Fig. 4.13(a) and (b) we plot the central frequency and the electrical 3dB bandwidth of the band-pass filter as a function of the optical source width, respectively. The inset of Fig. 4.13(a) represents the normalized electrical response.

(a)   (b)
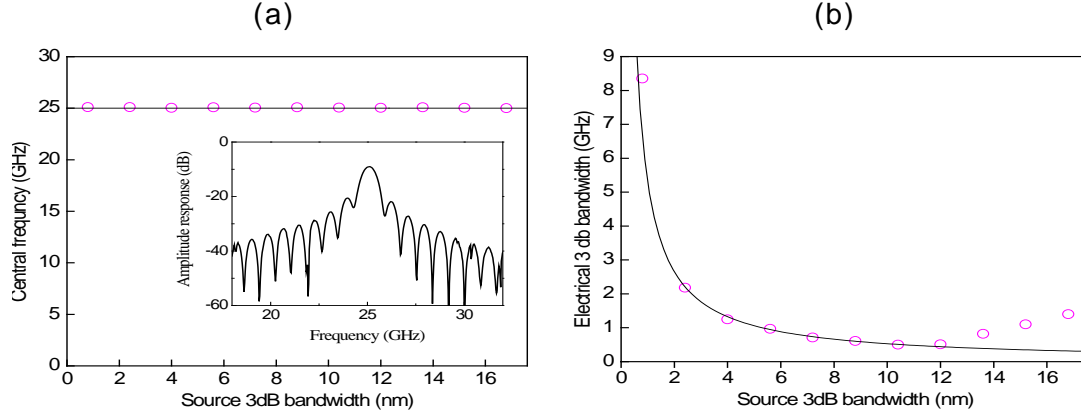
Fig. 4.13 Experimental characterization of the electrical response measured at 25 GHz: (a) central frequency of the band-pass filter as a function of the OBS 3dB width with the normalized electrical response as inset. (b) 3dB bandwidth as a function of the OBS width: experimental measurements ($\bigcirc$) and theoretical prediction (—).

Fig. 4.13(a) shows that the central position of the band-pass window ($\bigcirc$) is not influenced by the optical source width and remains almost constant over the tested range. On the contrary, Fig. 4.13(b) shows that the experimental electrical 3dB bandwidth of the band-pass filter ($\bigcirc$) decreases as the optical source width increases. In correspondence of 5.6 nm, which is the spectral width of the OBS employed in the previous experimental analysis, we find an electrical 3dB bandwidth around 1 GHz confirming the results of Fig. 4.6 and 4.9. This trend is maintained as long as the OBS width is kept lower than 12 nm. From that source width, we measure an experimental increment of the electrical 3dB bandwidth of the band-pass window.

The reader may observe how the experimental points start to differ from the solid line (—) corresponding to the theoretical prediction when the OBS width approaches 12 nm. Indeed, the theoretical prediction curve comes from the analytical study reported in Chapter 3 where, the term depending on the third order dispersion parameter, β_3, in the Taylor expansion, has been voluntary neglected. In practice, the condition under which the effects of the third order dispersion parameter can be neglected, is reflected directly in a condition on the critical 3dB source width $\delta\omega_C$ which is given by the following expression:

$$\delta\omega_c \approx \frac{1}{\sqrt{|\beta_3|L\Omega}} \quad (4.12)$$

Therefore, we deduce that the disagreement found between the experimental points and the theoretical model is due to the presence of the dispersion slope parameter whose effect, on the band-pass filter, is a

broadening of the 3dB bandwidth for a given frequency of operation. Although the third order dispersion parameter is always physically present, the experimental curve of Fig. 4.13(b) shows that its effect is important only from a critical value of the source width. In other words, while the source width is maintained below the critical value, the effect of β_2 over the electrical bandwidth of the band-pass filter is dominant with respect to the dispersion slope one and, therefore, the impact of dispersion slope can be neglected.

Since the theoretical prediction is in a good agreement with the experimental limitation of 12 nm, we validate the choice of a 5.6 nm OBS as good as to neglect the effects of β_3 in the experimental characterization presented in the current section. Note that, when the optical source exceeds the critical bandwidth limitation, the broadening of the band-pass window is also a function of the electrical frequency of operation in such a way that, as the electrical frequency increase, the 3dB bandwidth gets wider. It has been demonstrated in [Mor 2006] that apart from a bandwidth increase, the band-pass window experiments also a small attenuation which should be taken into account for the viability of transmissions especially at higher electrical frequencies. Finally, the results of Fig. 4.13(b) show clearly that, in all cases, a transmission window with an electrical 3dB bandwidth higher than 1 GHz is always achieved.

4.1.5 Experimental evaluation of the transmission performance in SMF links.

In this subsection, we verify the transmission capabilities of the two proposed system configurations with special emphasis on the differences between them and comparing the results with those obtained employing a conventional laser source and a broadband source without the insertion of the MZI. For this purpose, the optical carrier generated by the OBS owns a 3dB width of 5.6 nm whereas a vector signal generator provides the downstream signal. Attending to the SCM scheme, the digital data is a 5 Mb/s QPSK-encoded PRBS that amplitude modulates electrical subcarriers in a range of 20 GHz and with an electrical power of 15 dBm. The transmission test is run over 10 Km of SMF using the same optical modulator and photodetector of the previous experimental characterization. A maximum 10.0% of EVM is kept as conventional criterion for the evaluation of the signal quality degradation [Let 2005].

Fig. 4.14 shows the EVM of the demodulated signal as a function of the subcarrier frequency when four different cases are tested. In Fig. 4.14(a), the optical carrier is firstly provided by a conventional laser source centred at 1550 nm (□) and secondly by OBS without the insertion of the MZI (○). In Fig. 4.14(b), the first (△) and second (▽) system configurations described above respectively has been tested. The band-pass window has been tuned at 10 GHz by setting an optical time delay of 14.2 ps for both configurations.

(a)   (b)
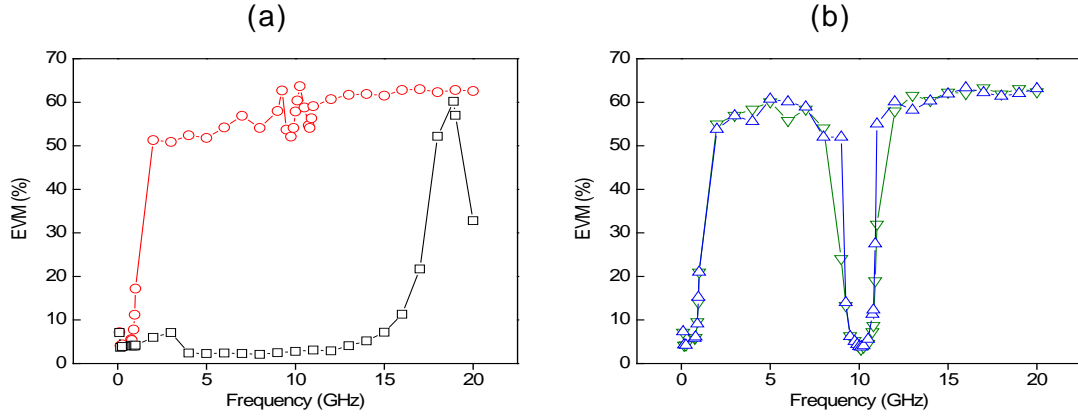
Fig. 4.14. EVM vs. subcarrier frequency employing (a) conventional laser source (□) and the OBS (○). (b) First (△), and the second (▽) system configuration when the band-pass filter is tuned at 10 GHz.

From Fig. 4.14(a), it can be observed that, when a conventional laser source is employed (□), the operative electrical range is limited to 15 GHz. That expected limitation is due to the presence of the first CSE notch at 18.7 GHz. In this case, the EVM of the recovered signal is always below 10.0% apart from the frequency region influenced by the CSE notch where the EVM goes over 50% and thus, a significant degradation of the signal quality is measured. When the laser is replaced by the OBS (○), the EVM is below 10.0% only in a very narrow 1.0 GHz electrical bandwidth, the low-pass region. For frequencies outside baseband, the signal quality reaches EVMs higher than 50.0%. Therefore, we verify that the transmission performance achieved in case of employing an OBS is severally limited by the effect of fiber chromatic dispersion over the optical source width.

When the OBS is combined with the MZI in accordance to first configuration (△), Fig. 4.14(b) shows acceptable performance in the baseband region and just in correspondence of the frequency range where the band-pass filter is tuned. This range has a bandwidth of 1 GHz around 10 GHz. Far from the baseband and the band-pass regions the transmission is clearly unviable. However, the MZI is key to allow the transmission over the electrical frequencies spanned by the band-pass filter where the OBS alone could not do it. Comparing curves (△) and (□) in correspondence of the band-pass frequency, the results obtained when the MZI is inserted are very similar to those reached with a conventional laser. When the second configuration is tested (▽), we do not observe significant differences in the results with respect to the first configuration. In fact the CSE is not influent in that band-pass region. Therefore, both system configurations are equivalent when the band-pass filter is tuned far from the first CSE notch.

In order to remark the difference between the two architectures, we plot in Fig. 4.15 the EVM as a function of the electrical subcarrier frequency for the first (△) and second (▽) configurations when the band-pass filter is tuned at different frequencies. For each frequency, the upper axis indicates the correspondent optical delay selected. The results obtained with a conventional laser (□) are also included into the plot.
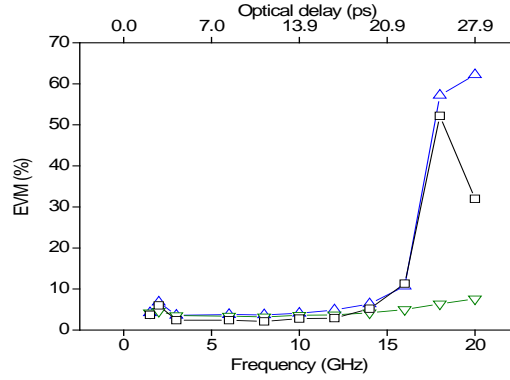
Fig. 4.15. EVM vs. subcarrier frequency using a conventional laser source (□) and an OBS in the first (△) and second (▽) system configuration.

Comparing the laser-based system (□) with the first configuration (△), in Fig. 4.15, we observe a similar degradation for both optical sources. In contrast, the second configuration (▽) allows to obtain EVM below 10.0% even for frequencies close to the first CSE notch performing better than the first configuration and the laser. For the second configuration, the slight EVM increasing at higher frequencies is just inherent to the electrical bandwidth of the modulator and photodetector used in the experimental setup.

4.1.6 Employment of MMF links.

In Chapter 3, we have demonstrated, that in third communication band, the limitations caused by fiber chromatic dispersion in presence of a broadband source, confine the transmission through both SMF and MMF-based links to a restrictive electrical operative range. Moreover, we have remarked that the fundamental difference between a SMF and a MMF channel is represented by the presence of another source of dispersion called modal dispersion and inherent to MMF propagation. Modal dispersion causes undesired amplitude fluctuations in the electrical response whose intensity increases with the distance, thus, imposing a significant limitation on the maximum allowed bandwidth-distance product (typically few GHz·km). However, the range of distances covered by a typical access network infrastructure is as short as to enable the transmission over MMF when techniques such as central launching are implemented [Haa 1993, Rad 1998, Yam 2007, Sim 2007]. Under this condition, the effect of the chromatic dispersion is dominant. In other words, once the modal coupling is minimized, both MMF and SMF links suffer the same transmission limitations regarding the employment of broadband sources operating in third communication band. Therefore, in this subsection, we validate the viability of inserting an MZI structure in order to enable the transport of RoF signals extending our solution to MMF links.

For this purpose, we have previously characterized the two system configurations described in Fig. 4.1 and 4.3 modeling a 35 nm-width optical source centred at 1556.54 nm and a 62.5-µm graded-index MMF as optical link with β_2=-18.47 ps/km^2 and β_3=0.142 ps/km^3 at the central wavelength of operation. The optical modulator owns an electrical 3dB bandwidth of 15 GHz. The MMF photodetector allows operations in a 23 GHz electrical bandwidth with a responsivity of 0.86 A/W. Figure 4.16 plots the theoretical

response obtained when the band-pass window is generated first at 5 GHz (—) and then at 20 GHz (—) in the following cases. Cases (a) and (b) refer to the first and second configuration, respectively, when 1 km of MMF is tested. Cases (c) and (d) correspond to the simulation with 10 km of MMF.

First configuration
(a)

Second configuration
(b)

(c)

(d)
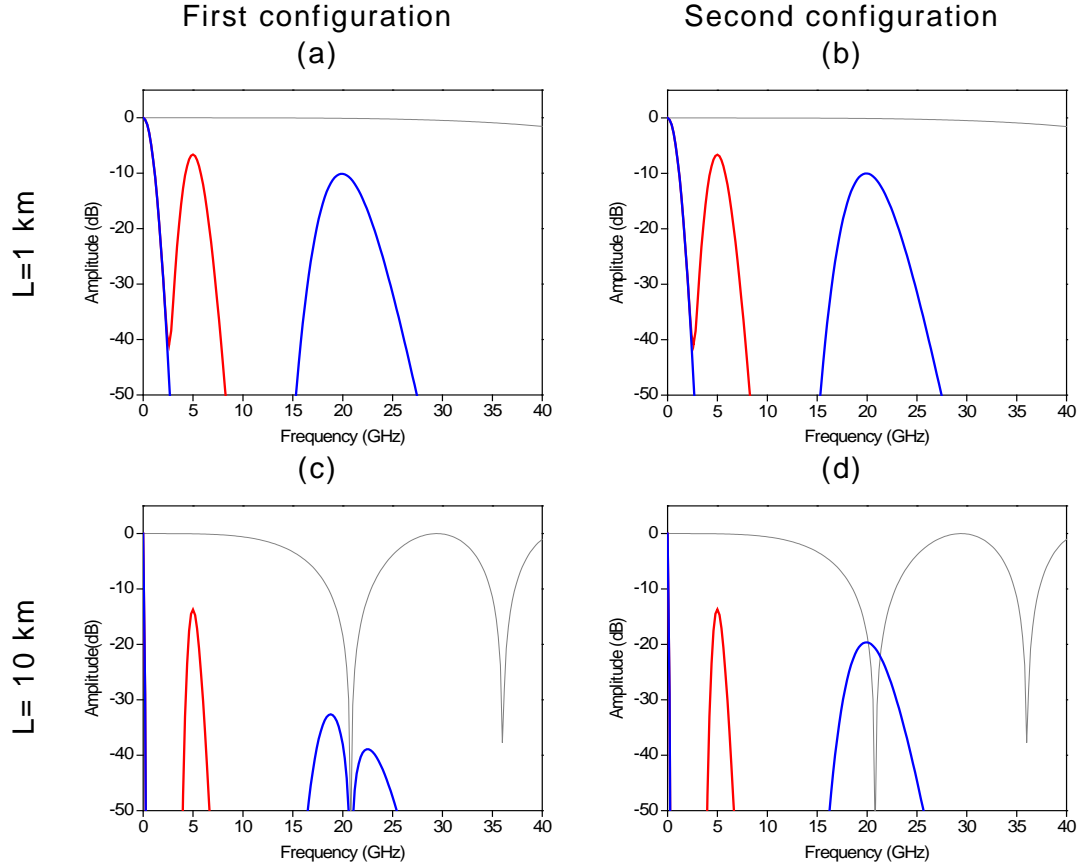
Fig. 4.16 Normalized theoretical electrical responses when the band-pass filter is tuned at 5 GHz (—) and 20 GHz (—). L = 1 km (a) first system configuration and (b) second system configuration. L=10 km (c) first system configuration and (d) second system configuration. CSE (—).

The theoretical amplitude responses shown in Fig 4.16(a) and (b) are very similar. We identify a common low-pass region with a bandwidth around 0.6 GHz due to effect of chromatic dispersion over the source width. Apart from the baseband region, the insertion of the MZI generates two transmission windows centred at 5 GHz (—) and 20 GHz (—). For 1 km of MMF, the first CSE notch is located around 66 GHz and, thus, its effect over the electrical response is negligible. Since the optical source width is larger than the critical width predicted by eq. 4.12, we observe also the effect of the dispersion slope parameter over the shape of the band-pass windows. In particular the increase of the 3dB bandwidth with the electrical frequency (from 1.5 GHz at frequency 5 GHz to 3.13 GHz at frequency 20 GHz) and a small decrease of the peak attenuation of the band-pass region (from -6.5 dB to -10.2 dB) common to both configurations.

In Fig. 4.16(c) and (d) we observe that, when 10 km of MMF are tested, the low-pass filtering effect at becomes more abrupt with respect to the one observed for 1 km of MMF as expected by the increasing of the factor $\beta_2 L$. It is reflected in the extremely narrow baseband region. In this case, the first CSE notch falls at 20.8 GHz (—) and the power fading,

caused by the CSE on the electrical response, increases with the electrical frequency. For the first configuration (c), it becomes critical especially for the band-pass window located at 20 GHz (—). However, provided the second configuration is implemented (d), the CSE is avoided just in correspondence of the spectral region around 20 GHz according to theory.

Since the spectacular tolerance of the second configuration to the CSE is once more confirmed, we have performed the experimental characterization of the second configuration employing a LED centred 1556.54 nm with 37 nm of 3dB width as optical carrier in the setup. The electrical signal is generated by a vector network analyzer limited to 20 GHz frequency range. Behind the modulator, the light is centrally launched into a 1.25 km transmission fiber length implemented with a 62.5 μm graded-index MMF. Figure 4.17 shows the experimental and theoretical MMF system responses when the transmission window is placed at different frequencies by tuning the MZI optical time delay.

(a) Experimental   (b) Theoretical
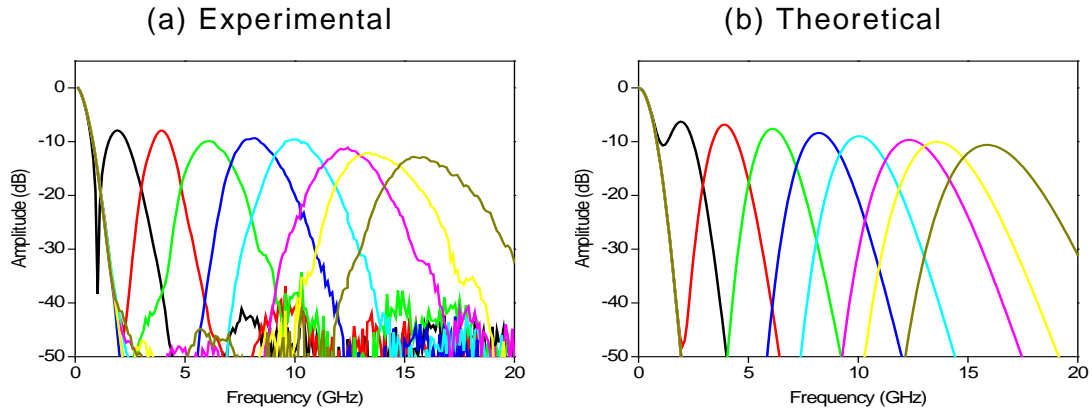
Fig. 4.17 Normalized (a) experimental and (b) theoretical amplitude responses of the second configuration when the band-pass filter is tuned at different electrical frequencies: 2 GHz (—), 4 GHz (—), 6 GHz (—), 8 GHz (—), 10 GHz (—), 12 GHz (—), 14 GHz (—) and 16 GHz (—).

As expected, Fig. 4.17(a) and (b) show a good agreement between theory and experimental results. All baseband regions have a 3dB bandwidth of 0.5 GHz and the transmission windows maintain an acceptable level of amplitude in the entire frequency range making viable the propagation of both baseband and RoF signals through the MMF link. The progressive amplitude decreasing and broadening of all pass-band windows is due to the effect of dispersion slope.

To complete the experimental characterization, Fig. 4.18(a) shows the experimental (○) and theoretical (—) central frequency of the band-pass filter as a function of the optical time delay, whereas, Fig. 4.18(b) shows the experimental (○) and theoretical (—) 3dB bandwidth evolution corresponding to the baseband as well as the experimental (□) and theoretical (—) 3 dB bandwidth of the band-pass windows.

100

(a)   (b)
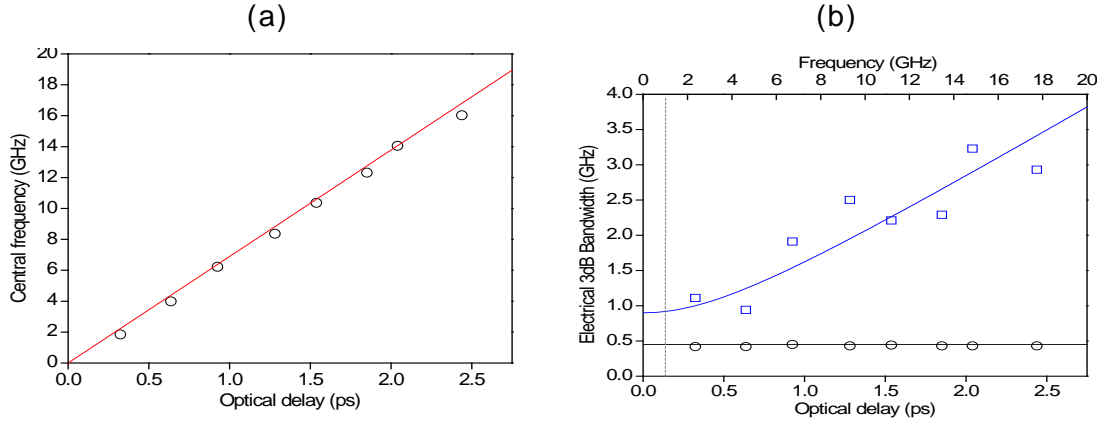
Fig. 4.18 Characterization of the band-pass window with respect to the optical time delay: (a) Experimental central frequency points (○) and theoretical slope (—). (b) 3dB bandwidth: baseband region experimental points (○) and theoretical curve (—); band-pass region experimental points (□) and theoretical curve (—).

In fig. 4.18(a), we observe a linear dependence between the central frequency of the band-pass window Ω_0 and the optical time delay $\Delta\tau$. The slope of the experimental points (○) agrees with the theoretical slope of 6.8 GHz/ps (—) calculated from eq. (4.5) using the link parameters β_2=-18.47 ps/km^2 and L=1.25 km.

With regard to the theoretical (—) and experimental (○) results of Fig. 4.18(b), the 3dB bandwidth at baseband exhibits small variations around 0.5 GHz when time delay is changed. In contrast, the electrical bandwidth of the band-pass filter (□) increases almost immediately with the frequency. This difference is due to the effect of the dispersion slope over the OBS spectrum at frequencies far from the baseband region and explains the changes of the band-pass window shape in Fig. 4.17(a) and (b). Indeed there is a frequency dependence on the parameter $\delta\omega_c$ in eq. 4.12. Substituting the experimental parameters in eq. 4.12, the electrical frequency from which the effect of dispersion slope becomes important is found to be around 1 GHz confirming the theoretical fit (—).

4.2 CWDM transport of RoF signals using spectrum sliced OBSs.

As described in Chapter 2, the spectral slicing is an effective WDM approach where the light from a single broadband source is subdivided into a set of narrower bands assigned to different subscribers. In this way, one single optical source, centralized at the CO, simultaneously generates light for all channels. The bandwidth characteristics of an OBS implies that, provided high input powers and low slicing losses are achieved, the generation of the carriers can be made with relaxed wavelength spacing conditions. It can avoid the complex and expensive use of temperature-sensitive coherent sources and slicing devices. In this context, the implementation of the spectral slicing technique is justified and potentially suitable for CWDM network environments, where the minimization of source-associated costs and transmitter complexity, rather than high-capacity, could be a fundamental target.

However, as demonstrated in Chapter 3, large bandwidth slices lead to an increase of chromatic dispersion-induced transmission limitations. In order

101

to allow the employment of spectrum sliced OBSs in third transmission band, the dispersion tolerant characteristics of the MZI structure demonstrated in section 4.1, can be conveniently exploited to reach RoF transport over a set of CWDM channels under a typical PON topology.

4.2.1 Description of the network architecture.

Figure 4.19 shows the architecture of the CWDM optical access network based on spectrum sliced OBS.
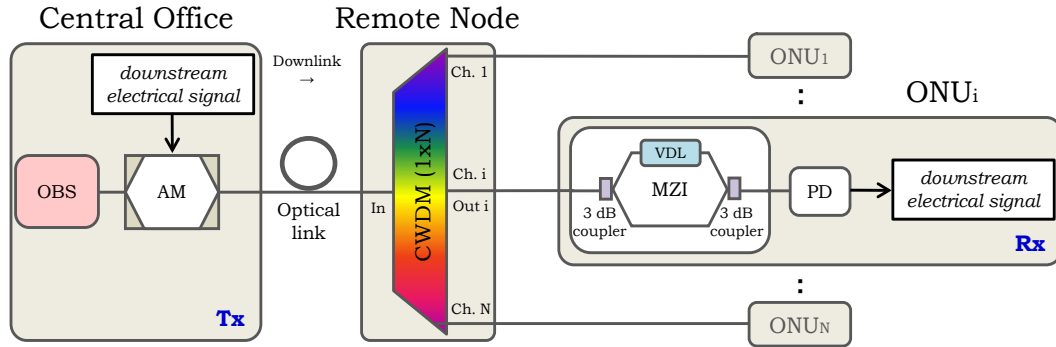
Fig. 4.19 Spectral slicing-based CWDM optical access network for the transport of RoF signals.

The architecture is composed by a CO connected by an optical link to a RN which feeds a number N of terminals ONUs as the customer premise equipment. Only the downstream path from the CO to the ONUs is shown in the figure for the sake of clarity. In the CO, the optical spectrum provided by a single OBS is amplitude modulated by the downstream electrical signal. The modulated optical field is launched into the optical link and after propagation it reaches the RN.

The architectural structure of the RN router is an example of how spectral slicing might be incorporated into an optical access network. In our design, the fundamental device employed for the implementation of the spectral slicing technique is a typical CWDM filter. The CWDM is composed by an input port and N output ports each one characterized by unique and adjacent spectral band-pass separated by the particular channel spacing of the device. With such structure, the working principle of the RN is as follows. Once the injected broadband light is launched into the input port, the multiplexer selects (slices) and passes through its output ports a different portion of the overall source's spectrum only if the selected slice falls within the corresponding CWDM channel spectral band. With such functionality, each slice can be used as optical carrier to convey the downstream signal. Therefore, the RN filters the broadband light provided by a single optical source into narrower bands and broadcast the information carried by each band through the network once a univocal correspondence between a given channel and an ONU is established.

Concretely, the spectral slicing approach creates an equivalent N-WDM scenario by exploiting the available optical bandwidth of a spectrum shared optical source to feed multiple ONUs at different locations. From a practical point of view, the great advantage with respect to a conventional WDM system built with multiple coherent lasers is a substantial minimization of inventory and management costs of the sources at the CO. In fact, the need

for well-defined wavelengths is avoided and precise tuning requirements are relaxed. Furthermore, it offers at the same time network scalability for channels and bandwidth scalability for users since the transmission capacity and the number of accommodated users can be varied by choosing conveniently the slicing device at the RN.

All ONUs are architecturally identical. The structure of the ONU receiver is simply composed by a MZI device followed by the photodetection circuit. Note that, the tunable MZI is opportunely placed in the ONU for two reasons. The first one is to exploit the CSE-free features offered by the second configuration tolerant to dispersion, as in the architecture the MZI is located after the optical modulator. The second reason is to allow "broadcast and select" applications in case of transmitting a combination of RoF signals employing the SCM technique. The MZIs could be alternatively placed in the RN immediately behind the CWDM, without changing any functionality with respect to the generation of the pass-band windows and the network performance. This solution would reduce the equipment installed at the ONU as well as the corresponding management which would be both centralized and performed remotely in the RN. The choice between the first and the second approach may depend on the degree of complexity that the provider can assume for the ONU and, thus, is directly associated to the number of ONUs deployed throughout the network. In any case, it shows the flexibility offered by the proposed architecture.

4.2.2 Experimental characterization.

The experimental characterization of the CWDM access network has been realized after implementing the scheme of Fig. 4.19. In the setup, the OBS installed at the CO is a C-L band EDFA-ASE light with a width of 85 nm centred at 1567.50 nm and with a total optical power of 19 dBm. The ASE spectrum is modulated with the broadcasted information using an EOM configured for conventional AM-DSB modulation.

Since N=4 ONUs are deployed, the CWDM installed at the RN is an $[1]_{In}$ x $[4]_{Out}$ based on thin film filter technology with high channel isolation and ITU-T grid compatible. The four spectral band-pass have a nominal center wavelength of 1531 nm (Ch.1), 1551 nm (Ch.2), 1571 nm (Ch.3) and 1591 nm (Ch.4). The channel spacing between central wavelengths is 20 nm. Each channel has a 17 nm bandwidth with insertion loss lower than 0.9 dB over the full band-pass. Therefore, the multiplexer slices the incoming broadband optical modulated spectrum into 4 narrower optical bands employed to carry the downstream information from the CO to ONU_1, ONU_2, ONU_3 and ONU_4, respectively.

Figure 4.20(a) and (b) show the optical spectrum of the ASE source and the combined optical spectrum measured at each output port of the CWDM as a result of the spectral slicing. As observed, apart from the optical loss accumulated from the CO to the RN, the spectral profile of each channel has a different power distribution. It is a consequence of the non uniform spectral power distribution of the ASE source. Figure 4.20(c) plots the spectra of the four sliced channels after passing through the MZI structure located at the correspondent ONU. The periodical amplitude variations in Fig. 4.20(c) result from the interferometric effect of the MZIs. In the example shown, the four channels present a common wavelength

periodicity around 2.3 nm obtained by setting optical time delays of 3.4 ps (—), 3.5 ps (—), 3.6 ps (—), and 3.7 ps (—). As observed, they are different because the optical carriers are centred at different wavelengths.
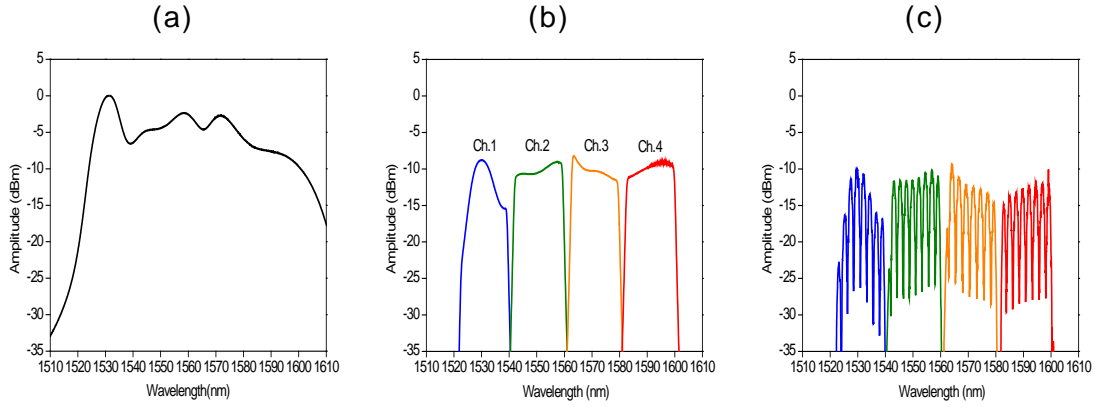
Fig. 4.20 (a) Optical spectrum of the OBS, (b) optical spectrum at the CWDM output ports with sliced channels centred at 1531 nm (—) 1551 (—), 1571 nm (—) and 1591 nm (—) and (c) optical spectra of the four channels at the output of the MZI installed at each ONU for an optical time delay of 3.4 ps (—) 3.5 ps (—), 3.6 ps (—) and 3.7 ps(—), respectively.

The characteristics of the implemented network, in terms of electrical response, have been measured employing both SMF and MMF optical links with a length of 5 km and 5.6 km, respectively. In both cases the EOM used in the setup has a 3dB electrical bandwidth of 15 GHz. The PDs employed for the SMF test have a 3dB bandwidth of 50 GHz and a responsivity of 0.63 A/W whereas PDs with a 3dB bandwidth of 23 GHz and a responsivity of 0.86 A/W are used in the MMF-based setup.
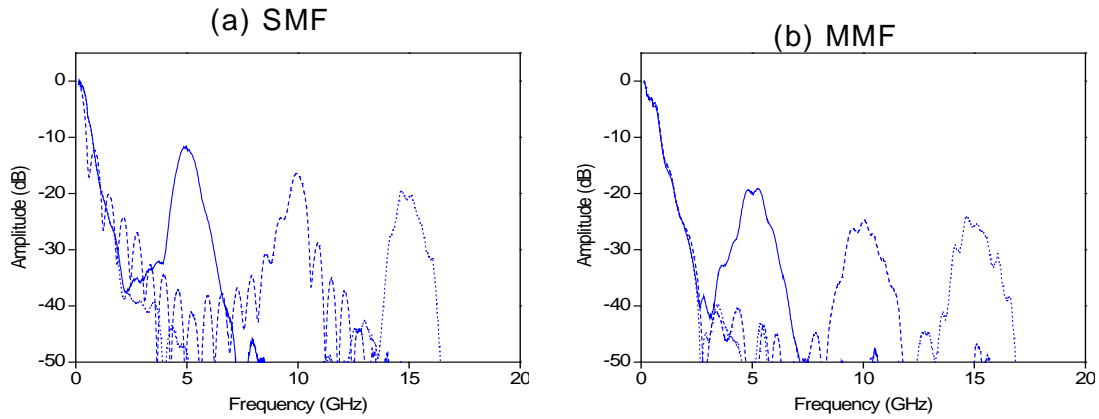
Fig. 4.21 Normalized experimental responses measured at ONU_1 when the band-pass windows are generated at 5 GHz (continuous trace), 10 GHz (dashed trace) and 15 GHz (dotted trace). (a) SMF, (b) MMF.

Figure 4.21(a) shows the electrical responses measured at ONU_1 when the band-pass windows are generated successively in three different regions centred at frequencies 5 GHz, 10 GHz and 15 GHz. The optical time delays have been set to 3.3 ps, 6.7 ps and 10.2 ps, respectively. Figure 4.21(b) shows the electrical responses measured at ONU_1 in the MMF case for optical delays of 2.7 ps, 5.3 ps and 7.9 ps are selected to place the band-pass filters at the same frequencies. The electrical responses show a common baseband region with a 3dB electrical

104

bandwidth around 0.5 GHz which is, as expected, the electrical operative range we would get without the insertion of the MZI.

In the SMF plot of Fig. 4.21(a), the high-frequency band-pass regions at 5 GHz, 10 GHz and 15 GHz have a 3dB bandwidths of 0.8 GHz, 0.6 GHz and 0.6 GHz with peak amplitude levels of -12 dB, -16 dB and -20 dB, respectively. The progressive attenuation experimented by the band-pass filters is due to the effect of the dispersion slope at higher frequencies.

In the MMF case, the band-pass windows have 1.0 GHz, 1.2 GHz and 1.1 GHz with peak amplitude levels of -20 dB, -25 dB and -26 dB, respectively. The peak amplitude levels are at most 8 dB below their correspondent levels of Fig. 4.21(a). This effect is caused by random fluctuations induced by the modal coupling.

From the results obtained, we deduce that the MZI structure modifies the propagation characteristics of the electrical transfer function enabling the transport of RoF signals. The same characterization has been carried out for all ONUs. As instance, Fig. 4.22(a) and (b) show the electrical response measured at all ONUs when all the MZIs generates a band-pass window at 5 GHz in case of SMF (a) and at 15 GHz in case of MMF (b).
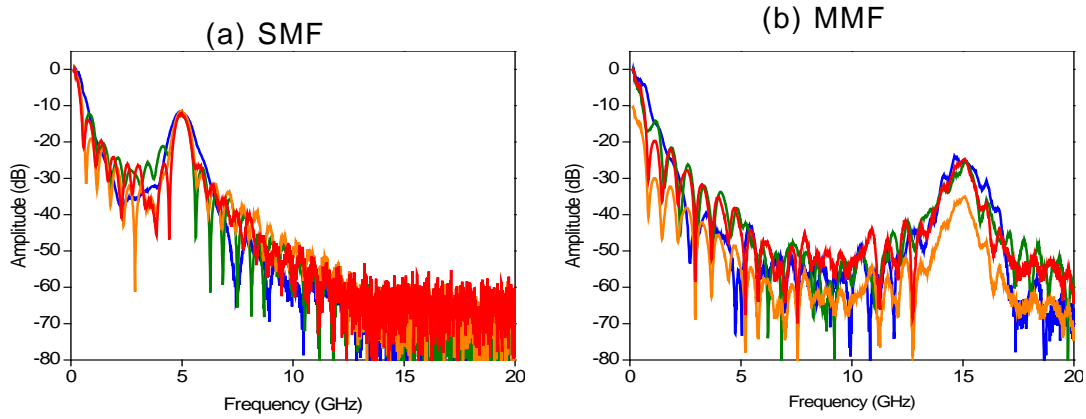
Fig. 4.22 Normalized experimental responses measured at ONU_1 (—) ONU_2 (—) ONU_3 (—) and ONU_4 (—) when the band-pass windows are generated at (a) 5 GHz for SMF and (b) 15 GHz for MMF.

Results similar to those represented in Fig. 4.21 have been obtained in Fig. 4.22. However, it can be observed that, independently of the tuning frequency and the optical link employed, each channel owns a different shape of the electrical response. It is due to the spectral dependence of the electrical response on the correspondent channel, which in turn, is set by the spectral profile the ASE source and the CWDM filter (see Fig. 4.20). The central frequency of the band-pass window depends on the optical delay introduced into the MZI of the corresponding ONU, the fiber dispersion value around the central wavelength of the selected channel, and the fiber length in accordance with eq. (4.5).

In Fig. 4.23(a) and (b) we show, for all channels, the linear dependence between the tunable central frequency of the band-pass window and the corresponding time delay.

105
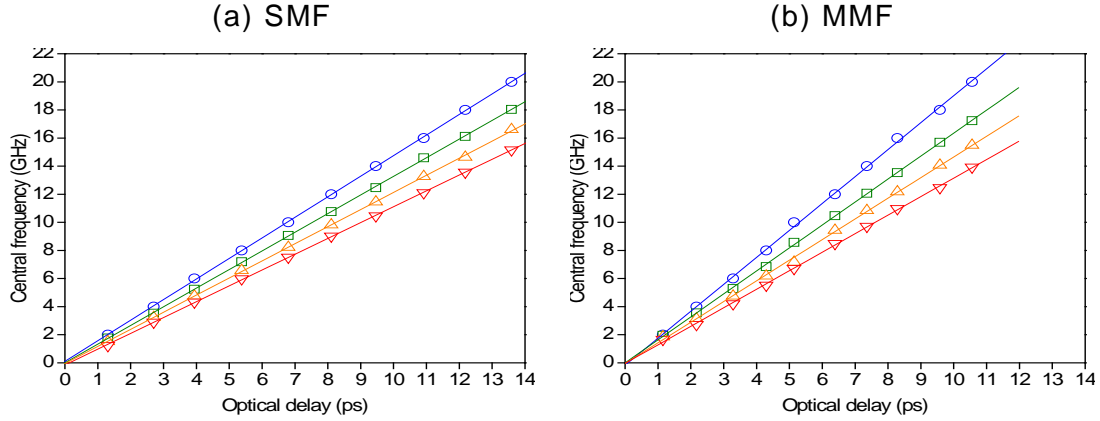
(a) SMF   (b) MMF

Fig. 4.23 Central frequency of the band-pass window vs. optical time delay measured at ONU$_1$ ($\bigcirc$), ONU$_2$ ($\square$), ONU$_3$ ($\triangle$) and ONU$_4$ ($\triangledown$). Theoretical slopes (—). (a) SMF, (b) MMF.

As expected, Fig. 4.23(a) and (b) show the linear relationship between the central frequency and the optical delay in the electrical operative range of the network around 20 GHz for all channels. Depending on the channel, the experimental points own different slopes. In the SMF case, the slope goes from 1.12 GHz/ps ($\triangledown$) to 1.46 GHz/ps ($\bigcirc$) indicating that for a given central frequency of the pass-band filter, higher time delays are required by channels at higher wavelengths. In the MMF case the slope increases from 1.31 GHz/ps ($\triangledown$) to 1.91 GHz/ps ($\bigcirc$) as the channel wavelength decreases. In both cases, the slope variations are due to the wavelength dependence of the chromatic dispersion parameter. The experimental points agree with the theoretical results (—).

4.2.3 Experimental evaluation of the network performance.

The performance offered by the proposed network is now evaluated through the transmission of RoF signals employing the SCM technique. The CO provides the electrical subcarrier for the transport of the downstream information and at each ONU the band-pass window is generated at the same subcarrier frequency. With regard to the downstream data we verify the flexibility of the network to the transport of different services by using different codification formats such as BPSK, QPSK and M-QAM as well as different bit rates. The evaluation of the quality of the received signals is made in terms of EVM, choosing conventional maximum criterion of 10.0% in case of BPSK and QPSK codifications and 6.0% for M-QAM codifications [Let 2005].

In the first set of experiments the transmission is run only between the CO and ONU$_1$ using the channel at 1531 nm with the aim of exploring the effect of the subcarrier frequency over the quality of the demodulated signal. The tested frequencies cover the available range of 20 GHz and the bit rate is set to a relatively low value of 5 Mb/s. Figure 4.24(a) and (b) plots the EVM as a function of the electrical subcarrier frequency for BPSK ($\square$), QPSK ($\bigcirc$), 16 QAM ($\triangle$) and 64-QAM ($\triangledown$) codifications.
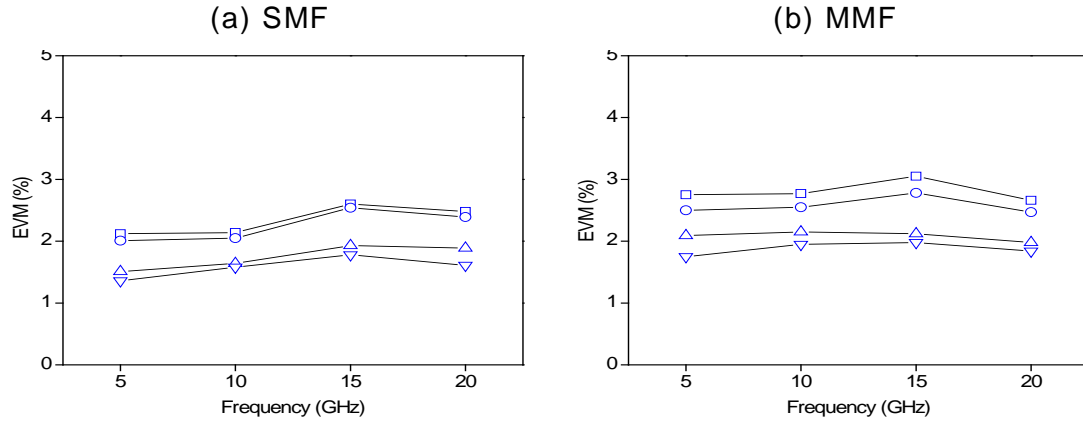
(a) SMF (b) MMF

Fig. 4.24 EVM vs. subcarrier frequency of the digital signal received at ONU$_1$ for codification formats BPSK (□) QPSK (○) 16-QAM (△) and 64-QAM (▽). (a) SMF, (b) MMF.

In both plots, the EVM of the received signal at ONU$_1$ ranges between 1.0% and 3.0% respecting the conventional criterion. The transmission quality is practically transparent to the subcarrier frequency. For a given frequency, the EVM improvement observed is just related to the codification type. In general the best quality, represented by EVM below 2.0%, is achieved by multilevel amplitude modulation formats (△,▽) due to their improved spectral efficiency. The back-to-back measured at the output of the EOM ranges between 1.3% and 1.5% in both cases.

In order to explore the overall transmission performance of the network we have performed another transmission tests including all channels and setting all electrical subcarriers and all band-pass windows to the maximum frequency of 20 GHz. Figure 4.25(a) and (b) show the results in terms of EVM related to the signal quality achieved at the four ONUs.
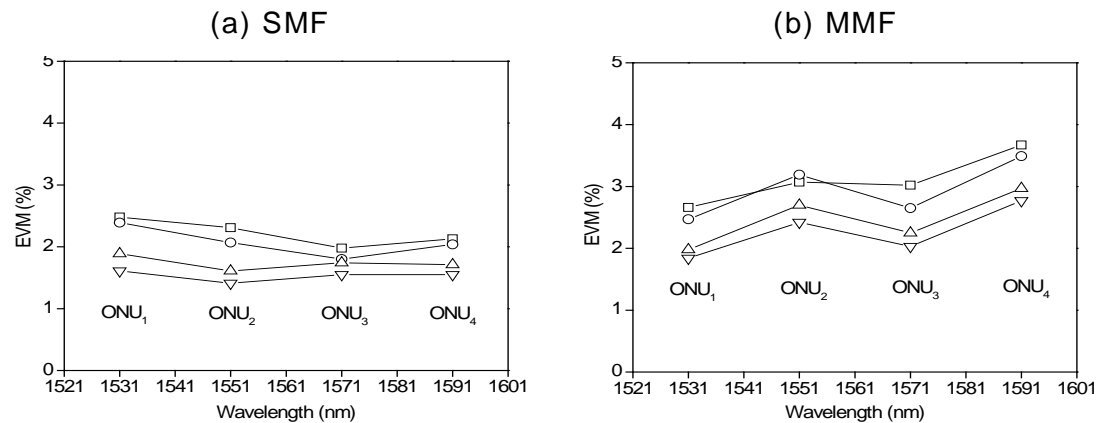
(a) SMF (b) MMF

Fig. 4.25 EVM vs. channel wavelength for codification formats BPSK (□) QPSK (○) 16-QAM (△) and 64-QAM (▽). (a) SMF, (b) MMF.

In both figures, the signal quality degradation undergoes by all channels follows a very similar trend characterized by EVMs not exceeding 3.0% and 4.0% for SMF and MMF respectively. As found in Fig. 4.24, the higher performance is achieved by 16-QAM and 64-QAM signals. The small variations observed between different channels are due to their different optical power distribution which depends mainly by the spectral profile of the OBS and the slicing of the CWDM. In case of MMF propagation this effect is further stressed by the modal coupling.

In the third test, we investigate the influence of the bit rate of the downstream traffic on the quality of the received signals. Considering first the transmission to ONU_4 as instance, we plot in Fig. 4.26(a) and (b) the EVM as a function of the bit rate for different codifications where the electrical subcarrier is set to 20 GHz. The maximum bit rate tested is limited by the demodulation bandwidth of the signal analyzer which is 25 MHz.
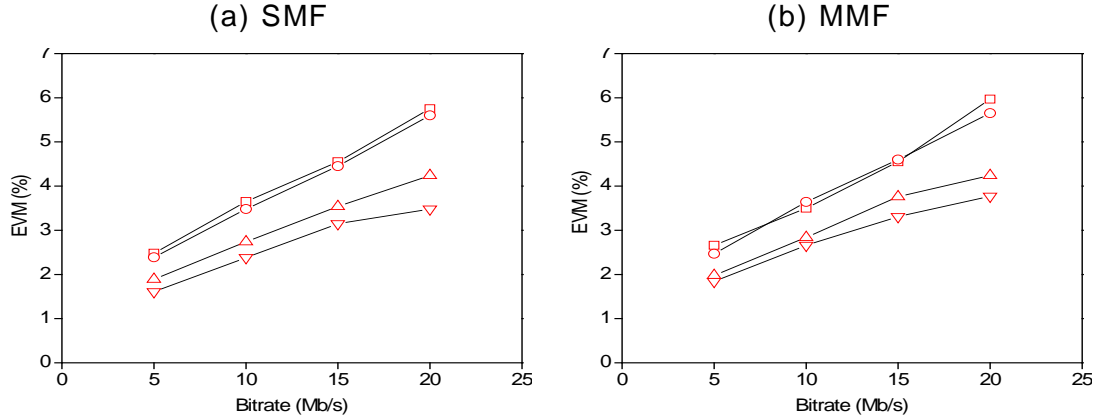
(a) SMF   (b) MMF

Fig. 4.26 EVM vs. bit rate of the downstream data received at ONU_4 for codification formats BPSK (□) QPSK (○) 16-QAM (△) and 64-QAM (▽). (a) SMF, (b) MMF.

Figure 4.26(a) and (b) show that the signal quality degradation increases with the bit rate with no significant differences between SMF and MMF. At minimum rates the EVMs are around 2.0% and 3.0%. At higher rates of 15 Mb/s and 20 Mb/s the EVM is kept below 5.0% and 6.0%, respectively. Again, the best performance is offered by M-QAM formats. In all cases, this behavior is due to a decrease of the signal to noise ratio at higher rates which is principally related to the demodulation bandwidth capabilities of the signal analyzer. Therefore, it is independent on the architecture. The behavior of the signal quality against the bit rate has been also evaluated for the remaining channels taking into account all modulation formats. Similar performance has been found implementing the SCM technique using 20 MB/s data modulating electrical tones at 20 GHz, which are the maximum capabilities of the implemented network.

Figure 4.27 summarizes these results displaying the constellation diagrams captured for the worst and the best channels after SMF (a) and MMF (b) propagation. Since the optical power distribution of the OBS and the CWDM slicing is not flat with the wavelength, in general the quality of the received symbols may vary from channel to channel as discussed before with the measurements of Fig. 4.25. However, the diagrams show that, for all type of codification, the symbols are received and demodulated with no significant degradation even in worst cases.

	BPSK	QPSK	16-QAM	64-QAM
(a) SMF worst case	EVM = 5.7% (Ch.1)	EVM = 5.6% (Ch.1)	EVM = 4.3% (Ch.1)	EVM = 3.6% (Ch.3)
(a) SMF best case	EVM = 3.8% (Ch.4)	EVM = 3.6% (Ch.4)	EVM = 3.0 % (Ch.4)	EVM = 2.7% (Ch.2)
(b) MMF worst case	EVM = 7.6% (Ch.4)	EVM = 6.8% (Ch.4)	EVM = 5.6% (Ch.4)	EVM = 4.8% (Ch.2)
(b) MMF best case	EVM = 5.9% (Ch.1)	EVM = 5.6% (Ch.1)	EVM = 4.2% (Ch.1)	EVM=3.7% (Ch.1)
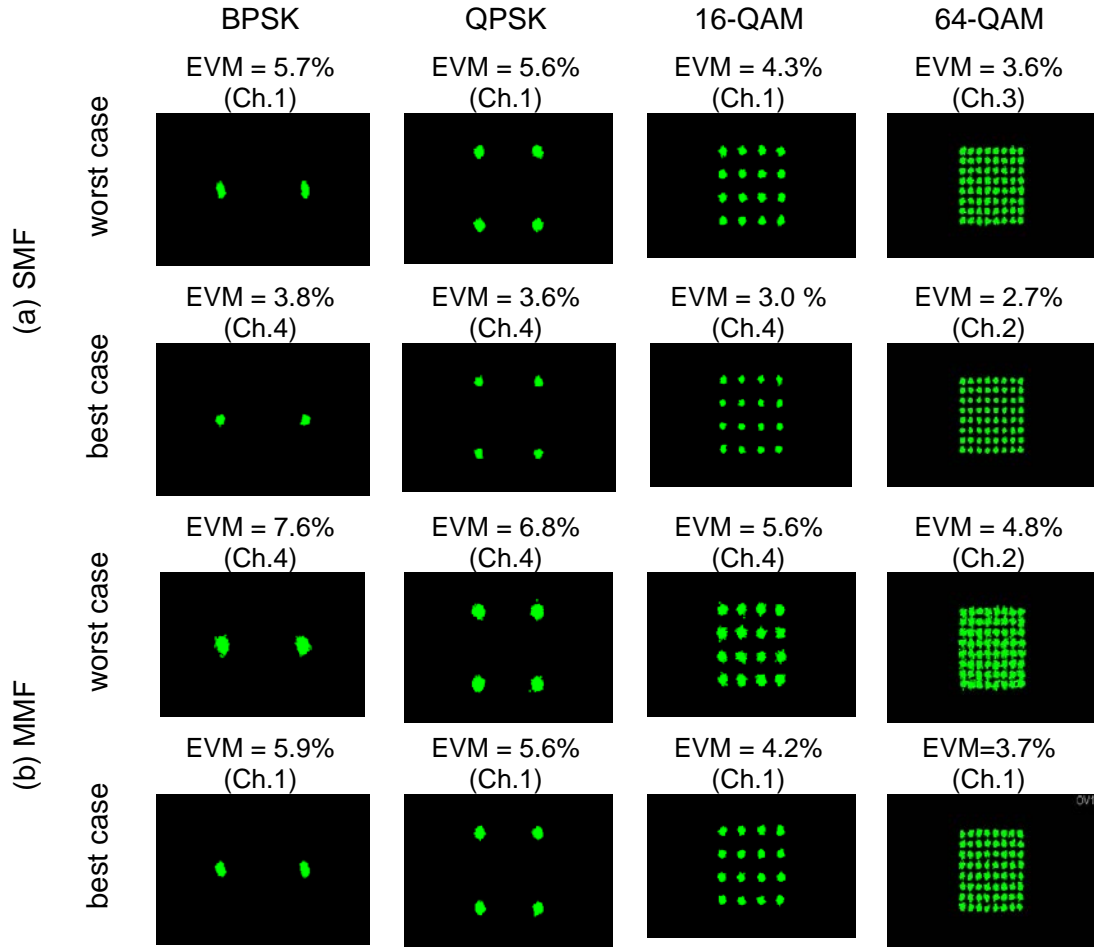
Fig. 4.27 Constellation diagrams for the best and the worst channels captured when the subcarrier frequency is set to 20 GHz and the bit rate is 20 Mb/s. (a) SMF, (b) MMF.

With this experimental validation we have demonstrated the viability of the proposed network. On one hand, the effectiveness and scalability of the spectral slicing approach applied to optical sources with a broad spectrum, and, on the other hand, the dispersion tolerant properties of the MZI structures, results in a powerful and flexible combination which makes our solution perfectly adaptable to the multichannel transport of RoF signals and very attractive for CWDM-PONs.

4.2.4 *Employment of phase modulation of the optical broadband source.*

In this subsection, we propose an alternative version of the spectral slicing-based CWDM optical access network for the transport of RoF signals in broadcasting mode. The main difference with respect to the previous network lies in the structure of the CO transmitter that employs phase modulation instead of the conventional DSB amplitude modulation of the optical carrier.

As described in Chapter 3, the PM-IM conversion process realized by the dispersive nature of the optical link when a coherent source is phase modulated, has a twofold advantage. First it allows the employment of the IM-DD scheme also for optical phase modulated signals. In this sense, the

PM format uses fiber chromatic dispersion as a positive factor. Second, the PM-IM conversion process generates a large band-pass transmission region through which the transport of RoF signals is permitted. In this context, the first configuration tolerant to dispersion would enable high frequency transport features equivalent to those achieved by a coherent source provided the tuning of the band-pass filter is made opportunely into the spectral region of the PM-IM curve. The schematic description of the proposed network is given in Fig. 4.28.
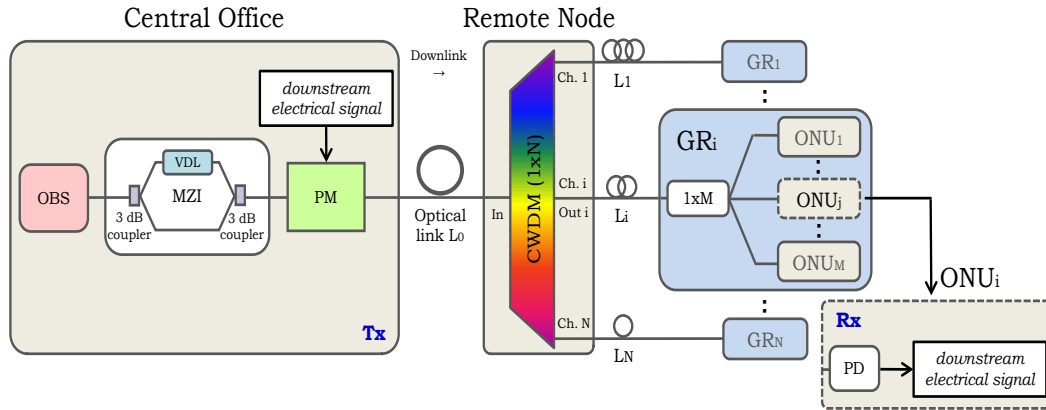
Fig. 4.28 Spectral slicing-based CWDM optical access network for the transport of RoF signals employing phase modulation of the optical broadband source.

In the CO transmitter, the OBS provides the optical field whose phase is modulated by the downstream data by means of a phase modulator. Prior to modulation the tunable MZI structure is inserted in accordance to the first configuration tolerant to dispersion. The resulting optical signal is launched into the optical link with length L_0 and reaches the RN. The RN, slices the incoming spectrum into N adjacent channels containing the same information. The N channels connect the RN with a number of N groups of ONUs (GR_1 to GR_N). In each group a passive (1xM) optical splitter is inserted to equally distribute the optical signal of the correspondent channel to M identically structured ONUs (ONU_1 to ONU_M) composed only by a photodetection circuit.

Since the network is designed to broadcast the same service to all remote groups, the cost associated to the MZI and the optical source can be shared among many users. However, as required in broadcast application, the optical time delay of the MZI must be previously tuned to generate at each remote group a band-pass transmission window that should be ideally centred at the same frequency of the service generated at the CO. In practice, since the optical channels have different wavelength, the central frequency of the band-pass filter may change due to the wavelength dependence of the chromatic dispersion.

In order to pre-compensate this effect and keep unchanged the central frequency of the band-pass filter, the feeding network between the RN and the N remote groups is composed by N fiber cables (L_1 to L_N) with a different length. For a given optical time delay, the central frequency of the band-pass windows and the fiber length are related by the following design equation:

$$\Omega_i = \frac{\Delta\tau}{\left|\beta_2\left(\lambda_i\right)\right|\left(L_0 + L_i\right)}, \ i = 1..N \quad (4.13)$$

where L_0 is the length of the link connecting the CO with the RN, and L_i is the length of the feeding channel. Note that, the physical distance between the RN and the location of the remote groups may be different from the fiber length L_i for practical reasons. In this case, a chirped FBG could be inserted in each group to modify the value of the dispersion and satisfy eq. 4.13.

In order to describe the electrical behavior of the transceiver we have implemented the scheme of Fig. 4.28 for N=4 and the same equipment of the experimental characterization of subsection 4.2.2 has been employed. In the experimental setup, the phase modulator has a 15 GHz bandwidth and the optical link is 20 km of SMF.

(a) (b)
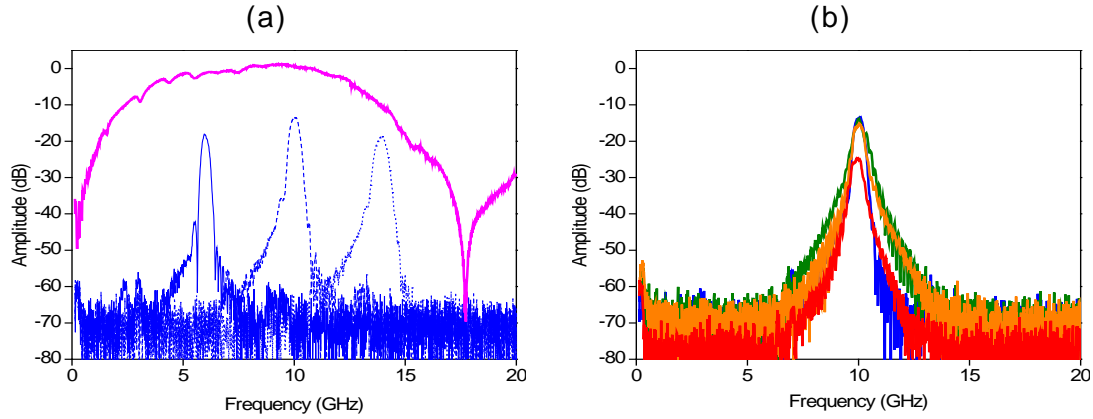
Fig. 4.29. (a) Normalized amplitude responses measured at GR_1 (Ch.1) with transmission window tuned alternatively at 6 GHz (continuous line), 10 GHz (dashed trace) and 14 GHz (dotted trace). Normalized PM-IM conversion curve measured by using a laser emitting at 1531 nm (—). (b) Normalized amplitude responses measured at all groups with channel centered at 1531 nm (—), 1551 nm (—), 1571 nm (—) and 1591 nm (—) and all band-pass windows generated at 10 GHz.

Fig. 4.29(a) shows the amplitude response measured at the first group, GR_1 which is fed by the channel centred at 1531 nm and supposing the presence of a single ONU in the group. The extra length of the optical SMF employed in the feeding plant is $L_1 = 5$ km. In the same plot is also included the experimental PM-IM curve (—) measured using a laser diode emitting at the same wavelength of the considered channel, 1531 nm. The PM-IM curve offers a 3dB bandwidth of 8.6 GHz around 10 GHz where the maximum PM-IM amplitude level is reached. In the case of Fig. 4.29(a) three different optical time delays are selected successively to open transmission windows at 6 GHz, 10 GHz and 14 GHz in the high-pass region of the PM-IM curve. Since the PM-IM curve is not frequency flat, the transmission window generated at 10 GHz is the only one showing the maximum peak amplitude. The peak amplitudes of the other two windows are 6 dB below.

A second test has been performed over all channels. Here all the band-pass windows are generated around 10 GHz which is the most favorable frequency according to the electrical transfer function of Fig. 4.29(a). Figure 4.29(b) plots the amplitude responses measured at each

group. Small differences are observed between the amplitude of the transmission windows of the first three groups comparing with the one of the fourth group. This effect is due to the spectral profile of the OBS employed which is not uniformly distributed as shown in Fig. 4.20(a).

The obtained results validate the employment of phase modulated OBSs combined with MZI structures as a solution highly compatible with the distribution of RoF signals over CWDM-based networks operating in the frequency range allowed by the PM-IM conversion function. Note that the operation range of the system is around 15 GHz. Moreover, the bandwidths of the amplitude responses of Fig. 4.29(b) are around 500 MHz. Therefore, our network potentially supports data rates up to hundreds of Mb/s with electrical subcarriers up to 15 GHz. At this point, we remark that the available operative range is determined mainly by the electrical bandwidth of the PM used in the experiment. In fact, operations at frequencies higher than 15 GHz can be potentially achieved provided higher bandwidth phase modulator is employed. Therefore the current operative limitation of the described network for high frequencies applications derives from the PM but it is not limited by the phase to intensity conversion curve.

With the aim of verify the transmission capabilities of the network, we have run the transport of QPSK and 64-QAM digital sequences at 5 Mb/s under the SCM technique. The evaluation of the signal quality degradation is made assuming as reference criterion a maximum 10.0% and 6.0% EVM for QPSK and 64-QAM data, respectively. The effect of the electrical SCM frequency on the quality of the signal received at GR_1 (Ch. 1) is firstly investigated. Fig. 4.30(a) plots the EVM as a function of the SCM frequency for QPSK ($\bigcirc$) and 64-QAM ($\triangledown$) data.
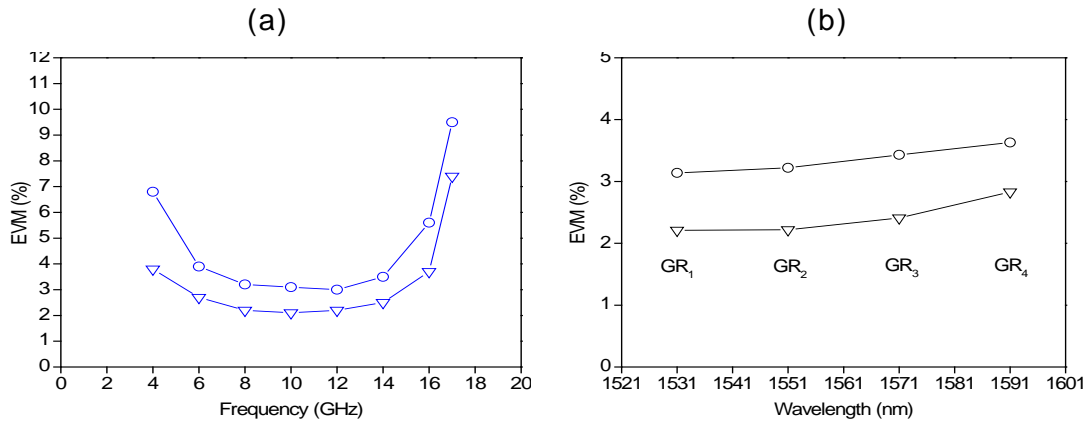
Fig. 4.30 (a) EVM vs. electrical subcarrier frequency measured at GR_1 for QPSK ($\bigcirc$) and 64-QAM ($\triangledown$) formats. (b) EVM over channel central wavelength when the bandpass window is tuned at 10 GHz. QPSK ($\bigcirc$) and 64-QAM ($\triangledown$) format.

As predicted by the PM-IM response and the amplitude responses of Fig. 4.29(a), the EVM increases at lower and higher frequencies and reaches minimum values around 10 GHz for both type of codifications. However, in case of QPSK the EVM is always below standard 10% in the tested SCM range with levels below 3.1% just around 10 GHz. The highest EVMs, 6.8% and 9.5%, are achieved at extreme frequencies far from the PM-IM maximum which are 4 GHz and 17 GHz, respectively. With 64-QAM, a good demodulation quality is obtained for electrical subcarriers up to 16 GHz. The worst case is observed at 17 GHz with an EVM of 7.4%, indeed. EVMs not exceeding 2.2% are found at subcarrier frequencies close to 10

GHz. In this test, the back-to-back was around 2.0%. Similar results have been obtained also with BPSK and 16-QAM formats after 20 km of SMF transmission.

To investigate the influence of the optical wavelength of the four CWDM channels, 5 Mb/s QPSK and 64-QAM data are broadcasted from the CO transceiver to each group after tuning the electrical transmission windows to 10 GHz. Figure 4.30(b) plots the experimental results in terms of EVM. The received signals always verifies the EVM criterion for both QPSK ($\bigcirc$) and 64-QAM ($\bigtriangledown$) formats and for all channels. The best results are achieved by GR_1 and GR_2 with EVM around 3.1% for QPSK and 2.2% for 64-QAM. According with the electrical responses of Fig. 4.29(b), the EVM values increase with the optical channel wavelength as a predictable effect induced by the different spectral power distribution of the channels. The worst case, resulting in an EVM of 3.6% (QPSK) and 2.8% (64-QAM), is measured at GR_4 which owns the band-pass window with the lower peak amplitude level.

However, even for the group with the poorest performance, the quality of the demodulated symbols is largely below the EVM limits established by the conventional criterion. The constellation diagrams displayed in Fig. 4.31 refer to the best and the worst case of the results presented in Fig. 4.30(b). They demonstrate that even in the worst case (GR_4) no significant errors are observed in the received symbols when the transmission window is tuned at 10 GHz.

GR_1 (Ch.1) GR_4 (Ch.4)

(a) QPSK   (b) 64-QAM   (c) QPSK   (d) 64-QAM
EVM = 3.1%   EVM = 2.2%   EVM = 3.6%   EVM = 2.8%
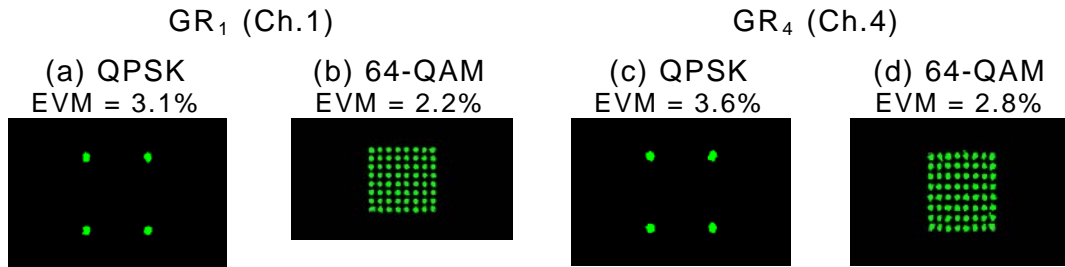
Fig. 4.31 Constellation diagrams in the best case GR_1 (a, b) and worst case GR_4 (c, d).

In the last test, the maximum number M of ONUs per group is experimentally estimated by splitting the total optical power received at each group. The experiment is performed considering SCM transmission of digital sequences on a subcarrier frequency of 10 GHz from the transceiver to the GR_1 and GR_4 which corresponds to the best and the worst channel respectively as found in Fig. 4.29(b) and 4.30(b).

In Fig. 4.32(a) and (b) the EVM is plot as a function of the number of ONUs which can be fed by splitting the optical power received at GR_1 ($\bigcirc$) and GR_4 ($\square$). The transmitted data are 5 Mb/s QPSK and 64-QAM, respectively.

Observing Fig. 4.32, for both groups an increase of the EVM is observed with the number of substations. In case of using QPSK format (a), the EVM is below standard 10.0% for a number of 8 ONUs per group. It means that the network allows good transmission performance for a total number M=32 of ONUs, being 4 the number of groups. Beyond 8 ONUs per group any splitting of the optical power produces a several degradation of

the received signal at BSG_4 ($\square$) which is the one that finally determines the system feeding capabilities.

When 64-QAM format is employed, such as in case (b), the EVM increases with the number of ONUs as well as in the previous case but the specification on the maximum EVM is achieved simultaneously by GR_1 ($\bigcirc$) and GR_4 ($\square$) only for a maximum number M=4 of ONUs. It leads to a total number of 16 ONUs deployable through the network. In case of more than 4 ONUs per group served, the available optical power is not as high as to guarantee a good broadcast transmission over the implemented link. However, considering the low capacity requirements of a CWDM access network, these results may be widely acceptable.

(a)   (b)
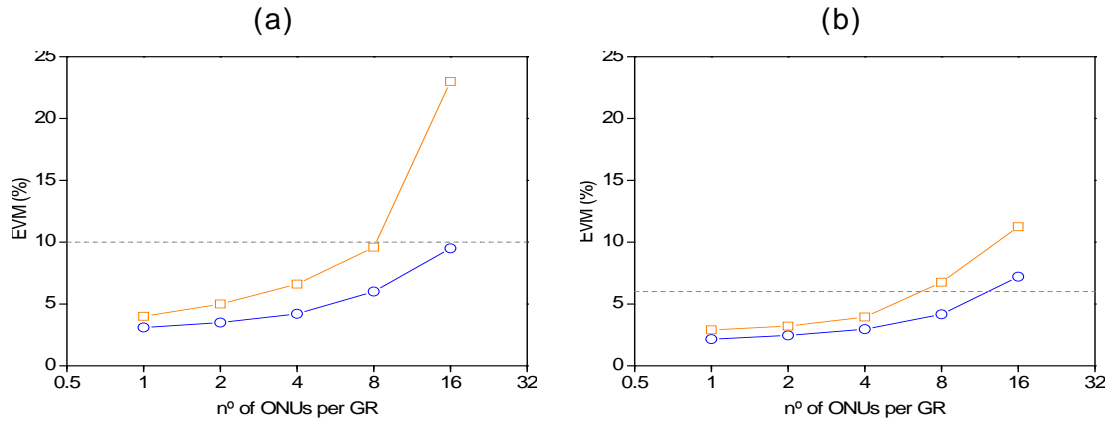
Fig. 4.32 EVM as a function of the number of ONUs per GR_1 ($\bigcirc$) and GR_4 ($\square$) for subcarrier frequency at 10 GHz and 5 Mb/s digital sequences modulated in (a) QPSK and (b) 64-QAM.

The possibility to extend the proposed network configuration to multiservice applications has been also investigated and successfully demonstrated through a simple upgrade of the CO transceiver of the system proposed in Fig. 4.28. In terms of experimental implementation the upgrade is based on inserting a N-way [1_{In}xN_{Out}] power splitter at the output of the OBS and a N-way [N_{In}x1_{Out}] optical combiner before the launching point. In the middle of them, N parallel MZI-PM structures are installed where each PM is fed by a different RoF signal and the pass-band window is opportunely tuned at the corresponding electrical frequency.

Although this architecture highlights once more the scalability issues of the MZI structures and spectral slicing, we found that, the overall network transmission performance depends strongly on the received optical power-per-channel, due to the OBS power splitting realized at the CO transmitter. Moreover, the installation of several MZI-PM structures would be also too expensive if N is high. However, these two limitations can be less significant in applications with a low number of channels.

4.2.5 Photonic suppression of non-linear distortion and all-optical frequency generation and up-conversion.

As described in Chapter 2, in optical WDM access networks designed to the transport of signals in the GHz band, the SCM scheme has been widely integrated in order to serve a larger number of end-users on a single WDM channel and, thus, improving the channel spectral efficiency. The SCM scheme is based on subdividing the radio frequency spectrum

114

transmitted by a single optical carrier in several independent radio channels. In this way the SCM scheme also provides a means to merge different communication services regardless of modulation formats and bit rates.

In a basic configuration of an SCM-WDM optical system n-independent high-speed digital signals are mixed by n-different μ-wave or mm-wave subcarriers. Then they are combined and optically modulated onto a single WDM channel. All WDM channels are then multiplexed and launched from the transmitter. At the RN an optical demultiplexer separates the WDM wavelengths for individual detection at the correspondent ONU where the digital signals can be finally recovered after detection at the SCM level.

For this operation, high-performance filters must be employed at the receiver to select and extract the content of one or various SCM signals within a given WDM wavelength without distorting and affecting the eventually baseband signals and/or other radio frequency channels assigned to the same or an adjacent ONU. In most of the cases the high bandwidth nature of the modulated subcarriers and the high-speed of digital data may require to perform these signal processing tasks directly in the optical domain overcoming the hardware limitations of the electronic processing, known in the literature as the "electronic bottleneck" [Cap 2005].

Another aspect that must be carefully taken into account is that the SCM technique requires a high degree of linearity to achieve the desired performance. In other words, any non linear distortion introduced by the transmitter, the optical link and the receiver, may induce undesired HD and IMD components in the SCM signal, as shown in eq.3.13 . In SCM links it has been found that the main factor limiting the receiver sensitivity is the optical modulation depth that could be obtained in the transmitter. This parameter, known as modulation index, is restricted by the non linear distortion generated in the optical modulator at high driving voltage levels, that is, when the optical modulator is driven electrically by one or several high amplitude electrical tones composing the SCM modulating signal [Loa 2003, Che 2006, Cou 2006, Lau 2006, Wu 2006, Lim 2007]. Therefore, one major source of non linear distortion is the inherently non linear electrical response of the optical modulator operating at large modulation indexes. Unfortunately, this is just the most likely driving condition in SCM schemes.

Various solutions have been proposed in order to combat the modulator-induced distortions and improve the dynamic range of optical links including optical feed forward [Lsm 2005], RF pre-distortion and adaptive predistortion methods [Lu 2004, Sha 2005] or SSB-AM format [Lim 2007, Mas 2007] among others. Successful results have been achieved at the expense of complex transmitters or the bandwidth limitations of the electronic processing.

In this context the electrical characteristics of the MZI can be conveniently exploited not only to surmount the transmission limitations caused by fiber chromatic dispersion, but also as an alternative way to perform the linearization of the optical modulator electrical response. In fact, the role played by the MZI is double since the band-pass window permits the transport of any signal falling into its spectral region and simultaneously rejects all undesired frequency components in adjacent bands. If these unwanted components are the distortion terms generated by

the optical modulator, the resulting effect is their suppression, which, as an added value, is made optically without the insertion of additional electronics devices.

The experimental validation of this concept has been realized by implementing the scheme of Fig. 4.33 for a 10 km of SMF-based optical link and for N=4.
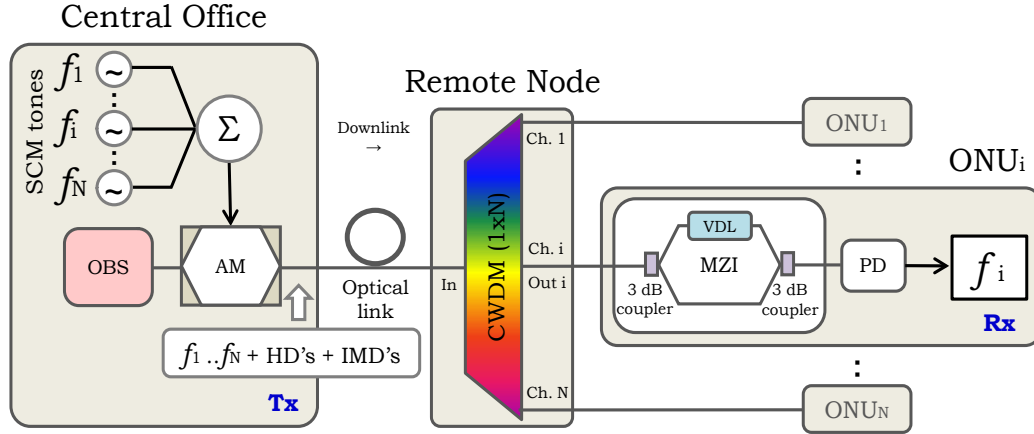
Fig. 4.33 Photonic suppression of the EOM distortions in SCM-WDM systems.

The first study is focused on the suppression of HD terms arising when the amplitude modulator is driven by a single large-amplitude electrical subcarrier.

Figure 4.34(a) plots the electrical response measured at the output of the optical modulator when an electrical tone at f_1=8 GHZ with 25 dBm of amplitude is used as driving input. Figure 4.34(b) plots the electrical transfer function measured at ONU_1 after photodetection when the band-pass window generated by the MZI is centred at 8 GHz and has a bandwidth of 320 MHz. A detail of the first harmonic spectrum is included as inset.
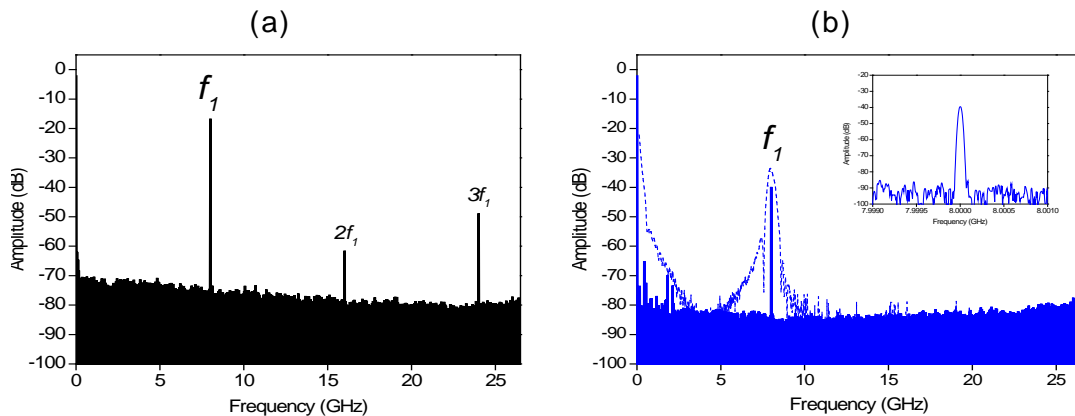
Fig. 4.34 Normalized amplitude response measured (a) after the EOM, (b) at ONU_1 after photodetection when the band-pass window of the MZI is tuned at 8 GHz (dashed trace).Inset: Detail of the electrical spectrum of the selected first harmonic.

In Fig. 4.34(a), we observe clearly the second and third harmonic distortion terms generated by the response of the modulator biased in the non linear region. As shown in Fig. 4.34(b), when the band-pass filter is generated at

8 GHz, the desired tone is selected and all undesired distortion terms are successfully filtered-out. Therefore the MZI realize intrinsically the linearization of the EOM response against HD distortion in a range of 25 GHz and with more than 40 dB of rejection.

With the same setup we demonstrate the optical generation and suppression of IMD products using the photonic filtering functionality realized by the MZI. In this case the amplitude modulator has been fed by the SCM sum of two tones at f_1=10 GHz and f_2=13 GHz with 25 dBm of amplitude each one directed to ONU_1 and ONU_2, respectively. Fig. 32(a) shows the electrical spectrum measured at the output of the EOM. Figure 4.35(b) and (c) plots the electrical response measured at ONU_1 and ONU_2.

(a) (b) (c)
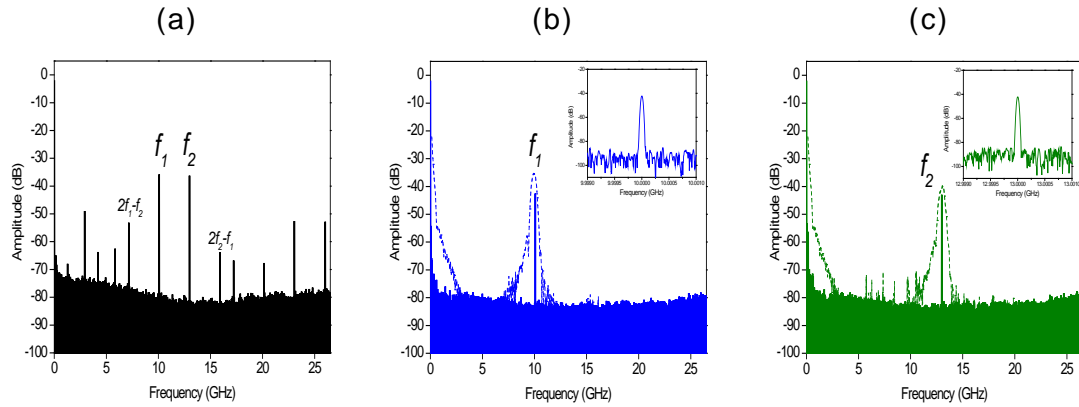
Fig. 4.35 Generation (a) and all-optical suppression of IMD terms at ONU_2 with band-pass window at 10 GHz (b) and at ONU_3 with band-pass window at 13 GHz (c). Insets: detail of the electrical spectrum of the selected subcarrier.

Figure 4.35(a) shows the HD and IMD components generated by the beating between the two SCM tones. Amongst others, the IMD products at $2f_1$-f_2 and $2f_2$-f_1 are generally more detrimental since they are in close proximity to the desired subcarriers. In order to receive only the 10 GHz subcarrier, the MZI inserted at ONU_1 generates a band-pass window at 10 GHz with a bandwidth of 420 MHz. The same operation is performed at ONU_2 but with a 460 MHz-bandwidth band-pass window tuned at 13 GHz which is the frequency of the second subcarrier. In both cases the resulting electrical spectrum is composed of a single harmonic component corresponding to the selected channel and free of any other unwanted distortion term. Therefore, owing to the filtering functionality of the MZI structure, also the IMD products have been successfully rejected in a range of 25 GHz.

In the previous discussion we have stated that the intrinsic non linearity of the electro optical modulation may be a problem in linear applications, such as, the distribution of GHz-band signals. It has been demonstrated that the photonic filtering process performed by the MZI is vital to the minimization of harmonic and intermodulation products especially when the modulation index is too large as in SCM signal distribution. However, for non linear applications, such as μ-wave and mm-wave generation and frequency up-conversion, the modulation index should not be too small to maximize the non linear effect of the optical modulator and ensure a good frequency multiplication or up-conversion efficiency. In these operations, the desirable signal is just one of the generated HD or IMD products, indeed.

To date, several techniques have been proposed to implement the µ-waves and mm-waves generation and up-conversion directly in the optical domain. Among them, the use two cascaded intensity modulators [Zha 2007, Chi 2008], the PM combination with dispersive links [Yao 2005, Zen 2005], the selective amplification of Brillouin scattering [Par 2007], and the employment of SOA non linearity such as XGM, [Seo 2003] XPM [Lee 2004] and FWM [Wan 2006] are the most relevant. Although high frequency mixing and conversion performance has been achieved, the major drawbacks of these techniques are related to the high complexity and poor stability of ultra narrowband filters employed, the need of high frequency electrical phase shifters making the approach not all-optical but hybrid. Moreover the power fading induced by fiber dispersion constrains the integration of complex dispersion compensation devices, and the complex use of coherent sources.

In our solution we take advantages of the non linear characteristics of the EOM and the high potential of the photonic filtering functionality offered by the MZI to implement simultaneously all-optical high-frequency mixing and up-conversion operations. In particular, the principle of the optical frequency generation and up-conversion scheme can be divided in two easy steps. The first step is to generate optically high-order harmonics by driving the amplitude modulator with a low or intermediate frequency electrical tone at the CO. The second step is to design the MZI at the ONU to have a band-pass window located just at the desired high-harmonic, which is the target up-converted signal, and rejecting all frequency components other than the up-converted one.

In order to demonstrate experimentally the technique we have adapted the scheme of Fig. 4.33 to our purpose by driving the optical modulator with the sum of an electrical signal at intermediate frequency f_{IF}=3 GHz and a local oscillation at f_{LO}=10 GHz and keeping the modulation index as high as possible in order to operate in the non linear region of the EOM. Under this conditions we choose the high order harmonic at the sum frequency f_{IF}+f_{LO}=13 GHz, as up-converted signal Therefore the transmission window, generated by the MZI at ONU_1, will be placed at 13 GHz.

Figure 33(a) shows the spectrum at the output of the EOM and Fig 33(b) plots the amplitude response measured at ONU_1 after photodetection when the MZI is tuned at 13 GHz.

As expected, the spectrum of Fig. 4.36(a) contains all the intermodulation products arisen from the beating between f_{IF} and f_{LO} among which the desired harmonic at 13 GHz can be identified. In Fig. 4.36(b) the band-pass window has a 460 MHz of bandwidth and, since it has been tuned at 13 GHz, the resulting effect is the selection of a pure tone corresponding to the up-converted signal with suppression of the remaining intermodulation products. The conversion efficiency, defined as the ratio of the electrical power of the up-converted signal at f_{IF}+f_{LO} to the detected electrical power of the intermediate frequency signal before up-conversion [Lee 2004, Par 2007], is found to be around -4.5 dB and can be improved by optimizing the input radio frequency components.

(a) (b)
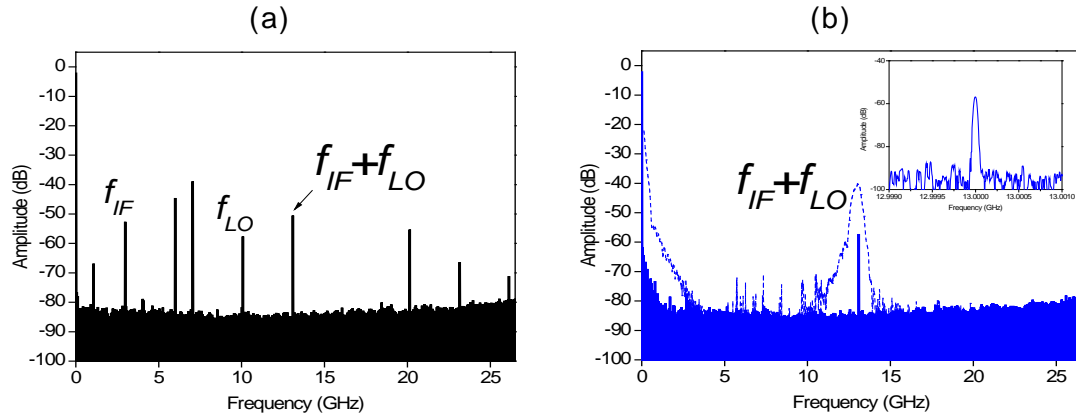
Fig. 4.36 Normalized amplitude response measured (a) after the EOM, (b) at ONU$_1$ after photodetection selecting the up-converted signal at 13 GHz. Inset: Detail of the electrical spectrum of the up-converted harmonic.

4.3 Full-duplex reconfigurable CWDM optical access network for wireless and wired services convergence.

Section 4.2 has been focused on the spectral slicing technique which is as a convenient strategy to replace many lasers by sharing the broadband spectrum of single OBS among many users of a PON. Since the transmission performance of OBS-based links has been found to be severely limited by fiber chromatic dispersion especially around the third band, MZI structures has been inserted at each ONU as an effective means to surmount such limitations and, thus, enable the transport of high frequency signals up to tens of GHz over multiple CWDM channels. To take a step forward, in this section we propose a novel and advanced CWDM optical access network architecture where, for the first time, bidirectional transmission and reconfigurable capacity assignment features are integrated. In addition, the proposed network performs the convergent transport of wireless and wired services using a light-sources centralized architecture.

4.3.1 Description of the network architecture.

The architecture of the full-duplex and reconfigurable CWDM optical access network is depicted in Fig. 4.37. The general architecture is composed by a CO connected to a RN via optical link and a group of N ONUs. In the CO, the optical field provided by a single OBS is first DSB-AM modulated by the downstream RoF signal and then broadcasted through the optical fiber in downlink direction. After propagation the optical modulated signal reaches the RN. At the RN the CWDM slices the incoming spectra into N adjacent channels (Ch.1 to Ch. N) each one transporting the same information, in this case. At the output ports of the CWDM a MZI structure is inserted in accordance to the second configuration, to permit the transport in the band-pass region centred at the same frequency of the downstream signal. Among all channels, a number i of them is dedicated to assure a fixed and unitary capacity assignment for each ONU whereas the remaining (N-i) are selected to supply an extra capacity service assignment.

119
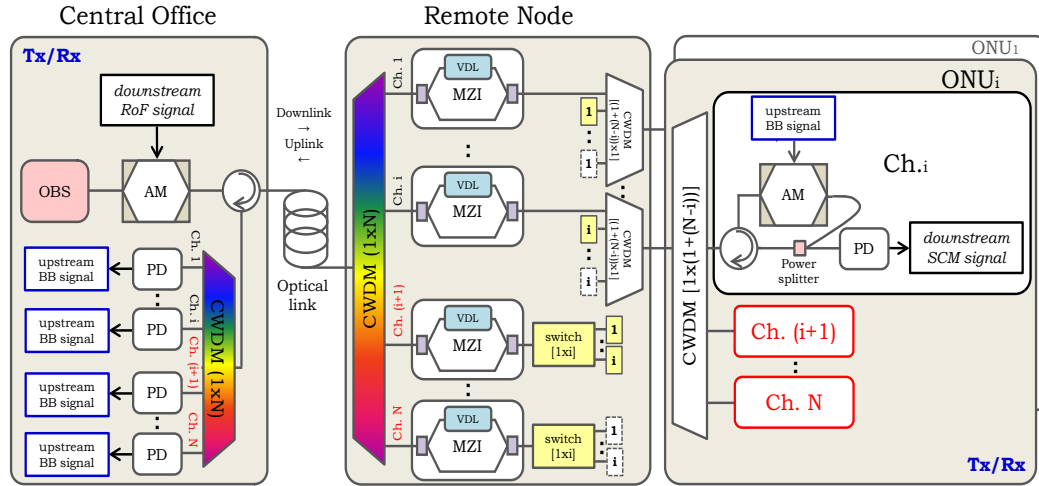
Fig. 4.37 Full-duplex and reconfigurable SCM-CWDM optical access network.

For each extra channel, the dynamical assignment of extra capacity is managed by a [1xi] optical switch, being i, the number of the switch output ports which also coincides with the number of fixed channels and ONUs. Depending on the demanding ONU, the configuration state of the optical switch is changed in order to select and route the extra service. For example, if ONU_i requires an enhancement of capacity, only the i-output port of one or more switches is enabled. Than the corresponding fixed and extra channels with index i are combined and routed to ONU_i through another CWDM. There are as CWDMs installed as the number of fixed channels. Being (N-i) the maximum number of extra channels available, the number of switches installed is also (N-i). Therefore, the CWDMs that combine the fixed and the (N-i) possible extra channels must have at least (1+(N-i)) input ports. The reconfigurable structure of the RN is thus compact and flexible to the addition of new users since the number of managed wavelengths is governed by the slicing capabilities of the particular CWDM.

The ONUs are all structurally identical. Each ONU receives the fixed and eventually all the extra channels which are first demultiplexed by a [1x(1+(N-i))] CWDM and then routed by means of an optical circulator toward the photodetection circuits where the channels are recovered separately. To perform the uplink transmission, a portion of the downlink power of the received channels is re-used by means of a power splitter and modulated by the upstream signals via amplitude modulators. Since the band-pass region has been already dedicated to the downlink transport of RoF signals, the upstream signals are modulated in the low-pass region of the electrical transfer function. This approach allows the convergent transport of wireless and wired service over the same infrastructure.

The upstream baseband signals are sent back to the network through the same optical circulator travelling a symmetrical round trip over the same optical fiber. At the CO, the optical circulator separates the downlink and uplink traffic and routes the upstream signals to a [1xN] CWDM followed by a set of N PDs for optical detection and data recovery.

With such a wavelength re-use approach, all ONUs are kept source-free and wavelength-independent agree with the centralization concept. It supposes a significant minimization of complexity and management

operations associated to the installation of additional light sources in the ONU. Moreover, since the installation and control of the MZIs is also centralized and performed at the RN, the ONU architecture is further simplified.

4.3.2 Experimental characterization and performance evaluation.

The proposed network architecture has been characterized experimentally by implementing the scheme of Fig. 4.37. For availability reasons, [1x4] CWDMs have been employed. Therefore, since N = 4, we have chosen i=3 as the number of fixed capacity channels whereas only one channel has been reserved for extra capacity assignment.

As in previous experimental implementations, the four channels resulting from the OBS slicing have central wavelengths: λ_1^F= 1531 nm (Ch.1), λ_2^F=1551 nm (Ch.2), λ_3^F=1571 nm (Ch.3) and λ_4^E=1591 nm (Ch. 4). The optical switch is a $[1]_{In}$ x $[4]_{Out}$ MEM switch with ultra-low insertion loss. The optical link is a 10 km of SMF length. The channel assignment as well as the correspondence with the CWDM ports is specified in Table 4.1 where the fixed and extra capacity channels are differentiated by color.

Table 4.1 Wavelengths plan.

Fixed capacity channels (nm)	Extra capacity channels (nm)	CWDM port	ONU
λ_1^F = 1531		1	1
λ_2^F = 1551		2	2
λ_3^F = 1571		3	3
	λ_4^E = 1591	4	

As described in subsection 4.3.1, the proposed network is envisioned to perform the bidirectional distribution of a given number of channels between the CO and a group of remote located ONUs through an integrated reconfigurable router. In order to implement and evaluate the reconfiguration capabilities of the network different routing scenarios must be previously defined. Based on the number of channels available and their assignment plan described in Table 4.1, we have defined and implemented three different routing scenarios for both downlink and uplink transmissions with no loss of generality.

In the first scenario each fixed channel is routed toward its own ONU in absence of any extra capacity service. This scenario emulates the network operative state under normal traffic conditions. In the second scenario a given ONU is fed by its correspondent fixed channel and requires the capacity extension represented by the extra channel. This case emulates an asymmetric capacity assignment under extra traffic demand conditions. In the last scenario the fixed channel is assigned to its correspondent ONU while the extra channel is routed to an adjacent ONU. This scenario is intended to investigate how the presence of the extra service in a given ONU affects the normal operability of an adjacent ONU. A schematic representation of the experimental routing scenarios is given

in Table 4.2 showing one of the three possible configurations for the second and third scenarios.

Table 4.2 Experimental routing scenarios.

	Scenario 1			Scenario 2			Scenario 3		
	Fixed		Extra	Fixed		Extra	Fixed		Extra
ONU$_1$	λ_1^F			λ_1^F			λ_1^F		
ONU$_2$		λ_2^F			λ_2^F	λ_4^E		λ_2^F	
ONU$_3$			λ_3^F			λ_3^F		λ_3^F	λ_4^E

For service differentiation in downlink direction, the downstream RoF signals is generated with the SCM technique where 5 Mb/s QPSK data modulates 5 GHz and 10 GHz electrical subcarriers for the fixed and extra capacity assignment, respectively. In uplink direction the baseband signal is an OOK modulated PRBS.

Figure 4.38 shows the electrical transfer function measured at ONU$_1$ (—), ONU$_2$ (—) and ONU$_3$ (—) when the MZIs are tuned at 5 GHz in accordance to the transmitted service. All baseband windows have a bandwidth between 0.3 GHz and 0.4 GHz whereas the band-pass region bandwidths are between 0.4 GHz and 0.5 GHz with relative maximum amplitude around -9 dB for the fixed channels and -12 dB for the extra channel. Also, electrical transfer function measured at ONU$_3$ (—) is shown when the bandpass window is generated at 10 GHz.
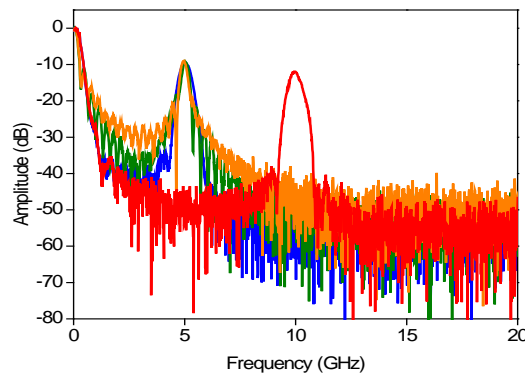
Fig. 4.38 Normalized amplitude response measured at ONU$_1$ (—), ONU$_2$ (—) and ONU$_3$ (—) with band-pass windows generated at 5 GHz. Amplitude response at ONU$_3$ (—) for a 10 GHz band-pass window.

In order to show the full-duplex transmission performance offered by the proposed reconfigurable optical access network, we evaluate first the downstream signal quality degradation in terms of EVM choosing a maximum EVM = 10.0%. All measurements have been made in accordance to the three scenarios defined above. In particular Fig. 4.39 plots the EVM as a function of the electrical power measured for CH$_1$ at ONU$_1$ (a), CH$_2$ at ONU$_2$ (b) and CH$_3$ at ONU$_3$ (c) when scenario 1 (□), scenario 2 (○), and scenario 3 (△) are implemented.

Downlink (Fixed channels)

(a) CH$_1$ (ONU$_1$) (b) CH$_2$ (ONU$_2$) (c) CH$_3$ (ONU$_3$)

($\square$) EVM=3.4% ($\bigcirc$) EVM=3.3% ($\triangle$) EVM=3.5%
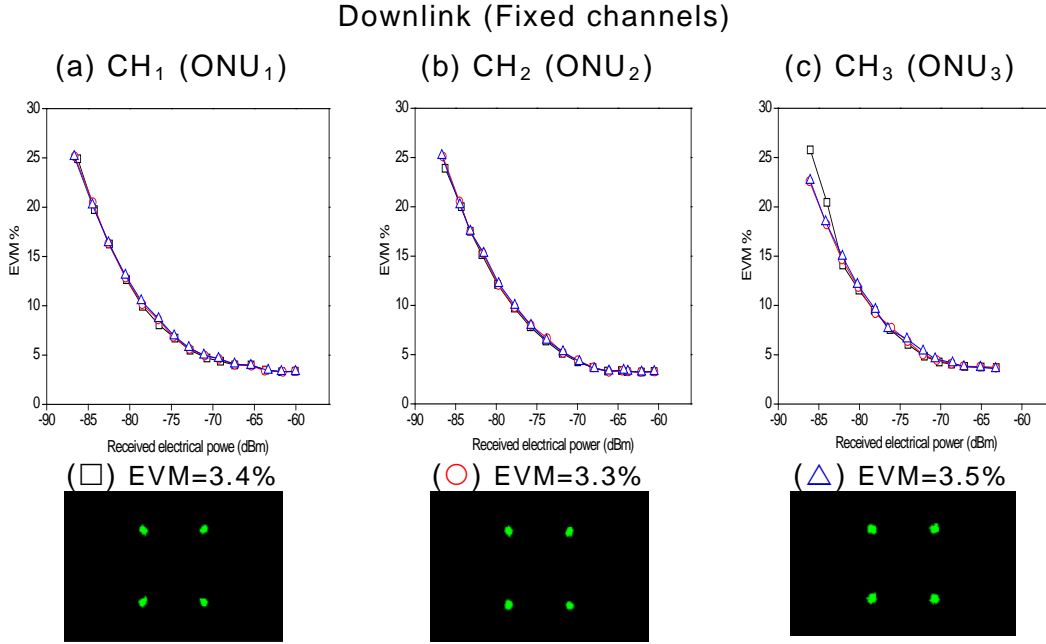
Fig. 4.39 EVM vs. received electrical power of the downstream signal transmission measured for fixed (a) CH$_1$ (ONU$_1$), (b) CH$_2$ (ONU$_2$) and (c) CH$_3$ (ONU$_3$) in routing scenario 1 ($\square$), 2 ($\bigcirc$) and 3 ($\triangle$). Constellation captured at ONU$_1$, ONU$_2$ and ONU$_3$ in the best demodulation case.

Considering the fixed CH$_1$ (measured at ONU$_1$) and the results (a) related to the first scenario ($\square$), the quality of the demodulated signal improves toward EVM between 3.0% and 4.0% when the power of the electrical signal received is around -65 dBm. When the second and third scenarios are implemented, the quality of the signal carried by CH$_1$ is practically not affected by the presence of the extra channel routed to the adjacent ONU$_2$ ($\bigcirc$) or to ONU$_3$ ($\triangle$). Observing cases (b) and (c), similar results have been achieved by measuring the signal degradation of fixed CH$_2$ (demodulated in ONU$_2$) and fixed CH$_3$ (demodulated in ONU$_3$). In fact, when scenario 2 and 3 are implemented, the quality of the signal carried by these channels is practically not affected by the presence of the extra channel 4 in their own ($\bigcirc$) or adjacent ($\triangle$) ONU. The good quality of transmission is also confirmed by the constellation diagrams captured in optimal receiving conditions plotted below each case for a particular scenario. However, the slight EVM variations observed from channel to channel reflect the different spectral characteristics of the CWDMs installed in each ONU.

It must be also remarked that for all channels, the signal demodulation is performed in a region where small variations of the electrical input power induces an abrupt increasing of the EVM. This region is governed by the electrical back-to-back of the transmitter whose EVM degradation is more appreciable at received electrical powers below -80 dBm. Therefore, such EVM degradation does not depend on the optical characteristics of the network.

The signal quality degradation of the extra channel 4 has been also measured at ONU$_2$, just as an example, in both scenario 2 ($\bigcirc$) and scenario 3 ($\triangle$). Figure 4.40 shows the corresponding EVM degradation.

Downlink (Extra channel)

CH$_4$ (ONU$_2$)

($\bigcirc$) EVM=3.2%   ($\triangle$) EVM=3.2%
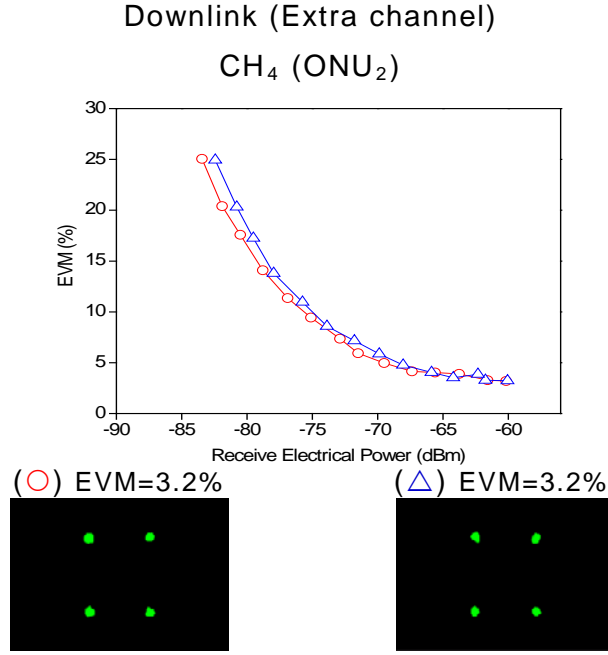
Fig. 4.40 EVM vs. received electrical power of the downstream signal transmission measured for extra CH$_4$ at ONU$_2$ in routing scenario 2 ($\bigcirc$) and routing scenario 3 ($\triangle$). Constellation diagrams captured at ONU$_2$ in the best demodulation case.

In Fig. 4.40, we observe that the degradation curves of the extra channel measured at ONU$_2$ are similar to those found for the fixed channels independently on which of the two scenarios is implemented. It demonstrates the reconfiguration capabilities of the network in downlink direction.

With regard to the uplink transmission, the upstream quality is evaluated using the bit error rate (BER) parameter fixing a minimum BER = 10^{-12} as conventional criterion. Fig. 4.41 shows the uplink BER measured as a function of the optical power received at the CO for three different bit rates, (a) 50 Mb/s, (b) 100 Mb/s and (c) 150 Mb/s. In particular the BER degradations of the signals carried by fixed CH$_1$, CH$_2$ and CH$_3$ in routing scenarios 1, 2, and 3, respectively, are plotted together with the back-to-back curve (dashed line).

Figure 4.41(a) indicates that, the uplink signal quality is successfully below the required minimum BER when the optical power received is higher than -24.4 dBm, -24.0 dBm, and -23.9 dBm for the first, second and third scenarios, respectively. The power penalty with respect to the back-to-back curve is around 0.8 dB in the worst case represented by CH$_3$. It means that the uplink transmission performance of the proposed network is very close to the ones achievable in the back-to-back configuration (dashed line). As observed in cases (b) and (c) of Fig. 38, at higher bit rates a higher optical power is required to maintain the same demodulation performance. For example, considering the curve relative to CH$_1$, in cases (b) and (c) the optical powers needed to reach a BER=10^{-12} are, respectively, 0.7 dB and 1.7 dB higher than the minimum value of -24.0 dBm found in case (a). It is due to the specific bandwidth limitations of the signal generation equipment used in the experimental setup.

Uplink (Fixed channels)

(a) 50 Mb/s　　　　(b) 100 Mb/s　　　　(c) 150 Mb/s
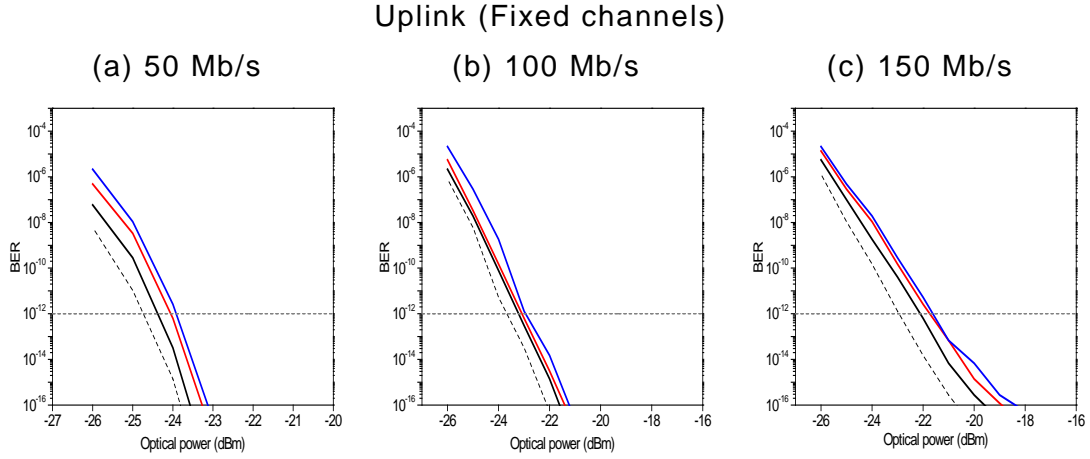
Fig. 4.41 BER vs. optical power for the uplink baseband signal transmission at bit rates (a) 50 Mb/s, (b) 100 Mb/s and (c) 150 Mb/s. CH_1 in scenario 1 (—),CH_2 in scenario 2 (—), and CH_3 in scenario 3 (—). Optical back-to-back curve (dashed line).

The uplink degradation of the extra channel, CH_4, has been also measured and is plotted in Fig. 4.42 for the same bit rates, 50 Mb/s (a), 100 Mb/s (b), and 150 Mb/s (c). In particular for each case, the BER degradation of the signal carried by extra CH_4 in routing scenario 2 and 3 are plotted together with the back-to-back curve (dashed line).

Uplink (Extra channel)

(a) 50 Mb/s　　　　(b) 100 Mb/s　　　　(c) 150 Mb/s
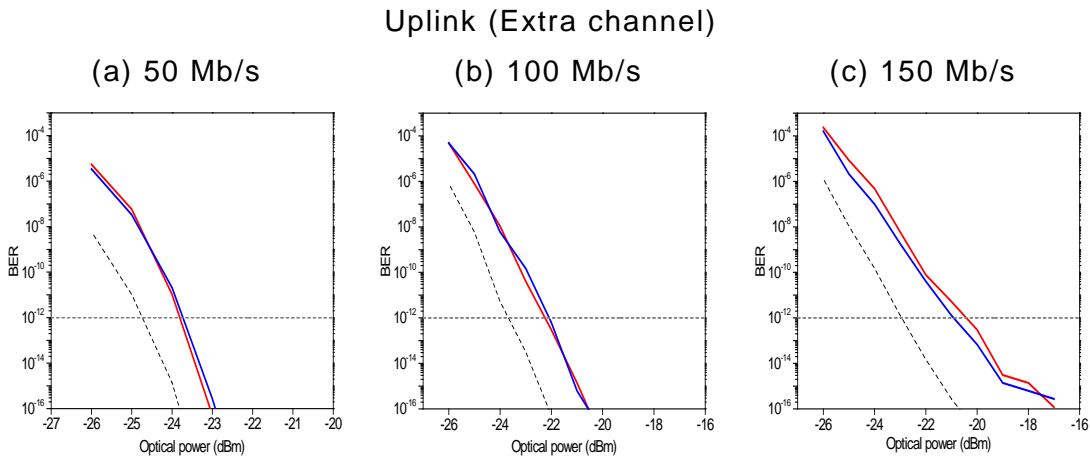
Fig. 4.42 BER vs. optical power for the uplink baseband signal transmission at bit rates (a) 50 Mb/s, (b) 100 Mb/s and (c) 150 Mb/s. Extra CH_4 in scenario 2 (—), and 3 (—). Optical back-to-back curve (dashed line).

Concerning the results shown in Fig. 4.42, the small difference with respect to the results shown in Fig. 4.41 is represented by the optical power level needed by the extra channel to reach the established BER. In case (a) this level is around -23.8 dBm in both scenarios. As the bit rate increases, the level is increased to -22.2 dBm (b) and to -20.3 dBm in (c) for the worst case (—). As a consequence also the power penalty with respect to the back-to-back curve (dashed line) increases slightly at higher bit rates.

4.4　Summary.

This chapter dealt with the theoretical and experimental validation of chromatic dispersion tolerant OBS-based optical transmission architectures

suitable for the transport of GHz-signals realized, for the first time to our knowledge, by incorporating fiber MZI structures. The effect of the insertion of the MZI structure in the link has been analytically described and experimentally investigated under two alternative system configurations. We have demonstrated that the photonic band-pass filtering effect of the MZI is a key property to enhance the operative electrical bandwidth allowed by the OBS in the presence of a dispersive link and, thus, enabling RoF signal transmission in the third optical transmission window.

The incorporation of a MZI structure presents a lower degree of implementation complexity compared with other chromatic dispersion compensation techniques addressed in the literature. Our strategy has been firstly implemented and validated in a single-channel optical transmission system employing the IM-DD scheme with external modulation of a broadband source in DSB-AM format and performing signal propagation over both SMF and MMF links. Concerning the generation of the transmitted signals, the SCM technique in the electrical domain has been used to imprint digital data onto electrical tones generated in the radio frequency band. In addition, we have used different codification types, such as, BPSK, QPSK, and M-QAM to demonstrate also the versatility of the proposed approach to the type of service.

In the second section of the chapter, the spectral characteristics of broadband sources and the incorporation of MZI structures has been exploited to build a multichannel optical transmission environment where the principal target is a minimization of the light sources-associated management complexity in the CO rather than an increasing of the overall capacity. In this context, we have proposed an OBS-based CWDM optical access network where expensive wavelength-specified lasers at the transmitter have been replaced by a single sliced OBS. The spectral slicing is an effective way to generate from a single broadband light, a group of adjacent narrower channels conveniently assigned to carry the information between CO and ONUs. Two alternative CWDM optical access networks have been validated. In the first one, the CO transmitter adopts DSB-AM modulation of the optical carrier, whereas, in the second one, PM format is employed as a mean to further simplify the transmitter complexity. As demonstrated in Chapter 3, for PM carriers, the dispersive nature of the fiber induces PM-IM conversion whose high-pass electrical response is well compatible with the accommodation and transport of RoF signals. This section also provides a brief demonstration of two more functionalities offered by the MZI: the photonic suppression of undesired HD- and IMD-induced distortion terms arising from the optical modulator in typical SCM systems and a novel scheme for all-optical microwaves mixing and up-conversion. Finally, in the third part of the chapter, we have described and experimentally validated a spectral slicing-based full-duplex reconfigurable access network. The transmission performance of the proposed network has been tested under typical routing scenarios demonstrating high quality signal reception of both downlink RoF and uplink baseband signals for service convergence.

4.5   References.

[Agr 2002]   G. P. Agrawal, "Fiber-optic communication systems", (John Wiley & Sons, Inc), 3rd edition, 2001.

[Cap 2005]   J. Capmany, B. Ortega, D. Pastor, S. Sales, "Discrete-time optical processing of microwave signals", J. Lightwave Technol., Vol. 23, pp. 702-723, 2005.

[Che 2006]   L. Cheng, S. Aditya, Z. Li, A. Nirmalathas, "Generalized Analysis of Subcarrier Multiplexing in Dispersive Fiber-Optic Using Mach-Zehnder External Modulator", J. Lightwave Technol., Vol. 24, pp. 2296-2304, 2006.

[Chi 2008]   H. Chi, J. Yao, "Frequency Quadrupling and Upconversion in a Radio Over Fiber Link", J. Lightwave Technol., Vol. 26, pp. 2706-2711, 2008.

[Cho 2006]   T.Cho, K.Kim "Effect of Third-Order Intermodulation on Radio-Over-Fiber Systems by a Dual-Electrode Mach-Zhender Modulator With ODSB and OSSB Signals", J. Lightwave Technol., Vol. 24, pp. 2052-2058, 2006.

[Haa 1993]   Z. Haas and M. A. Santoro, "A mode-filtering scheme for improvement of the bandwidth-distance product in multimode fiber systems", J. Lightwave Technol., Vol. 11, pp. 1125-1131, 1993.

[Hun 1996]   D. B. Hunter, R. A. Minasian, "Microwave optical filters using in-fiber Bragg grating arrays," IEEE Microw. Guided Wave Lett., Vol. 6, pp. 103-105, 1996.

[Ism 2005]   T. Ismail, C. P. Liu, J. E. Mitchell, A. J. Seed, "Feed-forward linearised uncooled DFB laser in a multi-channel broadband wireless over fibre transmission at 5.8 GHz", in Proc. MWP, pp. 115-118, Oct. 2005.

[Lau 2006]   P. Laurêncio, S. O. Simões, M. C. R. Medeiros, "Impact of the Combined Effect of RIN and Intermodulation Distortion on OSSB/SCM Systems", J. Lightwave Technol., Vol. 24, pp. 4250-2262, 2006.

[Lee 2004]   J.S. Lee, H.-J. Song, W.B. Kim, M. Fujise, Y.-H. Kim. J.-I. Song, "All-optical harmonic frequency upconversion of radio over fibre signal using cross-phase modulation in semiconductor optical amplifier", Electron. Lett., Vol. 40, 2004.

[Let 2005]   C. Lethien, C. Loyez, J-P. Vilcot, "Potentials of Radio over Multimode Fiber Systems for the In-Buildings Coverage of Mobile and Wireless LAN applications" IEEE Photon. Technol. Lett., Vol. 17, pp. 2793-2795, 2005.

[Lim 2007]   C. Lim, A. Nirmalathas, K.-L. Lee, D. Novak, R. Waterhouse, "Intermodulation Distortion Improvement for Fiber–Radio Applications Incorporating OSSB+C Modulation in an Optical Integrated-Access Environment", J. Lightwave Technol., Vol. 25,

pp. 1602-1612, 2007.

[Loa 2003]   A. Loayssa, C. Lim, A. Nirmalathas, D. Benito, "Optical Single-Sideband Modulator for Broad-Band Subcarrier Multiplexing Systems", IEEE Photon. Technol. Lett., Vol. 15, pp. 311-313, 2003.

[Lu 2004]   H.-H. Lu, S.-J. Tzeng, Y.-L. Liu, "Intermodulation Distortion Suppression in a Full-Duplex Radio-on-Fiber Ring Network", IEEE Photon. Technol. Lett., Vol. 16, pp. 602-604, 2004.

[Mas 2007]   B. Masella, X. Zhang, "Linearized Optical Single-Sideband Mach–Zehnder Modulator for Radio-Over-Fiber Systems", IEEE Photon. Technol. Lett., Vol. 19, pp. 2024-2026, 2007.

[Mor 2002]   J. Mora, B. Ortega, J. Capmany, J. L. Cruz, M. V. Andres, D. Pastor, S. Sales, "Automatic tunable and reconfigurable fiber optic microwave filters based on a broadband optical source sliced by uniform fiber Bragg gratings", Opt. Express, Vol. 10, pp. 1291-1298, 2002.

[Mor 2003]   J. Mora, B. Ortega, M. V. Andrés, J. Capmany, J. L. Cruz, D. Pastor, S. Sales, "Tunable all-optical negative multi-tap microwave filters based on uniform fiber Bragg gratings", Opt. Lett., Vol. 28, pp. 1308-1310, 2003.

[Mor 2006]   J. Mora, B. Ortega, A. Díez, J. L. Cruz, M. V. Andrés, J. Capmany, D. Pastor, "Photonic Microwave Tunable Single-Bandpass Filter Based on a Mach–Zehnder Interferometer", J. Lightwave Technol., Vol. 24, pp. 2500-2508, 2006.

[Pas 2002]   D. Pastor, B. Ortega, J. Capmany, S. Sales, A. Martinez, P. Muñoz, "Flexible and tunable microwave filters based on arrayed waveguide gratings", in Proc. IEEE Int. Top. Meet. Microw. Photon. (MWP), pp. 189-192, 2002.

[Par 2007]   C. I S. Park, C. G. Lee, C.-S. Park, "Photonic Frequency Upconversion Based on Stimulated Brillouin Scattering", IEEE Photon. Technol. Lett., Vol 19, pp. 777-779, 2007.

[Rad 1998]   L. Raddatz, I. H. White, D. G. Cunningham, M. C. Nowell, "An Experimental and Theoretical Study of the Offset Launch Technique for the Enhancement of the Bandwidth of Multimode Fiber Links", J. Lightwave Technol., Vol. 16, 324-331, 1998.

[Sha 2005]   A. R. Shah, B. Jalali, "Adaptive equalisation for broadband predistortion linearisation of optical transmitters," Proc. Inst. Electr. Eng. Optoelectron., Vol. 152, no. 1, pp. 16-32, Feb. 2005.

[Seo 2003]   Y.-K. Seo, J.-H. Seo, W.-Y. Choi, "Photonic Frequency-Upconversion Efficiencies in Semiconductor Optical Amplifiers", IEEE Photon. Technol. Lett., Vol. 15, pp. 751-753, 2003.

[Sim 2007]   D. H. Sim, Y. Takushima, Y. C. Chung, "Transmission of 10-Gb/s and 40-Gb/s signals over 3.7 km of multimode fiber using mode-field matched center launching technique", in Proceedings of OFC 2007, (Anaheim, USA, 2007), OTuL3.

[Wan 2006]   Q. Wang, H. Rideout, F. Zeng, J. Yao, "Millimeter-Wave
Frequency Tripling Based on Four-Wave Mixing in a
Semiconductor Optical Amplifier", IEEE Photon. Technol. Lett.,
Vol 18, pp. 2460-2462, 2006.

[Wu 2006]   C. Wu, X. Zhang, "Impact of Nonlinear Distortion in Radio Over
Fiber Systems With Single-Sideband and Tandem Single-
Sideband Subcarrier Modulations", J. Lightwave Technol., Vol.
24, pp. 2076-2090, 2006.

[Yam 2007]   S. S. Yam and F. Achten, "Toward 100 Gbits/s Ethernet with
broad wavelength window multimode fiber", J. Opt. Netw., Vol. 6,
pp. 527-534, 2007.

[Yao 2005]   J. Yao, G. Maury, Y. Le Guennec, B. Cabon, "All-Optical
Subcarrier Frequency Conversion Using an Electrooptic Phase
Modulator", IEEE Photon. Technol. Lett., Vol 17, pp. 2427-2429,
2005.

[Zhang 2007] J. Zang, H. Chen, M. Chen, T. Wang, S. Xie, "A photonic
microwave frequency quadrupler using two cascaded intensity
modulators with repetitious optical carrier suppression", Photon.
Technol. Lett., Vol 19, pp. 1057-1059, 2007.

[Zen 2005]   F. Zeng, J. Yao, "All-Optical Microwave Mixing and Bandpass
Filtering in a Radio-Over-Fiber Link", IEEE Photon. Technol.
Lett., Vol 17, pp. 899-901, 2005.

Chapter 5

Light sources centralized full-duplex optical transmission architectures based on the PolMUX technique

5.1   Introduction: historical background and applications.

Electromagnetic waves, such as light, exhibit polarization. The polarization is defined as the orientation of the electric field vector at a point in the space over one period of the oscillation. The geometric figure traced by the electric vector upon a stationary plane perpendicular to the direction of propagation is a description of the state of polarization (SoP) of the electromagnetic wave [Bor 1999].

Since the last two decades the vectorial nature of light, represented by polarization, has been regarded as a key parameter. Light polarization provides, in fact, a further degree of freedom which has been readily exploited for multiple purposes. In optical fiber communications, the two most representative applications of this concept are the realization of an alternative modulation format and the possibility to multiplex various optical signals into a single optical channel.

Initially, the SoP of a fully polarized lightwave has been employed as a modulation parameter to generate an alternative modulation format called PolSK. A conceptual representation of the PolSK modulation format is given in Fig. 5.1.
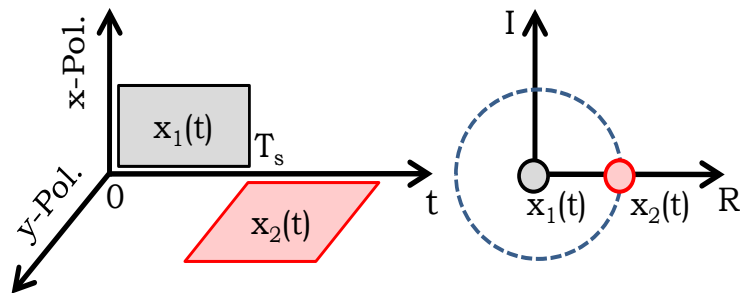
Fig. 5.1 Polarization shift keying modulation format.

In its first binary version (2-PolSK), two light signals at the same frequency and linearly polarized with orthogonal SoPs are associated to the two information levels or bit states, '0' and '1' and coded by a polarization modulator before fiber launching [Die 1987, Cal 1988]. Further extensions to multilevel PolSK (M-PolSK) modulation schemes are possible by encoding the information in a constellation of M signals given by different points in the three-dimensional Stokes space as proposed by [Ben 1990]. A complete theoretical description and performance evaluation of binary and multilevel PolSK modulation schemes is reported in [Ben 1992, Bet 1992].

Validations of the PolSK coding with high feasibility as a modulation format are presented in [Hu 2003, Chi 2005] and also very recently in [Cho 2009, Liu 2010, Wan 2010] confirming PolSK as a promising alternative choice to both envelop-modulation and phase modulation schemes.

On the other hand, the degree of freedom provided by light polarization has been regarded as a concrete opportunity to increase the spectral efficiency and the transmission capacity of a single-wavelength optical channel. The idea, proposed for the first time in 1986 by C. Herard and A. Lacourt [Her 1986], is based on equally splitting an optical field into two or even three components with lineal SoP and employ them as optical carriers to transmit simultaneously independent data streams over the same wavelength. Since in this case, the polarization parameter is employed to multiplex different optical signals into a single shared optical channel, the technique has been called polarization division multiplexing (PDM) also known as PolMUX, see Fig. 5.2.
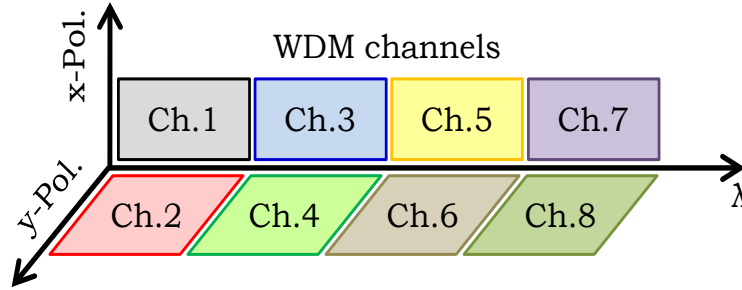
Fig. 5.2 Polarization division multiplexing principle.

For the case of a 2-channels PolMUX system, the PolMUX signal consists of two linearly polarized optical fields with orthogonal SoP generated by the same optical carrier, each one modulated by the corresponding electrical signal. Given a reference plane x-y normal to the z propagation axis of the electromagnetic field, the analytical expression of the PolMUX signal is given as follows:

$$\vec{E}_{POLMUX}(t) = \sqrt{P_{Ch,1}}e^{j\omega_o t}m_1(t)\cdot\vec{u}_x + \sqrt{P_{Ch,2}}e^{j\omega_o t}m_2(t)\cdot\vec{u}_y \quad (5.1)$$

where $P_{ch.1}$ and $P_{ch.2}$ are the average optical powers of both PolMUX channels, $m_1(t)$ and $m_2(t)$ are their corresponding modulation envelopes, and ω_0 is the frequency of the optical carrier.

A complete theoretical investigation of the optical PolMUX is presented in [Her 1991, Eva 1992] whereas the first significant experimental demonstration of a PolMUX-based optical transmission system is found in [Hil 1992]. Here, two 2 Gb/s BPSK data sets are multiplexed on each one of two orthogonal SoPs for a total 2x2 Gb/s single-channel transmission over 45 km of SMF. This publication paved the way to the employment of PolMUX in the optical communications area.

The attractive possibility of doubling the fiber information per-channel has led to integrate the PolMUX scheme especially in optical core network environments where high spectral efficiency and transmission capacity are very relevant (i.e. dense and ultra dense traffic packaging in long haul and ultra-long haul optical transmission links). In this context, up to 1.6 b/s/Hz spectral efficiency and 10 Tb/s aggregate capacity has been achieved

experimentally combining PolMUX with WDM technology [Chr 1996, Ito 2000, Big 2001] and other promising values have been achieved by using the even more complex technique such as the optical code division multiplexing (OCDM) [Sot 2002]. During the last decade and also thanks to the employment of highly spectrally efficient modulation formats, such as differential quadrature phase shift keying (DQPSK) and multilevel quadrature amplitude modulation (M-QAM), a wide series of laboratory experiments and record-breaking improvements up to 11 b/s/Hz of spectral efficiency and 69.1 Tb/s of aggregate capacity, have followed one after the other in order to target the single-wavelength 100 Gb/s transport and facilitate the use of digital signal processing at lower symbol rates [Wre 2003, Cho 2004, Mil 2005, Gna 2006, Flu 2008, Gav 2010]. Further investigations on DWDM transmission using PolMUX in combination with OFDM are reported in [Tak 2010, Ami 2010, Sch 2010].

The principal source of impairment observed in PolMUX systems is the coherent crosstalk between the two polarization channels induced by polarization mode dispersion (PMD) and polarization dependent loss (PDL). PMD is a stochastic phenomenon due to the random birefringence of optical fibers and components which unpredictably modifies the SoP of the signals causing a loss of orthogonality between the two polarization tributaries during the propagation [Nel 2000, Bof 2008, Wan 2009]. PDL usually occurs in optical components whose insertion loss varies with the SoPs of the input signals [Tsa 2005]. Both effects can become a problem particularly in long-haul transmissions when temperature variations and mechanical perturbations of the fiber conduct decrease the tolerance to PMD and when a large number of PDL elements are concatenated. Therefore, a mechanism to track and stabilize the SoP of the PolMUX signals is needed at the end of the fiber link before polarization demultiplexing [Mar 2006, Yao 2007, Bof 2009]. However, the effectiveness and advantage of PolMUX employment in optical core networks is undoubted and a significant amount of research is expected to take place in this area over the next years.

The exploitation of PolMUX in optical access networks started in 2009. Unlike long-haul core networks, where distance-bandwidth products are sufficiently large to leverage high implementation costs and short-term flexibility is not a primary goal, the access network platform requires a cost-efficient and flexible distribution and integration of different emerging broadband services to remain attractive and practical. In this context, the potential of the PolMUX method to carry information on two orthogonally polarized wavelengths generated by the same optical source has been conceived as valid alternative to run simultaneous transmission of independent services.

The suitability of the PolMUX scheme for access networks is demonstrated in [Tse 2009] for independent transmission of baseband and RoF services on a single wavelength after our first demonstration of the feasibility of the PolMUX technique in optical access networks [Gra 2009]. In [Qia 2010] the PolMUX scheme is proposed and implemented to provide a separate delivery of wired peer-to-peer data and wired multicast data at the same bit rates carried by two PolMUX wavelengths. To enable both cost-effective distribution of various services and bandwidth granularities, the combination of PolMUX with WDM and OFDM is now a solution regularly deployed also in the access segment. A substantial difference between the employment of PolMUX scheme in core and access networks

is that, in the last case, lower link distances increase the tolerance to PMD and PDL penalties. As it can be discussed next, although the control and maintenance of orthogonality is always an intrinsic issue in transmission and processing of PolMUX carriers, this tolerance is an advantage that highly relaxes SoP stabilization requirements. Therefore, PolMUX seems to be a multiplexing technique even more appropriate to optical access networks than core networks.

5.2 Light sources centralized full-duplex optical transmission system based on the PolMUX technique.

As described in Chapter 2, each strategy oriented to the centralization of the light sources presents different technical issues. Generally, the strategies based on the downlink wavelength "re-use" exhibit certain technical restrictions and may increase the architecture complexity. On the other hand, the centralization schemes based on the uplink wavelength supply are easy to scale but may increase inventory costs and management of the CO transceiver due to the high number of extra light-sources required. In this context, we propose and demonstrate a novel and effective implementation of a light-sources centralized architecture based on the PolMUX technique for optical access networks.

5.2.1 Description of the transmission architecture and principle of operation.

The schematic diagram depicted in Fig. 5.3 illustrates the light-sources centralized optical transmission architecture and the principle of operation of the PolMUX technique with special emphasis on the principal components required at the CO and ONU for its practical implementation.
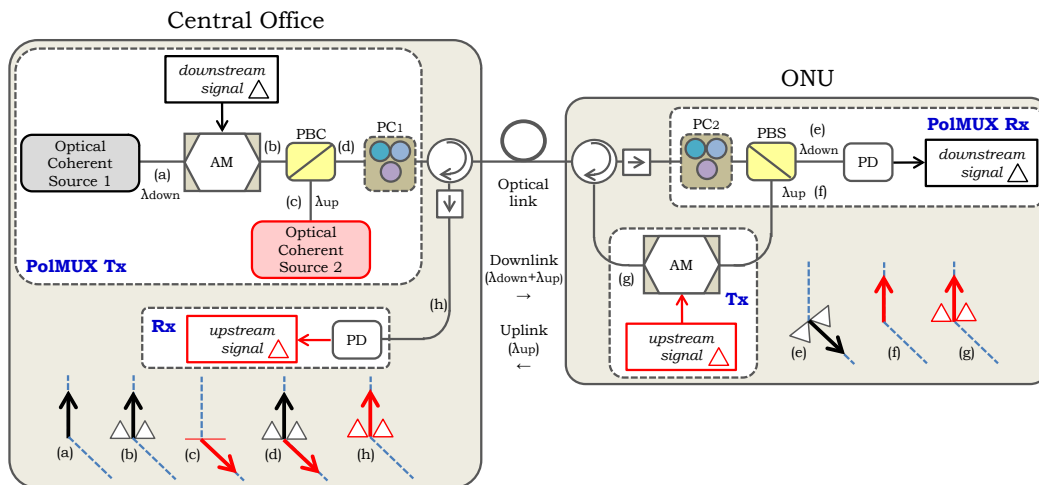
Fig. 5.3 Light sources centralized full-duplex optical transmission system based on the PolMUX technique.

The architecture is composed by a CO and a single ONU interconnected by the optical link. Both CO and ONU are composed by a transmitter (Tx) and a receiver (Rx) block described as follows.

At the CO, two conventional and linearly polarized optical coherent sources (lasers) provide two optical fields centered at wavelengths λ_{down} and λ_{up}, see points (a) and (c) of Fig. 5.3. The only difference between the two optical fields is that their SoPs are forced to be orthogonal to each other. We take advantage of the degree of freedom provided by polarization to arbitrarily make the following association. The first optical field, λ_{down}, is chosen as optical downlink carrier for the downlink transmission (CO to ONU). The second optical field, λ_{up}, takes the role of optical carrier engaged for the uplink transmission (ONU to CO). The optical carrier λ_{down} is DSB-AM modulated by the downstream signal by means of an EOM (see point (b)). The optical uplink carrier is left as a CW light. The two orthogonally polarized optical carriers are multiplexed in a polarization beam combiner (PBC) and launched into the optical link (see point d). The structure described above is called CO PolMUX Tx.

At the receiver section of the ONU, called ONU PolMUX Rx, a polarization beam splitter (PBS) divides the input optical field in two orthogonally polarized components obtaining the separation of the two PolMUX carriers at the output. The first optical carrier, λ_{down}, (see point (e)) enters the PD where the downstream signal is recovered. The second optical carrier, λ_{up}, is sent to the transmitter block of the ONU (see point (f)). The ONU Tx is composed only by an EOM which modulates the optical CW, λ_{up}, employing the upstream signal as electrical input. Then, the modulated uplink carrier (see point (g)) is routed back to the CO through an optical circulator. Note that, the uplink transmission runs over the same optical fiber. The optical circulator is inserted to uncouple the downlink and uplink signals and the optical isolator minimizes the optical crosstalk between λ_{down} and λ_{up} due to spurious reflections. Finally, in the CO Rx block, another optical circulator routes the uplink modulated optical carrier towards the PD (see point (h)) where, the upstream signal is recovered.

As explained, the PolMUX technique exploits the degree of freedom coming from the light polarization to multiplex two orthogonally polarized optical carriers into the same optical channel. The two carriers are provided by two optical coherent sources both centralized at the CO. In this way, the concept of light-sources centralization is practically implemented since no additional light-source is installed at the ONU which is left source-free, colorless and functionally simple. Moreover, the implementation of the PolMUX technique requires only a single optical fiber for both downlink and uplink transmission reducing the size of the external plant.

The principal devices employed to implement the PolMUX technique are the PBC, located at the CO, and the PBS, inserted in the ONU. The remaining components of the architecture are typical electro-optic and optic-electro converters, the optical sources and signal generators which are always present in typical optical transmission architectures. With regard to the generation and provisioning of the optical light-sources, this architecture follows the extra wavelength supply approach. In fact, the optical uplink carrier is generated at the CO by an extra optical source representing the "seed" light for the ONU. We will demonstrate later that, thanks to the characteristics of the PolMUX principle, the employment of two different optical sources for the downlink and uplink transmission is not really an indispensable requirement.

The success of the PolMUX technique depends on the degree of polarization orthogonality of the two PolMUX carriers before entering the

PBS. Since the polarization orthogonality may be lost during the propagation, a device employed to perform such polarization tracking and control, has been inserted in the system of Fig. 5.3. This important device is an automatic high tracking speed polarization controller (PC). In practice, the success of the polarization demultiplexing can be evaluated by measuring a parameter called polarization extinction ratio (PER). This parameter shows the ratio between the optical powers of the two orthogonally polarized fields at the output of the PBS. In accordance to the analytical expression in (5.1), the PER can be defined as follows:

$$PER = \frac{P_{Ch,1}}{P_{Ch,2}} \quad (5.2)$$

where $P_{ch.1}$ and $P_{ch.2}$ are the average optical powers of the two PolMUX carriers associated to wavelengths λ_{down} and λ_{up}, respectively.

Therefore, the main functionality of the PC is to set a certain PER between both PolMUX carriers. This condition is mandatory for the success of the PolMUX technique and must be verified especially when the two PolMUX carriers are finally separated at the ONU. Based on this assertion, a logical position of the PC would be the ONU. However, as the lector may observe, the place where the polarization monitoring and control is realized, has been left arbitrarily optional into the scheme of Fig. 5.3. In fact, the PC can be located either at the ONU PolMUX RX prior the splitting of the two PolMUX carriers, or at the CO PolMUX Tx immediately after the PBC. In Fig. 5.3 we have indicated as PC_1 and PC_2 these two alternative options, respectively.

The option to choose the location of the PC, without modifying the functioning of the PolMUX principle, is based on the following intuitive consideration. When the PC is located at the CO, it is capable of setting the required PER between the PolMUX carriers combined before the downlink propagation. Besides this operation, the PC can be also used to supervise and, in case of polarization misalignments, automatically rectify the SoP of the uplink optical carrier received after the round trip. In fact, once the upstream signal is received at the CO, its quality can be always taken as "feedback" information about the degree of orthogonality of the two PolMUX carriers remotely received at the ONU. This assumption is further supported by the fact that the two PolMUX carriers are originally generated in orthogonal polarization at the CO and that any polarization rotation along the fiber affects both SoPs in the same way. In other words, a good/bad quality of the upstream signal demodulated at the CO automatically means that also the downstream signal has been demodulated correctly/incorrectly at the ONU. Under this condition, each of the two positions of the PC are conceptually equivalent. Therefore, the orthogonality between the PolMUX carriers can be always monitored and maintained either locally at the ONU, using PC_2, or remotely at the CO, using PC_1 and taking the SoP of the uplink carrier as a reference. This remote control is possible since unwanted variations of polarization are slow compared to the time transit of the uplink transmission. Note that, commercially available PCs are capable to track and restore remotely any unwanted variation of polarization offering a fast speed response in the order of few microseconds.

Although the position of the PC is conceptually indifferent, it is practically very influent. The insertion of a PC in the ONU, in fact, grows

the complexity and cost of its architecture and constrains the operator to perform locally the monitoring and control of the polarization as well as all the operations required in case of polarization misalignments. This drawback may become particularly unfavorable when the access infrastructure addresses several ONUs. By contrast, when the PC is installed at the CO, or equivalently, when PC_1 is used instead of PC_2, the ONU becomes free from all polarization maintenance devices and management issues, which are placed and performed remotely at the CO, respectively. It represents an added benefit in the practical implementation of the PolMUX approach.

5.2.2 Experimental characterization.

In line with the description made in the previous subsection, we provide an experimental characterization of the PolMUX-based optical transmission architecture. For this purpose we implement the scheme of Fig. 5.3 connecting the CO and the ONU with a few meters optical SMF link. In the experimental setup the optical downlink and uplink carriers are centered at wavelengths λ_{down}=1550.12 nm and λ_{up}=1550.92 nm respectively with a wavelength separation $\Delta\lambda$=0.8 nm. The optical power of λ_{down} is set to 10 dBm whereas the optical power of λ_{up} is 12 dBm. Both carriers are provided by a multi-wavelength optical source using only two of the available tunable lasers. In this case, being the wavelength separated by 0.8 nm, the PolMUX approach is equivalent to a conventional 2-channels WDM system. Here we want to remark that, keeping a wavelength separation between the two optical carriers is not a constraint. It is done just to better visualize and measure the PER that can be achieved at the ONU by means of the PC. Figure 5.4 shows the optical spectra measured in different points of the experimental setup provided PC_1 or PC_2 is employed.

In particular, Figure 5.4(a) plots the optical spectrum measured at the output of the CO PolMUX Tx. We observe that the two optical carriers are multiplexed together into the same optical channel at the CO. The downlink optical carrier is modulated by the downstream signal whereas the uplink optical carrier is kept unmodulated.

Fig 5.4(b) plots the optical spectrum measured at the first output of the PBS of the ONU PolMUX Rx. Before entering the PBS, the PC provides a PER between λ_{down} and λ_{up} to an acceptable value. Just as an example, a PER = 45 dB is achieved to permit a correct separation of the two PolMUX carriers. In this way, the optical amplitude of the downlink carrier is maximized before its photodetection allowing a correct reception of the downstream data.

Figure 5.4(c) shows the optical spectrum measured at the output of the EOM in the ONU Tx. The uplink optical carrier, λ_{up}, is amplitude modulated by the upstream signal before the round trip. Note that, as occurred with the downlink carrier (case (b)), also the optical amplitude of the uplink carrier is simultaneously maximized at the second output of the PBS. In fact, the same value of PER is achieved as a result of the polarization splitting performed by the PBS.

The optical spectrum measured at the CO Rx after the round trip and before the PD is shown in Fig 5.4(d). Since only few meters separate the CO from the ONU, the PER remains practically unchanged as well as the optical amplitude of the uplink carrier. In this way, the demultiplexing

process performed at the ONU assures a correct reception of the upstream signal.
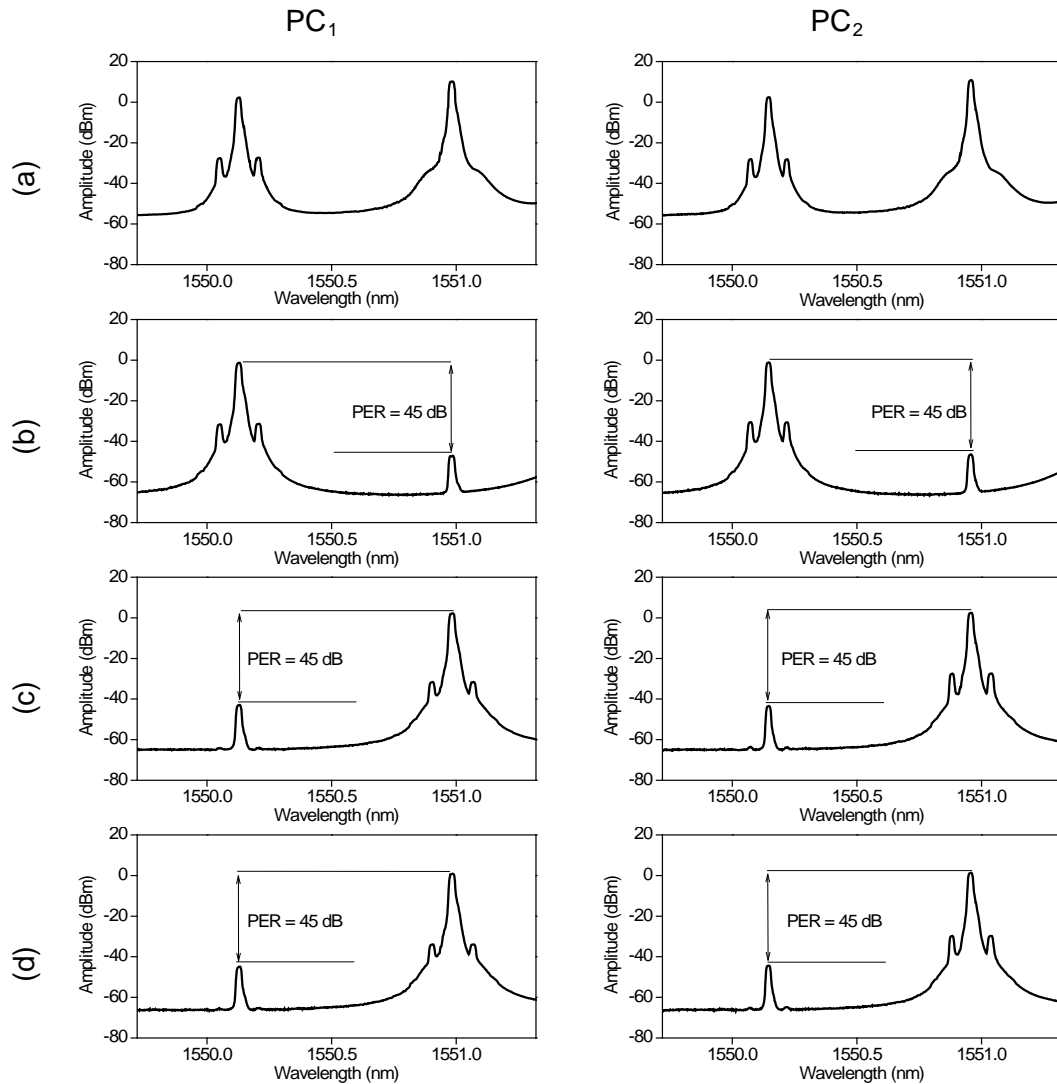
Fig. 5.4 Optical spectrum measured in case of employing PC1 (left side) or PC2 (right side): (a) output of CO PolMUX Tx, (b) output of the PBS in the ONU PolMUX Rx for a PER = 45 dB, (c) output of the EOM in the ONU Tx and (d) before PD in the CO Rx.

Some considerations can be made with regard to the power losses experienced by the PolMUX carrier throughout the link. Comparing Fig. 5.4(b) and 5.4(d), there is a difference of around 1 dB of optical power loss in excess for the uplink optical carrier with respect to the downlink one, which is not caused by the PolMUX scheme itself. Actually, it is caused by the round trip and specifically by the two optical circulators inserted at the CO and ONU to perform the corresponding routing operations. Therefore, a correct analysis and comparison of the effects of the architecture on the downlink and uplink performance may require a power compensation of all PolMUX-independent losses generated in the round trip. In other words, it should be assured that the downlink and the uplink optical carrier have the same optical power before leaving the CO and ONU, respectively (see Fig. 5.4(a) and (c)). This consideration explains the 2 dB-unbalanced input optical power between the two optical sources we initially set at the CO. Due to the round trip of the uplink optical carrier, the power compensation

between λ_{down} and λ_{up} must be always upgraded in case of inserting an optical fiber link of a given length or others optical devices. The power compensation is easily made by knowing the amount of their optical losses and decreasing (unbalancing) the input optical power of the downlink optical carrier in order to compensate for this amount.

From Fig. 5.4 it can be observed clearly that the results obtained for PC_1 and PC_2 are almost identical, as expected. It confirms the intuitive consideration made in the previous subsection and means that the spectral characteristics of the analyzed architecture and the behavior of the PolMUX technique are practically independent on the place where the monitoring and control of polarization is realized. In both cases a high PER can be achieved between λ_{down} and λ_{up} allowing a correct demultiplexing process at the ONU receiving end. Therefore, for practical reasons, the employment of PC_1 is an effective option.

Using the same setup as above, the experimental characterization of the optical transmission architecture based on the PolMUX technique continues exploring the effect of the wavelength separation between the two PolMUX carriers, λ_{down} and λ_{up}, on the achievable PER. To proceed with this test, the central wavelength of the downlink optical carrier, λ_{down}, has been kept to a fixed value of 1550.12 nm. The central wavelength of the uplink optical carrier, λ_{up}, has been decreased in steps of 0.2 nm from the initial value of 1550.92 nm ($\Delta\lambda=0.8$ nm) to 1550.12 nm ($\Delta\lambda=0$ nm). At each step we have extracted the PER. Figure 5.5 plots the PER as a function of the wavelength separation, $\Delta\lambda$, for the downlink ($\square$) and the uplink ($\bigcirc$) PolMUX carrier when the PER is set initially to 10 dB and successively to 20 dB and 30 dB. Again, the alternative use of PC_1 in case (a) and PC_2 in case (b) has been considered for a matter of completeness.
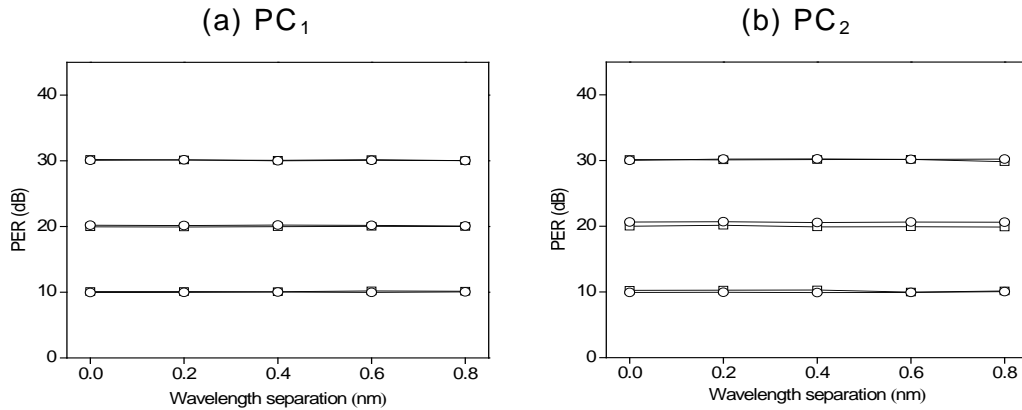
Fig.5.5 PER vs. $\Delta\lambda$ for the downlink ($\square$) and the uplink ($\bigcirc$) optical carrier when the initial PER is set to 10, 20 and 30 dB employing (a) PC_1 and (b) PC_2.

From Fig. 5.5(a), It can be observed that, in case of employing PC_1, the PER is practically constant with $\Delta\lambda$ for the two PolMUX carriers independently of which polarization crosstalk level is established at the beginning of the test. Indeed, the PER variations observed when the wavelength spacing, $\Delta\lambda$, decreases from 0.8 nm to 0.0 nm never exceeds a 1.0% of their initial value. Also using PC_2, (case (b)) the PER is almost flat when $\Delta\lambda$ is changed. Here too, the PER variations are bounded in a 1.0%. It means that the wavelength separation between the PolMUX carriers can be reduced to a minimum of 0.0 nm without modifying the performance of the PolMUX scheme in terms of achievable PER.

In other words, once a certain level of orthogonality is set, it is always possible to assign the same optical wavelength for the two optical carriers simply by taking $\lambda_{down}=\lambda_{up}$. This possibility has an important and favorable practical implication. The improvement brought by using a single optical wavelength for both downlink and uplink carriers is clear if we consider that the employment of a single wavelength doubles the spectral efficiency of the link and, at the same time, halves the implementation costs related to the wavelength provisioning if the two optical carriers are generated by the same optical source. The possibility of employing only a single optical source has been mentioned beforehand and is now demonstrated. It represents another positive feature of the PolMUX strategy and, as described later, it is especially useful and effective in multichannel scenarios where two or more optical full-duplex channels are deployed into the network.

To finalize the experimental characterization we present an interesting study about the influence of the optical link length on the degree of orthogonality which can be achieved by the two PolMUX carriers during the propagation. This study is illustrated by Fig. 5.6 where the PER is plotted over the optical fiber link length for the downlink (□) and the uplink (○) carrier using the two alternative positions of the PC.

The curves show that values of PER higher than 50 dB can be achieved in both downlink and uplink directions over distances not exceeding 10 km. As the distance increases, the maximum PER starts to decrease. However, it can be maintained over acceptable levels around 45 dB even at higher lengths. This behavior is independent of the PC position. Considering that all the lengths under test reflect a typical set of distances covered by an access infrastructure, the results achieved are very promising for the integration of the PolMUX technique into the access network architecture.

(a) PC$_1$ (b) PC$_2$
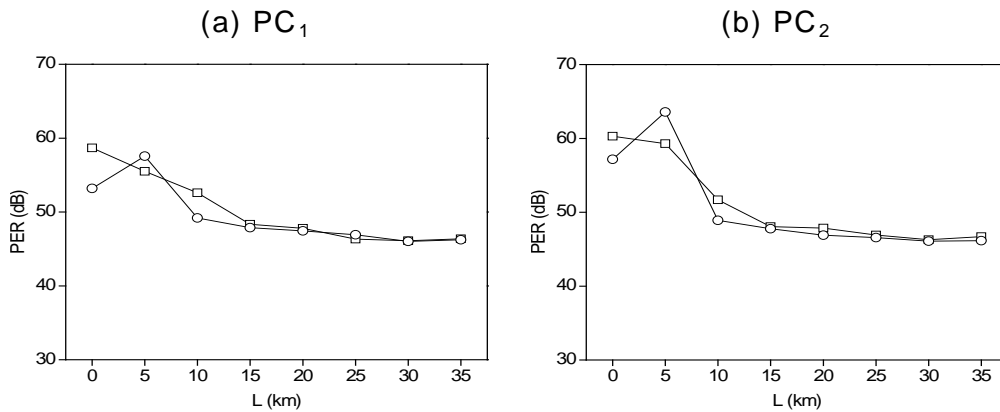
Fig. 5.6 PER vs. L for downlink (□) and uplink (○) optical carriers using (a) PC$_1$ and (b) PC$_2$.

5.2.3 Experimental evaluation of the system performance.

When the PolMUX technique is employed the degree of orthogonality of the two PolMUX carriers has a fundamental and direct impact on the transmission performance of the architecture. After demonstrating that the most convenient architectural configuration is the one where the polarization monitoring and control are realized remotely at the CO, we study the degradation induced by the PolMUX technique on the quality of

downstream and upstream signals carried by the correspondent PolMUX wavelengths referring to the case of employing PC_1.

In the experimental setup the downlink carrier is centered at λ_{down}=1550.12 nm and has a power of 10 dBm, whereas, the uplink carrier is centred at λ_{up}=1550.92 with 12 dBm of power. For the generation of the down- and upstream traffic we implement the SCM scheme by amplitude modulating an f_{RF}=10 GHz electrical subcarrier with a 5 Mb/s QPSK-encoded PRBS. The electrical input power of the SCM tone is set to 7 dBm. Since phase modulated electrical signals are transmitted, the EVM is used as figure of merit to evaluate the signal degradation. We establish a maximum EVM of 10.0% as conventional criterion. In the testing procedure the PC has been adjusted progressively in order to set the polarization crosstalk from a minimum of 0.0 dB to a maximum of 45 dB in steps of 5 dB and recording the EVM at each step. The EVM as a function of the PER is plotted for the downstream (□) and upstream (○) data considering a 0 km link. The results of this test are plotted in Fig. 5.7.
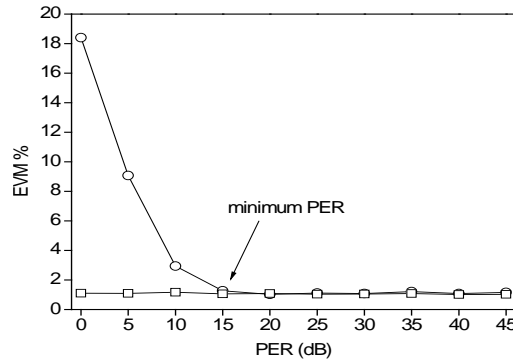
Fig. 5.7 EVM vs. PER for the downstream (□) and upstream (○) signal demodulation after 0 km of SMF propagation.

From Fig. 5.7 we observe that the EVM values reached by the downstream signal (□) are always around 1.0% independently on the PER. With regard to the quality of the upstream signal (○), the EVM values are very close to those obtained by the downstream one while the PER level is kept higher than 15 dB. Once the 15 dB threshold is crossed, the upstream data quality drastically starts to deteriorate with EVMs ranging from 2.9% for a PER=10 dB to 18.4% at the minimum PER. It can be clearly deduced that in case of low levels of orthogonality, the quality of the downlink and uplink signals is not affected in the same measure.

This important result is justified as follows. Due to the PolMUX principle, the optical spectrum photodetected at the ONU is composed by the downlink optical modulated carrier, λ_{down}, and the uplink optical carrier, λ_{up}, which is still a CW or, equivalently, only an unmodulated dc component. In this situation the downlink carrier is not perturbed by the amplitude level of the dc component even if their amplitude levels are comparable, which means a low PER. Therefore, the quality of the downstream signal received at the ONU will be acceptable independently of the degree of orthogonality between the PolMUX carriers. By contrast, when the PER is low, the optical spectrum photodetected at the CO Rx will present the two PolMUX carriers with the corresponding downstream and upstream data side bands. It happens because at the ONU an undesired

portion of the power of the downlink modulated carrier leaks through the uplink path and, thus, undergoes a back propagation to the CO together with the uplink modulated carrier. The amount of this power leakage is governed by the PER and produces interference between the side bands of the downstream and upstream signals. The interference increases as the PER decreases reducing drastically the quality of the upstream signal as shown in the curve of Fig. 5.7. In conclusion we affirm that, for a 0 km link, a minimum PER of 15 dB can be assumed as a criterion to guarantee a correct separation of the PolMUX carriers and, consequently, an acceptable and equal quality of both downstream and upstream demodulated signals.

As an example, Fig. 5.8 plots the optical spectra measured at the ONU Rx (a) and at the CO Rx (b) when the PER between the two PolMUX carriers is set to 0 dB. Fig. 5.8 (c) and (d) shows the optical spectra of the downlink and uplink transmission respectively but provided the PER is set to 30 dB.
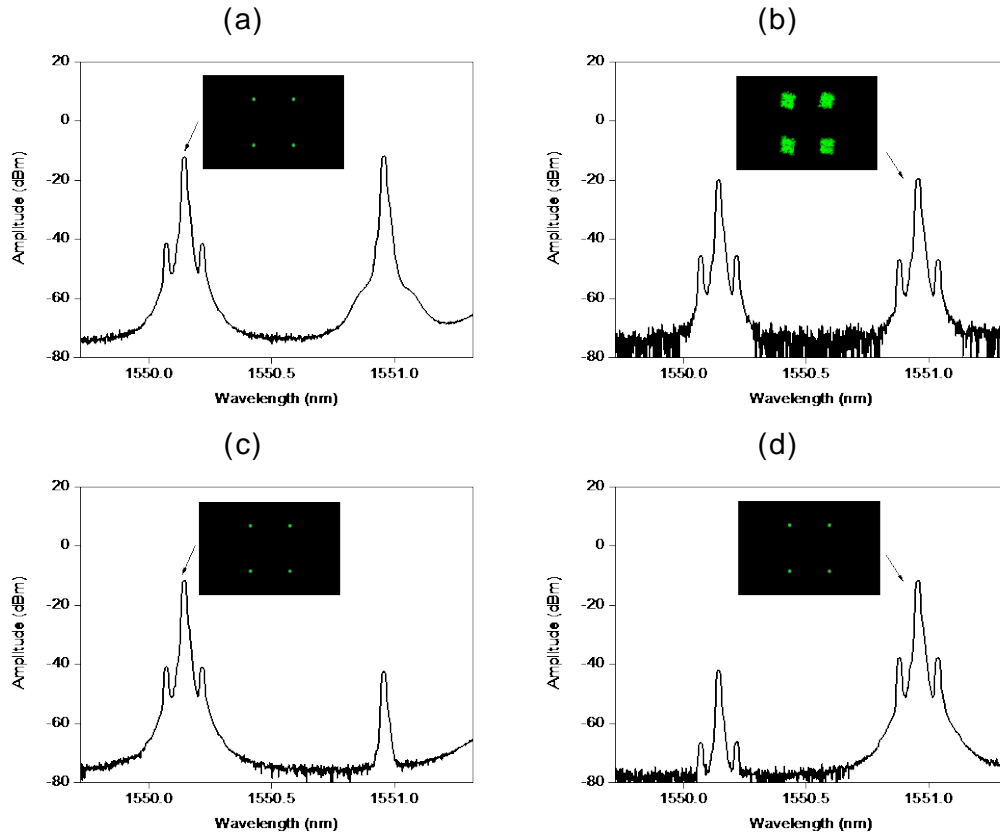
Fig. 5.8 Optical spectrum measured after 0 km transmission at (a) ONU PolMUX Rx and (b) CO Rx when PER=0 dB. Optical spectrum measured at (c) ONU PolMUX Rx and (d) CO Rx when PER=30 dB. The corresponding insets represent the constellation diagrams of the downstream (EVM=1.1%) and upstream (EVM=17.5%) signal when PER=0 dB and the downstream (EVM=1.0%) and upstream (EVM=1.0%) signal when PER=30 dB.

Figure 5.8(a) shows the optical spectrum measured at the PBS output of the ONU PolMUX RX when the PER is 0 dB. As expected, it can be observed that both downlink and uplink optical carriers present the same amplitude level and, thus, they are not correctly extracted at the ONU. Due to the power leakage of the downlink carrier, an identical consideration can

142

be made after observing the optical spectrum measured at the CO Rx shown in Fig. 5.8 (b).

Under this condition, we have experimentally performed the demodulation of the down- and upstream signals carried by λ_{down} and λ_{up}, respectively. The constellation diagram related to the downstream signal is captured at the ONU PolMUX Rx whereas the constellation diagram of the upstream signal is captured at the CO Rx. Both are shown together with the correspondent received optical spectra as insets of Fig. 5.8(a) and (b), respectively. For a PER=0 dB we find that the downstream signal is correctly demodulated with an EVM=1.1%. On the contrary an EVM=17.5% indicates that the upstream signal quality is largely lower than the downstream one. It means that the interference between the downstream and upstream signals, generated by a PER largely lower than the minimum established by the criterion, is significant only for the upstream signal and invalidates completely the PolMUX principle.

Let's consider the case of setting the PER to 30 dB which verifies the criterion. The corresponding optical spectra, measured at the ONU PolMUX Rx and at the CO Rx, are plotted in Fig 5.8 (c) and (d), respectively. In both figures, it can be appreciated the difference imposed by the PER on the amplitude level of the PolMUX carriers. After performing the full-duplex transmission, the downstream signal is demodulated with an EVM=1.0% at the ONU PolMUX Rx maintaining almost the same signal quality as the case (a) when the PER was set to 0 dB. Since the two PolMUX carriers are kept orthogonally polarized, a better behavior is observed after demodulating the upstream signal at the CO Rx. In fact, the increasing of PER from 0 dB to 30 dB produces a big improvement of the upstream signal quality unlike case (b). It is confirmed by an EVM of 1.0% which is very close to the one measured for the downstream signal. The great improvement of the signal quality can be also appreciated by observing the two constellation diagrams inserted in Fig 5.8(c) and (d) representing the downstream and the upstream demodulated symbols constellations, respectively. As expected, when the polarization demultiplexing is performed in a way that the two PolMUX optical carriers are kept separated with a high PER, the PolMUX system assures high quality demodulation performance. Note that all results show in Fig. 5.8 agree with the ones exposed in Fig. 5.7 corresponding to a PER=0 and 30 dB.

We have performed the same experimental evaluation but in case of inserting a 10 km of SMF between the CO and the ONU. In the experimental setup two laser sources centered at the same wavelengths as before, λ_{down}=1550.12 nm and λ_{up}=1550.92 nm, are employed to generate the downlink and uplink carriers, respectively. The input optical power of λ_{down} is set to 8 dBm, whereas, the input optical power of λ_{up} is set to 12 dBm. Note that, with respect to the optical power levels employed in the previous experimental evaluation (0 km case), we have compensated the 0.2 dB/km of optical loss induced by the fiber. It has been done by reducing the input optical power of λ_{down} by 2 dB, which is the total amount of optical loss accumulated in 10 km. Figure 5.9 plots the EVM over the PER for the downstream (□) and upstream (○) signal measured when the PER is varied progressively by means of the PC inserted in the CO. The optical back-to-back (△) measured at the output of the EOM is also included in the graph.

143
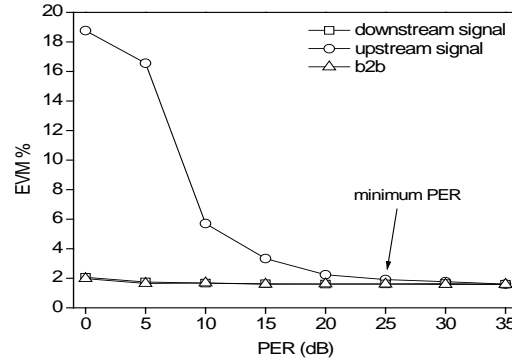
Fig. 5.9 EVM vs. PER for the downstream (□)
and upstream signal (○) transmission over 10
km of SMF link. Optical back-to-back (△).

With regard to the downlink transmission (□), the EVM reaches excellent values between 1.6% and 2.0% over the entire range tested. By contrast the EVM of the upstream signal (○) is very close to the downstream values only while the PER is kept higher than 25 dB. When the PER is lower than 25 dB, the quality of the upstream signal undergoes degradation. Comparing Fig. 5.9 with Fig. 5.7, the EVM follows the same behavior but we find an EVM degradation induced by the optical fiber loss. We can confirm that the presence of a 10 km SMF link modifies the value of minimum PER required. In fact, while for 0 km of optical link, a minimum PER=15 dB was sufficient to assure equal and correct downstream and upstream signal demodulation, in this case it is necessary a minimum PER=25 dB to achieve a comparable transmission performance.

This result is explained considering that the propagation runs over a SMF link which is not a polarization maintaining medium. In other words, the orthogonality between the two PolMUX carriers becomes inevitably more vulnerable to PMD and PDL-induced crosstalk during the propagation through the optical fiber. Therefore a higher PER must be kept to secure the orthogonality. From Fig. 5.9 it can be observed that, when the PER is kept around 25-30 dB, the signal quality of the downstream and upstream signals is preserved verifying the conventional EVM specification. Experimentally we have demonstrated in Fig. 5.6 that the PC located at the CO can sufficiently maintain this degree of orthogonality during the transmission over 10 km and even longer distances (up to 35 km).

Since the back-to-back EVMs are very close to those measured for the downlink transmission, we affirm that the PolMUX technique does not introduce a significant degradation on the signals quality.

As a concluding example, for the case of 10 km SMF link, we plot in Fig. 5.10 the optical spectra measured at the ONU Rx (a) and at the CO Rx (b) after setting 0 dB of PER. Cases (c) and (d) correspond to the same test but for a PER of 30 dB.
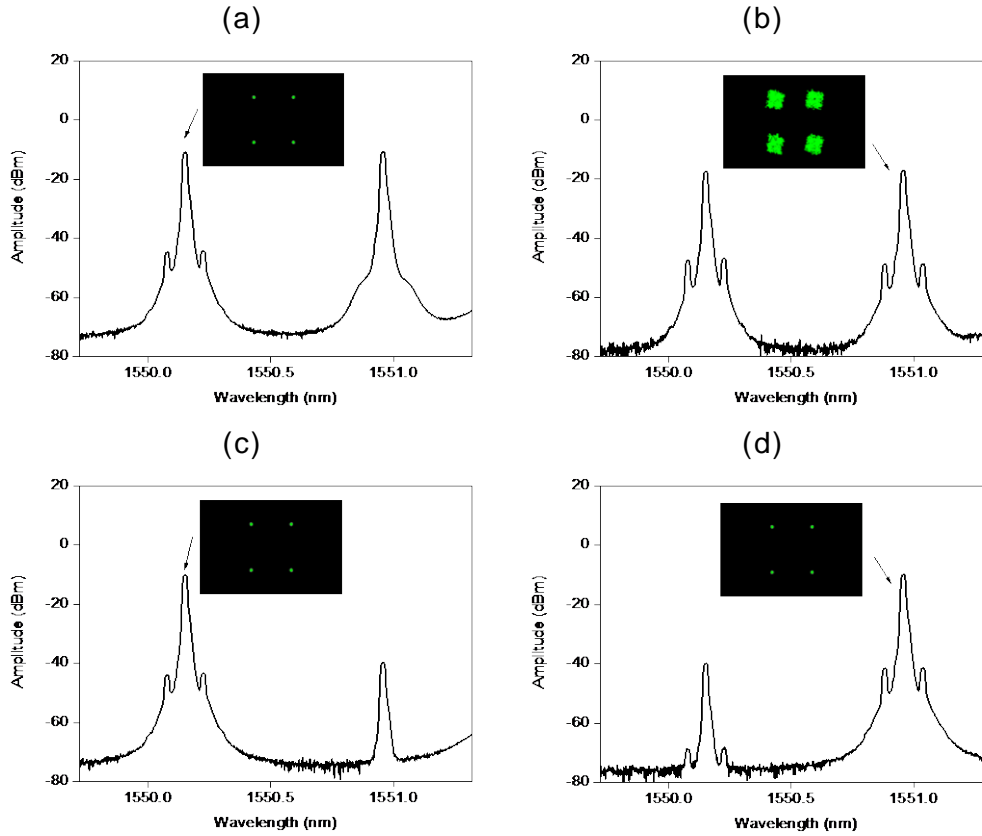
Fig. 5.10 Optical spectrum measured after 10 km of SMF propagation at (a) ONU PolMUX Rx and (b) CO Rx when PER=0 dB. Optical spectrum measured at (c) ONU PolMUX Rx and (d) CO Rx when PER=30 dB. The corresponding insets represent the constellation diagrams of the downstream (EVM=1.9%) and upstream (EVM=19.7%) signal when PER=0 dB and the downstream (EVM=1.7%) and upstream (EVM=1.6%) signal when PER=30 dB.

From Figure 5.10(a) and (b) we observe that, in absence of a polarization crosstalk, the PolMUX carrier cannot be completely separated at the ONU and consequently also at the CO. In this condition we expect the same transmission performance discussed in the previous example. In fact, the EVM measured after the downlink and uplink propagation are 1.9% and 19.7% respectively. The constellation diagrams inserted are representative of this case and confirm that the quality degradation undergone by the upstream signal is drastically higher than the downstream one. When the PER is set to 30 dB both carriers are correctly separated, as shown in Fig. 5.10(c) and (d). As a result, the quality of the upstream signal improves and becomes comparable with the quality of the upstream one. For that reason the constellation diagrams of the corresponding insets (downstream EVM=1.7% and upstream EVM=1.6%) are practically indistinguishable.

5.3   Reconfigurable WDM optical access network using the PolMUX technique.

In the previous section we have proposed and experimentally demonstrated, for the first time, a full-duplex and light-sources centralized transmission system based on the PolMUX technique. The first advantage brought by the PolMUX technique, with respect to other proposed centralized light-sources strategies, is a minimization of the cost/complexity of the ONU which is kept color-less, source-free, and easy to manage.

It has been demonstrated that, keeping the SoP of the two PolMUX optical carriers as orthogonal as possible, they are separated correctly at the ONU and, in consequence, high demodulation performance can be achieved in both directions of propagation. The polarization tracking and control operations are performed by a single automatic PC, which, as an added value, can be conveniently located at the CO rather than the ONU. As a proof of concept, we have demonstrated high quality full-duplex transmission of digital signals over 10 km of SMF demonstrating that even higher distances can be covered always provided an acceptable polarization extinction ratio between the PolMUX carriers is guaranteed.

Another important issue of the PolMUX approach is that the transmission performance is independent of the wavelength separation between the two optical carriers. It means that both the downlink and uplink PolMUX carriers can be generated by the same optical wavelength supplied by a single coherent source. Apart from doubling the spectral efficiency of the channel, this issue brings an important economical and practical advantage to the architecture. In fact it halves the number of optical sources that must be installed and facilitates the wavelength upgrading as well. Here, the characteristics of the PolMUX strategy result very adaptable and convenient especially in high capacity networks where several optical sources are employed to setup multichannel transmission between the CO and ONUs.

In this context we make a step forward by proposing for the first time a novel WDM optical access network combining dynamic channels assignment and PolMUX technique. Network reconfigurability is realized by means of a very compact and bandwidth-efficient wavelength router based on AWG and all optical switching technology. On the other hand, the PolMUX technique is employed as a light-sources centralization strategy to perform the uplink transmission keeping source-free and color-less ONUs. The employment of the PolMUX approach adds important and favorable implications. Indeed, owing to the PolMUX principle, the bandwidth-per-channel required by the router for wavelength distribution between the CO and each ONU is halved. It leads to a substantial optimization of capacity resources and increases simultaneously the scalability and the flexibility of the network to add more wavelengths in real-time operations.

The integration of the PolMUX technique into the reconfigurable node is demonstrated for different wavelength routing scenarios where the WDM channels are dynamically allocated by the router depending of the ONU demand. Moreover the full-duplex transmission performance of the network is tested with the distribution of digital signals generated in accordance to the SCM scheme. The results achieved show high quality of transmission directions and a great flexibility to manage different services.

5.3.1 Description of the network architecture.

Figure 5.11 shows the architecture of the reconfigurable WDM optical access network.
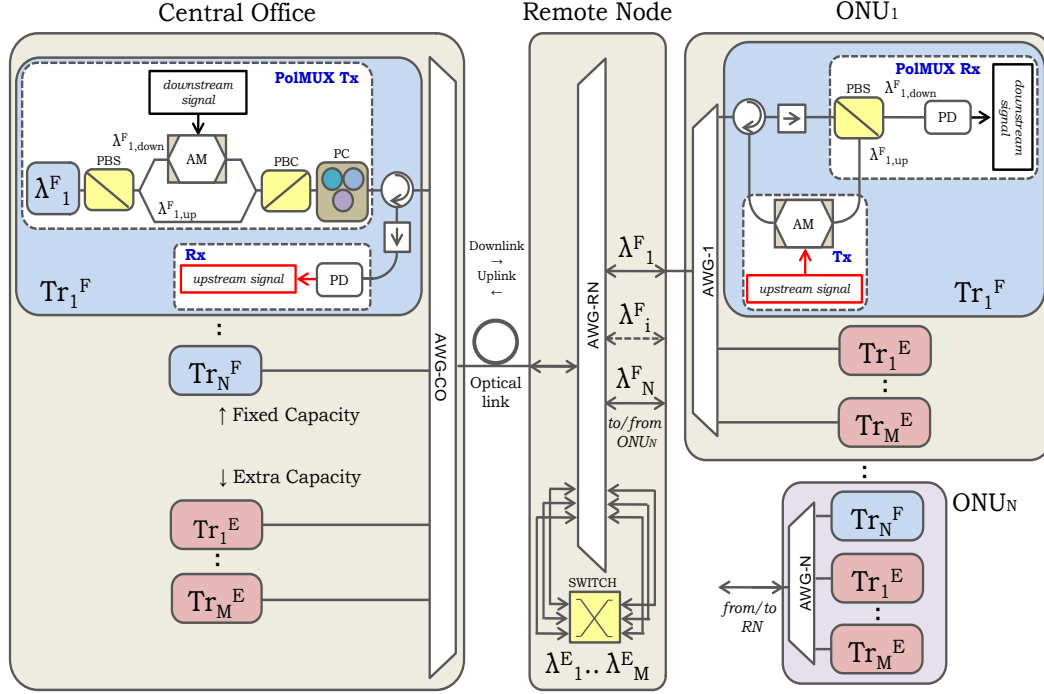
Fig. 5.11 PolMUX-based full-duplex and reconfigurable WDM optical access network.

In accordance with a typical PON topology, the network is composed by a CO, the optical link, a RN and a group of ONUs described as follows.

The CO contains a set of optical transceivers. A number N of them (from Tr_1^F to Tr_N^F) is reserved to the fixed capacity assignment whereas a number M of them (from Tr_1^E to Tr_M^E) is reserved to the extra capacity assignment. The architecture of all fixed and extra transceivers is identical. Each CO transceiver is composed by a PolMUX transmitter structure (CO PolMUX Tx) and a receiver (CO Rx) already described in subsection 5.2.1. A small variation has been introduced in the structure of the CO PolMUX Tx. In fact, as observed in Fig. 5.11, only a single optical source (instead of two) is employed to supply simultaneously the two PolMUX carriers at the same wavelength, the modulated $\lambda^F_{1,down}$ and the unmodulated $\lambda^F_{1,up}$. The separation and orthogonality between them is set by the PBS inserted immediately after the optical source centred at λ_1^F. In such a way two orthogonally polarized optical fields are generated with equally spliced power levels. The remaining part of the CO PolMUX Tx is kept structurally identical to the one described in section 5.2.1 where a PC is centralized in the CO to remotely set and control the degree of orthogonality between the PolMUX carriers during the propagation. Therefore, in the CO a number (N+M) of transceivers provide a pair of optical PolMUX carriers for the downlink and uplink transmission. Following the schematic diagram of Fig. 5.11, each pair of PolMUX carriers at the output of its correspondent transceiver is multiplexed by an $[N+M]_{In}$ x $[1]_{Out}$ AWG wavelength multi/demultiplexer. At the output of the AWG-CO all fixed and extra wavelengths are combined in each port and propagated in downlink direction through the optical link.

The RN is a very compact and flexible wavelength router based on a cyclic $[N+M]_{In}$ x $[N+M]_{Out}$ AWG (AWG-RN) [Ort 2007], where N and M are the number of the fixed and extra capacity channels, respectively. The network capacity is dynamically reconfigured in both downlink and uplink direction by means of a simple $[M]_{In}$ x $[M+N-1]_{Out}$ optical switch, being N and M the number of fixed and extra capacity channels, respectively. In downlink direction the AWG-RN performs a demultiplexing operation feeding each ONU with its correspondent set of PolMUX wavelengths. Symmetrically, in uplink direction, the AWG-RN multiplexes and forwards the uplink wavelengths from each ONU back to the CO. A number of N ports are always used by the AWG-RN to provide the bidirectional routing of the N wavelengths. In this way a fixed unitary capacity assignment is assured for each ONU. In addition, depending on the actual service demand, all ONUs are allowed to increase their total bandwidth by a number of extra channels. In fact, when extra capacity is required, the reconfiguration state of the optical switch can dynamically changed in order to enable a maximum number of M ports of the AWG-RN and, thus, supply the M extra capacity wavelengths. The extra wavelengths are launched back from the optical switch to the input ports of the AWG-RN and emerge from the output ports assigned to the demanding ONU. Thanks to the PolMUX approach, each pair of PolMUX carriers fills the same spectral portion. In turn the spectral efficiency of the AWG-RN is doubled. Therefore, in terms of spectral efficiency, the characteristics of the RN described above are better exploited than the one of the remote routers proposed in others contributions.

Moreover, the key feature of an all-optical switch is, as the name implies, that the signal is kept in the optical domain throughout the switching and routing process. In short, a clear advantage over conventional optic-electro-optic switches is that all-optical switches are transparent to the data rate and codification format of the electrical information carried by the optical signal. In addition, photonic switches can also send bidirectional data on the same single fiber port, something that conventional switches cannot do. Currently there exists a wide variety of all-optical switches commercially available in scalable configurations up to 256x256.

Following the network description all ONUs are identically composed by an optical AWG and a set of (M+1) optical transceivers structured in two principal blocks: the ONU PolMUX receiver (ONU PolMUX Rx) and the ONU transmitter (ONU Tx), also described in section 5.2.1. The first ONU transceiver is reserved to the unit capacity channel or, equivalently, the associated fixed capacity wavelength λ_1^F. Here, operations such as photodetection and demodulation of the downlink carrier, $\lambda_{1,down}^F$, as well as the modulation and back-distribution of the uplink carrier, $\lambda_{1,up}^F$, are realized once the two optical PolMUX carriers have been separated by the PBS. The remaining M extra transceivers execute the same operations but with the extra capacity wavelengths. In order to route the (M+1) channels, each ONU employs a $[1]_{In}$ x $[M+1]_{Out}$ AWG. Note that, the maximum number of ONUs deployed in the network agrees exactly with the number of fixed capacity wavelengths supplied by the CO, which is N. Owing to the integration of the PolMUX scheme, all ONUs present the same structure where all receiving and transmitting operations are performed with a minimized number of components in a way perfectly compatible with the reconfigurable architecture of the network.

5.3.2 Experimental characterization.

In order to experimentally characterize the proposed network, we implement the scheme of Fig. 5.11 by taking N = 4 and M = 2 as the number of fixed and extra capacity channels, respectively. The four fixed wavelengths identified as λ_1^F, λ_2^F, λ_3^F and λ_4^F and the two extra wavelengths, λ_2^E and λ_2^E, are simultaneously provided by a multi-wavelength optical source in accordance to the ITU WDM 0.8 nm-spacing grid for operation in third transmission band. The AWGs employed in the CO and in each of the four ONUs are $[40]_{In}$ x $[1]_{Out}$ and $[1]_{In}$ x $[40]_{Out}$ respectively with a larger number of ports than required for availability reasons. The AWG of the RN is a cyclic $[18]_{In}$ x $[18]_{Out}$ AWG. All AWGs are thermally controlled for matching and stabilization into the ITU grid. Since in our experimental setup M+N = 6, the AWG-RN largely satisfies the number of input and output ports required with high scalability to accommodate more channels. Note that all AWGs offer high wavelength resolution since the wavelength channel spacings is 0.8 nm according to the ITU channel allocation. The optical switch is a $[8]_{In}$ x $[8]_{Out}$ micro electro mechanical (MEM) switch providing channel selection between different input and output fibers with low insertion loss. The transmission is run over a 10 km of SMF. The wavelengths plan and the corresponding ONU assignment is specified in Table 5.1 where fixed and extra channels are differentiated by color.

Table 5.1 Wavelengths plan.

Fixed capacity wavelengths (nm)	Extra capacity wavelengths (nm)	ONU
λ_1^F = 1532.32		1
λ_2^F = 1533.12		2
λ_3^F = 1533.92		3
λ_4^F = 1534.72		4
:	:	:
	λ_2^E = 1545.12	
	λ_1^E = 1545.92	

The optical spectrum of the wavelengths plan corresponding to Table 5.1, has been measured at the output of the AWG-CO as shown in Fig. 5.12.

During the experimental measurements, the input optical power of the fixed capacity wavelengths has been set to 9 dBm and the input optical power of the extra capacity wavelengths has been increased by 4 dB in order to pre-compensate the insertion loss of the AWG-RN (around 3.5 dB) and the optical switch (around 0.5 dB) suffered by the extra capacity wavelengths in case of extra service demand. In this way both fixed and extra wavelengths reach the photodetector with roughly the same power level allowing a better comparison between them and a more realistic evaluation of the network performance. Figure 5.12 also shows that there are around 7 dBm of optical loss accumulated by all wavelengths at the

output of the AWG-CO. They are mainly due to the AWG-CO and the polarization devices in the CO.
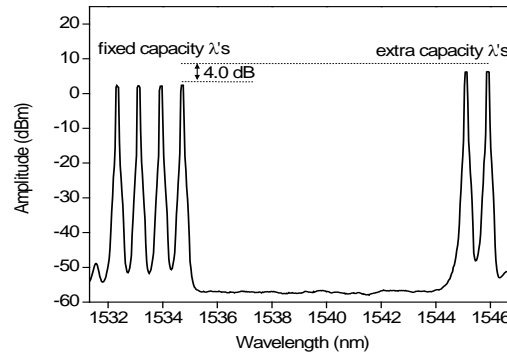
Fig. 5.12 Optical spectrum of the wavelengths plan measured at the output of the AWG-CO.

The proposed network is designed to perform a bidirectional distribution of services between the CO and a ONUs through a cyclic AWG-based router. The technical characteristics of the AWG-RN and the optical switch make the network reconfigurable in such a way that, apart from a fixed capacity assignment, the router is also capable to assign dynamically a number of extra channels. In practice such traffic reconfiguration can be implemented and evaluated for different routing scenarios where an extra service demand from one or more ONUs implies that one or more extra channels must be routed to them.

Taking into account the wavelength plan defined in Table 5.1 and with no loss of generality, we have implemented two different routing scenarios whose schematic representation is given in Table 5.2. In the first scenario the extra wavelengths, λ_1^E and λ_2^E, are assigned to ONU_3. This scenario emulates the case of maximum capacity demand from one single ONU. In the second scenario λ_1^E is assigned to ONU_1, whereas, λ_2^E is routed to ONU_2. The second scenario is a clear example of network resource-sharing between two different ONUs. In both scenarios, a fixed capacity service is always assured by routing all fixed wavelengths to their corresponding ONUs.

Table 5.2 Experimental routing scenarios.

	Scenario 1						Scenario 2					
	Fixed channels				Extra channels		Fixed channels				Extra channels	
ONU_1	λ_1^F						λ_1^F					λ_1^E
ONU_2		λ_2^F						λ_2^F			λ_2^E	
ONU_3			λ_3^F		λ_2^E	λ_1^E			λ_3^F			
ONU_4				λ_4^F						λ_4^F		

The routing table of the $[18]_{In} \times [18]_{Out}$ AWG-RN used in the experimental setup is given in Table 5.3.

As observed in Table 5.3, all fixed and extra wavelengths enter input port In_1 of the AWG-RN. The output ports Out_1 to Out_4 are reserved in ascending order to the distribution of the fixed capacity wavelengths between the CO and ONUs 1 to 4. The last two ports, Out_{17} and Out_{18}, are reserved to the routing of the extra wavelengths, λ_2^E and λ_1^E, respectively. Note that, the port assignment of the extra wavelengths is made in descending order starting from the last output port of the AWG-RN, Out_{18}. In this way the central part of the AWG-RN spectral grid is kept available for the progressive addition of new fixed and/or extra wavelengths. This approach shows the great flexibility and scalability of the network to manage a higher number of ONUs and/or a higher reconfiguration capacity.

With regard to the scenarios implemented, the routing table of the AWG-RN is such that, for the first scenario, the extra wavelengths, λ_1^E and λ_2^E, are routed back from Out_{18} and Out_{17} to input ports In_{16} and In_{15}, respectively. In this way they will emerge from Out_3 together with the fixed channel λ_3^F to reach ONU$_3$. In the second scenario, the extra channel, λ_1^E, follows the routing path Out_{18}-In_{18} in order to emerge from Out_1 with the fixed channel λ_1^F and reach ONU$_1$, whereas, the extra channel, λ_2^E, follows the routing path Out_{17}-In_{16} in order to emerge from Out_2 and reach ONU$_2$ with the fixed channel λ_2^F.

Table 5.3 Routing table of the [18]$_{In}$x[18]$_{Out}$ AWG-RN.

		ONU$_1$	ONU$_2$	ONU$_3$	ONU$_4$	ONU$_5$	..	Extra channels		
		Output ports								
		Out$_1$	**Out$_2$**	**Out$_3$**	**Out$_4$**	Out$_5$	..	Out$_{16}$	**Out$_{17}$**	**Out$_{18}$**
	In$_1$	λ_1^F	λ_2^F	λ_3^F	λ_4^F	λ_5^F	..	λ_3^E	λ_2^E	λ_1^E
	In$_2$	λ_2^F	λ_3^F	λ_4^F	λ_5^F	λ_6^F				
	In$_3$	λ_3^F	λ_4^F	λ_5^F	λ_6^F					
	In$_4$	λ_4^F	λ_5^F	λ_6^F						
	In$_5$	λ_5^F	λ_6^F							
	In$_6$	λ_6^F								
Input ports	:	:								
	In$_{15}$	λ_4^E	λ_3^E	λ_2^E	λ_1^E					
	In$_{16}$	λ_3^E	λ_2^E	λ_1^E						
	In$_{17}$	λ_2^E	λ_1^E							
	In$_{18}$	λ_1^E								

The optical spectra measured at the output channels of the AWG-RN are given in Fig. 5.13 for (a) scenario 1 and (b) scenario 2, respectively.

(a) Scenario 1   (b) Scenario 2
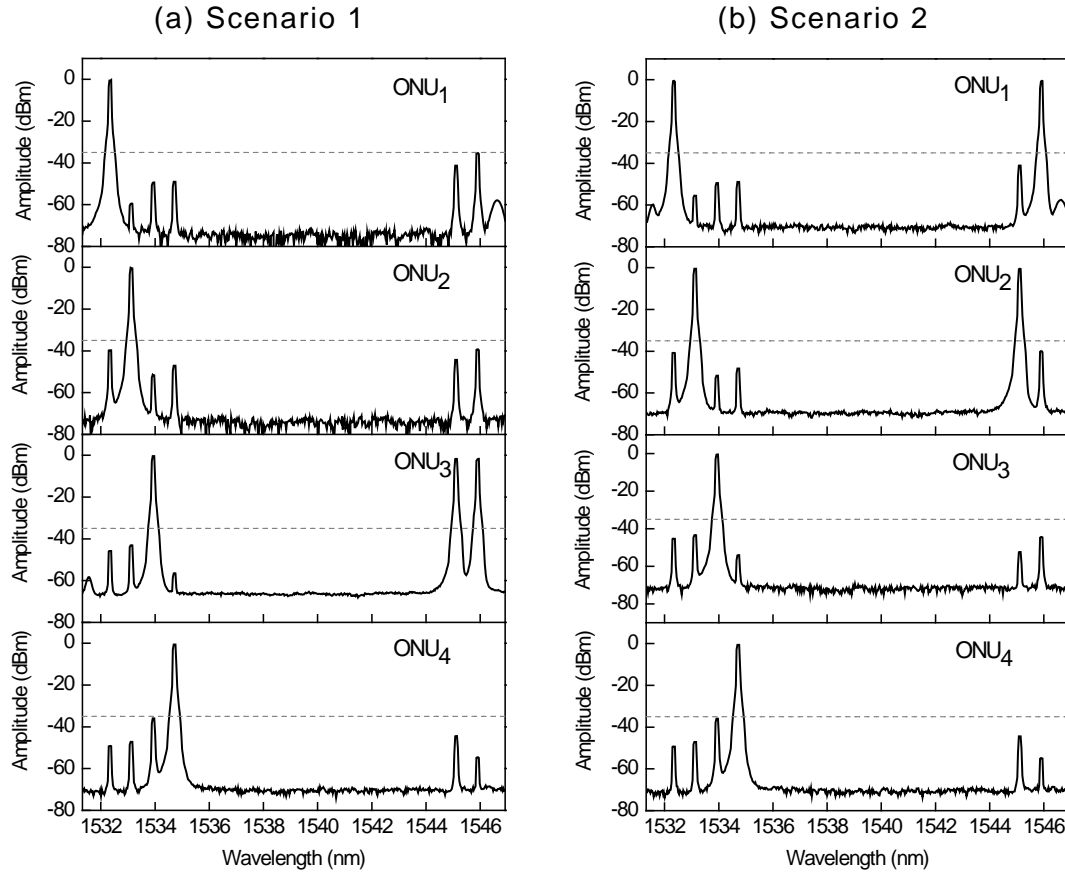
Fig 5.13 Optical spectra measured at the AWG-RN outputs in downlink direction. (a) scenario 1 and (b) scenario 2.

From Fig. 5.13 it can be observed the correct assignment of the four fixed wavelengths to their corresponding ONUs in the two scenarios. In Fig. 5.13(a) the two extra wavelengths are routed together to ONU_3 and, thanks to the pre-compensation of the input optical power, they emerge from the AWG-RN with a similar power level of the fixed wavelength. Note that, the amplitude level of all fixed wavelengths decreases by an amount of 2.5 dBm with respect to the power level of Fig. 5.12. This power penalty is due to the AWG-RN loss and is common to both scenarios. Note that for the extra wavelengths the power decreasing is higher since they cross the AWG-RN two times through the switch. In Fig. 5.13(b) the extra wavelength λ_1^E is received by ONU_1 while the extra wavelength λ_2^E is routed to the adjacent ONU_2 according to the second scenario. Also in this case, all fixed and extra wavelengths are received with similar amplitude levels. Independently of the implemented scenario it can be observed that each ONU, apart from the corresponding set of wavelengths, receives also a small amount of the optical power from other adjacent channels. This power leakage is due to the unavoidable inter-channel crosstalk of the AWG-RN and, depending on the filtering characteristics of the AWG-RN, it may vary from band to band. However, in any case, the crosstalk level is higher than 35 dB (see dashed line of Fig. 5.13) and does not affect significantly the routing operations. The experimental results demonstrate the effectiveness of the reconfigurable wavelength assignment and, thus, the integration of the PolMUX scheme in a reconfigurable node.

5.3.3 *Experimental evaluation of the network performance.*

Once characterized the network and demonstrated its routing capability, we have performed a full-duplex transmission test over a 10 km of SMF. For this purpose, the optical switch has been configured according to the wavelength assignment of the two scenarios defined above. Before running the transmission the orthogonality between all PolMUX carriers has been set to a PER=30 dB by means of the PCs installed at the CO. With regard to the generation of the down- and upstream traffic we have implemented the SCM scheme. A maximum 10% EVM has been established as conventional criterion for signal quality evaluation in the QPSK case, whereas a maximum of 6 % is established for M-QAM signals.

(a) Degradation of fixed and extra capacity channels.

In the experimental setup of this first set of measurements the service transported by each fixed wavelength is, just as instance, a 5 Mb/s QPSK data modulating its own 10 GHz electrical subcarrier in downlink and uplink transmission. To differentiate the fixed services from the extra services each extra capacity channel transports 10 Mb/s 64-QAM data modulating 5 GHz SCM tones also in downlink and uplink transmission.

With no loss of information the following measurements are referred to channels λ_1^F and λ_3^F corresponding to assigned ONU_1 and ONU_3, respectively. Figure 5.14 plots the downlink EVM (a) and the uplink EVM (b) as a function of the received electrical power when the input electrical power is varied from a maximum of 15 dBm to a minimum of -5 dBm. The EVM curves indicates the degradation of the signal carried by λ_1^F in scenario 1 ($\square$) and scenario 2 ($\square$) and the degradation of the signal carried by λ_3^F in scenario 1 ($\bigcirc$) and scenario 2 ($\bigcirc$). The optical back-to-back ($\triangle$) measured at the output of the optical modulator is also included.
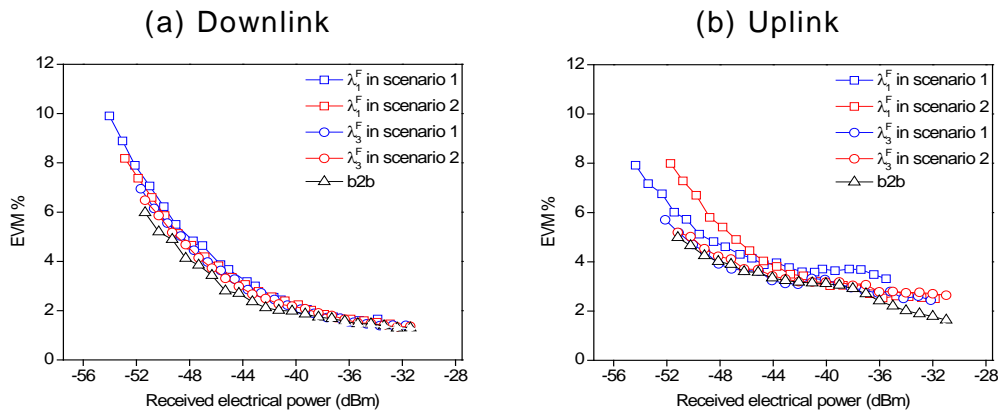
(a) Downlink   (b) Uplink

Fig. 5.14 EVM vs. received electrical power measured for fixed channels λ_1^F and λ_3^F in both scenarios in (a) downlink and (b) uplink propagation. Optical back-to-back ($\triangle$).

Considering the downlink transmission, Fig 5.14 (a) shows an expected improvement of the received signal quality with the received electrical power. In a range of 20 dBm and, independently of the scenario, the EVM reached at ONU_1 and ONU_3 goes from minimum values of 1.4% up to maximum values not exceeding 10.0%. This means that both ONUs demodulate their respective downstream signals with an acceptable quality

153

which becomes very high especially for electrical powers higher than -37 dBm.

Comparing the same channel in the two scenarios we observe small EVM fluctuations due to a different amount of crosstalk induced by the adjacent channels. On the other hand, the EVM fluctuations between channel 1 and 3 are due to the power distribution of the AWG employed in the RN which depends on the specific band. Another reason is that the AWGs of ONU_1 and ONU_3 are not identical. At lower electrical powers all curves are above the back-to-back one with small channel-to-channel variations due to the unequal characteristics of the optical components used in the setup. However, the results obtained are very close to the back-to-back curve and become practically indistinguishable, especially when the received power increases. Analogous considerations can be made for the results of the uplink transmission shown in Fig 5.14(b). Again, at the CO transceivers, the quality of the demodulated signals carried by channel 1 and 3 improves with the electrical power and never exceeds the EVM criterion. Note that, although not included in the plots, similar results have been measured also for the signals carried by wavelengths λ_2^F and λ_4^F.

In the same test, the quality of those signals carried by the extra channels λ_1^E and λ_2^E has been also measured in both scenarios. Figure 5.15(a) and (b) shows the downlink and uplink EVM degradation, respectively. The curves refer to the transmission of λ_1^E in scenario 1 ($\square$) and scenario 2 ($\square$) and the transmission of λ_2^E in scenario 1 ($\bigcirc$) and scenario 2 ($\bigcirc$) including the optical back-to-back ($\triangle$) into the plots.
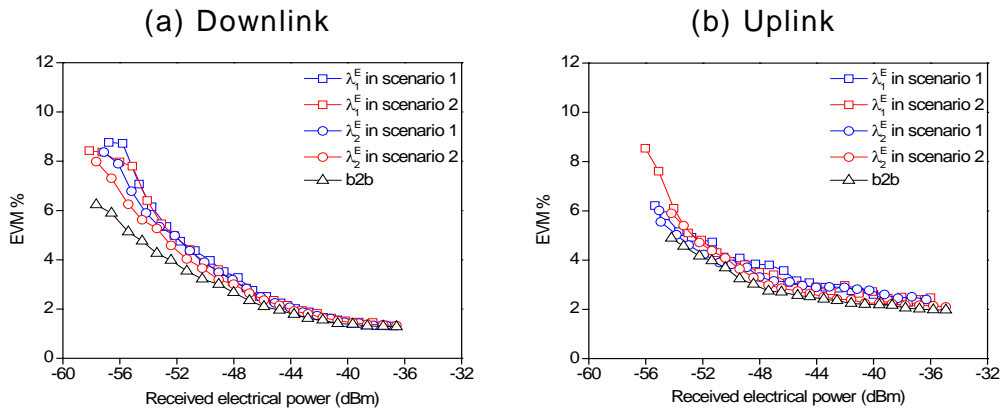
Fig. 5.15 EVM vs. received electrical power measured for extra capacity wavelengths λ_1^E and λ_2^E in both scenarios in (a) downlink and (b) uplink propagation. Optical back-to-back ($\triangle$).

For both scenarios the downlink signal degradation, shown in Fig. 5.15(a) is characterized by the improvement of the EVM with the received electrical power. As in the previous case minimum EVMs around 1.3% and maximum EVM not higher than 8.0% are reached in a range of 20 dB. This result is independent of the scenario and, especially when the received power is higher than -38 dBm, all curves overlap each others. We remark that the extra capacity channels do not affect each others neither when they are routed to the same ONU (scenario 1) nor when they are routed to adjacent ONUs (scenario 2). Note that also in case of injecting extra capacity wavelengths into the network, all curves are very close to the back-to-back one showing a negligible degradation introduced by the system in presence of dynamical service assignment. Figure 5.15 (b) shows

very similar EVM results in uplink transmission. In resume, the results of Fig. 5.14 and Fig. 5.15 demonstrate that, in case of extra capacity demand, the network performance does not vary significantly with respect to a fixed capacity routing. In other words, the transmission performance is transparent to the traffic distribution.

(b) Impact of the electrical subcarrier frequency.

Here, the influence of the electrical subcarrier frequency on the network performance is experimentally studied in order to validate the adaptability of the network to the SCM scheme.

Figure 5.16 plots the downlink EVM (a) and the uplink EVM (b) as a function of the electrical subcarrier frequency for an input electrical power of 12 dBm which has been set as reference level to achieve an acceptable photodetected power. Although all fixed wavelengths have been transmitted and measured in the actual test, to avoid redundancy of information, we show only the results related to the fixed capacity distribution of wavelengths λ_1^F and λ_3^F. In particular, the EVM curves refer to the degradation of digital signals carried by λ_1^F in scenario 1 ($\square$) and scenario 2 ($\square$) and λ_3^F in scenario 1 ($\bigcirc$) and scenario 2 ($\bigcirc$) including the back-to-back ($\triangle$) curve. In this first test, each fixed wavelength transports 5 Mb/s QPSK data modulating its corresponding subcarrier frequency while the extra capacity channels, λ_1^E and λ_2^E, transport 10 Mb/s 64-QAM data modulating subcarriers set to a fixed value of 5 GHz.
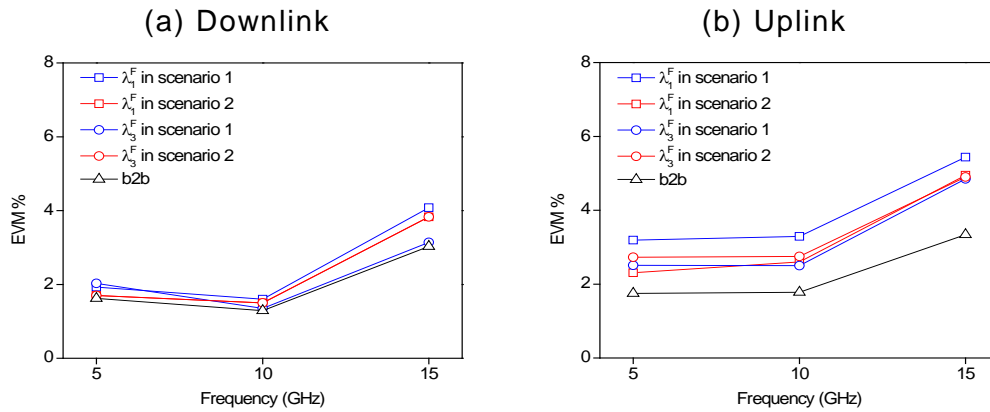
Fig. 5.16 EVM vs. SCM frequency measured for fixed channels λ_1^F and λ_3^F in different scenarios in (a) downlink and (b) uplink transmission. Optical back-to-back ($\triangle$).

Observing Fig. 5.16(a) and (b) the quality degradation of digital signals carried by channels 1 and 3 is characterized by EVM fluctuations around 2.0% and 3.0% for the first two subcarriers tested, 5 GHz and 10 GHz. This evolution is independent on the implemented scenario. At the higher subcarrier frequency, 15 GHz, the quality worsens to 3.1% -4.0% and 4.8%-5.4% in the downlink and uplink directions, respectively. This last EVM increase of the EVM is only due to the bandwidth limitations of the EOMs used in the experimental setup. However, even in the worst case, the EVM is always largely below 10.0%. It demonstrates the versatility of the network to support the SCM scheme and, thus, the flexible transmission of different services.

With regard to the extra service demand Fig 5.17(a) and (b) show the experimental results measured for extra wavelengths, λ_1^E and λ_2^E. In this second test both extra channels are carrying 10 Mb/s 64-QAM data modulating electrical subcarriers at the corresponding frequency while all the fixed wavelengths are carrying 5 Mb/s QPSK data modulated onto SCM tones set to a fixed value of 10 GHz. Also in this case the EVM values are similar to the ones in Fig. 5.16 where they never exceeded the maximum established level. Therefore we conclude that the impact of the electrical subcarrier frequency on the signal quality is transparent to the variable network capacity assignment.
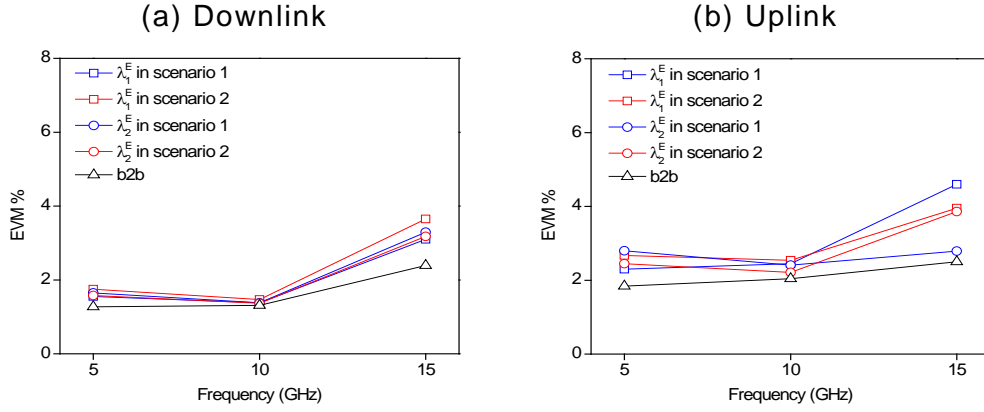
(a) Downlink   (b) Uplink

Fig. 5.17 EVM vs. SCM frequency for extra channels λ_1^E and λ_2^E in different scenarios in (a) downlink and (b) uplink transmission. Optical back-to-back ($\triangle$).

(c) Impact of the signal bit rate.

The network performance is now evaluated against variations of the bit rate imposed on the digital signals modulating the SCM carriers. In the first test all fixed capacity channels transport QPSK signals with the corresponding bit rate and modulating electrical subcarriers at 10 GHz. The two extra services are 10 Mb/s 64-QAM data modulating 5 GHz subcarriers. In Fig. 5.18 the EVM is plotted as a function of the bit rate for fixed channels, λ_1^F and λ_3^F, considering both scenarios in (a) downlink and (b) uplink direction.
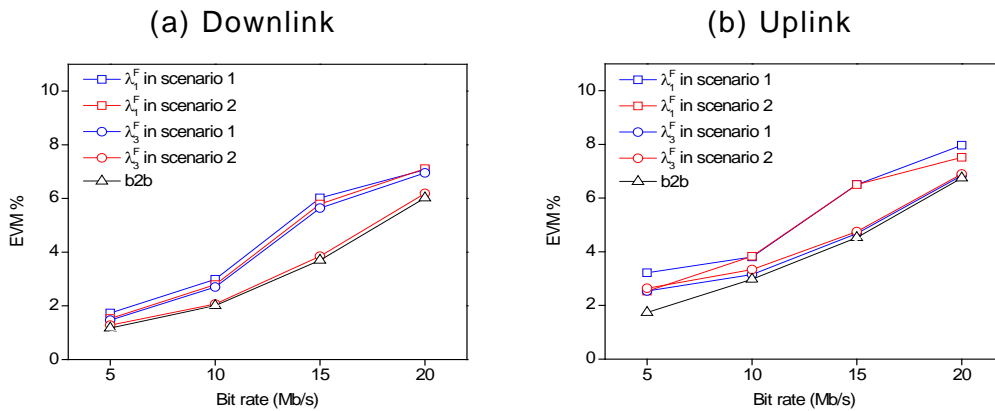
(a) Downlink   (b) Uplink

Fig. 5.18 EVM vs. bit rate for fixed capacity wavelengths λ_1^F and λ_3^F in the two scenarios in (a) downlink and (b) uplink propagation. Optical back-to-back ($\triangle$).

156

As observed in Fig. 5.18(a) at the lower bit rate the EVM is around 2.0%. As the bit rate increases the degradation of the signal quality becomes more important and reaches EVM around 6.0% and 7.0%. The worsening of the signal quality with the bit rate is common to all scenarios and an analogous trend is found in uplink direction, as shown in Fig. 5.18(b). This degradation is induced by the particular bandwidth characteristics of the devices employed in the receiving structures of the CO and ONUs and in particular it is due to the demodulation bandwidth of the photodetector. Therefore this degradation can be mitigated easily with the employment of photodetectors with a higher demodulation bandwidth. Our experimental setup permits, however, a correct signal demodulation of downstream and upstream signals since the EVM does not exceeds the maximum 10.0% criterion.

In the second test we evaluate the EVM degradation as a function of the bit rate for the two extra channels. Here the signals carried by λ_1^E and λ_2^E are 64-QAM data with the corresponding bit rate modulating electrical subcarriers at 5 GHz whereas all fixed services are set to 5 Mb/s QPSK data modulating 10 GHz subcarriers. In Fig. 5.19 the EVM is plotted as a function of the bit rate for extra channels, λ_1^E and λ_2^E, considering both scenarios in (a) downlink and (b) uplink direction.
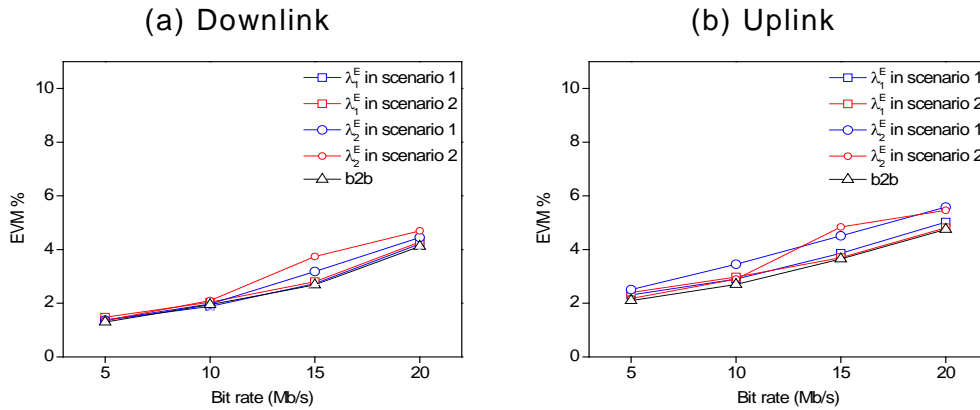
(a) Downlink   (b) Uplink

Fig. 5.19 EVM vs. bit rate for extra services carried by λ_1^E and λ_2^E in both scenarios in (a) downlink and (b) uplink propagation. Optical back-to-back (△).

Independently on the wavelength and scenario the quality of the downstream and upstream extra services is acceptable at lower bit rates. We observe again the increase of the EVM with the bit rate, however, it is somewhat slighter than the previous case, due to a better tolerance of the 64-QAM format to higher bit rates. Actually the EVM does not exceed 5.0% even in the worst case of 20 Mb/s.

5.4   Summary.

This chapter dealt with the experimental implementation and validation of centralized light-sources full-duplex optical transmission system and network architectures where, as far as we know, the PolMUX technique has been, for the first time, incorporated as a novel strategy to minimize the architecture complexity of the ONU, in accordance with the centralization purposes of the network.

The study has been organized as follows. First we have contextualized the application environment of the PolMUX technique with a brief historical background on the employment of light polarization in optical communications systems and networks.

Secondly, the principle of operation of the PolMUX technique and the fundamental optical components required for its practical implementation have been also detailed together with an exhaustive experimental characterization of the centralized light-sources system architecture where coherent sources are employed to generate the down- and uplink carriers at the CO. A single-channel full-duplex optical transmission system based on the PolMUX strategy has been experimentally validated through the evaluation of the transmitted signal quality degradation in both down- and uplink directions of propagation.

Finally, the PolMUX approach has been incorporated in centralized light-source reconfigurable WDM-based optical access network architecture for full-duplex multichannel transmissions where high-capacity demand and low architecture complexity of the ONU are required. The performance of the network has been evaluated for different routing scenarios where both fixed and reconfigurable capacity assignment have been implemented.

The PolMUX strategy is fundamentally based on the versatility offered by the polarization of light. The PolMUX principle, in fact, uses light polarization as a degree of freedom to efficiently multiplex two orthogonal optical fields at the same wavelength into the same optical channel. Under this principle, the optical carriers required for the downlink and uplink transmission can be provided only by a single coherent light source centralized at the CO. In this way, no additional light-source is installed at the ONU which becomes completely source-free and color-less. As technical and economical implications, complexity, fabrication costs and power consumption of the ONU are drastically minimized at the same time.

The tracking and control of polarization are strictly necessary for the success of a PolMUX approach. We have demonstrated that the orthogonality, in terms of PER, between the PolMUX carriers can be always adjusted and maintained higher than 25 dB during the propagation over tens of kilometers of optical link. It assures a correct demodulation of the downlink and uplink carrier at the ONU and CO respectively. As an added value, the ONU becomes polarization-independent once that all polarization monitoring and control operations are realized remotely from the CO. The effectiveness of PolMUX technique is reflected also in the size of the external plant since all full-duplex transmissions run over a single-fiber topology link.

It has been demonstrated that the PolMUX scheme can be successfully integrated into a multichannel transmission scenario such as a reconfigurable WDM optical access network. It is fully compatible with all routing operations performed for both fixed and extra reconfigurable capacity assignment. In addition, owing to the PolMUX versatility, the architecture scalability and service upgrading can be improved and facilitated in real time by adding new light-sources at the CO without significant changes in the network infrastructure and especially in the ONU and the RN. The spectral efficiency of the PolMUX scheme allows a compact and scalable RN with no waste of bandwidth. It means higher capacity at minimum cost as required in such kind of dynamical networks.

The evaluation of network performance has been carried out considering the full-duplex transmission of different services through different routing scenarios where, depending on the actual demand, extra capacity wavelengths have been assigned dynamically to different ONUs. In all cases the EVM of the demodulated channels always verified the conventional requirements independently of the scenario and direction of propagation.

We have also demonstrated that the network is also compatible with the SCM technique in the electrical domain. The signal quality in terms of EVM is almost transparent to variations of the codification type and bit rate once bandwidth limitations of the experimental equipment are overcome. In this way, the spectral efficiency of the network can be further increased with a substantial improvement of the network flexibility.

The effectiveness and potentialities of the proposed PolMUX approach for the light-sources centralization as well as the interesting possibility of realize polarization-insensitive ONUs by means of remote polarization tracking and control, has been considered and studied very recently also in [Jun 2010] showing that the application of the PolMUX technique is an important topic currently under research.

5.5 References.

[Ami 2010]   A. A. Amin, H. Takahashi, I. Morita, H. Tanaka, "100-Gb/s Direct-Detection OFDM Transmission on Independent Polarization Tributaries", IEEE Photon. Technol. Lett., Vol. 22, pp. 468-470, 2010.

[Ben 1990]   S. Benedetto, P. Poggiolini, "Combined Amplitude and Polarization Shift Keying Optical Coherent Modulation", Electron. Lett., Vol. 26, pp. 918-919, 1990.

[Ben 1992]   S. Benedetto, P. Poggiolini, "Theory of Polarization Shift Keying Modulation", IEEE Trans. on Comm., Vol. 40, pp. 708-721, 1992.

[Bet 1992]   S. Betti, G. De Marchis, E. Iannone, "Polarization Modulated Direct Detection Optical Transmission Systems", J. Lightwave Technol., Vol. 10, pp. 1985-1997, 1992.

[Big 2001]   S. Bigo, Y. Frignac, G. Charlet, W. Idler, S. Borne, H. Gross, R. Dischler, W. Poehlmann, P. Tran, C. Simonneau, D. Bayart, G. Veith, A. Jourdan, J. Hamaide, "10.2 Tbit/s (256x42.7Gbit/s PDM/WDM) transmission over 100km TeraLight fiber with 1.28 bit/s/Hz spectral efficiency", in Proc. Optical Fiber Communications Conf. (OFC), Anaheim, CA, 2001, Paper PD25.

[Bof 2008]   P. Boffi, M. Ferrario, L. Marazzi, P. Martelli, P. Parolari, A. Righetti, R. Siano, M. Martinelli, "Measurement of PMD tolerance in 40-Gb/s polarization-multiplexed RZ-DQPSK", Opt. Express, Vol. 16, pp. 13398-13404, 2008.

[Bof 2009]   P. Boffi, M. Ferrario, L. Marazzi, P. Martelli, P. Parolari, A. Righetti, R. Siano, M. Martinelli, "Stable 100-Gb/s POLMUX-DQPSK Transmission with Automatic Polarization Stabilization", IEEE Photon. Technol. Lett., Vol. 21, pp. 745-747, 2009.

[Bor 1999]   M. Born, E. Wolf "Principles of Optics", Seventh Edition, Cambridge University Press, 1999.

[Cal 1988]   R. Calvani, R. Caponi, F. Cisternino, "Polarization Phase-Shift Keying: A Coherent Transmission Technique with Differential Heterodyne Detection", Electron. Lett., Vol. 24, pp. 642-643, 1988.

[Chi 2005]   N. Chi, L. Xu, S. Yu, P. Jeppesen, "Generation and transmission performance of 40 Gbit/s polarisation shift keying signal", Electron. Lett., Vol. 41, 2005.

[Cho 2004]   P. S. Cho, G. Harston, C. J.Kerr, A. S. Greenblatt, A. Kaplan, Y. Achiam, G. Levy-Yurista, M. Margalit, Y. Gross, and J. B. Khurgin, "Investigation of 2 b/s/Hz 40-Gb/s DWDM transmission over 4x100 km SMF-28 fiber using RZ-DQPSK and polarization multiplexing", IEEE Photon. Technol. Lett., Vol. 16, pp. 656-658, 2004.

[Cho 2009]   C. W. Chow, C. H. Yeh, "Signal re-modulation without power sacrifice for carrier distributed hybrid WDM-TDM PONs using PolSK", Opt. Commun., Vol. 282, pp. 1294-1297, 2009.

[Chr 1996]   A. R. Chraplyvy, A. H. Gnauck, R. W. Tkach, J. L. Zyskind, J. W. Sulhoff, A. J. Lucero, Y. Sun, R. M. Jopson, F. Forghieri, R. M. Derosier, C. Wolf, A. R. McConnick, "1-Tb/s Transmission Experiment", IEEE Photon. Technol. Lett., Vol. 8, pp. 1264-1266, 1996.

[Die 1987]   E. Dietrich, B. Enning, R. Gross, H. Knupke, "Heterodyne Transmission of a 560 Mbit/s Optical Signal by Means of Polarization Shift Keying", Electron. Lett., Vol. 23, pp. 421-422, 1987.

[Eva 1992]   S. G. Evangelides, L. F. Mollenauer, J. P. Gordon, N. S. Bergano, "Polarization Multiplexing with Solitons", J. Lightwave Technol. Vol. 10, pp. 28-35, 1992.

[Flu 2008]   C.R.S. Fludger, T. Duthel, D. van den Borne, C. Schulien, E-D. Schmidt, T. Wuth, J. Geyer, E. De Man, Giok-Djan Khoe, H. de Waardt, "Coherent Equalization and PolMux-RZ-DQPSK for Robust 100GE Transmission", J. Lightwave Technol., Vol. 26, pp. 64-72, 2008.

[Gav 2010]   G. Gavioli, E. Torrengo, G. Bosco, A. Carena, V. Curri, V. Miot, P. Poggiolini, F. Forghieri, S. J. Savory, L. Molle, R. Freund, "NRZ-PM-QPSK 16 100 Gb/s Transmission Over Installed Fiber With Different Dispersion Maps", IEEE Photon. Technol. Lett., Vol. 22, pp. 371-373, 2010.

[Her 1991]   C. Herard, A. Lacourt, "New multiplexing technique using polarization of light", Applied Optics, Vol. 30, pp. 222-231, 1991.

[Hil 1992]   P. M. Hill, R. Olshansky, W. K. Burns, "Optical Polarization
              Division Multiplexing at 4 Gb/s", IEEE Photon. Technol. Lett., Vol.
              4, pp. 500-502, 1992.

[Hu 2003]   E. Hu, Y. Hsueh, K. Shimizu, K. Wong, N. Kikuchi, M. Marhic, L.
              Kazovsky, "4-level direct-detection polarisation shift-keying (DD-
              PolSK) system with phase modulators", in Proc. OFC'2003,
              Atlanta, GA, USA, paper FD2, 2003.

[Gna 2006]   A. H. Gnauck et al., "12.3-Tb/s C-Band DQPSK Transmission at
              3.2 b/s/Hz Spectral Efficiency", Paper Th4.1.2, ECOC2006, 2006.

[Gra 2009]   J. Mora, B. Ortega, J. Capmany, F. Grassi, "Bi-directional Optical
              Aceess Network based on POLMUX Technique Using Centralized
              Light Sources", in proceeding of MWP 2009, Th 4.9, 2009.

[Ito 2000]   T. Ito, K. Fukuchi, K. Sekiya, D. Ogasahara, R. Ohhira, T. Ono,
              "6.4 Tb/s (160 x 40 Gb/s) WDM transmission experiment with 0.8
              bit/s/Hz spectral efficiency", in Proceedings of European
              Conference on Optical Communications, Munich, Germany, 2000,
              Paper PD1.1.

[Jun 2010]   H.-D. Jung, N.-C. T. C. Okonkwo, E. Tangdiongga, T. Koonen,
              "10Gb/s Bi-directional Symmetric WDM-PON System based on
              POLMUX Technique with Polarization Insensitive ONU", in
              Proceedings of OFC 2010, paper OTuL3.

[Mar 2006]   M. Martinelli, P. Martelli, S. M. Pietralunga, Polarization
              Stabilization in Optical Communications Systems", J. Lightwave
              Technol., Vol. 24, pp. 4172-4183, 2006.

[Mil 2005]   B. Milivojevic, A. F. Abas, A. Hidayat, S. Bhandare, D. Sandel, R.
              Noé, M. Guy, M. Lapointe, "1.6-b/s/Hz 160-Gb/s 230-km RZ-
              DQPSK polarization multiplex transmission," IEEE Photon.
              Technol. Lett., Vol. 17, pp. 495-498, 2005.

[Nel 2000]   L. E. Nelson, H. Kogelnik, "Coherent crosstalk impairments in
              polarization multiplexed transmission due to polarization mode
              dispersion", Opt. Express, Vol. 7, pp. 350-361, 2000.

[Liu 2010]   B. Liu, X. Xin, L. Zhang, J. Yu, Q. Zhang, C. Yu, "A WDM-OFDM-
              PON architecture with centralized lightwave and PolSK-modulated
              multicast overlay", Opt. Express, Vol. 18, pp. 2137-2143, 2010.

[Ort 2007]   B. Ortega, J. Mora, G. Puerto, J. Capmany, "Symmetric
              reconfigurable capacity assignment in a bidirectional DWDM
              access network", Opt. Express, Vol. 15, pp. 16781-16786, 2007.

[Qia 2010]   D. Qian, N. Cvijetic, J. Hu, T. Wang, "108 Gb/s OFDMA-PON With
              Polarization Multiplexing and Direct Detection", J. Lightwave
              Technol., Vol. 28, pp. 484-493, 2010.

[Sch 2010]   B. J. C. Schmidt, Z. Zan, L. B. Du, A. J. Lowery, "120 Gbit/s Over
              500-km Using Single-Band Polarization-Multiplexed Self-Coherent
              Optical OFDM", J. Lightwave Technol., Vol. 28, pp. 328-335,
              2010.

[Sot 2002]   H. Sotobayashi, W. Chujo, K.-I. Kitayama, "1.6-b/s/Hz 6.4-Tb/s QPSK-OCDM/WDM (4 OCDMx40 WDMx 40 Gb/s) Transmission Experiment Using Optical Hard Thresholding", IEEE Photon. Technol. Lett., Vol. 14, pp. 555-557, 2002.

[Tak 2010]   H. Takahashi, A. A. Amin, S. L. Jansen, I. Morita, H. Tanaka, "Highly Spectrally Efficient DWDM Transmission at 7.0 b/s/Hz Using 8x65.1-Gb/s Coherent PDM-OFDM", J. Lightwave Technol., Vol. 28, pp. 406-414, 2010.

[Tsa 2005]   I. Tsalamanis, E. Rochat, M. C. Parker, S. D. Walker, "Polarization Dependent Loss and Temperature Fluctuations Effect on Degree of Orthogonality in Polarization Multiplexed Arrayed Waveguide Grating Based Distribution Networks", IEEE J. of Quantum Electron., Vol. 41, pp. 945-950, 2005.

[Tse 2009]   C. P. Tsekrekos, T. Kuri, K.-I. Kitayama, "Simultaneous Transmission of Millimeter-Wave and Baseband Signals Using Wavelength Interleaving and Polarization Multiplexing for an Integrated Reconfigurable Access Network", IEEE Photon. Technol. Lett., Vol. 21, pp. 1597-1599, 2009.

[Wan 2009]   Z. Wang, C. Xie, X. Ren, "PMD and PDL impairments in polarization division multiplexing signals with direct detection", Opt. Express, Vol. 17, pp. 7993-8004, 2009.

[Wan 2010]   R. Wang, S. Fu, P.P. Shum, C. Lin, "10 Gbit/s WDM-PON using downstream PolSK coded by polarization modulator and upstream intensity re-modulation", Electron. Lett., Vol. 46, 2010.

[Wre 2003]   C. Wree, N. Hecker-Denschlag, E. Gottwald, P. Krummrich, J. Leibrich, E.-D. Schmidt, B. Lankl, W. Rosenkranz, "High spectral efficiency 1.6-b/s/Hz transmission (8x40 Gb/s with a 25-GHz grid) over 200-km SSMF using RZ-DQPSK and polarization multiplexing", IEEE Photon. Technol. Lett., Vol. 15, pp. 1303-1305, 2003.

[Yao 2007]   X. S. Yao, L.-S. Yan, B. Zhang, A. E. Willner, J. Jiang, "All-optic scheme for automatic polarization division demultiplexing", Opt. Express, Vol. 15, pp. 7407-7414, 2007.

Chapter 6

Conclusions and future prospects

6.1 Conclusions.

In this Thesis we have investigated and proposed different novel full-duplex and reconfigurable broadband optical access architectures based on WDM technology with the aim of minimize complexity and costs of next generation WDM-PONs. In particular, the investigation has dealt with two specific topics depending on whether the access network requires low or high capacity transport of broadband services.

All-optical networks are becoming a reality, driven by recurrent needs for capacity and by the necessity to remove electronic bottlenecks. In this context WDM is promising to be the technology of choice for meeting the current and future user's demand in fiber-optic communication networks. Originally used to increase the long-haul transmission capacity, today's efforts are moving WDM technology into the access domain in order to serve residential and business subscribers. Here also, the WDM-PON is becoming the most attractive solution to achieve high-capacity distribution of multiple services in a simple fiber-shared topology satisfying also information protection and security issues.

In conventional WDM-PONs the channels are univocally assigned and distributed from/to the CO to/from each ONU or BS. In steady traffic conditions, the channel allocation is fixed. However, depending on the actual demand, some or all terminal subscribers may need to adjust their usage of resources causing asynchronous changes in traffic conditions. In these cases, the architecture should provide dynamic capacity allocation by means of flexible channels allocation. In this way, all distributed services can be dynamically accommodated in response to the actual traffic load and users needs. Due to the advantages of photonic technology, the optical routing of channels is a rapid and efficient candidate to realize such network capacity reconfiguration and monitoring functions.

In addition, RoF is an already mature technique that allows transmission of analog radio frequency signals. Today RoF can be easily integrated into WDM-PONs creating a perfect symbiosis between the fixed and wireless access worlds. In this context, the spectrally efficient SCM technique is a powerful multiplexing approach for the analog broadcasting of video services according to new digital TV and HDTV standards. Recently, an obvious and versatile extension of SCM technique has been also proposed for the converged transport of mixed digital (or baseband) FTTx and analog RoF signals at microwave or millimeter wave frequencies. In such hybrid solutions the last mile paths of the access network can be covered by optical fibers (for example, in FTTx applications MMF is often preferred for its easy installation inside buildings and cost-effectiveness with respect to SMF) and conventional radio links without the need of separate wired and wireless access infrastructures.

Despite of these well-recognized features and capabilities, WDM-PONs are still far from being widely deployed and commercialized as they may be cost-prohibitive due to complex transceivers architecture. In fact the inherent multi-access nature of WDM technology may require several wavelength-specified sources at the CO for the downlink transmission. All wavelengths must be monitored and controlled to exactly match the optical band-pass region of the multiplexing/demultiplexing device. For the uplink transmission a single optical source at each ONU transceiver is strictly necessary causing the need for a wavelength-dependent ONU per each PON customer. Today, finding simple and cost-effective solutions for such requirements is becoming a new challenge.

Therefore the current state and specifications of WDM access networks justifies the two main contributions of this Thesis focused on advanced WDM optical architectures designed to satisfy the actual and diversified demand of capacity and broadband services while keeping low the architecture cost and complexity by means of concepts such as dynamic capacity reconfiguration, service convergence and centralization of light source provisioning and control.

6.1.1 Converged signal transmission using optical broadband sources.

The first contribution of the Thesis concerns to an optical access platform with low capacity requirements which aims to the centralized, reconfigurable and converging transport of baseband and RoF signals using optical broadband sources (OBSs). Concretely, we propose the theoretical analysis and experimental validation of dispersion-tolerant optical systems based on the employment of optical broadband sources in third communication band and whose adaptability to the transport high frequency RoF signals is realized, for the first time to our knowledge, by means of optical interferometric structures.

The photonic band-pass transmission response of the interferometric structure has been proved to be a key feature in order to overcome the chromatic dispersion-induced effect arising from the spectral width of the source, which is the major cause of the system operative bandwidth limitations. Under convenient selection of the time delay between its two optical branches, the interferometric structure is capable of optically generating a band-pass transmission window in the electrical system response in such a way that the transport of RoF signals is allowed. By changing the optical time delay using a variable delay line, the band-pass window can be also tuned in a wide GHz range only limited by the photodetector bandwidth. The incorporation of a interferometric structure to reduce the impact of fiber chromatic dispersion offers a relatively low degree of implementation complexity and opens the possibility to transmit RoF signals employing cost-effective OBSs in optical access platforms. In addition, we have demonstrated that the position of the interferometric structure just behind the electro optical modulator opens, at the same time, a viable alternative to mitigate the carrier suppression effect in comparison to other dispersion compensation techniques.

Our innovative solution has been firstly validated in a single-channel transmission over SMF and MMF links using the IM-DD scheme with external modulation of DSB-AM optical carriers. Concerning the generation and transport of the electrical signals, the RoF technique has been

incorporated in combination with the SCM scheme to improve the link bandwidth utilization. Moreover, for the binary information, different codifications, such as, BPSK, QPSK and M-QAM have been applied demonstrating the service flexibility of the proposed approach.

Secondly, the spectral characteristic of OBSs and the ability of the interferometric structures have been exploited to build a multichannel transmission scenario with principal target the minimization of the light sources-associated costs at the CO transceiver rather than an increasing of capacity. In this context, the research has addressed the experimental implementation of a CWDM-PON access architecture where expensive and wavelength-specific lasers at the CO transceiver has been efficiently replaced by a single OBS. Here, the spectral slicing technique applied to the OBS has been indispensable to divide the broad spectrum of the OBS into narrower CWDM channels for broadcasting the same information to different ONUs.

For the architecture of the CO transceiver, we have also proposed the adoption of phase modulation of the optical carrier as a good alternative to conventional amplitude modulation. In presence of phase modulated optical carriers, we have demonstrated that the dispersive nature of SMF and MMF induces the phase-to-intensity conversion effect whose band-pass response is perfectly compatible with the accommodation of RoF signals using the interferometric approach.

At this point, we have highlighted and experimentally demonstrated two more functionalities offered by the interferometric structure: the photonic suppression of undesired HD and IMD terms arising from the non linear response of the external modulator in SCM systems and the all-optical microwaves generation and up-conversion.

This work on the converged signal transmission over broadband sources has been completed with the experimental implementation of a full-duplex reconfigurable access node contemplating both fixed and dynamical channel assignment of different services over different routing scenarios.

The remote node architecture adopts a simple scheme where the dynamical assignment of extra capacity channels is accomplished by means of optical switches. Depending on the demanding ONU, the configuration state of each switching device can be changed in order to select and route the extra service. The RN architecture is compact and offers flexibility to the addition of new users depending on the slicing capabilities of the CWDM device.

For the uplink transmission, at each ONU, a portion of the downlink carrier power is re-used and modulated by the upstream signal. In this way, all ONUs are kept source-free and wavelength-independent avoiding the inventory costs and management operations associated to the installation of additional light sources at the ONU. Moreover, since the installation and control of the interferometric structures are centralized at the RN, the ONU architecture is further simplified. The upstream signals are modulated in the low-pass region of the electrical transfer function leaving the high frequency band for the to downstream transmission. This approach offers the required downstream wireless and upstream wired service convergence.

6.1.2 High capacity bidirectional signal transmission using the PolMUX technique.

The second contribution of the thesis is devoted to the experimental implementation and demonstration of high-capacity full-duplex optical transmission systems where the polarization multiplexing (PolMUX) technique is employed for the first time in the access network as a novel strategy to minimize the cost and complexity of the ONU in accordance with the centralization concept. The PolMUX strategy is fundamentally based on the versatility offered by the polarization of light. The principal characteristics and improvements brought by the PolMUX scheme with respects to other light-sources centralization strategies are resumed as follows. The PolMUX principle uses light polarization as a degree of freedom to efficiently multiplex two orthogonal optical fields at the same wavelength into the same optical channel. Under this principle, the optical carriers required for the downlink and uplink transmission can be provided only by a single coherent light source centralized at the CO. In this way, no additional light-source is installed at the ONU which becomes completely source-free and wavelength-independent. Therefore, complexity and fabrication costs of the ONU may be drastically minimized at the same time.

In this line, the research contemplates two stages. In the first stage, the experimental characterization of a single-channel full-duplex optical transmission system based on the PolMUX approach is made along with the experimental evaluation of the signal quality degradation in both down- and uplink directions of propagation. The results remark that the tracking and control of polarization are strictly necessary for the success of the PolMUX strategy. However, the tests carried throughout the experimental validation, demonstrate that the orthogonality between the PolMUX carriers can be always adjusted and maintained during the propagation over tens of kilometers assuring a correct demodulation of the PolMUX carriers by using advanced high-speed polarization controllers. As an added value, in our architecture, the ONU can be also kept polarization-independent since all polarization monitoring and control operations are realized remotely at the CO. The effectiveness of the PolMUX technique is reflected also in the size of the external plant since all full-duplex transmissions run over a single-fiber topology instead of using a pair of separate fibers.

In a second stage, the PolMUX scheme is integrated in a full-duplex reconfigurable WDM-based optical access network architecture for multichannel communications. Here the WDM networking defines an environment of application with higher capacity. The transmission performance of the network is evaluated through different routing scenarios where both fixed and reconfigurable capacity assignment are implemented. Owing to the PolMUX versatility, the architecture scalability and service upgrading can be improved and facilitated by adding new light-sources at the CO without significant changes in the network infrastructure and especially in the ONU and the RN. The spectral efficiency of the PolMUX scheme allows a compact and scalable RN based on a cyclic AWG whereas dynamical routing is accomplished by an optical switch. The experimental validation demonstrates also that the PolMUX approach is also compatible with the SCM technique and that the signal quality in terms of EVM is almost transparent to variations of the codification type and bit rate provided that bandwidth limitations of the experimental equipment are

overcome. In this way, the spectral efficiency of the architecture can be further increased with a substantial improvement of service flexibility.

6.2   Future prospects.

Concerning the two significant contributions of the Thesis, the author would like to mention some interesting lines which have been kept open for future research and development.

- Regarding the insertion of the interferometric structure in the CO transceiver architecture, it could be interesting to investigate some other possible configurations in order to allow not only broadcast but also unicast distribution on an individual basis. Also, the possibility to employ cascaded interferometric structures could be also evaluated in order to select different frequency bands from the incoming broadcast signal.

- In the PolMUX transmission scheme, the employment of MMF has not been considered. Here, it could be interesting to study the influence of modal dispersion over the SoP of the PolMUX carriers, and, thus, the transmission performance of the PolMUX system.

- So far, the effects of the optical channel filtering have been neglected in both contributions. However, some interaction between channels, such as, the optical crosstalk mechanism due to imperfect WDM optical components is expected and should be considered as it may leads to unwanted wavelengths interfering with the desired optical channel and implies small additional system performance power penalties.

- In multiple-wavelength transmission, the effects of fiber non-linearities such as SPM, cross-phase modulation (XPM), four-wave mixing (FWM), stimulated Raman scattering (SRS) and stimulated Brillouin Scattering (SBS) may become significant. Although not contemplated in this Thesis, the crosstalk due to the optical fiber non linearities should be taken into account as it may depend on the subcarrier frequency, the channel spacing and the optical power. The analysis and measurement of such crosstalk dependence constitutes a new line of research in order to extend the use of our system configurations also to the long-haul transmission. In this context, the adoption of new modulation formats such as optical duobinary, carrier-suppressed return-to-zero (CS-RZ), and DPSK could be introduced mostly because of their transmission properties in terms of tolerance to GVD and/or resilience to optical fiber non linearities, but also because some of them might allow for an increased spectral efficiency.

- We have mentioned that the size of the outside plant is also critical when deploying an access network. The kilometers of fiber that are deployed and the number of optical fusions needed to connect the ONUs to the CO depends not only on the network topology but also on the number of fibers used for the down- and up-stream

transmission. In the direction of a cost affordable FTTH system, it is reasonable to consider a single-fiber (1-F) solution outside plant for reducing the amount of fiber to be installed. Despite this architecture is very attractive, its main limiting factor is that light is being transmitted in both directions over the same fiber at the same wavelength. In fact, due to signals propagating in opposite directions, the transmission performance may be seriously degraded by the presence of Rayleigh backscattering (crosstalk between the signal travelling in one direction and the backscattering from the signal that travels in the opposite direction) of counter-propagating signals, as well as from crosstalk caused by possible lumped reflections of passive components. The effects and minimization of Rayleigh backscattering, an important and unavoidable limiting interference in bidirectional single-fiber and single-wavelength systems, and other reflection mechanisms could be another interesting topic to be extensively studied in the future.

In conclusion, research in optical access networks is of primary importance to meet the actual and forecasted subscriber's demand. Representative solutions proposed to date exhibits a wide variety of technological and architectural approaches. Differences among these alternative designs typically derive from differing assumption on fundamental requirements and issues such as network capacity, subscriber's bandwidth, service transparency and user's scalability, dynamical traffic routing, external plant size, availability and cost of various competing technologies. All these factors make the design of optical access networks very challenging and in most cases, no one specific design is optimal in all circumstances. Although currently optimized access architectures for the transport of digital and analog services may have an important near-term window of opportunity, optical fiber access completely based on WDM technology should ultimately emerge as the architecture of choice due to its superior performance. Upgrading current-generation TDM-based PONs is, therefore, a challenge, and, as remarked in various points of this work, the major goal is to provide an economic solution to enable a large scale deployment of WDM-PONs in the future.

However, design considerations other than cost and transceivers complexity could become important in this future upgrading path. For example, the most convenient access topology may not strictly remain a conventional tree. The fiber layout may be adapted to star and ring topologies or probably an agile combination of them depending on specific geographic conditions and operator's needs. The network topology should be especially versatile in order to satisfy user's mobility in wireless areas or when the deployment of a new access infrastructure is required to provide coverage in punctual events with high concentration of fixed or mobile subscribers. Therefore, although this thesis focuses on optical access solutions, the real-world implementation of access networks will probably be a hybrid integration of fiber, radio and even free-space optics physical layers to provide the best possible service to the end user seamlessly. In this context, the interfaces between such different infrastructures are still creating interesting research areas with further challenges such as the minimization of size and power consumption of some or all units composing the network.

I. Index of figures

Index of figures

II. Index of tables

Index of tables

III. List of acronyms

10GEPON	10 Gigabit Ethernet Passive Optical Network
ADSL	Asymmetric Digital Subscriber Line
AM	Amplitude Modulation
AON	Active Optical Network
APON	Asynchronous Transfer Mode Passive Optical Network
ASE	Amplified Spontaneous Emission
ATM-PON	Asynchronous Transfer Mode Passive Optical Network
AWG	Arrayed Wavelength Grating
BER	Bit Error Rate
BPON	Broadband Passive Optical Network
BS	Base Station
CATV	Cable Television
CD	Coherent Detection
CO	Central Office
CSE	Carrier Suppression Effect
CW	Continuous Wave
CWDM	Coarse Wavelength Division Multiplexing
DCA	Dynamic Channel Allocation
DCF	Dispersion Compensating Fiber
DFB	Distributed Feedback Laser
DPSK	Differential Phase Shift Keying
DQPSK	Differential Quadrature Phase Shift Keying
DSB	Double Side Band
DSL	Digital Subscriber Line
DWDM	Dense Wavelength Division Multiplexing
EAM	Electro Absorption Modulator

EDFA	Erbium Doped Fiber Amplifier
EFM	Ethernet in the First Mile
EMI	Electromagnetic Immunity
EOM	Electro Optical Modulator
EPON	Ethernet Passive Optical Network
FBG	Fiber Bragg Grating
FCA	Fixed Channel Allocation
FPLD	Fabry-Perot Laser Diode
FSAN	Full Service Access Network
FT	Fourier Transform
FTTB	Fiber to the Building
FTTC	Fiber to the Curb
FTTH	Fiber to the Home
FTTN	Fiber to the Node
FTTP	Fiber to the Premise
FTTx	Fiber to the x
FWHM	Full Width at Half Maximum
FWM	Four Wave Mixing
GDM	Group Diversity Multiplexing
GPON	Gigabit Passive Optical Network
GVD	Group Velocity Dispersion
HD	Harmonic Distortion
HDTV	High Definition Television
HFC	Hybrid Fiber Coaxial
IEEE	Institute of Electrical and Electronics Engineers
IMD	Inter Modulation Distortion
IM-DD	Intensity Modulation Direct Detection
ISI	Inter Symbol Interference
ITU	International Telecommunication Union

LED	Light Emitting Diode
LiNbO$_3$	Lithium Niobate
LO	Local Oscillator
LTI	Linear Time Invariant
MAC	Media Access Control
MEM	Micro Electro Mechanical
MIMO	Multiple Input Multiple Output
MMF	Multi Mode Fiber
M-QAM	Multilevel Quadrature Amplitude Modulation
MZI	Mach-Zehnder Interferometer
MZM	Mach-Zehnder Modulator
OBS	Optical Broadband Source
OCDM	Optical Code Division Multiplexing
ODC	Optical Dispersion Compensation
OFDM	Optical Frequency Division Multiplexing
OFM	Optical Frequency Multiplication
ONU	Optical Network Unit
P2MP	Point To Multipoint
P2P	Point To Point
PBC	Polarization Beam Combiner
PBS	Polarization Beam Splitter
PC	Polarization Controller
PD	Photodetector
PDL	Polarization Dependent Loss
PDM	Polarization Division Multiplexing
PER	Polarization Extinctio Ratio
PM	Phase Modulation
PMD	Polarization Mode Dispersion
PM-IM	Phase to Intensity Modulation

PolMUX	Polarization Multiplexing
PON	Passive Optical Network
PSD	Power Spectral Density
RoF	Radio over Fiber
SA	Service Area
SBS	Stimulated Brillouin Scattering
SCM	Subcarrier Multiplexing
SMF	Single Mode Fiber
SOA	Semiconductor Optical Amplifier
SoP	State of Polarization
SPM	Self Phase Modulation
SRS	Stimulated Raman Scattering
SSB	Single Side Band
TDM	Time Division Multiplexing
VDL	Variable Delay Line
VDSL	Very High Bit Rate Digital Subscriber Line
WDM	Wavelength Division Multiplexing
XPM	Cross Phase Modulation

IV. List of publications

Publications on International Journals:

- F. Grassi, J. Mora, B. Ortega, J. Capmany, "Subcarrier multiplexing tolerant dispersion transmission system employing optical broadband sources", Opt. Express, Vol.17, pp. 4740-4751, 2009.

- F. Grassi, J. Mora, B. Ortega, J. Capmany, "Centralized light-source optical access network based on polarization multiplexing", Opt. Express, Vol.18, pp. 4240-4245, 2010.

- F. Grassi, J. Mora, B. Ortega, J. Capmany, "Radio over fiber transceiver employing phase modulation of an optical broadband source", Opt. Express, Vol.18, pp. 21750-21756, 2010.

- F. Grassi, J. Mora, B. Ortega, J. Capmany, "Low cost SCM-WDM radio over fiber system employing optical broadband sources for multimode and singlemode fiber", peer-review in Opt. Express.

- F. Grassi, J. Mora, B. Ortega, J. Capmany, "WDM optical access network for full-duplex and reconfigurable capacity assignment based on PolMux technique", peer-review in Opt. Express.

Publications on International Conferences and Exhibitions:

- F. Grassi, J. Mora, B. Ortega, J. Capmany, "20 GHz Radio over Fiber signal transport using optical broadband sources over multimode and singlemode fibers", in Proc. of the 14th European Conference on Networks and Optical Communications (NOC 2009) and 4th Conference on Optical Cabling and Infrastructure (OC&I 2009), Valladolid, Spain, pp. 257-263, 2009.

- F. Grassi, J. Mora, B. Ortega, J. Capmany, "Experimental evaluation of the Transmission in a Low Cost SCM/WDM Radio over Fiber System Employing Optical Broadband Sources and Interferometric Structures", in Proc. of the 11th International Conference on Transport Optical Networks (ICTON 2009), Ponta Delgada, Island of S. Miguel, Azores, Portugal, pp. 1-4, 2009.

- F. Grassi, J. Mora, B. Ortega, J. Capmany, "Experimental SCM Transmission System Employing Optical Broadband Sources Free from Carrier Suppression Effect", in Proc. of the 9th IASTED International Conference on Wireless and Optical Communications (WOC 2009), Banff, Alberta, Canada, pp. 110-115, 2009.

- F. Grassi, J. Mora, B. Ortega, J. Capmany, "GHz-Multichannel SCM-WDM transmission over multimode fiber links employing an optical broadband source", in Proc. of the IEEE International Topical Meeting on Microwave Photonics (MWP2009), Valencia, Comunidad Valenciana, Spain, 2009.

- F. Grassi, J. Mora, B. Ortega, J. Capmany, "Low cost Radio over Fiber transceiver using phase signal modulation", in Proc. of the IEEE

International Topical Meeting on Microwave Photonics (MWP2009), Valencia, Comunidad Valenciana, Spain, 2009.

- J. Mora, B. Ortega, J. Capmany, F. Grassi, "Bidirectional optical access network based on PolMUX technique using centralized light sources", in Proc. of the IEEE International Topical Meeting on Microwave Photonics (MWP2009), Valencia, Comunidad Valenciana, Spain, 2009.

- F. Grassi, J. Mora, B. Ortega, J. Capmany, "Suppression of Harmonic and Intermodulation Distortion for SCM-WDM RoF Systems based on the Spectral Slicing of Optical Broadband Sources", in Proc. of the 2010 Conference on Laser and Electro-Optics and the Quantum Electronics and Laser Science Conference (CLEO/qels2010), San Jose, California, United States of America, 2010.

- F. Grassi, J. Mora, B. Ortega, J. Capmany, "All- Optical Microwave Up-Conversion using an Optical Broadband Source and a Mach-Zehnder Interferometer", in Proc. of the 2010 Conference on Laser and Electro-Optics and the Quantum Electronics and Laser Science Conference (CLEO/qels2010), San Jose, California, United States of America, 2010.

- F. Grassi, J. Mora, B. Ortega, J. Capmany, "Bidirectional transmission of digital signals in a WDM-PolMUX optical access network", in Proc. of the IEEE International Topical Meeting on Microwave Photonics (MWP2010), Montréal, Québec, Canada, 2010.

- B. Ortega, J. Mora, M. Bolea, F. Grassi, J. Capmany, "Microwave photonics solutions for in-building networks signal transmission", in Proc. of the 2010 OSA Access Networks and In-house Communications (ANIC 2010), Karlsruhe, Germany, paper AThA2, pp. 21-23, 2010.

Publications on National Conferences and Exhibitions:

- F. Grassi, J. Mora, B. Ortega, J. Capmany, "Fuentes Ópticas Anchas para Transmisión de Señales RoF en Redes Ópticas WDM-PON de Bajo Coste", in Proc. Of the XXIV Simposium Nacional de la Unión Científica Internacional de Radio (URSI 2009), Santander, Cantabria, Spain, pp. 181, 2009.

- F. Grassi, J. Mora, Manuel Rius, B. Ortega, J. Capmany, "Red de Acceso óptica WDM-PolMUX con control remoto de la polarización", in Proc. Of the XXV Simposium Nacional de la Unión Científica Internacional de Radio (URSI 2009), Bilbao, Vizcaya, Spain, 2010.

Other publications:

- G. Puerto, J. Mora, B. Ortega, J. Capmany, F. Grassi, "Fiber-Bragg Grating-Based Architectures for Reconfigurable Services in In-Building Networks", in Proc. of the 2010 Conference on Laser and Electro-Optics and the Quantum Electronics and Laser Science Conference (CLEO/qels2010), San Jose, California, United States of America, 2010.